

This item was submitted to [Loughborough's Research Repository](#) by the author.
Items in Figshare are protected by copyright, with all rights reserved, unless otherwise indicated.

The development of ICP-MS methods for the study of biomedical problems particularly those involving nucleic acids

PLEASE CITE THE PUBLISHED VERSION

PUBLISHER

© Peter D. Winship

PUBLISHER STATEMENT

This work is made available according to the conditions of the Creative Commons Attribution-NonCommercial-NoDerivatives 4.0 International (CC BY-NC-ND 4.0) licence. Full details of this licence are available at: <https://creativecommons.org/licenses/by-nc-nd/4.0/>

LICENCE

CC BY-NC-ND 4.0

REPOSITORY RECORD

Winship, Peter D.. 2019. "The Development of ICP-MS Methods for the Study of Biomedical Problems Particularly Those Involving Nucleic Acids". figshare. <https://hdl.handle.net/2134/17387>.



University Library

Author/Filing Title WINSHIP, P.D.

Class Mark T
.....

Please note that fines are charged on ALL
overdue items.

FOR REFERENCE ONLY

0403603560



The Development of ICP-MS
Methods for the Study of
Biomedical Problems Particularly
those Involving Nucleic Acids

By


Peter D. Winship

A Doctoral Thesis

**Submitted in Partial Fulfilment of the Requirements for the Award
of Degree of Doctor of Philosophy of Loughborough University**

21st June 2007

© by Peter D. Winship 2007

	Loughborough University Pekington Library
Date	8/2008
Class	T
Acc No.	0403603560

“How quickly one accepts the incredible if only one sees it enough.”

- Richard Matheson, I Am Legend

Abstract

Inductively coupled plasma mass spectrometry (ICP-MS) is a well established and versatile technique for the elemental analysis of a wide spectrum of samples. For a majority of the elements that can be analysed by ICP-MS limits of detection in the order of sub ng l⁻¹ levels can be attained. However, a number of these elements have problems associated with them that lead to a restriction of the limits of detection that can be achieved. Phosphorus and Sulphur are two such elements that exhibit poorer limits of detection, the improvement of which would be highly desirable to the ICP-MS analyst.

Six methods for the measurement of ³¹P and ³²S isotopes have been developed with the aim of avoiding the spectroscopic interferences at the native *m/z* ratios of 31 and 32 respectively. These approaches have utilised a hexapole collision cell, a ‘cold/cool plasma’ and an experimental ICP torch bonnet. Via the collision cell and ‘cold/cool plasma’ approaches the isotopes of interest were either converted to different species for successful measurement at an alternative *m/z* ratio or interfering species were removed allowing measurement at the native *m/z*. Limits of detection achieved by these approaches were comparable with those quoted in the literature and by ICP-MS instrument manufacturers. The approach using the torch bonnet was not successful in attenuating spectroscopic interferences; however, it did show potential for continuing as an area of research. The development of these six methods is discussed in Chapter 2.

As an application of the successful methods developed for the measurement of ³¹P and ³²S isotopes, DNA (and its associated components) was selected for study as this bio-molecule is comprised of approximately 10 % phosphorus. DNA in solution was successfully quantified by these methods and DNA components, studied during polymerase chain reaction processes and in single nucleotide polymorphisms, were qualified. The application of these methods to the study of DNA and its components is discussed in Chapter 3.

As part of a collaboration between the Loughborough University Atomic Spectroscopy Research Group and the Cancer Biomarkers and Prevention Group at the University of Leicester, ICP-MS was employed in the investigation of the interactions between two Pt based anti-cancer drugs (cisplatin and oxaliplatin) and their biological target DNA. For this collaboration, DNA was the interest common to both groups. The interaction of each of these drugs with known quantities of DNA was measured by ICP-MS and binding constant data was calculated for use as the basis of a clinical test for drug efficacy in cancer patients. The binding constant data showed that the interaction between drug and target is particularly inefficient. This area of research is discussed in Chapter 4.

The potential for ICP-MS interface modification was also explored. Two modified designs are discussed that may prove to be advantageous for the transport of ions between the atmospheric pressure conditions of the ICP ion source and the vacuum conditions of the mass spectrometer. One of these designs was successfully manufactured and produced positive data. Research into this design is being furthered by the Thermo Electron Corporation, the discussion of which is in Chapter 5.

A further collaboration was established with both the Biomaterials-related Infection Group of the School of Medical and Surgical Sciences and the Polymer Group of the School of Mechanical, Materials and Manufacturing Engineering at the University of Nottingham. Here ICP-MS was employed in the measurement of silver leaching from a silver nano-particle impregnated polymer material that could be used in the production of catheters. Silver leaching from a catheter is potentially desirable due to its anti-microbial properties. The study of this leaching revealed that significant quantities of silver were being transferred from the polymer into surrounding human serum media over the period of seven days and beyond. For the most part this work was routine ICP-MS measurement, and did not involve research or development, so does not take part in the main body of this thesis. This work is discussed in Appendix 5.

Dedicated to my beautiful wife Joanne.

**For her unlimited love, encouragement and support and her ability to point out
my very few faults.**



Figure A. The Radiant Joanne Winship, 8th May 2004.

Acknowledgements

I would like to extend my appreciation to the large number of people who devoted both time and energy to the work that is described in this thesis making it the success that it was. Without the support from each of these individuals I would not have been able to overcome the obstacles that I encountered during the course of this research.

I would like to thank the Thermo Electron Corporation (Winsford, United Kingdom) for both their financial and instrumental support. Without such support this research would not have been able to go ahead.

I owe a huge debt of gratitude to Dr Barry Sharp, my supervisor, and Dr Helen Reid for all of their support, guidance, ideas and good humour over the past five years. I am exceptionally grateful to both of you.

For their generosity of expertise and time I would also like to thank David Wilson, Trevor Brown, Ashley Gilmour, Sarabjit Mastana, Bob Ludlum, Chris Harrington, Rachel Le Pla, Don Jones, Peter Farmer, John Spray and Stuart Pinkney.

A huge thank you goes to my Mother and Father, Claire, Dave and Charlotte, Steve and Ellie, Granny Winship, Kevin, Kelly, Sophie and Michaela as well as the Claytons (Ron, Chris, Simon, Gemma and the five boys) for everything that you all do to support me on a daily basis. Another huge thank you goes to my friends and second family for keeping a smile on my face; it is my privilege to know you all: Mark Landon, Ciaran O'Connor, Karen Tappenden, Stuart 'Spudgun' and Vicky Aldridge, Sam Kerr, Dhinesh Asogan, Monica Felepe-Sotelo, Jo Wragg, Barry Sharp and Helen Reid.

I would also like to acknowledge the following individuals, in no particular order, for their daily inspiration.

The Man, James Ellroy, Elmore Leonard, Peter Stormare, Guy Fawkes, The Rik Mayall, Adrian Edmondson, Henry 'The Fonz' Winkler, Bender the Robot, Pierre Boule, Philip Eisner, Rex Pickett, The Market Square Bakery, J.K. Rowling, Frank Miller, Johnny Cash, Richard Stark, Richard Matheson, The Creator of Blueberry Muffins, Rammstein, John Carpenter, Debra Hill, Matt Groening, Joanne Harris, Eddie Izzard, Carl Hiaasen, Metallica, The Employees of Starbucks, Chuck Palahniuk, The Hooters Girls, Homer Simpson, The Late Douglas Adams, Alice Cooper, Eeyore (The Lamb With One Vertebrae Too Many), Mario, Telly Savalas, Terry Pratchett, Kid Rock, Oliver Cromwell, George A. Romero, Guy Burt, Bryan Singer, Stephen King, Michael Chiklis, Will Ferrell, Peter Kay, Jim Bowen, Rob Grant, Doug Naylor, William Shatner, Ranulph Fiennes, Mike Stroud, Ernest Hemingway, Jim Henson, Slash, Sheryl Crow, Stephen Fry, The Good People of Las Vegas, Kenny Rogers, Philip K. Dick, Cartman, Kenny, Kyle and Stan.

Contents

Abstract.....	3
Acknowledgements.....	6
Contents.....	7
List of Figures	12
List of Tables.....	20
Glossary of Abbreviations	28

Chapter 1. An Introduction to ICP-MS Analysis

1.1. An Introduction to ICP-MS	34
1.1.1. The Design and Operation of an ICP-MS Instrument	36
1.1.2. Sample Introduction in ICP-MS Analysis	39
1.1.3. Mass Spectrometry Employed in ICP-MS Analysis.....	42
1.2. Limitations of ICP-MS Analysis.....	45
1.2.1. Spectroscopic Interferences	45
1.2.2. Non-Spectroscopic Interferences	47
1.3. Kinetic Energy Issues Associated with ICP-MS Analysis.....	52
1.3.1. Causes of Ion Kinetic Energy Spread	52
1.3.2. The Significance of Ion Kinetic Energy Spread	55
1.3.3. Advantageous Ion Energy Effects	55
1.4. Collision and Dynamic Reaction Cells	57
1.4.1. Collision Cells.....	57
1.4.2. Dynamic Reaction Cells	57
1.4.3. Ion-Molecule Chemistry of Collision and Dynamic Reaction Cells	58
1.5. “Cold/Cool Plasma”	61
1.6. The Application of ICP-MS in Biological Samples.....	63
1.6.1. Biological Samples in Clinical Science	63
1.6.2. Biological Samples in the Environment	64
1.7. Thesis Aims and Objectives	65

Chapter 2. Method Development Studies for the Determination of Phosphorus and Sulphur Isotopes by ICP-MS

2.1. The Determination of Phosphorus and Sulphur by ICP-MS	69
2.1.1. The Limitations of ³¹ P and ³² S Determination by ICP-QMS.....	70
2.1.2. Alternative Techniques for the Determination of ³¹ P and ³² S	72
2.2. Aims of Research.....	75

2.3. Experimental Details.....	77
2.4. The Development of Methods to Overcome ^{31}P and ^{32}S Isotope Interferences	79
2.4.1. Method 1: The Determination of $^{31}\text{P}^{16}\text{O}^+$ and $^{32}\text{S}^{16}\text{O}^+$ Ions in a Collision Cell Incorporating He and O_2 Under IKEE Conditions	79
2.4.2. Method 2: The Determination of $^{31}\text{P}^{16}\text{O}^+$ and $^{32}\text{S}^{16}\text{O}^+$ Ions in a Collision Cell Incorporating O_2 Only Under IKEE Conditions.....	90
2.4.3. Method 3: Selective Removal of Polyatomic Ions in a Collision Cell Incorporating He Collision Gas Under KED Conditions	99
2.4.4. Method 4: The Determination of $^{31}\text{P}^{16}\text{O}^+$ and $^{32}\text{S}^{16}\text{O}^+$ Ions Formed Under ‘Cold/Cool Plasma’	107
2.4.5. Method 5: The Determination of $^{31}\text{P}^{16}\text{O}^+$ and $^{32}\text{S}^{16}\text{O}^+$ Ions Formed by ‘Cold/Cool’ Plasma Incorporating an Additional O_2 Nebuliser Flow	114
2.4.6. Method 6 (Part 1): The Exclusion of Entrained Atmospheric Gases from the ICP	118
2.4.7. Method 6 (Part 2): The Exclusion of Entrained Atmospheric Gases from the ICP	124
2.5. The Calculation of Method Limit of Detection (LOD).....	131
2.5.1. LOD Calculation 1	131
2.5.2. LOD Calculation 2	131
2.5.3. A Comparison of LOD’s	132
2.6. Conclusions	134

Chapter 3. The Application of Methods Developed for the Determination of ^{31}P and ^{32}S and the Study of DNA and Related Material by ICP-MS

3.1. Genomics	138
3.2. Aims of Research.....	140
3.3. The Application of Developed Methods	140
3.4. DNA Quantification by Methods 2, 3, 4 and 5	141
3.5. The Analysis of DNA Samples Separated on an Agarose Gel Plate by ICP-MS Employing Method 2	146
3.6. The Study of DNA Replication by Polymerase Chain Reaction...	149
3.7. The Study of Single Nucleotide Polymorphisms by HPLC-ICP-MS	153
3.8. Conclusions for the Application of ^{31}P and ^{32}S ICP-MS Methods	158

Chapter 4. The Measurement of Platinum Based Anticancer Drugs and DNA by ICP-MS

4.1. Disease and Metal Based Complexes.....	161
4.2. Cancer and Cancer Treatments.....	161
4.2.1. Cisplatin	162
4.2.2. Oxaliplatin	164
4.2.3. Types of Drug-Target Interaction Exhibited by Cisplatin and Oxaliplatin and Other Metal Based Drug Complexes	165
4.2.4. The Effect of Cisplatin and Oxaliplatin Binding on DNA Structure.....	168
4.2.5. DNA Repair Mechanisms and Drug Resistance.....	168
4.2.6. Cancer Treatments and Drug Efficacy.....	169
4.2.7. Previous Studies of Cisplatin and Oxaliplatin Exposure to DNA	170
4.3. Aims of Research.....	173
4.4. The Study of DNA and Pt Based Drug Interactions <i>In Vitro</i> by ICP-QMS.....	174
4.4.1. Study 1	174
4.4.2. Study 2	183
4.4.3. Studies 3 and 4	192
4.4.4. The Analysis of Study 4 Centrifuge Filters	214
4.4.5. Study 5	222
4.5. The Calculation of DNA and Pt Based Drug Formation Constants (K_f) and Adduct Ratios.....	230
4.5.1. Formation Constant (K_f) Theory.....	230
4.5.2. Formation Constant (K_f) and Adduct Ratios: Calculations	234
4.5.3. Formation Constant (K_f) and Adduct Ratios: Discussion and Conclusions.....	242
4.6. Conclusions and Further Work.....	245

Chapter 5. The Development of ICP-MS Interface Structures

5.1. The ICP-MS Interface	247
5.1.1. Deposition problems within the ICP-MS Interface	248
5.1.2. Ion Kinetic Energy Spread Associated with the ICP-MS Interface.....	248
5.2. Previous Approaches to Tackling ICP-MS Interface Problems...	250
5.2.1. Skimmer Cone Geometry	250
5.2.2. Sample and Skimmer Cone Separation	251
5.2.3. Three Cone Interface	252
5.3. The Development of an Adapted ICP-MS Interface for the Reduction of Ion Deposition.....	253

5.3.1. The Temperature Environment of an ICP-MS Interface Expansion Chamber	256
5.3.2. Manufacture and Testing of an Adapted ICP-MS Interface for the Reduction of Ion Deposition	258
5.3.3. The Development of an Adapted ICP-MS Interface for the Reduction of Ion Deposition: Conclusion.....	262
5.4. The Development of an ICP-MS Interface with a Gradual Pressure Reduction	263
5.4.1. The Transitions Required for a Gradual Interface Pressure Reduction	263
5.4.2. A Potential Approach to a Gradual Interface Pressure Reduction.....	265
5.4.3. The Development of an ICP-MS Interface with a Gradual Pressure Reduction: Conclusion.....	268
5.5. Conclusions	269

Chapter 6. General Conclusions and Future Work

6.1. The Development of Methods for the Determination of ^{31}P and ^{32}S Isotopes by ICP-MS.....	271
6.1.1. Hexapole Collision Cell Methods.....	271
6.1.2. ‘Cold/Cool Plasma’ Methods.....	272
6.2. The Application of Methods Developed for the Determination of ^{31}P and ^{32}S Isotopes by ICP-MS	273
6.3. The Analysis of Platinum Based Anti-Cancer Drugs and DNA by ICP-MS.....	275
6.4. The Development of ICP-MS Interface Structures	276
References	277
Appendices	287

List of Figures

Figure 1. A Periodic Table of the Elements Showing Detection Limits and Ionisation Potential Data for the Useable Elements by ICP-MS.	35
Figure 2. A Schematic of a Typical ICP-MS Instrument.	37
Figure 3. A Diagram of the Barrel Shock Region Produced in the Interface of an ICP-MS Instrument.	38
Figure 4. The "Ion Energy Rollercoaster" Diagram. ¹⁰²	53
Figure 5. A Graph Comparing $m/z = 31$ Signal with V_h for the Analysis of 2% HNO_3 Blank and $1000 \mu\text{g l}^{-1}$ P Solutions (Reaction Gases: $\text{He} = 0.2 \text{ ml min}^{-1}$ and $\text{O}_2 = 0.3 \text{ ml min}^{-1}$) ($V_q = +1 \text{ V}$).	82
Figure 6. A Graph Comparing $m/z = 47$ Signal with V_h for the Analysis of 2% HNO_3 Blank and $1000 \mu\text{g l}^{-1}$ P Solutions (Reaction Gases: $\text{He} = 0.2 \text{ ml min}^{-1}$ and $\text{O}_2 = 0.3 \text{ ml min}^{-1}$) ($V_q = +1 \text{ V}$).	83
Figure 7. A Graph Comparing $m/z = 32$ Signal with V_h for the Analysis of 2% HNO_3 Blank and $1000 \mu\text{g l}^{-1}$ S Solutions (Reaction Gases: $\text{He} = 0.2 \text{ ml min}^{-1}$ and $\text{O}_2 = 0.3 \text{ ml min}^{-1}$) ($V_q = +1$).	83
Figure 8. A Graph Comparing $m/z = 48$ Signal with V_h for the Analysis of 2% HNO_3 Blank and $1000 \mu\text{g l}^{-1}$ S Solutions (Reaction Gases: $\text{He} = 0.2 \text{ ml min}^{-1}$ and $\text{O}_2 = 0.3 \text{ ml min}^{-1}$) ($V_q = +1 \text{ V}$).	84
Figure 9. A Survey Data Mass Spectrum Generated During the Method 1 IKEE Experimental Work.	88
Figure 10. A Graph Comparing $m/z = 31$ Signal with V_h for the Analysis of 2% HNO_3 Blank and $1000 \mu\text{g l}^{-1}$ P Solutions (Reaction Gas: $\text{O}_2 = 0.3 \text{ ml min}^{-1}$) ($V_q = +1 \text{ V}$).	91
Figure 11. A Graph Comparing $m/z = 47$ Signal with V_h for the Analysis of 2% HNO_3 Blank and $1000 \mu\text{g l}^{-1}$ P Solutions (Reaction Gas: $\text{O}_2 = 0.3 \text{ ml min}^{-1}$) ($V_q = +1 \text{ V}$).	91
Figure 12. A Graph Comparing $m/z = 32$ Signal with V_h for the Analysis of 2% HNO_3 Blank and $1000 \mu\text{g l}^{-1}$ S Solutions (Reaction Gas: $\text{O}_2 = 0.3 \text{ ml min}^{-1}$) ($V_q = +1 \text{ V}$).	92
Figure 13. A Graph Comparing $m/z = 48$ Signal with V_h for the Analysis of 2% HNO_3 Blank and $1000 \mu\text{g l}^{-1}$ S Solutions (Reaction Gas: $\text{O}_2 = 0.3 \text{ ml min}^{-1}$) ($V_q = +1 \text{ V}$).	92
Figure 14. Graphs Exhibiting Signal Response as a Function of Concentration for the ^{31}P and ^{32}S Isotopes Employing 'Method 2'	97
Figure 15. A Graph Comparing $m/z = 31$ Background Subtracted Signal for the Analysis of 2 % HNO_3 Blank and $200 \mu\text{g l}^{-1}$ P Solutions when Varying He Flow Rate (ml min^{-1}) Under Different KED Conditions (KED Spread = +1 V).	101
Figure 16. A Graph Comparing $m/z = 31$ Signal Sample : Blank Ratio for the Analysis of 2 % HNO_3 Blank and $200 \mu\text{g l}^{-1}$ P Solutions when Varying He Flow Rate (ml min^{-1}) Under Different KED Conditions (KED Spread = +1 V).	101
Figure 17. A Graph Comparing $m/z = 31$ Background Subtracted Signal for the Analysis of 2 % HNO_3 Blank and $200 \mu\text{g l}^{-1}$ P Solutions when Varying He Flow Rate (ml min^{-1}) Under Different KED Conditions (KED Spread = +2 V).	102
Figure 18. A Graph Comparing $m/z = 31$ Signal Sample : Blank Ratio for the Analysis of 2 % HNO_3 Blank and $200 \mu\text{g l}^{-1}$ P Solutions when Varying He Flow Rate (ml min^{-1}) Under Different KED Conditions (KED Spread = +2 V).	102
Figure 19. A Graph Comparing $m/z = 31$ Background Subtracted Signal for the Analysis of 2 % HNO_3 Blank and $200 \mu\text{g l}^{-1}$ P Solutions when Varying He Flow Rate (ml min^{-1}) Under Different KED Conditions (KED Spread = +3 V).	103

Figure 20. A Graph Comparing $m/z = 31$ Signal Sample : Blank Ratio for the Analysis of 2 % HNO_3 Blank and 200 $\mu\text{g l}^{-1}$ P Solutions when Varying He Flow Rate (ml min^{-1}) Under Different KED Conditions (KED Spread = +3 V).....	103
Figure 21. A Graph Exhibiting Signal Response as a Function of Concentration for the ^{31}P Isotope Employing ‘Method 3’.....	107
Figure 22. A Graph Comparing $m/z = 31$ Signal with Forward Power (W) for the Analysis of 2 % HNO_3 Blank and 1000 $\mu\text{g l}^{-1}$ P Solutions.	109
Figure 23. A Graph Comparing $m/z = 47$ Signal with Forward Power (W) for the Analysis of 2 % HNO_3 Blank and 1000 $\mu\text{g l}^{-1}$ P Solutions.	109
Figure 24. A Graph Comparing $m/z = 32$ Signal with Forward Power (W) for the Analysis of 2 % HNO_3 Blank and 1000 $\mu\text{g l}^{-1}$ S Solutions.	110
Figure 25. A Graph Comparing $m/z = 48$ Signal with Forward Power (W) for the Analysis of 2 % HNO_3 Blank and 1000 $\mu\text{g l}^{-1}$ S Solutions.	110
Figure 26. Graphs Exhibiting Signal Response as a Function of Concentration for the ^{31}P and ^{32}S Isotopes Under ‘Method 4’.....	113
Figure 27. The Variation of $m/z = 47$ Signal with O_2 Nebuliser Gas Flow Introduction for the Analysis of 2 % HNO_3 Blank and 1000 $\mu\text{g l}^{-1}$ P Solutions.....	115
Figure 28. The Variation of $m/z = 48$ Signal with O_2 Nebuliser Gas Flow Introduction for the Analysis of 2 % HNO_3 Blank and 1000 $\mu\text{g l}^{-1}$ S Solutions.....	115
Figure 29. Graphs Exhibiting Signal Response as a Function of Concentration for the ^{31}P and ^{32}S Isotopes Employing Method 5 Conditions.....	117
Figure 30. A Schematic of the Torch Bonnet Design (Dimensions Measured in mm).	119
Figure 31. A Comparison of P Standard Concentration ($\mu\text{g l}^{-1}$) with $m/z = 31$ Signal (cps) for Analysis Under Standard Conditions and with the Torch Bonnet in Position.	120
Figure 32. A Graph Comparing S Standard Concentration ($\mu\text{g l}^{-1}$) with $m/z = 32$ Signal (cps) for Analysis Under Standard Conditions and with the Torch Bonnet in Position.	121
Figure 33. A Graph Comparing P and S Standard Concentration ($\mu\text{g l}^{-1}$) with $m/z = 115$ Signal (cps) for Analysis Under Standard Conditions and with the Torch Bonnet in Position.....	121
Figure 34. A Schematic of the Second Torch Bonnet Design (Dimensions Measured in mm).....	125
Figure 35. A Graph Comparing P Standard Concentration ($\mu\text{g l}^{-1}$) with $m/z = 31$ Signal (cps) for Analysis Under Standard Conditions and with the Second Torch Bonnet Design in Place.....	126
Figure 36. A Graph Comparing S Standard Concentration ($\mu\text{g l}^{-1}$) with $m/z = 32$ Signal (cps) for Analysis Under Standard Conditions and with the Second Torch Bonnet Design in Place.....	127
Figure 37. A Graph Comparing P and S Standard Concentration ($\mu\text{g l}^{-1}$) with $m/z = 115$ Signal (cps) for Analysis Under Standard Conditions and with the Second Torch Bonnet Design in Place.	127
Figure 38. The Common Approach to the Calculation of Limit of Detection.....	131
Figure 39. The Equation used to Calculate Limit of Detection Signal (More Realistic Approach).	132
Figure 40. A Structural Diagram of Nucleotides That Make Up The DNA Molecule.	139

Figure 41. A Standard Additions Graph Comparing P Standard Conc ⁿ ($\mu\text{g l}^{-1}$) with $m/z = 47$ Signal (cps) for a Series of P Spiked 2000 $\mu\text{g l}^{-1}$ DNA Solns Under Method 2 Conditions.	142
Figure 42. A Standard Additions Graph Comparing P Standard Conc ⁿ ($\mu\text{g l}^{-1}$) with $m/z = 31$ Signal (cps) for a Series of P Standard Solns and P Spiked 200 $\mu\text{g l}^{-1}$ DNA Solns Under Method 3 Conditions.	143
Figure 43. A Standard Additions Graph Comparing P Standard Conc ⁿ ($\mu\text{g l}^{-1}$) with $m/z = 47$ Signal (cps) for a Series of P Standard Solns and P Spiked 200 $\mu\text{g l}^{-1}$ DNA Solns Under Method 4 Conditions.	143
Figure 44. A Standard Additions Graph Comparing P Standard Conc ⁿ ($\mu\text{g l}^{-1}$) with $m/z = 47$ Signal (cps) for a Series of P Standard Solns and P Spiked 200 $\mu\text{g l}^{-1}$ DNA Solns Under Method 5 Conditions.	144
Figure 45. A Graph Comparing Number of Thermocycles with $m/z = 47$ Signal for the Analysis of a PCR Process Employing ICP-MS Method 2.	151
Figure 46. The UV Chromatogram of Oligonucleotides 2 and 3 Separated and Detected by HPLC-ICP-MS (Absorbance Versus Retention Time (Minutes)).	156
Figure 47. The ICP-MS Chromatogram of Oligonucleotides 2 and 3 Separated and Detected by HPLC-ICP-MS.	156
Figure 48. A Structural Diagram of Cisplatin.	163
Figure 49. A Structural Diagram of Oxaliplatin.	164
Figure 50. A Diagram of the Most Common Binding Interactions between <i>cis</i> -diammine Pt Adducts and the Purine Molecular Bases of a DNA Strand (Not to Scale).	166
Figure 51. A Diagram of the Most Common Binding Interactions between (<i>trans</i> -R,R)-diamino-cyclohexane Pt Adducts and the Purine Molecular Bases of a DNA Strand (Not to Scale).	167
Figure 52. A Graph Comparing P Spike Concentration ($\mu\text{g l}^{-1}$) with $m/z = 47$ Signal (cps) for Sample 1 : 1 000 000 and External Standards.	178
Figure 53. A Graph Comparing Pt Spike Concentration ($\mu\text{g l}^{-1}$) with $m/z = 194$ Signal (cps) for Sample 1 : 1 000 000 and External Standards.	179
Figure 54. A Graph Comparing Pt Spike Concentration ($\mu\text{g l}^{-1}$) with $m/z = 195$ Signal (cps) for Sample 1 : 1 000 000 and External Standards.	179
Figure 55. A Graph Comparing Number of Cisplatin Molecules Per DNA Nucleotide with Corrected $m/z = 194$ and 195 Signal (cps).	188
Figure 56. A Graph Comparing Pt Standard Concentration ($\mu\text{g l}^{-1}$) with $m/z = 194$ and 195 Signal (cps).	188
Figure 57. A Bar Chart Comparing $m/z = 31$ Signals (cps) Between DNA/Cisplatin Samples Studied During Study 2.	189
Figure 58. A Graph Comparing Number of Cisplatin Molecules Per DNA Nucleotide with Corrected $m/z = 194$ and 195 Signal (cps) for Study 3.	199
Figure 59. A Graph Comparing Number of Oxaliplatin Molecules Per DNA Nucleotide with Corrected $m/z = 194$ and 195 Signal (cps) for Study 3.	199
Figure 60. An External Calibration Graph Comparing Pt Standard Concentration ($\mu\text{g l}^{-1}$) with $m/z = 194$ and 195 Signal (cps) for both DNA/Cisplatin and DNA/Oxaliplatin Samples Studied During Study 3.	200
Figure 61. A Bar Chart Comparing $m/z = 31$ Signals (cps) Between DNA/Cisplatin Samples Studied During Study 3.	200
Figure 62. A Bar Chart Comparing $m/z = 31$ Signals (cps) Between DNA/Oxaliplatin Samples Studied During Study 3.	201

Figure 63. A Graph Comparing Number of Cisplatin Molecules Per DNA Nucleotide with Corrected $m/z = 194$ and 195 Signal (cps) for Study 4.....	201
Figure 64. A Graph Comparing Number of Oxaliplatin Molecules Per DNA Nucleotide with Corrected $m/z = 194$ and 195 Signal (cps) for Study 4.	202
Figure 65. An External Calibration Graph Comparing Pt Standard Concentration ($\mu\text{g l}^{-1}$) with $m/z = 194$ and 195 Signal (cps) for DNA/Cisplatin Samples Studied During Study 4.....	202
Figure 66. An External Calibration Graph Comparing Pt Standard Concentration ($\mu\text{g l}^{-1}$) with $m/z = 194$ and 195 Signal (cps) for DNA/Oxaliplatin Samples Studied During Study 4.....	203
Figure 67. A Bar Chart Comparing $m/z = 31$ Signals (cps) Between DNA/Cisplatin Samples Studied During Study 4.....	203
Figure 68. A Bar Chart Comparing $m/z = 31$ Signals (cps) Between DNA/Oxaliplatin Samples Studied During Study 4.....	204
Figure 69. A Bar Chart Comparing $m/z = 194$ Signals (cps) Between Centrifuge Filter Leachate Solutions of the DNA/Cisplatin Samples Studied for Study 4.....	216
Figure 70. A Bar Chart Comparing $m/z = 195$ Signals (cps) Between Centrifuge Filter Leachate Solutions of the DNA/Cisplatin Samples Studied for Study 4.....	216
Figure 71. A Bar Chart Comparing $m/z = 194$ Signals (cps) Between Centrifuge Filter Leachate Solutions of the DNA/Oxaliplatin Samples Studied for Study 4.....	217
Figure 72. A Bar Chart Comparing $m/z = 195$ Signals (cps) Between Centrifuge Filter Leachate Solutions of the DNA/Oxaliplatin Samples Studied for Study 4.....	217
Figure 73. A Bar Chart Comparing $m/z = 31$ Signals (cps) Between Centrifuge Filter Leachate Solutions of the DNA/Cisplatin Samples Studied for Study 4.....	218
Figure 74. A Bar Chart Comparing $m/z = 31$ Signals (cps) Between Centrifuge Filter Leachate Solutions of the DNA/Oxaliplatin Samples Studied for Study 4.....	218
Figure 75. An External Calibration Graph Comparing Pt Standard Concentration ($\mu\text{g l}^{-1}$) with $m/z = 194$ and 195 Signal (cps) for the Centrifuge Filter Leachate Solutions of the DNA/Cisplatin and DNA/Oxaliplatin Samples Studied for Study 4.	219
Figure 76. An External Calibration Graph Comparing DNA Based Pt Standard Concentration (ng l^{-1}) with $m/z = 194$ and 195 Signal (cps) for the Untreated DNA/Cisplatin and DNA/Oxaliplatin Samples Solutions Studied During Study 5.	224
Figure 77. A Graph Comparing Number of Drug Molecules Per Nucleotide with the ICP-MS Measured Pt Concentration for the Study of Cisplatin Exposed DNA Samples (Study 5).....	227
Figure 78. A Graph Comparing Number of Drug Molecules Per Nucleotide with the ICP-MS Measured Pt Concentration for the Study of Oxaliplatin Exposed DNA Samples (Study 5).....	228
Figure 79. The Equilibrium Reaction between DNA Nucleotides and Pt Based Drug Molecules.....	230
Figure 80. The Equation Required for the Determination of a Formation Constant (K_f).....	231
Figure 81. The Altered Equation Required for the Determination of a Formation Constant (K_f).....	232
Figure 82. Additional Equations Used During the Conversion of Study Data to Components Required for the Calculation of K_f and Number of Adducts Formed. a) An Equation for the Calculation of the Number of Nucleotides Per Litre. b) An Equation for the Calculation of the Number of Pt Atoms Exposed Per Litre.	

c) An Equation for the Calculation of the Number of Drug-Target Adducts Formed Per Litre. d) An Equation for the Calculation of the Number of Adducts formed Per DNA Nucleotide.	233
Figure 83. The Deflected Shock at a Small Tip Angle Skimmer Cone.	254
Figure 84. The Deflected Shock at a Large Tip Angle Skimmer Cone.	254
Figure 85. The Suggested Deflected Shock Arising from Supersonic Flow Against an Additional Plate and Orifice.	255
Figure 86. An Equation Comparing Pre/Post Sampler Orifice Pressures with Mach Number.	257
Figure 87. An Equation Comparing Pre/Post Sampler Orifice Temperatures with Mach Number.	257
Figure 88. A Schematic of the Second (Four Rod) ICP-MS Interface Structure.	261
Figure 89. A Diagram Showing a Potential Plate Stack Interface Structure Design for the Gradual Reduction of Pressure in the Expansion Chamber.	267
Figure 90. An Isotopic Abundance Table.	289
Figure 91. A Photograph of the Two Torch Bonnets Manufactured for the Exclusion of Entrained Atmospheric Gases from the ICP.	313
Figure 92. A Photograph of the First Torch Bonnet Design Placed Within the Instrument Torch Box.	313
Figure 93. A Photograph of the Second Torch Bonnet Design Placed Within the Instrument Torch Box.	316
Figure 94. A Graph Comparing Added P Concentration ($\mu\text{g l}^{-1}$) with $m/z = 47$ Signal (cps) for Samples 1-5 (C110) and External Standards.	341
Figure 95. A Graph Comparing Added Pt Concentration ($\mu\text{g l}^{-1}$) with $m/z = 194$ Signal (cps) for Samples 1-5 (C110) and External Standards.	341
Figure 96. A Graph Comparing Added Pt Concentration ($\mu\text{g l}^{-1}$) with $m/z = 195$ Signal (cps) for Samples 1-5 (C110) and External Standards.	341
Figure 97. A Graph Comparing Added P Concentration ($\mu\text{g l}^{-1}$) with $m/z = 47$ Signal (cps) for Samples 6-10 (C110 Duplicate) and External Standards.	341
Figure 98. A Graph Comparing Added Pt Concentration ($\mu\text{g l}^{-1}$) with $m/z = 194$ Signal (cps) for Samples 6-10 (C110 Duplicate) and External Standards.	341
Figure 99. A Graph Comparing Added Pt Concentration ($\mu\text{g l}^{-1}$) with $m/z = 195$ Signal (cps) for Samples 6-10 (C110 Duplicate) and External Standards.	341
Figure 100. A Graph Comparing Added P Concentration ($\mu\text{g l}^{-1}$) with $m/z = 47$ Signal (cps) for Samples 11-15 (C109) and External Standards.	342
Figure 101. A Graph Comparing Added Pt Concentration ($\mu\text{g l}^{-1}$) with $m/z = 194$ Signal (cps) for Samples 11-15 (C109) and External Standards.	342
Figure 102. A Graph Comparing Added Pt Concentration ($\mu\text{g l}^{-1}$) with $m/z = 195$ Signal (cps) for Samples 11-15 (C109) and External Standards.	342
Figure 103. A Graph Comparing Added P Concentration ($\mu\text{g l}^{-1}$) with $m/z = 47$ Signal (cps) for Samples 16-20 (C109 Duplicate) and External Standards.	342
Figure 104. A Graph Comparing Added Pt Concentration ($\mu\text{g l}^{-1}$) with $m/z = 194$ Signal (cps) for Samples 16-20 (C109 Duplicate) and External Standards.	342
Figure 105. A Graph Comparing Added Pt Concentration ($\mu\text{g l}^{-1}$) with $m/z = 195$ Signal (cps) for Samples 16-20 (C109 Duplicate) and External Standards.	342
Figure 106. A Graph Comparing Added P Concentration ($\mu\text{g l}^{-1}$) with $m/z = 47$ Signal (cps) for Samples 21-25 (C108) and External Standards.	343
Figure 107. A Graph Comparing Added Pt Concentration ($\mu\text{g l}^{-1}$) with $m/z = 194$ Signal (cps) for Samples 21-25 (C108) and External Standards.	343

Figure 108. A Graph Comparing Added Pt Concentration ($\mu\text{g l}^{-1}$) with $m/z = 195$ Signal (cps) for Samples 21-25 (C108) and External Standards.	343
Figure 109. A Graph Comparing Added P Concentration ($\mu\text{g l}^{-1}$) with $m/z = 47$ Signal (cps) for Samples 26-30 (C108 Duplicate) and External Standards.	343
Figure 110. A Graph Comparing Added Pt Concentration ($\mu\text{g l}^{-1}$) with $m/z = 194$ Signal (cps) for Samples 26-30 (C108 Duplicate) and External Standards.	343
Figure 111. A Graph Comparing Added Pt Concentration ($\mu\text{g l}^{-1}$) with $m/z = 195$ Signal (cps) for Samples 26-30 (C108 Duplicate) and External Standards.	343
Figure 112. A Graph Comparing Added P Concentration ($\mu\text{g l}^{-1}$) with $m/z = 47$ Signal (cps) for Samples 31-35 (C107) and External Standards.	344
Figure 113. A Graph Comparing Added Pt Concentration ($\mu\text{g l}^{-1}$) with $m/z = 194$ Signal (cps) for Samples 31-35 (C107) and External Standards.	344
Figure 114. A Graph Comparing Added Pt Concentration ($\mu\text{g l}^{-1}$) with $m/z = 195$ Signal (cps) for Samples 31-35 (C107) and External Standards.	344
Figure 115. A Graph Comparing Added P Concentration ($\mu\text{g l}^{-1}$) with $m/z = 47$ Signal (cps) for Samples 36-40 (C107 Duplicate) and External Standards.	344
Figure 116. A Graph Comparing Added Pt Concentration ($\mu\text{g l}^{-1}$) with $m/z = 194$ Signal (cps) for Samples 36-40 (C107 Duplicate) and External Standards.	344
Figure 117. A Graph Comparing Added Pt Concentration ($\mu\text{g l}^{-1}$) with $m/z = 195$ Signal (cps) for Samples 36-40 (C107 Duplicate) and External Standards.	344
Figure 118. A Graph Comparing Added P Concentration ($\mu\text{g l}^{-1}$) with $m/z = 47$ Signal (cps) for Samples 41-45 (C106) and External Standards.	345
Figure 119. A Graph Comparing Added Pt Concentration ($\mu\text{g l}^{-1}$) with $m/z = 194$ Signal (cps) for Samples 41-45 (C106) and External Standards.	345
Figure 120. A Graph Comparing Added Pt Concentration ($\mu\text{g l}^{-1}$) with $m/z = 195$ Signal (cps) for Samples 41-45 (C106) and External Standards.	345
Figure 121. A Graph Comparing Added P Concentration ($\mu\text{g l}^{-1}$) with $m/z = 47$ Signal (cps) for Samples 46-50 (C106 Duplicate) and External Standards.	345
Figure 122. A Graph Comparing Added Pt Concentration ($\mu\text{g l}^{-1}$) with $m/z = 194$ Signal (cps) for Samples 46-50 (C106 Duplicate) and External Standards.	345
Figure 123. A Graph Comparing Added Pt Concentration ($\mu\text{g l}^{-1}$) with $m/z = 195$ Signal (cps) for Samples 46-50 (C106 Duplicate) and External Standards.	345
Figure 124. A Graph Comparing Added P Concentration ($\mu\text{g l}^{-1}$) with $m/z = 47$ Signal (cps) for Samples 51-55 (C105) and External Standards.	346
Figure 125. A Graph Comparing Added Pt Concentration ($\mu\text{g l}^{-1}$) with $m/z = 194$ Signal (cps) for Samples 51-55 (C105) and External Standards.	346
Figure 126. A Graph Comparing Added Pt Concentration ($\mu\text{g l}^{-1}$) with $m/z = 195$ Signal (cps) for Samples 51-55 (C105) and External Standards.	346
Figure 127. A Graph Comparing Added P Concentration ($\mu\text{g l}^{-1}$) with $m/z = 47$ Signal (cps) for Samples 56-60 (C105 Duplicate) and External Standards.	346
Figure 128. A Graph Comparing Added Pt Concentration ($\mu\text{g l}^{-1}$) with $m/z = 194$ Signal (cps) for Samples 56-60 (C105 Duplicate) and External Standards.	346
Figure 129. A Graph Comparing Added Pt Concentration ($\mu\text{g l}^{-1}$) with $m/z = 195$ Signal (cps) for Samples 56-60 (C105 Duplicate) and External Standards.	346
Figure 130. A Graph Comparing Added P Concentration ($\mu\text{g l}^{-1}$) with $m/z = 47$ Signal (cps) for Samples 61-65 (C104) and External Standards.	347
Figure 131. A Graph Comparing Added Pt Concentration ($\mu\text{g l}^{-1}$) with $m/z = 194$ Signal (cps) for Samples 61-65 (C104) and External Standards.	347
Figure 132. A Graph Comparing Added Pt Concentration ($\mu\text{g l}^{-1}$) with $m/z = 195$ Signal (cps) for Samples 61-65 (C104) and External Standards.	347

Figure 133. A Graph Comparing Added P Concentration ($\mu\text{g l}^{-1}$) with $m/z = 47$ Signal (cps) for Samples 66-70 (C104 Duplicate) and External Standards.....	347
Figure 134. A Graph Comparing Added Pt Concentration ($\mu\text{g l}^{-1}$) with $m/z = 194$ Signal (cps) for Samples 66-70 (C104 Duplicate) and External Standards.....	347
Figure 135. A Graph Comparing Added Pt Concentration ($\mu\text{g l}^{-1}$) with $m/z = 195$ Signal (cps) for Samples 66-70 (C104 Duplicate) and External Standards.....	347
Figure 136. A Graph Comparing Added P Concentration ($\mu\text{g l}^{-1}$) with $m/z = 47$ Signal (cps) for Samples 91-95 (C101) and External Standards.	348
Figure 137. A Graph Comparing Added Pt Concentration ($\mu\text{g l}^{-1}$) with $m/z = 194$ Signal (cps) for Samples 91-95 (C101) and External Standards.	348
Figure 138. A Graph Comparing Added Pt Concentration ($\mu\text{g l}^{-1}$) with $m/z = 195$ Signal (cps) for Samples 91-95 (C101) and External Standards.	348
Figure 139. A Graph Comparing Added P Concentration ($\mu\text{g l}^{-1}$) with $m/z = 47$ Signal (cps) for Samples 96-98 (C101 Duplicate) and External Standards.....	348
Figure 140. A Graph Comparing Added Pt Concentration ($\mu\text{g l}^{-1}$) with $m/z = 194$ Signal (cps) for Samples 96-98 (C101 Duplicate) and External Standards.....	348
Figure 141. A Graph Comparing Added Pt Concentration ($\mu\text{g l}^{-1}$) with $m/z = 195$ Signal (cps) for Samples 96-98 (C101 Duplicate) and External Standards.....	348
Figure 142. An External Calibration Graph Comparing Ag Standard Concentration ($\mu\text{g l}^{-1}$) with $m/z = 107$ and 109 Signal (cps) for a Series of Ag Calibration Standards.....	407

List of Tables

Table 1. A Table of Resolutions Required to Separate Analyte Ions from Interfering Ions.....	44
Table 2. Reactions Taking Place Between Ionic and Neutral Species in a Collision/Reaction Cell.....	60
Table 3. A Table of Potential Interferences with Regard to K, Ca and Fe Isotopes...	61
Table 4. A Table of P and S Isotopes, their Abundances, IP and Polyatomic Ion Interferences.....	70
Table 5. A Comparison of ^{31}P and ^{32}S Limit of Detection Data for Elemental Analysis Techniques.....	74
Table 6. A Table of Typical PQ ExCell ICP-MS Instrument Parameters.....	77
Table 7. Reaction Data for Oxidation of $^{31}\text{P}^+$, $^{32}\text{S}^+$, $^{47}\text{Ti}^+$ and Associated Polyatomic Ions.....	80
Table 8. Analyte Oxide Ion Signal to Analyte Ion Signal Ratio for Data Generated During IKEE He/O ₂ and O ₂ Only $^{31}\text{P}^{16}\text{O}^+$ and $^{32}\text{S}^{16}\text{O}^+$ Formation Maximisation Experiments.....	96
Table 9. The $m/z = 31$ Signal Reduction Observed when the Torch Bonnet was in Position.....	122
Table 10. The $m/z = 115$ Signal Reduction Observed when the Torch Bonnet was in Position.....	124
Table 11. The $m/z = 31$ Signal Reduction Observed when the Second Torch Bonnet was in Position.....	128
Table 12. The $m/z = 115$ Signal Reduction Observed when the Second Torch Bonnet was in Position.....	129
Table 13. LOD's Calculated by both Approaches for Methods 2, 3, 4 and 5.....	133
Table 14. A Summary and Comparison of Methods Developed for the Measurement of ^{31}P and ^{32}S Isotopes by ICP-MS.....	136
Table 15. The Overall Molecular Mass of Individual DNA Nucleotides.....	138
Table 16. Quantification Data for the Analysis of 200 and 2000 $\mu\text{g l}^{-1}$ DNA Solutions by Methods 2, 3, 4 and 5.....	145
Table 17. Data Accrued During the Analysis of the Agarose Gel Leachate by ICP-MS Employing Method 2 Conditions.....	147
Table 18. The Oligonucleotide Sequences Studied by HPLC-ICP-MS.....	154
Table 19. Chromatographic Conditions Employed During the Study of Oligonucleotide Sequences by HPLC-ICP-MS.....	155
Table 20. Retention Times Acquired Following the Study of Oligonucleotides by HPLC-ICP-MS Employing Method 2.....	157
Table 21. Preparation Details for the Samples Investigated During Study 1.....	176
Table 22. ^{31}P Isotope Content of the DNA/Cisplatin Samples Studied by ICP-MS.....	180
Table 23. ^{194}Pt Isotope Content of the DNA/Cisplatin Samples Studied by ICP-MS.....	181
Table 24. ^{195}Pt Isotope Content of the DNA/Cisplatin Samples Studied by ICP-MS.....	182
Table 25. Preparation Details for the Samples Investigated During Study 2.....	185
Table 26. ^{194}Pt Isotope Content of the DNA/Cisplatin Samples Analysed During Study 2.....	190
Table 27. ^{195}Pt Isotope Content of the DNA/Cisplatin Samples Analysed During Study 2.....	191
Table 28. Preparation Details for the Cisplatin Samples Investigated During Study 3.....	194

Table 29. Preparation Details for the Oxaliplatin Samples Investigated During Study 3.	195
Table 30. Preparation Details for the Cisplatin Samples Investigated During Study 4.	196
Table 31. Preparation Details for the Oxaliplatin Samples Investigated During Study 4.	197
Table 32. ¹⁹⁴ Pt Isotope Content of the DNA/Cisplatin Samples Analysed During Study 3.	205
Table 33. ¹⁹⁵ Pt Isotope Content of the DNA/Cisplatin Samples Analysed During Study 3.	206
Table 34. ¹⁹⁴ Pt Isotope Content of the DNA/Oxaliplatin Samples Analysed During Study 3.	206
Table 35. ¹⁹⁵ Pt Isotope Content of the DNA/Oxaliplatin Samples Analysed During Study 3.	207
Table 36. ¹⁹⁴ Pt Isotope Content of the DNA/Cisplatin Samples Analysed During Study 4.	210
Table 37. ¹⁹⁵ Pt Isotope Content of the DNA/Cisplatin Samples Analysed During Study 4.	211
Table 38. ¹⁹⁴ Pt Isotope Content of the DNA/Oxaliplatin Samples Analysed During Study 4.	212
Table 39. ¹⁹⁵ Pt Isotope Content of the DNA/Oxaliplatin Samples Analysed During Study 4.	213
Table 40. ¹⁹⁴ Pt Isotope Content of the Untreated DNA/Cisplatin Sample Solutions Analysed During Study 5.	225
Table 41. ¹⁹⁴ Pt Isotope Content of the Untreated DNA/Oxaliplatin Sample Solutions Analysed During Study 5.	226
Table 42. ¹⁹⁵ Pt Isotope Content of the Untreated DNA/Cisplatin Sample Solutions Analysed During Study 5.	226
Table 43. ¹⁹⁵ Pt Isotope Content of the Untreated DNA/Oxaliplatin Sample Solutions Analysed During Study 5.	227
Table 44. Further Data Generated During the Calculation of K _f and the Ratio of Number of Adducts Per DNA Nucleotide for the Cisplatin Exposed DNA Samples Analysed During Study 2.	235
Table 45. Further Data Generated During the Calculation of K _f and the Ratio of Number of Adducts Per DNA Nucleotide for the Cisplatin Exposed DNA Samples Analysed During Study 3.	236
Table 46. Further Data Generated During the Calculation of K _f and the Ratio of Number of Adducts Per DNA Nucleotide for the Oxaliplatin Exposed DNA Samples Analysed During Study 3.	237
Table 47. Further Data Generated During the Calculation of K _f and the Ratio of Number of Adducts Per DNA Nucleotide for the Cisplatin Exposed DNA Samples Analysed During Study 4.	238
Table 48. Further Data Generated During the Calculation of K _f and the Ratio of Number of Adducts Per DNA Nucleotide for the Oxaliplatin Exposed DNA Samples Analysed During Study 4.	239
Table 49. Further Data Generated During the Calculation of K _f and the Ratio of Number of Adducts Per DNA Nucleotide for the Cisplatin Exposed DNA Samples Analysed During Study 5.	240

Table 50. Further Data Generated During the Calculation of K_f and the Ratio of Number of Adducts Per DNA Nucleotide for the Oxaliplatin Exposed DNA Samples Analysed During Study 5.	241
Table 51. A General Comparison of K_f Values and Numbers of Drug-Nucleotide Adducts Formed Per DNA Nucleotide Between Studies 2 to 5.	242
Table 52. Calculated Transition Pressures and Numbers of Transition ‘Chambers’ for a Gradual Pressure Reduction in the ICP-MS Interface.	264
Table 53. A Table of Examples of Spectroscopic Interferences in ICP-MS.	290
Table 54. A Table of ICP-MS Instrument Parameters for Method 1: The Determination of $^{31}\text{P}^{16}\text{O}^+$ and $^{32}\text{S}^{16}\text{O}^+$ Ions in a Collision Cell Incorporating He and O_2 Under IKEE Conditions.	292
Table 55. Data Generated During IKEE ($\text{He} = 0.2 \text{ ml min}^{-1}$ and $\text{O}_2 = 0.3 \text{ ml min}^{-1}$) $^{31}\text{P}^{16}\text{O}^+$ and $^{32}\text{S}^{16}\text{O}^+$ Formation Maximisation Experiments.	293
Table 56. A Table of ICP-MS Instrument Parameters for Method 2: The Determination of $^{31}\text{P}^{16}\text{O}^+$ and $^{32}\text{S}^{16}\text{O}^+$ Ions in a Collision Cell Incorporating O_2 Only Under IKEE Conditions.	294
Table 57. Data Generated During IKEE ($\text{O}_2 = 0.3 \text{ ml min}^{-1}$) $^{31}\text{P}^{16}\text{O}^+$ and $^{32}\text{S}^{16}\text{O}^+$ Formation Maximisation Experiments.	295
Table 58. Data Generated During the Analysis of P and S Calibration Standards by ICP-MS Employing ‘Method 2’ Conditions.	296
Table 59. A Table of ICP-MS Instrument Parameters for Method 3: Selective Removal of Polyatomic Ions in a Collision Cell Incorporating a He Collision Gas Under KED Conditions.	297
Table 60. Data Accrued During the Analysis of 2 % HNO_3 Blank and $200 \mu\text{g l}^{-1}$ P solutions Using a Collision Cell with Various He Flows and KED Conditions (KED Spread = +1 V).	298
Table 61. Data Accrued During the Analysis of 2 % HNO_3 Blank and $200 \mu\text{g l}^{-1}$ P solutions Using a Collision Cell with Various He Flows and KED Conditions (KED Spread = +2 V).	301
Table 62. Data Accrued During the Analysis of 2 % HNO_3 Blank and $200 \mu\text{g l}^{-1}$ P solutions Using a Collision Cell with Various He Flows and KED Conditions (KED Spread = +3 V).	303
Table 63. Data Generated During the Analysis of P Calibration Standards by ICP-MS Employing Method 3 Conditions.	304
Table 64. A Table of ICP-MS Instrument Parameters for Method 4: The Determination of $^{31}\text{P}^{16}\text{O}^+$ and $^{32}\text{S}^{16}\text{O}^+$ Ions Formed Under ‘Cool/Cold Plasma’.	305
Table 65. Data Generated During Reduced Forward Power Signal Optimisation Experiments for a HNO_3 Blank Solution ($V_q = +1\text{V}$).	306
Table 66. Data Generated During Reduced Forward Power Signal Optimisation Experiments for a $1000 \mu\text{g l}^{-1}$ P Solution ($V_q = +1\text{V}$).	307
Table 67. Data Generated During Reduced Forward Power Signal Optimisation Experiments for a $1000 \mu\text{g l}^{-1}$ S Solution ($V_q = +1\text{V}$).	308
Table 68. Data Accrued for Calibration Experiments Carried out for ‘Method 4’.	309
Table 69. A Table of ICP-MS Instrument Parameters for Method 5: The Determination of $^{31}\text{P}^{16}\text{O}^+$ and $^{32}\text{S}^{16}\text{O}^+$ Ions Formed Under ‘Cool/Cold Plasma’ Incorporating an Additional O_2 Nebuliser Flow.	310
Table 70. Data Generated During the Introduction of O_2 to the Nebuliser Flow Whilst Analysing Under ‘Cold/Cool Plasma’ Conditions Described in Section 2.4.4.	311

Table 71. Data Accrued for Calibration Experiments Carried out Under ‘Method 5’ Conditions.....	312
Table 72. A Table of ICP-MS Instrument Parameters for Method 6 (Part 1): The Exclusion of Entrained Atmospheric Gases from the ICP.	314
Table 73. Data Generated from the Study of P and S Standard Solutions Spiked with $1 \mu\text{g l}^{-1}$ In by ICP-MS both with and without ICP Enclosure with the First Torch Bonnet Design.....	315
Table 74. A Table of ICP-MS Instrument Parameters for Method 6 (Part 2): The Exclusion of Entrained Atmospheric Gases from the ICP.	317
Table 75. Data Generated from the Study of P and S Standard Solutions Spiked with $1 \mu\text{g l}^{-1}$ In by ICP-MS both with and without ICP Enclosure with the Second Torch Bonnet Design.	318
Table 76. A Table of ICP-MS Instrument Parameters for the Analysis of a $2000 \mu\text{g l}^{-1}$ DNA Solution Via Measurement of the ^{31}P Isotope Employing Method 2: The Determination of $^{31}\text{P}^{16}\text{O}^{+}$ and $^{32}\text{S}^{16}\text{O}^{+}$ Ions in a Collision Cell Incorporating O_2 Only Under IKEE Conditions.....	320
Table 77. A Table of ICP-MS Instrument Parameters for the Analysis of a $200 \mu\text{g l}^{-1}$ DNA Solution Via Measurement of the ^{31}P Isotope Employing Method 3: Selective Removal of Polyatomic Ions in a Collision Cell Incorporating a He Collision Gas Under KED Conditions.....	321
Table 78. A Table of ICP-MS Instrument Parameters for the Analysis of a $2000 \mu\text{g l}^{-1}$ DNA Solution Via Measurement of the ^{31}P Isotope Employing Method 4: The Determination of $^{31}\text{P}^{16}\text{O}^{+}$ and $^{32}\text{S}^{16}\text{O}^{+}$ Ions Formed Under ‘Cool/Cold Plasma’.	322
Table 79. A Table of ICP-MS Instrument Parameters for the Analysis of a $200 \mu\text{g l}^{-1}$ DNA Solution Via the Measurement of the ^{31}P Isotope Employing Method 5: The Determination of $^{31}\text{P}^{16}\text{O}^{+}$ and $^{32}\text{S}^{16}\text{O}^{+}$ Ions Formed by ‘Cool/Cold Plasma’ Incorporating an Additional O_2 Nebuliser Flow.....	323
Table 80. Data Generated During the Standard Additions Analysis of DNA and P Standard Solutions by Methods 2, 3, 4 and 5.	324
Table 81. A Table of ICP-MS Instrument Parameters for the Analysis of DNA Samples, Separated on an Agarose Gel Plate, Via Measurement of the ^{31}P Isotope Employing Method 2: The Determination of $^{31}\text{P}^{16}\text{O}^{+}$ and $^{32}\text{S}^{16}\text{O}^{+}$ Ions in a Collision Cell Incorporating O_2 Only Under IKEE Conditions.....	325
Table 82. A Table of ICP-MS Instrument Parameters for the Analysis of DNA Replication by Polymerase Chain Reaction, Via Measurement of the ^{31}P Isotope Employing Method 2: The Determination of $^{31}\text{P}^{16}\text{O}^{+}$ and $^{32}\text{S}^{16}\text{O}^{+}$ Ions in a Collision Cell Incorporating O_2 Only Under IKEE Conditions.	326
Table 83. Data Generated During the Analysis of Separated Amplified DNA Sequence Samples by ICP-MS Employing Method 2.	327
Table 84. A Table of ICP-MS Instrument Parameters for the Analysis of Single Nucleotide Polymorphisms, Via Measurement of the ^{31}P Isotope Employing Method 2: The Determination of $^{31}\text{P}^{16}\text{O}^{+}$ and $^{32}\text{S}^{16}\text{O}^{+}$ Ions in a Collision Cell Incorporating O_2 Only Under IKEE Conditions.....	328
Table 85. A Table of ICP-MS Instrument Parameters for the Analysis of Single Nucleotide Polymorphisms, Via Measurement of the ^{31}P Isotope, Employing Method 4: The Determination of $^{31}\text{P}^{16}\text{O}^{+}$ and $^{32}\text{S}^{16}\text{O}^{+}$ Ions Formed Under ‘Cool/Cold Plasma’.....	329
Table 86. DNA/Cisplatin Initial Sample Preparation Details (Study 1).....	331
Table 87. Details of Pre-Analysis Sample Treatment for Study 1.....	332

Table 88. A Table of ICP-MS Instrument Parameters for the Analysis of DNA and Cisplatin Interactions <i>In Vitro</i> , Via Measurement of the ³¹ P and ^{194,195} Pt Isotopes, Employing Method 2: The Determination of ³¹ P ¹⁶ O ⁺ and ³² S ¹⁶ O ⁺ Ions in a Collision Cell Incorporating O ₂ Only Under IKEE Conditions (Study 1).	336
Table 89. Data Accrued During the Analysis of DNA/Cisplatin Samples (Study 1).	337
Table 90. Recovered, Cisplatin Exposed, DNA UV Spectroscopy Data (Study 2).	349
Table 91. Incubation Pre-Treatment Data for DNA/Drug Samples Analysed During Study 2.	351
Table 92. Centrifugation Pre-Treatment Data for DNA/Drug Samples Analysed During Study 2.	351
Table 93. Final Pre-Concentration Data for DNA/Cisplatin and DNA/Oxaliplatin Samples Analysed During Study 2.	352
Table 94. A Table of ICP-MS Instrument Parameters for the Analysis of DNA and Cisplatin Interactions <i>In Vitro</i> , Via Measurement of the ^{190,192,194,195,196,198} Pt Isotopes, Employing Standard Conditions (Study 2).	353
Table 95. Mean Raw Data Accrued Following Analysis of the DNA/Cisplatin Samples During Study 2.	354
Table 96. Corrected Data Accrued Following Analysis of the DNA/Cisplatin Samples During Study 2.	354
Table 97. Mean Data for a Series of Pt Standard Solutions Analysed with the DNA/Cisplatin Samples During Study 2.	355
Table 98. Recovered, Cisplatin Exposed, DNA UV Spectroscopy Data (Study 3).	356
Table 99. Recovered, Oxaliplatin Exposed, DNA UV Spectroscopy Data (Study 3).	358
Table 100. Recovered, Cisplatin Exposed, DNA UV Spectroscopy Data (Study 4).	360
Table 101. Recovered, Oxaliplatin Exposed, DNA UV Spectroscopy Data (Study 4).	363
Table 102. Incubation Pre-Treatment Data for DNA/Drug Samples Analysed During Study 3.	366
Table 103. Centrifugation Pre-Treatment Data for DNA/Drug Samples Analysed During Study 3.	367
Table 104. Incubation Pre-Treatment Data for DNA/Cisplatin Samples Analysed During Study 4.	368
Table 105. Incubation Pre-Treatment Data for DNA/Oxaliplatin Samples Analysed During Study 4.	369
Table 106. Centrifugation Pre-Treatment Data for DNA/Cisplatin Samples Analysed During Study 4.	370
Table 107. Centrifugation Pre-Treatment Data for DNA/Oxaliplatin Samples Analysed During Study 4.	371
Table 108. Final Pre-Concentration Data for DNA/Cisplatin and DNA/Oxaliplatin Samples Analysed During Study 3.	372
Table 109. Final Pre-Concentration Data for DNA/Cisplatin Samples Analysed During Study 4.	373
Table 110. Final Pre-Concentration Data for DNA/Oxaliplatin Samples Analysed During Study 4.	374
Table 111. A Table of ICP-MS Instrument Parameters for the Analysis of DNA, Cisplatin and Oxaliplatin Interactions <i>In Vitro</i> , Via Measurement of the ^{190,192,194,195,196,198} Pt Isotopes, Employing Standard Conditions (Study 3).	375

Table 112. Mean Raw Data Accrued Following Analysis of the DNA/Cisplatin Samples During Study 3.	376
Table 113. Corrected Data Accrued Following Analysis of the DNA/Cisplatin Samples During Study 3.	376
Table 114. Mean Raw Data Accrued Following Analysis of the DNA/Oxaliplatin Samples During Study 3.	377
Table 115. Corrected Data Accrued Following Analysis of the DNA/Oxaliplatin Samples During Study 3.	377
Table 116. Mean Data for a Series of Pt Standard Solutions Analysed with the DNA/Cisplatin and DNA/Oxaliplatin Samples During Study 3.	378
Table 117. A Table of ICP-MS Instrument Parameters for the Analysis of DNA and Cisplatin Interactions <i>In Vitro</i> , Via Measurement of the ^{190,192,194,195,196,198} Pt Isotopes, Employing Standard Conditions (Study 4).	379
Table 118. A Table of ICP-MS Instrument Parameters for the Analysis of DNA and Oxaliplatin Interactions <i>In Vitro</i> , Via Measurement of the ^{190,192,194,195,196,198} Pt Isotopes, Employing Standard Conditions (Study 4).	380
Table 119. Mean Raw Data Accrued Following Analysis of the DNA/Cisplatin Samples During Study 4.	381
Table 120. Corrected Data Accrued Following Analysis of the DNA/Cisplatin Samples During Study 4.	382
Table 121. Mean Raw Data Accrued Following Analysis of the DNA/Oxaliplatin Samples During Study 4.	383
Table 122. Corrected Data Accrued Following Analysis of the DNA/Oxaliplatin Samples During Study 4.	384
Table 123. Mean Data for a Series of Pt Standard Solutions Analysed with the DNA/Cisplatin Samples During Study 4.	385
Table 124. Mean Data for a Series of Pt Standard Solutions Analysed with the DNA/Oxaliplatin Samples During Study 4.	385
Table 125. Sample Preparation Details for the Analysis of Cisplatin Study 4 Centrifuge Filter Leachates.	386
Table 126. Sample Preparation Details for the Analysis of Oxaliplatin Study 4 Centrifuge Filter Leachates.	387
Table 127. A Table of ICP-MS Instrument Parameters for the Analysis of DNA/Cisplatin and DNA/Oxaliplatin Centrifuge Filter Leachate Solutions, Via Measurement of the ^{190,192,194,195,196,198} Pt Isotopes, Employing Standard Conditions.	388
Table 128. Mean Data for a Series of Pt Standard Solutions Analysed with Centrifuge Tube Leachate Solutions of the DNA/Cisplatin and DNA/Oxaliplatin Samples of Study 4.	389
Table 129. Mean Raw Data Accrued Following Analysis of the Centrifuge Filter Leachate Solutions of the DNA/Cisplatin Samples of Study 4.	390
Table 130. Mean Raw Data Accrued Following Analysis of the Centrifuge Filter Leachate Solutions of the DNA/Oxaliplatin Samples of Study 4.	391
Table 131. Recovered, Cisplatin Exposed, DNA UV Spectroscopy Data (Study 5).	392
Table 132. Recovered, Oxaliplatin Exposed, DNA UV Spectroscopy Data (Study 5).	394
Table 133. A Table of ICP-MS Instrument Parameters for the Analysis of DNA/Cisplatin and DNA/Oxaliplatin Interactions <i>In Vitro</i> , Via Measurement of the ^{190,192,194,195,196,198} Pt Isotopes, Employing Standard Conditions (Study 5). ...	396

Table 134. Mean Data for a Series of DNA Based Pt Standard Solutions Analysed with the Untreated DNA/Cisplatin and DNA/Oxaliplatin Samples During Study 5.	397
Table 135. Mean Raw Data Accrued Following Analysis of the Untreated DNA/Cisplatin Sample Solutions Analysed During Study 5.	398
Table 136. Mean Raw Data Accrued Following Analysis of the Untreated DNA/Oxaliplatin Sample Solutions Analysed During Study 5.	398
Table 137. A Table of ICP-MS Instrument Parameters for the Analysis of Deionised Water and Human Serum Leachate Solutions, Via Measurement of ^{107,109} Ag Isotopes Employing Standard Conditions.....	405
Table 138. Mean Data Generated Following the ICP-MS Analysis of Leachate Samples and Ag Standards.	406
Table 139. Silver Content of Each Leachate Sample, Calculated Via External Calibration.	407

Glossary of Abbreviations

Abbreviation	Word/Title/Term	Further Detail
AAS	Atomic Absorption Spectroscopy	-
amu	Atomic Mass Unit	Unit used within mass spectrometry referring to resolution
ATP	Adenosine Triphosphate	-
Bar	-	Unit of pressure
°C	Degrees Centigrade	Unit of temperature described by the centigrade scale
CC	Collision Cell	-
CID	Collisionally Induced Dissociation	-
cm	Centimetre	Unit of length dimension ($\times 10^{-2}$ m)
cps	Counts Per Second	Unit referring to the ICP-MS signal, the number of ion counts measured in a second
CTP	Cytosine Triphosphate	-
CVC	Central Venous Catheter	-
DC	Direct Current	-
DRC	Dynamic Reaction Cell	-
DNA	Deoxyribose Nucleic Acid	-
dNTP	Deoxynucleotidetriphosphate	-
EIE	Easily Ionisable Element	-
E_k	Kinetic Energy	-
eV	Electronvolt	A unit of energy equal to the work done on an electron in moving it through a potential difference of one volt
FAAS	Flame Atomic Absorption Spectroscopy	-
FDA	Food and Drug Administration	-
γ	Ratio of Heat Capacity at Constant Pressure to Heat Capacity at Constant Volume	-
g	Gram	Unit of mass
GC	Gas Chromatography	-
GF-AAS	Graphite Furnace Atomic Absorption Spectroscopy	-
GTP	Guanine Triphosphate	-
HPLC	High Performance Liquid Chromatography	-
ΔH_r	Enthalpy of Reaction	A thermodynamic property of a system

Abbreviation	Word/Title/Term	Further Detail
ICP-MS	Inductively Coupled Plasma Mass Spectrometry	-
ICP-QMS	Inductively Coupled Plasma Quadrupole Mass Spectrometry	-
ICP-OES	Inductively Coupled Plasma Optical Emission Spectroscopy	-
ICP-ToFMS	Inductively Coupled Plasma Time of Flight Mass Spectrometry	-
IKEE	Ion Kinetic Energy Effect	-
IP	Ionisation Potential	Parameter describing the energy required to ionise an atom, measured in electron volts (eV)
K	Kelvin	Unit of temperature described by the Kelvin scale
kcal mol⁻¹	Kilocalories Per Mole	Unit describing enthalpy of reaction
KED	Kinetic Energy Discrimination	-
k_r	Rate Constant	The constant in an expression for the rate of a chemical reaction in terms of concentrations or activities
LA-ICP-MS	Laser Ablation Inductively Coupled Plasma Mass Spectrometry	-
LC-MS	Liquid Chromatography Mass Spectrometry	-
l min⁻¹	Litres Per Minute	Unit of flow rate
LOD	Limit of Detection	-
m	Metre	Unit of length dimension
M	Mole	Unit of the amount of a substance
M	Mach Number	-
M²⁺	Doubly Charged Ion	-
mBar	Millibar	Unit of pressure (x 10 ⁻³ Bar)
mg	Milligram	Unit of mass (x 10 ⁻³ g)
MHz	Megahertz	Unit for the measurement of frequency (x 10 ³ Hz)
mg ml⁻¹	Milligrams Per Millilitre	Unit of concentration (same as g l ⁻¹)
ml min⁻¹	Millilitres Per Minute	Unit of flow rate (x 10 ⁻³ l min ⁻¹)
mm	Millimetre	Unit of length dimension (x 10 ⁻³ m)
mM	Millimole	Unit of the amount of a substance (x 10 ⁻³ M)

Abbreviation	Word/Title/Term	Further Detail
MWCO	Molecular Weight Cut-Off	-
<i>m/z</i>	Mass-To-Charge Ratio	-
NADH	Nicotinamide Adenine Dinucleotide	Reduced form
NADPH	Nicotinamide Adenine Dinucleotide Phosphate	Reduced form
nm	Nanometre	Unit of length dimension (x 10 ⁻⁹ m)
NMR	Nuclear Magnetic Resonance	-
P₀	Pressure Within the ICP Ion Source	-
P_i	Pressure Within the Isentropic Core of the Expansion	-
PCR	Polymerase Chain Reaction	An artificial nucleic acid replication/amplification process
PCR-SSCP	Polymerase Chain Reaction Single Strand Conformation Polymorphism	-
pmol	Picomole	Unit of the amount of a substance (x 10 ⁻¹² M)
RAM	Relative Atomic Mass	-
RF	Radio Frequency	-
RMM	Relative Molecular Mass	-
RNA	Ribonucleic Acid	-
RPM	Revolutions Per Minute	-
RSD	Relative Standard Deviation	A statistical parameter
s	Second	Unit of time dimension
SD	Standard Deviation	A statistical parameter
SFC	Supercritical Fluid Chromatography	-
SNP	Single Nucleotide Polymorphism	-
T₀	Temperature Within the ICP Ion Source	-
T_i	Temperature Within the Isentropic Core of the Expansion	-
TBE	Tris-Borate Buffer	-
TRA	Time Resolved Analysis	-
TTP	Thymine Triphosphate	-
µg	Microgram	Unit of mass (10 ⁻⁶ g)
µg l⁻¹	Micrograms Per Litre	Unit of concentration
µl	Microlitre	Unit of volume (10 ⁻⁶ l)
µl min⁻¹	Microlitres Per Minute	Unit of flow rate (x 10 ⁻⁶ l min ⁻¹)
µm	Micrometre	Unit of length dimension (x 10 ⁻⁶ m)

Abbreviation	Word/Title/Term	Further Detail
μM	Micromole	Unit of the amount of a substance ($\times 10^{-6}$ M)
UV	Ultra-Violet	Electromagnetic radiation having wavelengths between 4 and 400 nm
V	Volt	Unit of electromotive force, force sufficient to carry one ampere of current against one ohm of resistance
V_h	Applied Hexapole Voltage	-
V_p	Plasma Potential	-
V_q	Applied Quadrupole Voltage	-
W	Watt	Unit of power, used here in the description of plasma forward and reflected power parameters

Chapter 1

An Introduction to ICP-MS Analysis

1.1. An Introduction to ICP-MS

Inductively coupled plasma mass spectrometry (ICP-MS) is a powerful atomic spectroscopy technique employed in the elemental analysis of metals and non-metals at ultra-trace levels. Devised by Gray and Houk in 1980, with the first commercial instruments available since 1983,^{1, 2} ICP-MS is the combination of an inductively coupled plasma (ICP) ion source and a mass spectrometer.²

The main attraction of ICP-MS as an atomic spectroscopy technique is its capability for low limits of detection (LOD), as low as sub part-per-trillion (ng l^{-1}) levels for some elements, and its wide dynamic range, of approximately four to eleven orders of magnitude.³⁻⁵ The ICP-MS LOD for an element is dependent on a number of factors, these include the following:

- The isotopic abundance and ionisation potential of the element under analysis, see the periodic table in Figure 1.⁶
- The type of gas(es) used to generate the ICP ion source and transport the sample through the plasma central channel, see sections 1.1.2.2 and 1.2.1.2.
- The instrumental conditions, particularly plasma forward power and nebulisation flow, see section 1.1.2.
- The type of mass spectrometer interfaced with the ICP ion source, see section 1.1.3.
- The physical state of the sample being introduced (solid, liquid or gaseous) and the method and conditions of introduction, see section 1.1.2.
- Any modifications made to the instrument. For example the implementation of collision or dynamic reaction cell technology and plasma-mass spectrometer interface modifications, see sections 1.3 and 1.4 and Chapter 5.

As can be seen in Figure 1 ICP-MS can successfully analyse approximately three quarters of the elements of the periodic table between concentrations of $< 1 \text{ ng l}^{-1}$ and $10 \text{ } \mu\text{g l}^{-1}$.^{4, 7}

Periodic Table of the Elements, Showing Detection Limits and Ionisation Potentials for useable Elements by ICP-MS Analysis

1 1 (99.9%) H 13.6																	2 4 (100%) He 24.6
3 7 (92.5%) Li 5.4	4 9 (100%) Be 9.3											5 11 (80.1%) B 8.3	6 12 (98.9%) C 11.3	7 14 (99.6%) N 14.5	8 16 (99.8%) O 13.6	9 19 (100%) F 17.4	10 20 (90.5%) Ne 21.6
11 23 (100%) Na 5.1	12 24 (79.0%) Mg 7.6											13 27 (100%) Al 6	14 28 (92.2%) Si 8.2	15 31 (100%) P 10.5	16 32 (95%) S 10.4	17 35 (75.8%) Cl 13	18 40 (99.6%) Ar 15.8
19 39 (93.3%) K 4.3	20 40 (96.9%) Ca 6.1	21 45 (100%) Sc 6.5	22 48 (73.8%) Ti 6.8	23 51 (99.8%) V 6.7	24 52 (83.8%) Cr 6.8	25 55 (100%) Mn 7.4	26 56 (91.7%) Fe 7.9	27 59 (100%) Co 7.9	28 58 (68.3%) Ni 7.6	29 63 (69.2%) Cu 7.7	30 64 (48.6%) Zn 9.4	31 69 (60.1%) Ga 6	32 74 (36.5%) Ge 7.9	33 75 (100%) As 9.8	34 80 (49.7%) Se 9.8	35 79 (50.7%) Br 11.8	36 84 (57%) Kr 14
37 85 (72.2%) Rb 4.2	38 88 (82.6%) Sr 5.7	39 89 (100%) Y 6.4	40 90 (51.5%) Zr 6.8	41 93 (100%) Nb 6.9	42 98 (24.1%) Mo 7.1	43 99 7.3	44 102 (31.6%) Ru 7.4	45 103 (100%) Rh 7.5	46 106 (27.3%) Pd 8.3	47 107 (51.8%) Ag 7.6	48 114 (28.7%) Cd 9	49 115 (95.7%) In 5.8	50 120 (32.6%) Sn 7.3	51 121 (57.3%) Sb 8.6	52 130 (33.8%) Te 9	53 127 (100%) I 10.5	54 132 (26.9%) Xe 12.1
55 133 (100%) Cs 3.9	56 138 (71.7%) Ba 5.2	57 139 (99.9%) La 5.6	72 180 (35.1%) Hf 7	73 181 (99.9%) Ta 7.9	74 184 (30.7%) W 8	75 187 (62.6%) Re 7.9	76 190 (26.4%) Os 8.7	77 193 (62.7%) Ir 9.1	78 195 (33.8%) Pt 9	79 197 (100%) Au 9.2	80 202 (29.8%) Hg 10.4	81 205 (70.5%) Tl 6.1	82 208 (52.4%) Pb 7.4	83 209 (100%) Bi 7.3	84 Po	85 At	86 Rn
87 Fr		88 Ra	89 Ac														

30
64 (48.6%)
Zn
9.4

Atomic Number
Most Abundant Isotope (Abundance)
Symbol
Ionisation Potential (eV)

< 1 ng l⁻¹ (ppt)

1-10 ng l⁻¹ (ppt)

10-100 ng l⁻¹ (ppt)

0.1-1 µg l⁻¹ (ppb)

1-10 µg l⁻¹ (ppb)

58 140 (88.5%) Ce 5.5	59 141 (100%) Pr 5.4	60 142 (27.1%) Nd 5.5	61 Pm	62 152 (26.7%) Sm 5.6	63 153 (52.2%) Eu 5.7	64 158 (24.8%) Gd 6.1	65 159 (100%) Tb 5.9	66 164 (28.2%) Dy 5.9	67 165 (100%) Ho 6	68 166 (33.6%) Er 6.1	69 169 (100%) Tm 6.2	70 174 (31.8%) Yb 6.3	71 175 (97.4%) Lu 5.4
90 232 (100%) Th 7	91 231 Pa	92 238 (99.3%) U 6.9	93 Np	94 Pu	95 Am	96 Cm	97 Bk	98 Cf	99 Es	100 Fm	101 Md	102 No	103 Lr

Figure 1. A Periodic Table of the Elements Showing Detection Limits and Ionisation Potential Data for the Useable Elements by ICP-MS.

ICP-MS is a particularly versatile analytical technique as it allows various approaches to sample introduction, interfacing with different mass spectrometry techniques and simple modification. Due to this versatility samples can be analysed in solid, liquid or gaseous states which in turn allows ICP-MS to be applied to a gamut of samples for which the analyst may require elemental composition data. Alongside other techniques, ICP-MS plays a dominant role in the elemental analysis of biological, geological, environmental and industrial samples, many of which could also be forensic samples.⁸⁻³⁸

Although ICP-MS exhibits the analytical benefits already mentioned, limitations are observed in the form of analyte interferences in the mass spectrum. These interferences appear for several reasons, see section 1.2. ICP-MS is also a relatively expensive analytical technique; a simple ICP-quadrupole mass analyser instrument costs in the range of £90 000 to £150 000. An instrument incorporating a high resolution mass spectrometer is almost double the cost of that of a quadrupole based instrument.

1.1.1. The Design and Operation of an ICP-MS Instrument

An inductively coupled plasma is generated in a horizontally-mounted, fused-silica, torch consisting of three concentric tubes (outer, middle and injector tubes).^{1, 4, 39} The plasma gas flows tangentially between the outer and middle tubes (≈ 12 to 17 l min^{-1}) whilst an auxiliary gas passes between the middle and injector tubes ($\approx 1 \text{ l min}^{-1}$).^{10, 40} When analysing liquid samples via a nebuliser and spray chamber arrangement a gas, typically Ar flowing at $\approx 1 \text{ l min}^{-1}$, carries the sample through the nebuliser and spray chamber and into the plasma.^{4, 10} After generation of the plasma it is this third gas flow that is responsible for “punching” a central channel through the plasma discharge.¹⁰

The last 2-3 cm of a standard ICP-MS torch sits centrally within a water cooled induction, or load, coil that provides an alternating current that produces an intense electromagnetic field. The load coil is powered by an RF generator producing

between 1.5 W and 2.5 W at 27 or 40 MHz.^{4, 39} On passage of the plasma gas through the torch and load coil, a high voltage spark causes some of the plasma gas atoms to ionise; the resulting free electrons are accelerated in the electromagnetic field which causes an ionisation cascade effect. A steady state plasma is formed as a result of this ionisation.

Samples are introduced into an ICP ion source positioned end on to a water cooled sample cone.^{4, 41} See Figure 2 for a typical schematic of the ICP-MS ion path. Following sample atomisation, excitation and ionisation in the central channel of the ICP source,^{5, 40} a large fraction of positively charged ions are directed from the ion source to the mass spectrometer via an interface that allows ions to be extracted whilst stepping from atmospheric pressure (1 Bar) to vacuum conditions ($\approx 10^{-7}$ mBar).^{5, 40}

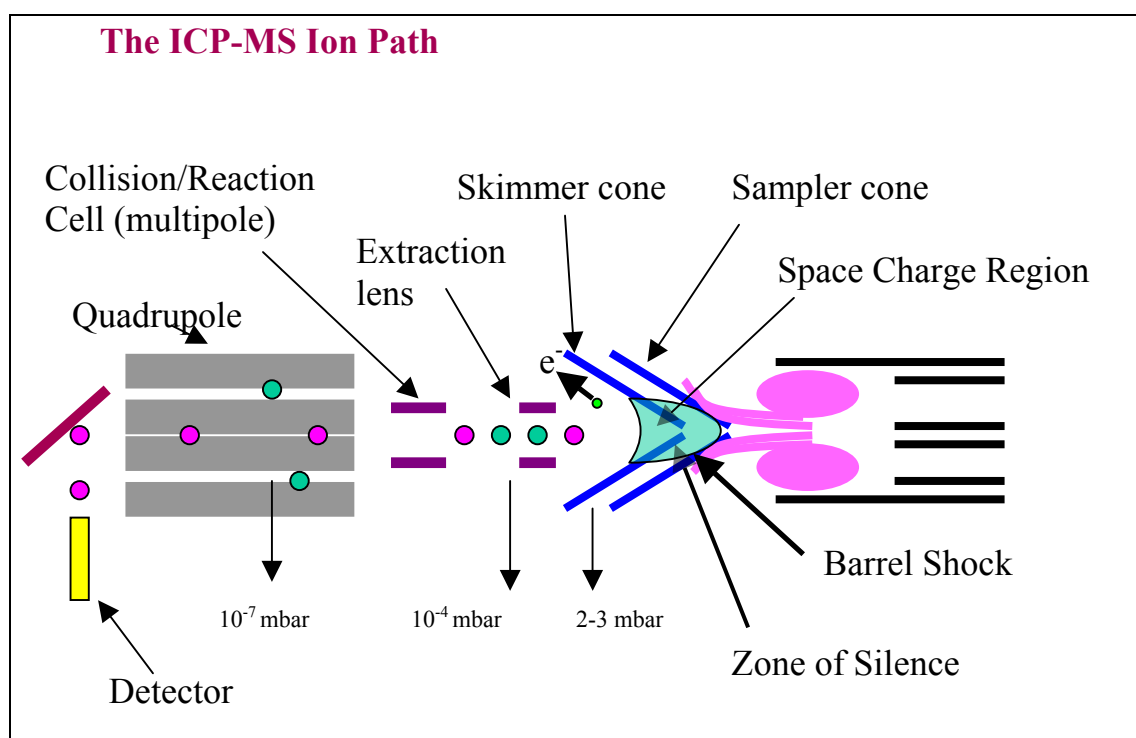


Figure 2. A Schematic of a Typical ICP-MS Instrument.

The fraction of ions sampled, from the ICP source, stream through an aperture (approximately 1 to 2 mm in diameter) in the centre of a nickel or platinum sample cone into a low pressure expansion chamber that maintains a pressure of

approximately 2 to 4 mBar, achieved using a mechanical pump, the remaining analyte ions impinge on the cone surrounding the orifice.^{2, 40, 41} In this chamber the ions are accelerated to speeds of approximately ten times the speed of sound due to rapid expansion which occurs due to the plunge in pressure. Due to this expansion a “barrel shock” region is formed and within this is an area known as the “zone of silence”.⁴² The front wall of this barrel shock region is known as a Mach Disc and it is from just behind this Mach Disc, in the zone of silence, that ions are removed (skimmed) for analysis, see Figure 3.^{4, 5, 7, 42} Ions are skimmed from this region via a cone, similar to the sample cone, known as the skimmer cone.

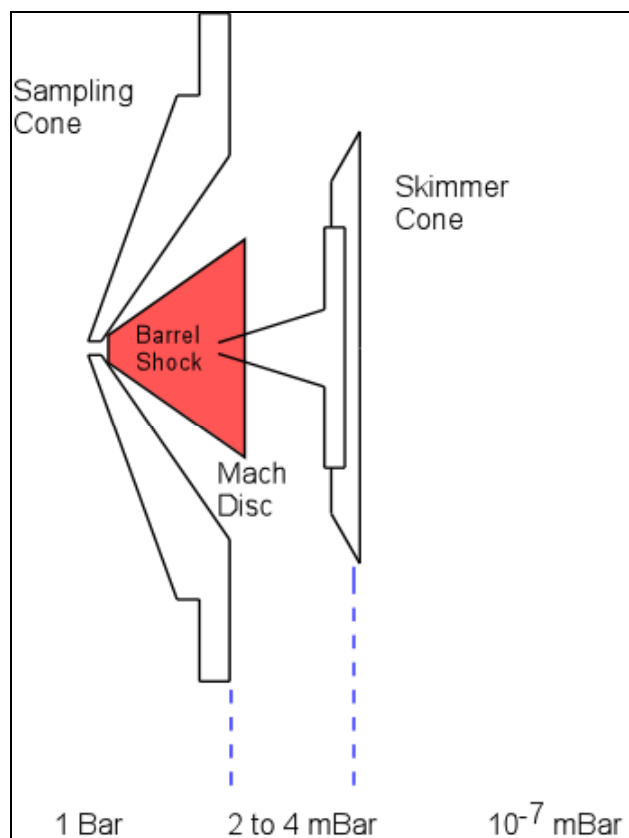


Figure 3. A Diagram of the Barrel Shock Region Produced in the Interface of an ICP-MS Instrument.

On the opposite side of the skimmer cone an ion beam is generated consisting of ions (originating from the analyte, plasma gas and torch box atmosphere), electrons and some surviving neutral species. This ion beam is then guided into a mass analyser by

means of an extraction lens that carries a negative potential (typically -300 V to -700 V).^{7, 42, 43} The constituents of the ion beam are then accelerated and focussed towards the entrance orifice of the mass analyser by a series of electrostatic lenses (carrying varying potentials, see section 1.3.1),^{2, 7, 43} during this process neutral species are removed from the beam and electrons are defocused.

Following filtering in a mass analyser ions are counted by a detector. For the work described in this report a dual mode detector was employed. Such a detector is capable of handling a large range of signals via two detection modes. For low signals, of less than 10^6 ion counts per second, a pulse counting output is used where ion impact onto a surface of high voltage releases primary electrons that impact again and continually release further electrons.^{4, 42} The resultant pulse charge is processed generating an analytical signal. For high signals (those of approximately 10^6 ion counts per second and above) the pulse charge is diverted, integrated and measured as a DC current.^{4, 42}

Following ion sampling and skimming it has been calculated that only, approximately, 0.7 % of the ions generated from a liquid sample (introduced via a nebuliser and spray chamber arrangement) in the plasma are detected by the mass analyser.⁴

1.1.2. Sample Introduction in ICP-MS Analysis

As highlighted previously, with the appropriate sample pre-treatment and introduction techniques, it is possible to analyse almost any type of sample (in solid, liquid or gaseous states) employing ICP-MS.

The most common approach to the introduction of samples into an ICP ion source is by the introduction of analytes in the form of liquids. With regard to liquid samples homogeneity can normally be guaranteed, this is analytically desirable. Such samples are typically introduced using a nebuliser and spray chamber arrangement of which there are many designs that may be used to transport a wide range of solutions with

differing viscosities or dissolved solid content.^{1, 4, 7, 44-46} Other methods of introducing liquid samples into an ICP source include the formation of volatile hydride species from the sample that can be transported into the plasma and direct insertion using injector tubes or pyrolytic graphite electrodes.^{2, 4, 5, 7, 40, 47-52}

Due to the ease of introducing liquid samples into the ICP source, the coupling of separation techniques such as high performance liquid chromatography (HPLC) with ICP-MS has become a routine application.^{1, 4, 7, 26, 53-57} With some system modification, the mobile phase, carrying separated analytes, exiting a liquid chromatography column can be introduced into a plasma via the typical nebuliser/spray chamber arrangement. The attraction of such a coupling is the potential for analyte pre-concentration and generation of data from both techniques that can lead to speciation of analytes within very varied sample types.^{4, 9, 11, 12, 26, 53-59} However, the introduction of such organic based mobile phases may be responsible for both spectroscopic and non-spectroscopic interferences (due to the presence of elevated concentrations of C and N isotopes), see section 1.2.2. The transport efficiency of liquid samples into an ICP ion source is particularly low as 85 to 90 % of the liquid aspirated is commonly discarded.⁴²

The introduction of gaseous samples into an ICP source is straight-forward. Some gaseous samples can be injected directly into the ICP or introduced via sampling loops or the nebuliser/injector flow of the plasma gas.^{4, 7} Similar to liquid samples, homogeneity can be guaranteed in a gaseous sample. Hydride species can also be evolved from some gaseous samples and transported into the source.^{2, 4, 5, 7, 42, 49, 50, 60} Similarly to that discussed previously, instrumental coupling with gas based separation techniques, such as gas chromatography (GC) or supercritical fluid chromatography (SFC), can free samples from possible interfering species and provide speciation information.^{4, 58} Compared with the introduction of liquids, the transport of gaseous samples into an ICP ion source is almost 100 % efficient.

Although more difficult than gaseous or liquid samples the introduction of solid samples into an ICP source is possible and such introduction can also be beneficial with regard to the evasion of some spectroscopic interferences (see section 1.2.1). The most common approach to the analysis of solid samples is to chemically digest or

decompose the sample and introduce it into the plasma as a solution.^{1, 4, 7} A solid digest solution also promotes sample homogeneity which can be problematic in other solid sampling techniques. However, such an approach is not appropriate for many solid samples so other methods have been developed and employed. Solid samples can be introduced by direct insertion, aerosols and vapours can be evolved and introduced from samples after processes such as arc and spark ablation, electrothermal vaporisation and laser ablation.^{2, 4, 21, 29, 30, 34, 47, 61-63} Solid samples can also be ground into powders prior to slurry formation and nebulisation.^{1, 2, 4, 5, 7, 42}

The use of laser ablation, as a technique for solid sampling, is rapidly growing in popularity. By firing a laser at a solid surface, small quantities of the solid in particulate form can be generated. This particulate solid sample can then be carried via a carrier gas, such as helium, into the ICP for elemental measurement. This sample introduction technique is an incredibly powerful analytical tool; however, it presents a number of challenges in the form of elemental fractionation as well as the usual solid sampling issues, see below. These challenges are currently being studied by research groups worldwide.

Although solid sample introduction can exhibit advantages in the form of analyte transport with a reduced matrix and minimum preparation there are limitations that the analyst must have a firm understanding of. A digested/decomposed solid sample may be accompanied by a concentrated or harsh matrix that could lead to spectroscopic and non-spectroscopic interferences. Aerosols and vapours generated from solid samples are commonly introduced into the plasma by a carrier gas, e.g. He or Ar.^{4, 64} The presence of this carrier gas is known to affect the mass spectral background as such a gaseous introduction is comparable to the employment of a mixed-gas plasma (see section 1.2.1). The greatest limitation for the analysis of solid samples is the lack of solid certified standard materials that can be analysed for reference data. This absence means that solid sampling methods do not generally reach the same quality of quantification as for a liquid sample introduction.

1.1.3. Mass Spectrometry Employed in ICP-MS Analysis

It is possible to interface an ICP ion source with various mass analysers for the elemental analysis of samples. Following ion formation within an ICP ion source a mass spectrometer can be used, either by dispersion or filtering, to determine ions according to their mass-to-charge ratio (m/z). The most important parameters concerning a mass spectrometer are upper mass limit, transmission efficiency and mass resolution.^{39, 65} These parameters vary, widely, between the different types of mass spectrometer available.

Composed of four parallel hyperbolic or circular rods, a quadrupole mass spectrometer separates ions according to their motion.^{1, 4, 7, 39, 42, 58, 65-67} A voltage composed of DC and RF components is applied between adjacent rods of the quadrupole and adjustment of these components affects the trajectory stability of the ions passing through. At certain rod voltage conditions some ions will have a stable trajectory and pass between the rods from one end of the quadrupole to the other whilst some will not and will be rejected.^{4, 58, 65, 67} In ICP-MS, quadrupoles are the most commonly used mass analysers as they are compact and relatively inexpensive. However, quadrupole mass analysers are limited as they have a restricted m/z range (typically 1 to 4000 amu) and a low resolution of approximately 300 (0.6 amu bandpass) is achieved.^{4, 58, 65, 67}

Time-of-flight (ToF) is a particularly simple method of mass spectrometry whereby the flight time of ions over a known distance (in a drift tube typically 1 m in length), is measured. Assuming that ions have the same kinetic energy (E_k), which is not normally the case (see section 1.3) then their velocity is determined by their mass, i.e. heavier ions arrive at the detector after lighter ions.³⁹ Several researchers have coupled ToF mass analysers to an ICP ion source obtaining LOD's in the range of 0.4 to 2.0 ng ml⁻¹, comparable to the limits obtained with a quadrupole.⁴ As a result of this research, commercial ICP-ToFMS instruments are now available.^{4, 11} The main benefit of employing a ToF mass analyser in ICP-MS is that the problem of E_k spread (see section 1.3) can be addressed by taking advantage of electrostatic reflectors, otherwise known as reflectrons, which compensate for variations in E_k .³⁹ However,

one significant limitation to the coupling of an ICP ion source to a ToF mass analyser lies in the transportation of ions between the two. Pulses, or “bundles”, of ions are carried away from the ion beam generated after the ICP and into the ToF analyser. The result of such a configuration is a particularly inefficient transport of ions which hinders the capability of limit of detection.

A double focussing magnetic sector mass spectrometer employs a combination of magnetic and electrical fields in order to focus ions according to their momentum which is a function of mass and velocity.^{4, 39, 42} Such a mass spectrometer allows the resolution of ion signals with small differences in m/z and is commonly composed of a source slit (allowing ions into the magnetic and electrical fields), a magnetic sector analyser, an electrostatic analyser, a collector slit and a detector.^{39, 42} The transmission of ions through a magnetic sector mass analyser is a function of resolution and resolution of such an instrument is controlled by the source and collector slits.

The main limitation, therefore, of employing such a mass spectrometer in ICP-MS is that resolution is gained at the expense of sensitivity.⁴ However, on comparison to quadrupoles, a magnetic sector mass analyser can be more sensitive (an additional order of magnitude in terms of sensitivity can be achieved). For example, in the comparison of a quadrupole based instrument with a sector field based instrument for the measurement of Pt in urine there was an approximate three fold improvement in the limit of detection when employing the sector field instrument (LOD's of 0.18 ng l⁻¹ and 0.05 ng l⁻¹ for quadrupole and sector field instruments respectively).⁶⁸ Examples of the resolution required to separate interfering signals in a mass spectrum can be seen in Table 1.^{4, 7, 42} Double focussing magnetic sector mass analysers are also very expensive and are much more difficult to interface with an ICP ion source.

Table 1. A Table of Resolutions Required to Separate Analyte Ions from Interfering Ions.

Isotope	Isotope Mass	Interfering Ion	Interfering Ion Mass	Resolution required
²⁸ Si	27.9769	¹⁴ N ₂ ⁺	28.0061	960
³¹ P	30.9738	¹⁴ N ¹⁶ O ¹ H ⁺	31.0058	970
³² S	31.9721	¹⁶ O ₂ ⁺	31.9898	1800
³⁹ K	38.9637	³⁸ Ar ¹ H ⁺	38.9706	5700
⁴⁰ Ca	39.9626	⁴⁰ Ar ⁺	39.9624	193000
⁵¹ V	50.9440	³⁵ Cl ¹⁶ O ⁺	50.9638	2600
⁵² Cr	51.9405	⁴⁰ Ar ¹² C ⁺	51.9624	2400
⁵⁶ Fe	55.9349	⁴⁰ Ar ¹⁶ O ⁺	55.9573	2500
⁷⁵ As	74.9216	⁴⁰ Ar ³⁵ Cl ⁺	74.9312	7800
⁸⁰ Se	79.9165	⁴⁰ Ar ₂ ⁺	79.9248	9700

High resolution mass spectrometers are widely employed in ICP-MS instruments in applications demanding lower LOD's and the removal of molecular ion interferences.^{9, 12, 38, 69-71}

1.2. Limitations of ICP-MS Analysis

Although ICP-MS, employing a low resolution quadrupole mass analyser, can boast excellent LOD's and linear ranges it is hindered, to a certain degree, by various sources of interference and transmission problems through the plasma-mass spectrometer interface. Interferences in ICP-MS can be divided into two categories; spectroscopic and non-spectroscopic interferences.^{1, 5, 7, 70, 72}

1.2.1. Spectroscopic Interferences

Spectroscopic interferences are defined as any enhancement of the analyte signal caused by atomic or molecular ion species of the same m/z as that of the analyte species.^{1, 5, 7, 36, 73} The major causes of such interference and available remedies are described as follows.

In an ICP-MS instrument employing a low resolution mass analyser signals originating from different isotopes can be observed at the same m/z , in such a situation these signals cannot be separated. Overlapping isotope signals of this kind are described as isobaric interferences.⁷ The degree of such interference depends on the quantity and properties of isotopes present in the plasma. Isobaric interference is therefore dependent on the analyte isotopes of interest, the type of plasma gas(es) being used, the sample matrix and entrained atmospheric gases.^{7, 73, 74} Isobaric interference can be assessed in the isotopic abundance table (Figure 90) in Appendix 1.

Ionic molecular species, otherwise known as polyatomic ions, may also interfere with the m/z signal of an analyte isotope.^{1, 5, 7, 75-80} Polyatomic ions are detected as the result of either atomisation survival within the ICP or formation from atomic ions and neutral species. Such formation occurs through combination or ionisation reactions at the plasma-mass spectrometer interface.^{7, 76} The presence of polyatomic ions can make elemental analysis by ICP-MS difficult and in some cases even the use of high

resolution mass spectrometry is not particularly beneficial.^{1, 5, 7, 79} Some of the more common examples of these polyatomic ions are those based on argon, $^{40}\text{Ar}^{14}\text{N}^+$, $^{40}\text{Ar}^{16}\text{O}^+$ and $^{40}\text{Ar}_2^+$ ions interfere with the measurement of ^{54}Fe , ^{56}Fe and ^{80}Se isotopes respectively. An extensive list of polyatomic ion interferences can be seen in Table 53 (Appendix 1).

Under certain plasma conditions doubly charged ions can be formed from some isotopes. The signal for such an ion in the mass spectrum appears at a m/z at half that of the same isotope carrying a single charge.^{4, 5, 74, 75, 81} Doubly charged ions can therefore cause interference in lower regions of the mass spectrum. Previously, however, the presence of doubly charged ions in the mass spectrum has been used to the benefit of the analyst. Jarvis *et al.*⁸² used the occurrence of Eu^{2+} ions to quantify $^{151,153}\text{Eu}$ at $m/z = 75.5$ and 76.5 avoiding interfering $^{135}\text{Ba}^{16}\text{O}^+$, $^{134}\text{Ba}^{16}\text{O}^1\text{H}^+$, $^{137}\text{Ba}^{16}\text{O}^+$ and $^{136}\text{Ba}^{16}\text{O}^1\text{H}^+$ ions at the native $m/z = 151$ and 153 . Further examples of doubly charged ions can be seen in Table 53 (Appendix 1).

With basic chemical knowledge most isobaric and doubly charged ion interferences can be predicted and avoided by the use of alternative isotopes, in the case of polyisotopic analytes, or by the careful selection of sample matrices, plasma gas(es) and plasma conditions. However, in the case of polyatomic ion interferences the prediction of their presence and degree of effect can be more difficult. Various methods are available to the analyst that can be used to limit polyatomic ion interferences, these include the following:

Although Ar is the most commonly used gas in the generation of an ICP the mass spectral background of such a plasma is dominated by Ar based spectroscopic interferences particularly between $m/z = 50$ and 80 .⁸³ Employing a plasma generated from alternative or mixed gases (such as N_2 , O_2 , H_2 , He, Xe, CH_4 , CHF_3 , C_2H_4 or compressed air) will provide a mass spectral background dominated by ions of a different m/z . Some such backgrounds will allow the analysis of certain m/z signals that are heavily interfered with when employing an Ar plasma.^{40, 84-89}

The problem of spectroscopic interferences may be tackled by the utilisation of collision or dynamic reaction cells. By bleeding reactive gases into a multipole

situated between the plasma-mass spectrometer interface and the mass analyser, through which the ion beam generated after the skimmer cone is passing, it is possible to react analyte or interfering ions to form product ions at an alternate m/z therefore allowing detection and quantification.^{33, 43, 59, 79, 90-96}

Spectroscopic interferences can also be overcome by deliberately altering the conditions of the ICP. Lowering the plasma forward power from the typical 1350 W to between 600 W and 900 W (known as the “cold/cool plasma” region) results in a plasma with a background spectrum dominated by the $^{14}\text{N}^{16}\text{O}^+$ ($m/z = 30$) ion rather than Ar based ions. Similar to the use of alternate or mixed gas plasmas, a different mass spectral background arising from a “cold/cool plasma” will allow the analysis of certain m/z 's without interference. The use of such a plasma is common in the determination of K isotopes at $m/z = 39$ and 41 .⁹⁷⁻⁹⁹ Low forward power plasmas operate at lower temperatures and have different plasma potentials than those run at the normal 1350 W. It is the variation of these two parameters that result in changes in atomisation and ionisation characteristics leading to a different mass spectral background.

Some spectroscopic interferences can be avoided by the employment of an alternative method of sample introduction. Although sometimes problematic, introduction techniques such as laser ablation, hydride generation and electrothermal vaporisation can be employed for this reason as they all involve transport of a sample in a pure form.^{2, 4, 21, 29, 30, 34, 40, 41, 47, 49, 50, 61-63} In many cases interferences arising from the presence of polyatomic ions can be resolved by the use of high resolution mass spectrometry coupled to the ICP ion source.^{4, 38, 69-71, 100}

1.2.2. Non-Spectroscopic Interferences

Non-Spectroscopic interferences are defined as any degradation in signal that arises as a result of physical or chemical parameters of the sample.^{4, 36} The major causes of such interference and approaches to compensate for them are described as follows.

Easily Ionisable Elements

Elements with a relatively low ionisation potential (such as Na, K, Ca, Rb and Cs) are described as easily ionisable elements (EIE's). Theoretically an excess of EIE's present in a sample can create a bias in the ionisation equilibrium of the ICP towards elements of a lower ionisation potential (IP). Such a bias could result in ionisation suppression of analyte elements exhibiting a higher ionisation potential.⁴ For example, in the analysis of a sample containing ^{31}P (IP = 10.5 eV) and an excess of Na (IP = 5.1 eV) a significant degree of suppression of the ionisation of ^{31}P may be expected. If such suppression is not anticipated, and taken into account through matrix matching of standards or internal standardisation, anomalous results might be obtained. In practise, however, the quantity of sample elements passing through the ICP in relation to the argon plasma gas will always be low so any non-spectroscopic interference effect that would arise due to the presence of EIE's would be minimal, if it occurred at all.

Physical Properties of a Sample

The physical properties of the sample being analysed and the method of delivering it into an ICP must be understood fully by the analyst so to estimate the degree of non-spectroscopic interference.

On introduction into an ICP, it would be expected that gaseous samples exhibiting a high vapour pressure would vary the width of the plasma central channel and therefore affect the local temperature and ionisation capability. If sample vapour pressure is high enough then the plasma may destabilise completely and extinguish. This effect must also be considered when employing sample introduction techniques that require the use of an alternative carrier gas to transport the sample into the plasma. For example, in laser ablation sample introduction a He carrier gas introduced into an Ar plasma is known to vary the properties of the ICP, such as temperature and plasma potential, as seen in the employment of a mixed gas plasma.⁴

The efficiency with which a liquid sample can be introduced into an ICP and analysed is dependent on an even greater number of physical properties. Viscosity, surface tension, density and vapour pressure all affect the efficiency with which a liquid can be nebulised and transported through a spray chamber into the ICP torch. Once in the torch, sample vapour pressure has the same effect on the plasma as that described for gaseous samples.⁴

As mentioned previously, the most common approach to the introduction of solid samples is to form a vapour and/or particle cloud from a sample surface. With regard to the introduction of such a vapour or particle cloud there are two main factors that can contribute to non-spectroscopic interference that must be considered. The first factor is the use of alternative carrier gases for the transportation of material into the ICP, this has already been discussed with regard to gaseous and liquid introduction in this section. The second factor is known as elemental fractionation. In basic terms elemental fractionation can be described as non-representative sampling, i.e. the signal response of the ICP-MS is not representative of the components of the sample. Although work is still being carried out to fully understand what causes this problem it is now generally believed that elemental fractionation can occur at three points during the sampling, transport and ionisation processes. During the sampling process bias can take place during the transfer of certain elements into the gas phase based on their physical properties such as melting and boiling points, vapour pressure, atomic and ionic radius, charge and speciation.⁶⁴ Generally the particles created during solid sampling are much larger than those generated during liquid sample nebulisation. These larger solid particles are thought to be significant with regard to deposition during sample transport and atomisation and ionisation efficiency within the ICP.⁶⁴ For these reasons the degree of elemental fractionation, therefore, differs widely between samples.⁶⁴ The problem of elemental fractionation highlights the necessity for matrix matched solid calibration standards which are not available for the majority of solid samples.

Sample Deposition within an Instrument

Analyte signal may be suppressed as a result of excessive sample deposition on the sample and skimmer cones during an analysis or if deposits are allowed to build up over time. If this takes place the orifice of either cone may block and the ion beam generated behind the skimmer cone will be affected, a signal of reduced or little intensity will result. This problem can be easily avoided assuming regular instrument cleaning and maintenance.

Space Charge Effects

“Space charge effect” describes a situation whereby a predominance of positive or negative charge causes a mutual repulsion amongst ions. In ICP-MS, the plasma species transported through the sample cone are primarily composed of positively charged ions, electrons and neutral atoms and molecules (originating from the analyte, plasma gas and entrained atmospheric gases). Because, throughout the instrument, ions and electrons are travelling at different velocities, the potential for the separation of charge and a breakaway from neutrality is high. If charge separation is sufficiently strong then repulsion between positive ions will take place. Such separation can influence ion trajectory as the ion beam passes into the mass analyser, unstable trajectories can result in a loss of analyte sensitivity.^{4, 72, 101}

Ion Kinetic Energy Spread

The degree of variation in kinetic energy (E_k) exhibited between ions of the same element can contribute to reductions in ion transmission and mass spectrometer resolution. The E_k of ions passing through the system is an important factor in terms of the ability to move between the various electrical environments of the instrument. A wide spread in E_k could lead to a significant proportion of ions of the same element being eliminated from the mass analyser prior to detection or interference with elements of a neighbouring mass. For a full description of the issue of ion kinetic energy effects see section 1.3.

With the careful design of an ICP-MS analysis most non-spectroscopic interferences can be anticipated and potentially minimised. The presence of EIE's in a sample can be limited to avoid ionisation bias towards elements of low IP and the evasion of highly concentrated samples, as well as regular instrument cleaning, can minimise the chances of orifice blocking in the sample and skimmer cones. Selection of appropriate sample pre-treatment and introduction techniques can help avoid some non-spectroscopic interferences derived from physical properties of the sample. Internal standardisation, standard addition and isotope dilution approaches are commonly employed in order to standardise non-spectroscopic interference.^{4, 22, 28, 39}

1.3. Kinetic Energy Issues Associated with ICP-MS Analysis

A subject that has been relatively overlooked with regard to interferences in ICP-MS is the kinetic energy (E_k) of ions, generated in the ICP, and the effect that such energy has on ion transmission through the instrument. E_k of ions transmitted through the ICP-MS can have both detrimental effects (with regard to ion transmission and mass spectral resolution as a result of E_k spread) and advantageous effects (with regard to ion control in a collision cell by KED and IKEE) on the determination of isotopes. Such effects are discussed in sections 1.3.1, 1.3.2 and 1.3.3.

1.3.1. Causes of Ion Kinetic Energy Spread

The E_k of ions generated in the plasma and transmitted through the plasma-mass spectrometer interface, ion optics and mass analyser is a function of an individual ion's mass and velocity. During passage through the instrument ion velocity can change according to the physical characteristics of the environment to which the ion is exposed. Between generation in the ICP source and detection, after filtering in a mass analyser, ions are subjected to several different environments in an ICP-MS that result in them experiencing a wide range of electrostatic energies. Such exposure has been described by Dexter *et al.* as an “ion energy rollercoaster”, see Figure 4.¹⁰² Environmental exposure to varying pressures, temperatures and electrical phenomena are seen to cause this “rollercoaster” which leads to a wide E_k spread amongst the ions transmitted.

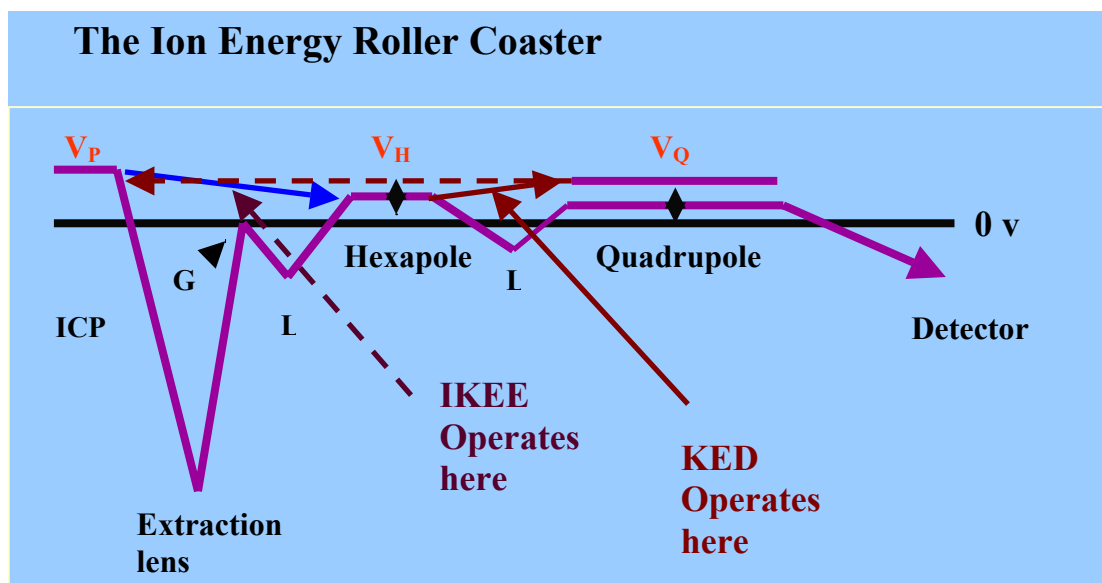


Figure 4. The "Ion Energy Rollercoaster" Diagram.¹⁰²

Figure 4 is a diagram that highlights the variation in electrical environment, with respect to 0 V, through which ions pass in the ICP-MS. The thick pink line, of the Figure 4 diagram, shows the variation in potential imposed on ions at different stages in the instrument relative to the 0 V black line. Although this diagram is a specific description for a Thermo PQ ExCell ICP-MS instrument the premise is similar for all quadrupole based ICP-MS instruments. The different stages, highlighted in Figure 4, during which ion energy is influenced significantly are described as follows:

Composed of positively charged ions, electrons and neutral species, the ICP ion source is an environment of high plasma potential (+9 V to +11 V) and high temperature (7000 K to 10 000 K for an Ar based plasma).^{4, 39} In this region the positive ions are fast moving and highly mobile due to the repulsion forces between themselves, the positive potential of the plasma and the high plasma temperatures.³⁹

As positive ions are drawn through the sample cone they are rapidly accelerated to supersonic velocities in the expansion chamber that buffers the ICP ion source operating at atmospheric pressure and the mass analyser at vacuum conditions.⁴ This acceleration takes place due to the environmental pressure transition (1 Bar to

approximately 2 to 4 mBar) and is described in the equation of Figure 86 in section 5.3.1.⁴

Following rapid acceleration and skimming of the bulk material in the expansion chamber, positive ions are subject to two significant factors that contribute to E_k spread. Firstly there is an attracting force acting on the ions in the form of a large negative potential, of approximately -600 V, applied to the extraction lens that sits behind the skimmer cone.⁴³ Such a large potential applied to the extraction lens is required because the entrance aperture leading into the electrostatic lenses is quite small. The extraction lens voltage is controlled via the instrument software. Secondly, between the back of the skimmer cone and the extraction lens “space charge effects” are known to be prevalent. Any mass repulsion between ions, in the beam generated after the skimmer cone, will have an affect on ion velocity and therefore E_k .

After passage through the extraction lens the bulk flow of ions is decelerated on approach to the slide valve that separates the low pressure expansion region and the vacuum conditions of the mass analyser multipole. This deceleration takes place as the slide valve is grounded so there are no attracting or repelling forces acting on the ions.

Beyond the slide valve the ions passing through are accelerated due to attraction towards negative voltage applied to a series of three electrostatic guiding lenses.⁴³ In the case of the Thermo PQ ExCell ICP-MS instrument the first of these lenses carries a potential of approximately -1 V whilst the second and third lenses carry potentials of approximately -50 V and -100 V respectively.

Following acceleration by the electrostatic lenses the ion flow is decelerated on entrance to the collision cell multipole, in this case a hexapole. This takes place due to repulsion by the positive potential applied to the multipole (typically +1 V to +10 V).²⁵ If the collision cell is in operation and a reaction gas has been bled into the hexapole then ions can be slowed further as a result of collisions between ionic and neutral species.¹⁰³ It should be noted that a collision cell or dynamic reaction cell multipole is not a standard feature of a quadrupole based ICP-MS instrument.

The collision cell multipole and mass analyser quadrupole are separated by a further guiding lens that carries a negative potential, this lens is responsible for ion acceleration before entrance to the quadrupole.⁴³ On passage into the quadrupole mass analyser the ion flow is accelerated or decelerated according to the potential applied. During typical analysis a potential of +1 V is applied to the quadrupole which has a decelerating effect on the ion flow.⁴³

The dual mode detector employed by the Thermo PQ ExCell ICP-MS typically carries a voltage of between -2500 V and -4000 V, therefore on exit of the quadrupole ions are subjected to a sudden acceleration into the detector for counting.

1.3.2. The Significance of Ion Kinetic Energy Spread

It is because the ions generated are exposed to the undulating conditions, described in section 1.3.1, that the E_k that they exhibit, following passage through the instrument, can be quite varied. The presence of this E_k variation can impair ion resolution and transmission, i.e. sensitivity. This variation in E_k can vary ion trajectory stability on passage through the quadrupole and hence determine whether or not it is filtered and detected. It is believed that any instrument modifications that can be made to lessen the drastic changes in ion velocity spread whilst maintaining ion transmission would improve ICP-MS LOD's for every element of the periodic table.

1.3.3. Advantageous Ion Energy Effects

As a result of the study of ion E_k within an ICP-MS instrument, with respect to collision and dynamic reaction cells, two distinct effects have been recognised. These two effects are known as kinetic energy discrimination (KED) and the ion kinetic energy effect (IKEE) and are described as follows:

Kinetic Energy Discrimination (KED)

Defined as the exclusion of slow, collision cell formed, ions from the mass analyser, kinetic energy discrimination (KED) is a particularly beneficial effect in analysis by ICP-MS. The passage of unwanted secondary or tertiary ions into the mass analyser can be limited, by KED, leading to a reduction in levels of interference.⁸³ During KED a “kinetic energy barrier” is established, between the collision cell and mass analyser multipoles, which ions must overcome in order to enter the mass analyser.^{83,}

91

The KED effect is achieved by setting the potential of a pressurised collision cell multipole slightly less positive than the mass analyser potential.⁸³ When this is the case collision product ions from the cell with the same energy as the collision cell potential are discriminated against and rejected before reaching the mass analyser. Analyte ions, generated within the ICP source, are typically of high energy due to exposure to high plasma potential and high temperatures so are allowed through to the mass analyser.^{83, 91, 96} KED can be used to exclude cell formed molecular ions from the quadrupole as they have a higher collisional cross section than analyte ions so undergo more thermalising collisions with the gaseous collision cell species.¹⁰⁴

Ion Kinetic Energy Effect (IKEE)

Ion kinetic energy effect (IKEE) is defined as the variation of collision cell reactivity by control of the input ion energy. Dexter *et al.*⁸³ studied the effects of IKEE and observed that the input ion E_k can be varied by alteration of the potential difference between the plasma (≈ 9 V) and a collision cell multipole (variable potential) in a Thermo PQ ExCell ICP-MS instrument. Dexter *et al.*⁸³ observed that increasing the collision cell multipole potential with respect to plasma potential resulted in an increase in the rate of exothermic reactions and a decrease in the rate of endothermic reactions. Here, IKEE has been highlighted as an area of research that may be beneficial for future analysis employing ICP-MS instruments and collision cell technology.

1.4. Collision and Dynamic Reaction Cells

Collision and dynamic reaction cells are enclosed, pressurised, multipoles (quadrupoles, hexapoles and octapoles) that can be employed as gas phase “test tubes” as part of the operation of an ICP-MS. Due to differences in stability boundaries of quadrupoles, hexapoles and octapoles, two types of cell have evolved and are in common use in ICP-MS today.

1.4.1. Collision Cells

Typically hexapole or octapole collision cells are positioned between the plasma-mass spectrometer interface and the mass analyser. Operating in an RF only mode these cells guide the ion beam that has been generated. On bleeding a reaction gas into such a cell, processes such as collisionally induced dissociation (CID) and ion-molecule reactions can be performed with the ionic species of the ion beam. As these cells are operated in an RF only mode the gas being introduced must be inert or of low reactivity in order to avoid the formation of secondary or tertiary ions that may have stable trajectories in the multipole and potentially interfere with the m/z of the analyte of interest. H_2 ,^{23, 33, 59, 83, 91, 93, 105-110} Xe ,^{33, 111} CH_4 ,³³ He ,^{15, 23, 59, 83, 91, 93, 105-111} O_2 ,³³ and N_2O ,¹⁰⁹ have been well documented as collision cell gases that can provide beneficial chemistries with regard to tackling spectroscopic interferences.

1.4.2. Dynamic Reaction Cells

The dynamic reaction cell is a pressurised quadrupole that, like the collision cell, is positioned between the instrument interface and the mass analyser. A reaction gas can be bled into the cell whilst being operated in an RF and DC mode. This type of cell can therefore discriminate against ions leaving the cell and entering the mass analyser according to the bandpass control. For this reason more reactive gases can

be incorporated into the device than can be in a collision cell as any secondary or tertiary reaction products can be removed before reaching the mass analyser. NH_3 ,^{17, 18, 33, 95, 109, 112-117} CH_4 ,^{18, 33, 95, 112, 114} H_2 ,^{18, 33, 113, 114, 116} and O_2 ,^{18, 33, 114, 117, 118} gases have been studied in a dynamic reaction cell in order to tackle spectroscopic interferences.

1.4.3. Ion-Molecule Chemistry of Collision and Dynamic Reaction Cells

During the operation of a collision or dynamic reaction cell several processes are known to take place between the components of the ion beam and the collision/reaction gas introduced. A scattering effect on the ions transported through the cell multipole can be produced by the cell gas. Such an effect can limit the number of ions reaching the mass analyser and hence reduce the overall sensitivity achieved. This effect is seen to be worse for ions of a lower mass compared to heavier ions.³³ The other processes that take place in a collision or dynamic reaction cell are collisional processes; these describe the interactions between ions and collision/reaction gas molecules and are discussed as follows:

Energy Transfer

By the means of a non-reactive collision, energy can be transferred from an ion to a neutral molecule. The degree of energy that can be transferred depends on the kinetic energy of each species involved in the collision. If multiple collisions occur in a collision or dynamic reaction cell between a high energy ion and a low energy neutral species then sequential loss of E_k from the ion occurs, this is known as energy damping. Such damping is extensive when there is a large neutral species to ion mass ratio in the cell.³³

Collisional Fragmentation

As described previously, during the collision between ionic and neutral species energy can be transferred to the neutral molecule. Such transferred energy, transformed partly into vibrational energy, can exceed molecular bond strength and a chemical bond may break resulting in fragmentation or dissociation of the molecule involved in the collision.³⁹ This process is known as collisionally induced dissociation (CID). In a collision or dynamic reaction cell, as part of an ICP-MS instrument, polyatomic ions or neutral species can be dissociated by collision with an inert gas such as He or Ar.³³ Such dissociation can occur through a single collision, although multiple collisions may be required where internal energy is accumulated until breaking point on each single collision. Although CID is a very useful tool in the fragmentation of large molecular ions in organic based mass spectrometry it is not a particularly efficient process for the removal of some low mass interfering polyatomic ions, chemical reaction can be a far more effective approach to this.^{33, 39, 66}

An example of the advantageous employment of CID in collision/reaction cell ICP-MS is the dissociation of the argon dimer ($^{40}\text{Ar}_2^+$, $m/z = 80$). By using Ar as a collision gas, in a cell, the dissociation of $^{40}\text{Ar}_2^+$ is 86 % efficient for single collision fragmentation.³³ The same effect can be achieved with He and H_2 collision gases but multiple collisions (4 or more) are required for dissociation.

Ion-Molecule Reactions

Reactive gases, such as H_2 , can be bled into a collision or dynamic reaction cell to remove unwanted low mass ions by chemical reaction. Typically the reaction gases bled into the cell are introduced at low pressures to avoid excessive scattering of ions in the cell.^{33, 66} Due to the presence of ionic and neutral species in the cell several important types of reaction are known to occur, as indicated in Table 2.³³

Table 2. Reactions Taking Place Between Ionic and Neutral Species in a Collision/Reaction Cell.

Reaction Type	Reaction Process	Example
Charge Transfer	$A^+ + B \rightarrow B^+ + A$	$^{40}\text{Ar}^+ + ^{14}\text{N}^1\text{H}_3 \rightarrow ^{40}\text{Ar} + ^{14}\text{N}^1\text{H}_3^+$
Proton Transfer	$\text{AH}^+ + B \rightarrow \text{BH}^+ + A$	$^{40}\text{Ar}^1\text{H}^+ + ^1\text{H}_2 \rightarrow ^{40}\text{Ar} + ^1\text{H}_3^+$
H Atom Transfer	$A^+ + \text{BH} \rightarrow \text{AH}^+ + B$	$^{40}\text{Ar}^+ + ^1\text{H}_2 \rightarrow ^{40}\text{Ar}^1\text{H}^+ + ^1\text{H}$
Oxidation	$A^+ + \text{BO} \rightarrow \text{AO}^+ + B$	$^{136}\text{Ce}^+ + ^{14}\text{N}_2^{16}\text{O} \rightarrow ^{136}\text{Ce}^{16}\text{O}^+ + ^{14}\text{N}_2$
Association	$A^+ + B \rightarrow \text{AB}^+$	$^{28}\text{Ni}^+ + ^{14}\text{N}^1\text{H}_3 \rightarrow ^{28}\text{Ni}^+ \cdot ^{14}\text{N}^1\text{H}_3$

Ion-molecule reactions that can take place in a collision or dynamic reaction cell are thermodynamically specific according to their enthalpy of reaction. For example, it is possible for $^{40}\text{Ca}^+$ ($m/z = 40$) to be resolved from $^{40}\text{Ar}^+$ ($m/z = 40$) employing a NH_3 reaction gas. Such resolution is possible because the reaction between the $^{40}\text{Ar}^+$ ion and NH_3 is fast (rate constant = $1.7 \times 10^{-9} \text{ cm}^3 \text{ molecule}^{-1} \text{ s}^{-1}$) compared to the slower reaction between the $^{40}\text{Ca}^+$ ion and NH_3 (rate constant $< 1.0 \times 10^{-13} \text{ cm}^3 \text{ molecule}^{-1} \text{ s}^{-1}$). This reaction specificity is also reflected in the ionisation potential of each species; $\text{Ar} = 15.76 \text{ eV}$, $\text{NH}_3 = 10.16 \text{ eV}$ and $\text{Ca} = 6.11 \text{ eV}$. The result of this is the attenuation of the $^{40}\text{Ar}^+$ ion whilst the $^{40}\text{Ca}^+$ ion is almost unaffected.^{33, 51}

By taking advantage of differences in reactivity between the analyte ions of interest and unwanted interfering ions selective reactions can be carried out by introducing various reaction gases into the cell. Such reactions have shown that the approach of employing these cells has been found to be effective in the reduction of some interfering polyatomic ions, with the same m/z value as the analyte ion, entering the mass analyser.

1.5. “Cold/Cool Plasma”

In an Ar based, quadrupole, ICP-MS instrument, under conventional operating conditions K, Ca and Fe isotopes are particularly difficult to analyse due to intense background signals at $m/z = 39, 40, 41, 42, 43, 43.5, 44$ and 56 .^{4, 6, 98, 99, 119} Such background signals occur due to isobaric interferences and spectroscopic interferences resulting from the presence of Ar based polyatomic ions and doubly charged ^{84,86,87,88}Sr isotopes.⁹⁹ Isobaric and spectroscopic interferences that typically affect the analysis of K, Ca and Fe isotopes are listed in Table 3.^{98,99,119}

Table 3. A Table of Potential Interferences with Regard to K, Ca and Fe Isotopes.

Analyte Isotope	Isobaric Interference	Polyatomic Ion Interference	Doubly Charged Ion Interference
³⁹ K	-	³⁸ Ar ¹ H ⁺	-
⁴⁰ K	⁴⁰ Ar ⁺ , ⁴⁰ Ca ⁺	³⁸ Ar ¹ H ₂ ⁺	-
⁴¹ K	-	⁴⁰ Ar ¹ H ⁺	-
⁴⁰ Ca	⁴⁰ Ar ⁺ , ⁴⁰ K ⁺	³⁸ Ar ¹ H ₂ ⁺	-
⁴² Ca	-	⁴⁰ Ar ¹ H ₂ ⁺	⁸⁴ Sr
⁴³ Ca	-	-	⁸⁶ Sr
⁴⁴ Ca	-	-	⁸⁸ Sr
⁴⁸ Ca	⁴⁸ Ti ⁺⁺	-	-
⁵⁴ Fe	⁵⁴ Cr ⁺	³⁸ Ar ¹⁶ O ⁺ , ⁴⁰ Ar ¹⁴ N ⁺	-
⁵⁶ Fe	-	⁴⁰ Ar ¹⁶ O ⁺	-
⁵⁷ Fe	-	⁴⁰ Ar ¹⁶ O ¹ H ⁺	-
⁵⁸ Fe	⁵⁸ Ni ⁺⁺	-	-

For some elements it is acceptable to analyse samples by collecting data at alternate isotopes. For example, for the analysis of Ca the isotope at $m/z = 44$ (2.09 % abundant) may be studied rather than the isotope at $m/z = 40$ (96.9 % abundant) that suffers both isobaric and spectroscopic interferences. However, for some elements the measurement of an alternative isotope is not possible. Instead, by substantially altering the operating conditions of the ICP-MS instrument, it is possible to change the composition of the plasma and hence change the dominant background ions in the

mass spectrum. By increasing the sampling depth of the plasma torch, lowering the plasma forward power and increasing the nebuliser flow a lower temperature “cool/cold plasma” is achieved.⁴ In the analysis of a 0.1 % HNO₃ solution under standard conditions the dominating ions observed were ⁴⁰Ar⁺ ($m/z = 40$), ⁴⁰Ar¹H⁺ ($m/z = 41$), ¹⁶O⁺ ($m/z = 16$) and ¹⁴N⁺ ($m/z = 14$).⁴ Large background signals were also seen for ⁴⁰Ar₂⁺ ($m/z = 80$) and ⁴⁰Ar¹⁶O⁺ ($m/z = 56$).⁴ When the same solution was analysed under “cool/cold plasma” conditions the background spectrum was different, being dominated by ¹⁴N¹⁶O⁺ ($m/z = 30$) ions. Under such conditions the formation of ⁴⁰Ar⁺ ($m/z = 40$) and ⁴⁰Ar¹H⁺ ($m/z = 41$) ions are suppressed leaving ions at $m/z = 39, 40$ and 41 relatively interference free.⁹⁷

The main disadvantage in employing “cool/cold plasma” conditions is that the formation of polyatomic ions, particularly oxide ions, originating from the sample matrix is more likely within the ICP. These effects can be reduced by the separation of the sample from its matrix or vice versa before introduction into the plasma which can be achieved by, for example, hydride generation, electrothermal vaporisation, laser ablation or coupled techniques such as HPLC.^{2, 4}

When used in conjunction with techniques for reducing a secondary discharge and methods for matrix removal, “cool/cold plasma” ICP-MS can be a very effective approach to analysis. Several groups have employed the “cool/cold plasma” technique in the analysis of ^{40,42,43,44,48}Ca, ^{39,40,41}K and ^{54,56,57,58}Fe isotopes that commonly suffer the interferences previously described.⁹⁷⁻⁹⁹ It has been shown that employing these conditions during the analysis of Ca, K and Fe isotopes the analyte signals can be easily separated from the background signal. Because of the low LOD's achieved, “cool/cold plasma” has become the approach for ultra-trace analysis of acids and waters in the semiconductor industry which has a requirement for high purity materials.^{4, 98, 99}

1.6. The Application of ICP-MS in Biological Samples

In recent years there has been an explosion in the number of publications involving the study of metals in biological systems by ICP-MS. The understanding of the role of metal species in the human body has become increasingly important and ICP-MS has been able to provide accurate quantitative data that could not, previously, have been produced by atomic absorption spectroscopy. Also, on interfacing with separation techniques such as HPLC, speciation data has provided enormous quantities of information that can describe biological systems.

1.6.1. Biological Samples in Clinical Science

From a clinical point of view there are three main areas in the study of these systems that ICP-MS can contribute to.¹²⁰ These three areas are described as follows:

Nutrition

ICP-MS has been used to determine the levels and speciation of metals in human body media such as blood, serum, plasma, urine and tissues following digestion or dilution. Such data has been used to associate the deficiency of essential elements (for example Cr, Mn, Mo, Fe, Co, Cu, Zn, Se and I) with diseases and disorders.^{94, 120-126} As ICP-MS is an isotope specific technique it has also been employed in the determination of the efficacy of metal supplementation. By supplementing the body with stable isotope enriched compounds and measuring isotope ratios in blood, serum and plasma the degree of metal uptake can be established. An example of such research has been supplementation with iron and selenium compounds.¹²³

Toxicology

The occurrence of metal poisoning in the body can be determined and quantified by employing ICP-MS. Exposure to As, Hg and Pb have been determined through the ICP-MS analysis of blood, plasma, urine and hair samples.¹²⁷ Such measurements are important in occupational medicine.¹²⁰

Currently there is a lot of research being carried out on implantable devices in the human body, particularly hip joint replacements. Such hip replacements based on two metal surfaces moving against each other generate significant quantities of particulate wear debris that can reside in the tissues surrounding the joint and can be circulated via the blood stream. ICP-MS has been employed in the quantification of metals such as Co, Cr and Mo in blood, serum and urine samples.¹²⁸⁻¹³¹ At present there is much debate with regard to the biological effect, if any, of such debris in the human body.

Pharmacology

The employment of ICP-MS in pharmacology can be viewed from two points of view. ICP-MS is used extensively in the study of metal based therapeutic compounds, such as the platinum based cisplatin and oxaliplatin (see Chapter 4). Blood, serum, tissues and isolated cells have been studied in the determination of drug/target interactions. The ICP-MS technique is also employed in the detection of inorganic impurities in materials and formulations used and produced in the synthesis of pharmaceutical compounds.^{132, 133} Such impurities typically originate from the use of catalysts and reaction vessels and control of which is essential with regard to the quality and safety of a drug.

1.6.2. Biological Samples in the Environment

ICP-MS is widely employed in the study of biological systems in the environment. Plant and animal life are commonly studied to establish the roles of metal species in

their biochemistry and also to determine the uptake of metals as a result of exposure to industrial processes. A very good example of this is the speciation analysis of As. Such work has shown that biological systems can absorb significant levels of As, however, the metal may not produce any detrimental effects as it can be present as a non-toxic species.

1.7. Thesis Aims and Objectives

Under sponsorship by the Thermo Electron Corporation (Winsford, Cheshire, United Kingdom) the initial aim of the work, carried out to attain the degree of doctor of philosophy was the following:

The improvement of limits of detection for the measurement of ^{31}P and ^{32}S isotopes by quadrupole based ICP-MS.

The reasons behind carrying out such work are described in sections 1.2.1 and 2.1.1. The work carried out towards this initial aim is described in Chapter 2. During the three years over which the work for this thesis was carried out three additional objectives evolved from the original aim, these are described as follows:

The study of deoxyribose nucleic acid (DNA) by ICP-QMS methods developed towards the original aim.

DNA in various matrices was studied as an application of the ^{31}P and ^{32}S methods developed. The DNA molecule consists of approximately 10 % phosphorus, present in the phosphate sugar backbone, so was viewed as an ideal compound for study. Qualification and quantification of DNA is typically undertaken via robust UV/Vis spectroscopy and fluorescence methods. It was the aim of this work to determine the

viability of ICP-QMS as a competing technique for the study of this compound. The work carried out towards this aim is described in Chapter 3.

The study of interactions between DNA and platinum based anti-cancer drugs (cisplatin and oxaliplatin) by ICP-QMS.

As a direct continuation of some of the work carried out towards the original aim a collaboration between the Loughborough University atomic spectroscopy research group and the cancer biomarkers and prevention group at the University of Leicester was established. The joint interest between these two groups lay in the study of DNA. In the case of the Loughborough group the study of the DNA molecule by ICP-QMS was of interest in terms of its phosphorus content. The interest for the Leicester group lay in DNA being the therapeutic target of the platinum based anti-cancer drugs cisplatin and oxaliplatin.

The study of the interaction between such drugs and their target should allow the calculation of binding constant data that could be used to fulfil one of the overall objectives of the Leicester group which is the development of a clinical blood test to establish drug efficacy of both cisplatin and oxaliplatin in individual patients. The aim behind this objective was the determination of a binding constant for the interaction between the cisplatin and oxaliplatin drugs and their biological target DNA (see Chapter 4).

The development of alternative ICP-MS interface structures to tackle non-spectroscopic interferences.

With regard to general instrument development, an area that has changed very little since the birth of ICP-MS instruments is the interface region. The current design of this region contributes to two significant forms of non-spectroscopic interference; sample deposition on the skimmer cone tip and analyte ion kinetic energy spread. Successfully overcoming these issues could improve the limits of detection for all of the elements measureable by ICP-MS. With the understanding of the processes that

take place in this region it was the aim of this work to tackle these two forms of interference via research into two additional structures that could be incorporated into the expansion chamber. The work carried out towards this third additional objective is described in Chapter 5.

Chapter 2

Method Development Studies for the Determination of Phosphorus and Sulphur Isotopes by ICP-QMS

2.1. The Determination of Phosphorus and Sulphur by ICP-MS

Phosphorus and sulphur are two elements that are crucial to all forms of life. Both elements are important in the steel and semiconductor industries as well as the food and petrochemical industries and in the analysis of environmental and geological samples, especially with respect to the concentration of sulphur in rain water (or “acid rain”), and the presence of phosphorus in ground waters that may establish leaching from chemical fertilisers.^{90, 92, 134}

Phosphorus species play a decisive role in the majority of metabolic steps of all organisms from the simplest to the most complex. Phosphorus is an important constituent of tissues, bones and teeth and cells.¹³⁵ Phosphorus forms the basis of the linking groups between units of the sugar esters of DNA and RNA, it is also present in the energy storing nucleotide triphosphates such as ATP and in coenzymes such as NADH and NADPH.¹³⁵⁻¹³⁷

Sulphur plays an enormous role in the biochemistry of cells, particularly in oxidation and reduction processes.¹³⁷ Occurring in the amino acids cysteine and methionine, sulphur is therefore present in any peptide containing more than twenty five amino acids, i.e. it is approximately 4 % abundant in peptides.^{136, 137}

The determination of phosphorus and sulphur isotopes is, therefore, important in the understanding of many biological processes. During the analysis of clinical samples the measurement of these two elements in relation to other elements of the periodic table can allow biochemical processes such as phosphorylation and metal based drug binding to be followed.¹³⁶ As mentioned in Chapter 1 ICP-MS exhibits very desirable characteristics in elemental analysis, these have been invaluable with regard to speciation work. Although ICP-MS has previously been applied to the analysis of complex biological and clinical samples it remains, somewhat, an untapped resource compared to techniques such as liquid chromatography mass spectrometry (LC-MS). It is hoped that in the coming years the potential of this technique will be fully realised.

2.1.1. The Limitations of ^{31}P and ^{32}S Determination by ICP-QMS

Although ICP-MS exhibits low limits of detection for many elements, the determination of the isotopes of phosphorus and sulphur (^{31}P , ^{32}S , ^{33}S , ^{34}S and ^{36}S) by Ar, quadrupole based, ICP-MS is relatively troublesome for three main reasons. Firstly, in relative terms, the ionisation potential of both elements is very high, 10.5 eV for phosphorus and 10.4 eV for sulphur.⁶ This means that on, entrance to the ICP, only approximately 33 % of phosphorus and sulphur atoms introduced will be ionised.¹³⁸ So, on comparison to other elements, for the same quantity of P or S introduced a lower number of ions are generated which restricts the LOD capability of the ICP-MS technique from the outset. Secondly both P and S are subject to two types of non-spectroscopic interference. The high ionisation potential of these elements means that they could be subject to ionisation suppression within the plasma when in the presence of elements of a lower IP (easily ionisable elements, EIE's) assuming that the species involved are present in high concentrations, see section 1.2.2.¹³⁹ Phosphorus and Sulphur are also described as “light elements” with regard to their atomic mass; this makes them more prone to matrix induced space charge effects, see section 1.2.2.^{72, 92, 101, 139} Thirdly the phosphorus and sulphur isotopes are typically subject to spectroscopic interference from polyatomic ions based on carbon, nitrogen, oxygen and hydrogen (elements common to all sample matrices and entrained atmospheric gases), see section 1.2.1.^{6, 7, 38, 73, 74, 79, 100, 139} Examples of these polyatomic ions can be seen in Table 4.^{6, 7, 38, 73, 74, 79, 100, 139}

Table 4. A Table of P and S Isotopes, their Abundances, IP and Polyatomic Ion Interferences.

Analyte Isotope	Abundance (%)	Ionisation Potential (eV)	Polyatomic Ion Interference
^{31}P	100	10.5	$^{14}\text{N}^{16}\text{O}^+\text{H}^+$, $^{15}\text{N}^{15}\text{N}^+\text{H}^+$, $^{15}\text{N}^{16}\text{O}^+$, $^{14}\text{N}^{17}\text{O}^+$, $^{13}\text{C}^{18}\text{O}^+$, $^{12}\text{C}^{18}\text{O}^+\text{H}^+$
^{32}S	95	10.4	$^{16}\text{O}_2^+$, $^{14}\text{N}^{18}\text{O}^+$, $^{15}\text{N}^{17}\text{O}^+$, $^{14}\text{N}^{17}\text{O}^+\text{H}^+$, $^{15}\text{N}^{16}\text{O}^+\text{H}^+$
^{33}S	0.75	10.4	$^{15}\text{N}^{18}\text{O}^+$, $^{14}\text{N}^{18}\text{O}^+\text{H}^+$, $^{15}\text{N}^{17}\text{O}^+\text{H}^+$, $^{16}\text{O}^{17}\text{O}^+$, $^{16}\text{O}_2^+\text{H}^+$, $^{32}\text{S}^+\text{H}^+$
^{34}S	4.21	10.4	$^{15}\text{N}^{18}\text{O}^+\text{H}^+$, $^{16}\text{O}^{18}\text{O}^+$, $^{17}\text{O}_2^+$, $^{16}\text{O}^{17}\text{O}^+\text{H}^+$, $^{33}\text{S}^+\text{H}^+$
^{36}S	0.02	10.4	$^{18}\text{O}_2^+$, $^{17}\text{O}^{18}\text{O}^+\text{H}^+$

Another problem with regard to the determination of P and S is that both elements are ubiquitous and are generally difficult to eliminate from blank sample solutions. This is another factor that contributes to the poorer LOD's observed in the ICP-MS technique. Successful elimination of P and S from blank solutions would require the use of ultra-pure reagents prepared in a "clean-room", such an approach to analysis introduces an escalation in cost.

The combination of each of these problems results in the LOD of phosphorus and sulphur being two to four orders of magnitude poorer than that of the majority of elements in the periodic table that can be analysed by ICP-MS. There are three main options for the reduction of interferences and the improvement of LOD for phosphorus and sulphur isotopes, these being:

1. The coupling of a high resolution mass spectrometer to an ICP source. The resolution capability of such a mass analyser can allow the analyte and interfering polyatomic ion peaks to be resolved.^{4, 7, 38, 69, 70, 100}
2. The use of collision or dynamic reaction cells to move the analyte m/z to an alternate part of the mass spectrum or to move the interfering species m/z to a different value.^{4, 33, 59, 79, 90-96}
3. Alternative sample introduction techniques can be employed to transport the sample into the plasma whilst minimising, or eliminating, the presence of elements originating from a sample matrix, for example electrothermal vaporisation.^{2, 4, 7, 40, 41, 47, 49, 50}

The limits of detection capable by the various commercial ICP-MS instruments are not widely advertised. However, Perkin Elmer have published that the LOD capability of their ELAN DRC II instrument is 0.01 to 0.1 $\mu\text{g l}^{-1}$ and 0.1 to 1 $\mu\text{g l}^{-1}$ for ^{31}P and ^{32}S isotopes, respectively.¹⁴⁰ Bandura *et al* have also published a DRC method for the measurement of ^{31}P and ^{32}S isotopes, employing an O_2 reaction gas, whereby LOD's of $< 0.1 \mu\text{g l}^{-1}$ and $< 0.2 \mu\text{g l}^{-1}$ were obtained.⁹⁰

2.1.2. Alternative Techniques for the Determination of ^{31}P and ^{32}S

^{31}P and ^{32}S isotopes may be determined by other elemental analysis techniques, these include the following.

Inductively Coupled Plasma Optical Emission Spectroscopy (ICP-OES)

Inductively coupled plasma optical emission spectroscopy (ICP-OES) is in many ways a very similar technique to ICP-MS. Both techniques are almost identical between the sample introduction and ICP sections of the instrument but differ on the detection of elements present within a sample. Whereas ICP-MS counts the number of ions produced following transport through the plasma via a mass analyser, ICP-OES quantifies the presence of elements by measurement of the emission of radiation released from excited atoms and ions within the ICP ion source. Elements of the periodic table mostly exhibit unique wavelengths of emission; it is these wavelengths that are measured.^{1, 3, 5, 42} The main difference between these two ICP techniques is that ICP-OES measures the presence of elements only whilst ICP-MS determines isotopes.

Although both ICP-MS and ICP-OES techniques display similarities with regard to non-spectroscopic interferences they also exhibit their own benefits. An ICP-OES instrument can be described as a “flow-by” technique compared to the “flow-into” description of ICP-MS. As an ion flow into a detector is not required in ICP-OES this technique is well suited to the analysis of highly concentrated samples that contain a significant degree of dissolved solids. Such solutions are problematic for ICP-MS with regard to non-spectroscopic interferences. For this reason, ICP-OES is commonly employed in the analysis of environmental samples (such as soil, rock and vegetation digests) and biological samples (such as blood, serum and bone).

With regard to the determination of the ^{31}P and ^{32}S isotopes by ICP-OES the main limitations of analysis lie in spectroscopic interference from the overlap of emission wavelengths. With regard to the determination of ^{31}P emission can be measured at

178.29 nm, 213.62 nm and 214.91 nm.⁵ However, interfering emission originating from Mn, S, Cr and Mo isotopes can be problematic.⁵ In the case of ³²S emission can be measured at 180.73 nm and 182.04 nm.⁵ The average ³¹P and ³²S LOD's exhibited by the ICP-OES technique can be seen in Table 5.

Flame Atomic Absorption Spectroscopy (FAAS)

Up to the late 1970's and early 1980's flame atomic absorption spectroscopy (FAAS) was the most widely used method for the trace analysis of metals.⁴² A radiation source, typically a hollow cathode lamp, is used to emit radiation of a wavelength unique to an analyte of interest. This radiation is directed through a flame atomiser, of variable gaseous composition, into which the sample is introduced. The quantity of radiation transmitted through the flame is measured and absorption by analyte atoms is calculated. This takes place when the radiation passes through a monochromator and hits a photomultiplier.^{1, 3, 42}

Although elemental analysis is now dominated by ICP based techniques, FAAS is still popular for the measurement of metals at the $\mu\text{g l}^{-1}$ level and above. FAAS is also attractive to the analyst as it is a far less expensive technique than ICP-OES or ICP-MS. As with ICP-OES, FAAS measures the presence of metal elements and cannot provide information on isotopic content of a sample. FAAS has difficulties with the measurement of phosphorus and cannot be employed for sulphur. The reason for this is that the emission wavelength of each element is below 200 nm which is outside the main emission region of standard hollow cathode lamps.¹ Under standard FAAS analysis the LOD of phosphorus is therefore very poor although its limit can be improved by employing a graphite furnace. Typical ³¹P and ³²S LOD's exhibited by FAAS are given in Table 5.

A Comparison of Techniques for the Determination of ³¹P and ³²S

Although there are a number of elemental analytical techniques available, with regard to many elements of the periodic table such techniques are complementary rather than

competitive as they exhibit similar LOD's (see Table 5) and dynamic ranges.³ For the measurement of ³¹P and ³²S, however, performance varies quite widely. Average LOD's for these elements, compared between the techniques, can be seen in Table 5.^{1, 3, 4, 42, 100, 141}

Table 5. A Comparison of ³¹P and ³²S Limit of Detection Data for Elemental Analysis Techniques.

Analytical Technique	³¹P LOD (µg l⁻¹)	³²S LOD (µg l⁻¹)
ICP-QMS (Perkin Elmer)⁹⁰	0.01 – 0.1	0.1 – 1
ICP-QMS (P.D. Winship Data, Four Separate Methods - See Sections 2.4.1 to 2.4.7 and 2.5)	0.69 - 14	1.23 – 80
ICP-MS (High Resolution)¹	0.05	0.01
ICP-OES¹	4 – 50	10
FAAS⁴²	50 000 – 75 000	-
GF-AAS⁴	30 – 130	-

2.2. Aims of Research

It was the aim of the research in this chapter to develop methods to tackle instrumental interferences and hence improve the LOD's of the ^{31}P and ^{32}S isotopes by quadrupole based ICP-MS. LOD's of these two isotopes are, comparatively, poor considering the capabilities of this instrument for many elements. The most obvious means of overcoming polyatomic ion interference in the mass spectrum would be the employment of a high resolution ICP-MS instrument; however, as previously discussed this is an expensive approach to elemental analysis. Six methods, via three different approaches, were studied in order to overcome some of the instrumental interferences described in sections 1.2.1 and 2.1. These six methods are described as follows:

Collision Cell Methods

- The determination of $^{31}\text{P}^{16}\text{O}^+$ ($m/z = 47$) and $^{32}\text{S}^{16}\text{O}^+$ ($m/z = 48$) ions formed in a hexapole collision cell incorporating He and O_2 as a buffer gas and reaction gas, respectively, under IKEE conditions.^{4, 33, 59, 79, 83, 90-96}
- The determination of $^{31}\text{P}^{16}\text{O}^+$ ($m/z = 47$) and $^{32}\text{S}^{16}\text{O}^+$ ($m/z = 48$) ions formed in a hexapole collision cell incorporating an O_2 only reaction gas under IKEE conditions.^{4, 33, 59, 79, 83, 90-96}
- The selective removal of polyatomic ions at $m/z = 31$ allowing the measurement of $^{31}\text{P}^+$ ions at their native m/z in a hexapole collision cell incorporating a He buffer gas under KED conditions.¹⁰⁴

Cold Plasma Methods

- The determination of $^{31}\text{P}^{16}\text{O}^+$ ($m/z = 47$) and $^{32}\text{S}^{16}\text{O}^+$ ($m/z = 48$) ions formed within the ICP under “cold/cool plasma” conditions.⁴

- The determination of $^{31}\text{P}^{16}\text{O}^+$ ($m/z = 47$) and $^{32}\text{S}^{16}\text{O}^+$ ($m/z = 48$) ions formed within the ICP under “cold/cool plasma” conditions incorporating an additional O_2 flow through the nebuliser.⁴

Torch Bonnet Method

- The limitation of atmospheric gas entrainment into the ICP ion source and the reduction of polyatomic ion formation at $m/z = 31$ and 32 employing an enclosed ICP source.¹³⁴

2.3. Experimental Details

The typical PQ ExCell ICP-MS instrumental conditions for the work carried out in this and other chapters are described in Table 6. The magnitude of each of the parameters are documented for each individual experiment both within the text section in which it is discussed and Appendix 2 (Tables 54, 56, 59, 64, 69, 72 and 74), Appendix 3 (Tables 76 to 79, 81, 82, 84 and 85), Appendix 4 (Tables 88, 94, 115, 121, 122, 131 and 137) and Appendix 5 (Table 141).

Table 6. A Table of Typical PQ ExCell ICP-MS Instrument Parameters.

Instrument Parameter	Parameter Value
Analyser Pressure	$\approx 10^{-7}$ mBar
Expansion Pressure	1.0 to 3.0 mBar
Nebuliser Pressure	2.6 to 2.8 Bar
Plasma Forward Power	Variable According to the Method Employed
Plasma Reflected Power	< 2 W
Plasma Gas: Cool Flow	12.5 to 13.0 l min ⁻¹
Plasma Gas: Auxilliary Flow	0.80 to 0.90 l min ⁻¹
Plasma Gas: Nebuliser Flow	0.90 to 1.20 l min ⁻¹
Torch Position: Sampling Depth	Variable to Establish Optimum Signal
Torch Position: Vertical	
Torch Position: Horizontal	
Extraction Lens Voltage	-300 V to -900 V
D1 Lens Voltage	-24 to -30 V
L1 Lens Voltage	-10.0 to +5.0 V
L2 Lens Voltage	-130 to -190 V
L3 Lens Voltage	-110 to -200 V
Focus Lens Voltage	+18 to +27 V
Applied Quadrupole Voltage	+1 V
Applied Hexapole Voltage: Standard Mode	-1.97 V
Applied Hexapole Voltage: Collision Cell Mode	+1 V to + 10 V

Any specific instrumental parameters that have been varied as part of these studies are described within the text associated with the work. Any other instrumentation that is employed during the work discussed in this thesis is described in its relevant section as well as associated parameters and their magnitude. Throughout this chapter the various voltage characteristics of the ICP ion source, the hexapole collision cell and the quadrupole mass analyser are stated.

Unless otherwise stated, for each experiment carried out three replicate readings were taken in order to allow the calculation of mean, standard deviation (SD) and relative standard deviation (RSD) data.

2.4. The Development of Methods to Overcome ^{31}P and ^{32}S Isotope Interferences

Six separate approaches to the measurement of ^{31}P and ^{32}S were studied, with the aim of overcoming the spectroscopic interferences previously described, and subsequent quantification experiments were performed, see sections 2.4.1 to 2.4.7. The hexapole collision cell of the PQ ExCell ICP-MS instrument was employed to produce alternate analyte oxide species, $^{31}\text{P}^{16}\text{O}^+$ and $^{32}\text{S}^{16}\text{O}^+$, for measurement at non-interfered m/z 's (as described in sections 2.4.1 and 2.4.2) and to remove interfering ions, $^{14}\text{N}^{16}\text{O}^+\text{H}^+$ and $^{16}\text{O}_2^+$ etc..., at the native m/z (as described in section 2.4.3). Similar to approaches using the collision cell, “cold/cool plasma” conditions were employed in order to produce the $^{31}\text{P}^{16}\text{O}^+$ and $^{32}\text{S}^{16}\text{O}^+$ ions in the ICP for measurement at $m/z = 47$ and 48. The introduction of additional oxygen to the ICP during analysis with “cold/cool plasma” conditions was also studied with the aim of maximising analyte oxide ion formation. Additionally, the use of an ICP torch bonnet was studied with the aim of reducing the entrainment of the gaseous atmosphere of the torch box into the plasma. By limiting the quantity of entrained gas it may be possible to reduce the formation of polyatomic ions based on nitrogen and oxygen.

2.4.1. Method 1: The Determination of $^{31}\text{P}^{16}\text{O}^+$ and $^{32}\text{S}^{16}\text{O}^+$ Ions in a Collision Cell Incorporating He and O_2 Under IKEE Conditions

Initial work was carried out into the determination of ^{31}P and ^{32}S isotopes by the formation and measurement of $^{31}\text{P}^{16}\text{O}^+$ ($m/z = 47$) and $^{32}\text{S}^{16}\text{O}^+$ ($m/z = 48$) ions in the hexapole collision cell incorporating He and O_2 collision/reaction gases. Previous research into collision and dynamic reaction cells has highlighted the formation of P and S oxide ions for isotope measurement. The formation of these oxide ion species can be appreciated by study of the $^{31}\text{P}^+$, $^{32}\text{S}^+$, $^{47,48}\text{Ti}^+$ and polyatomic ion reaction data, see Table 7.⁹⁰

Table 7. Reaction Data for Oxidation of $^{31}\text{P}^+$, $^{32}\text{S}^+$, $^{47}\text{Ti}^+$ and Associated Polyatomic Ions.

Reaction	Reaction Enthalpy Change, ΔH_r (kcal mol$^{-1}$)	Reaction Rate Constant, k_r (molecule$^{-1}$ cm3 s$^{-1}$)
$\text{P}^+ + \text{O}_2 \rightarrow \text{PO}^+ + \text{O}$	-71.4	5.3×10^{-10}
$\text{S}^+ + \text{O}_2 \rightarrow \text{SO}^+ + \text{O}$	-6.2	1.8×10^{-11}
$\text{NO}^+ + \text{O}_2 \rightarrow \text{NO}_2^+ + \text{O}$	57.4	$< 1.0 \times 10^{-11}$ (No Reaction)
$\text{NOH}^+ + \text{O}_2 \rightarrow \text{NO}_2\text{H}^+ + \text{O}$	19.3	No Data
$\text{Ti}^+ + \text{O}_2 \rightarrow \text{TiO}^+ + \text{O}$	-46.1	5.0×10^{-10}

According to the reaction data of Table 7 the formation of $^{31}\text{P}^{16}\text{O}^+$ readily takes place in the presence of $^{31}\text{P}^+$ and O_2 as it is strongly exothermic ($\Delta H_r = -71.4$ kcal mol $^{-1}$) and proceeds fairly quickly ($k_r = 5.3 \times 10^{-10}$ molecule $^{-1}$ cm 3 s $^{-1}$). In the case of $^{32}\text{S}^{16}\text{O}^+$, formation does not take place as readily or at as fast a rate ($\Delta H_r = -6.2$ kcal mol $^{-1}$ and $k_r = 1.8 \times 10^{-11}$ molecule $^{-1}$ cm 3 s $^{-1}$).⁹⁰ Oxidation reactions for the polyatomic ions present at $m/z = 31$ and 32 with O_2 are endothermic and do not take place under thermal conditions. On the formation of P and S oxide species with measurement at $m/z = 47$ and 48 an issue that would normally have to be considered is interference from the presence of contaminating $^{47,48}\text{Ti}^+$ ions. However, Ti also readily reacts with O_2 to form the oxide species at $m/z = 63$ and 64 ($\Delta H_r = -46.1$ kcal mol $^{-1}$ and $k_r = 5.0 \times 10^{-10}$ molecule $^{-1}$ cm 3 s $^{-1}$) so Ti contamination is not a significant problem.

On the introduction of O_2 gas into the collision cell two effects of interaction on the ion beam passing through the hexapole are recognised. The result of collision of O_2 molecules with the $^{31}\text{P}^+$ and $^{32}\text{S}^+$ ions can either be the successful formation of analyte oxide species or no reaction leaving the interacting species in their original state. If there is no reaction between the species then the collision will lead to a degree of scattering of the ionic species. For use of the collision cell, the hexapole must be pressurised. Due to the size of the O_2 molecule and the limitation of control of gases entering the cell to 0.1 ml min $^{-1}$ then at this stage of research it was believed that a buffer gas, in this case He, would be required in order to maintain pressurisation whilst not relying on the O_2 reaction gas that may lead to a detrimental degree of analyte ion scattering.

The variation of the collision/reaction gas flows in the cell revealed optimum flows of 0.2 ml min^{-1} and 0.3 ml min^{-1} for He and O₂, respectively. Whilst employing these optimum gas flows, IKEE was studied to determine whether or not the formation of the desired ionic oxide species could be maximised for the improvement of ³¹P and ³²S LOD. Normally the applied hexapole (collision cell) voltage is negative compared to the quadrupole voltage; this allows a maximum transmission of ions. Under IKEE conditions an opposite polarity is in place (hexapole voltage positive compared to quadrupole voltage), here analyte ions are slowed on entrance to the hexapole allowing an increased residence time in the cell. As residence time increases more collisions take place between these ions and the He and O₂ present in the cell.

Experimental Details

Whilst incorporating the He and O₂ gas flows into the hexapole, described in this section, the $m/z = 31, 32, 47$ and 48 signals (corresponding to the ³¹P⁺, ³²S⁺, ³¹P¹⁶O⁺ and ³²S¹⁶O⁺ ions) were studied during the analysis of the following samples:

- 2 % HNO₃ (as a blank solution).
- 1000 µg l⁻¹ P in a 2 % HNO₃ matrix.
- 1000 µg l⁻¹ S in a 2 % HNO₃ matrix.

During this study the applied hexapole voltage (V_h) was varied with respect to the plasma potential (V_p), which is assumed to be constant at approximately +9 V, in order to determine whether an IKEE would be beneficial to the formation of ionic P and S oxide species. The voltage applied to the mass analyser quadrupole (V_q) was set at a constant value of +1 V (previous experimentation has shown that the variation of V_q contributes little to IKEE). An unshielded ICP torch was employed during this analysis and it should be noted that if a shielded plasma was used the data obtained would be associated with different V_h 's. The general instrumental conditions under which this work was carried out can be seen in Table 54 (Appendix 2).

Results and Discussion

The data for this study are given in Table 55 (Appendix 2). Plots for ^{31}P analysis are given in Figures 5 and 6 whilst plots for ^{32}S can be seen in Figures 7 and 8.

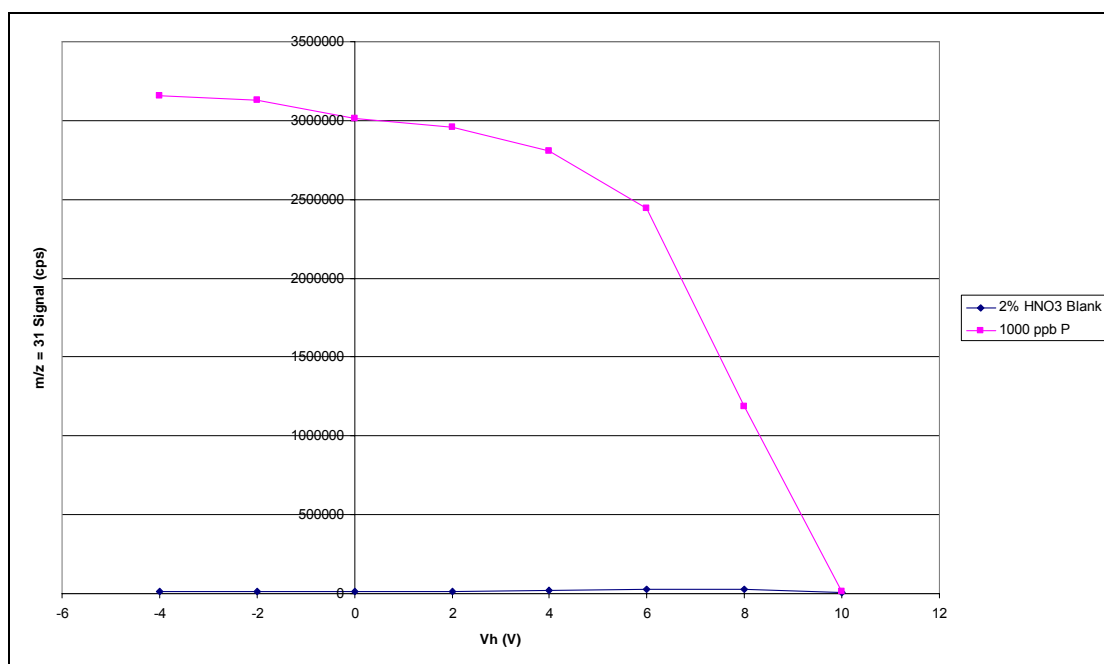


Figure 5. A Graph Comparing $m/z = 31$ Signal with V_h for the Analysis of 2% HNO_3 Blank and 1000 $\mu\text{g l}^{-1}$ P Solutions (Reaction Gases: $\text{He} = 0.2 \text{ ml min}^{-1}$ and $\text{O}_2 = 0.3 \text{ ml min}^{-1}$) ($V_q = +1 \text{ V}$).

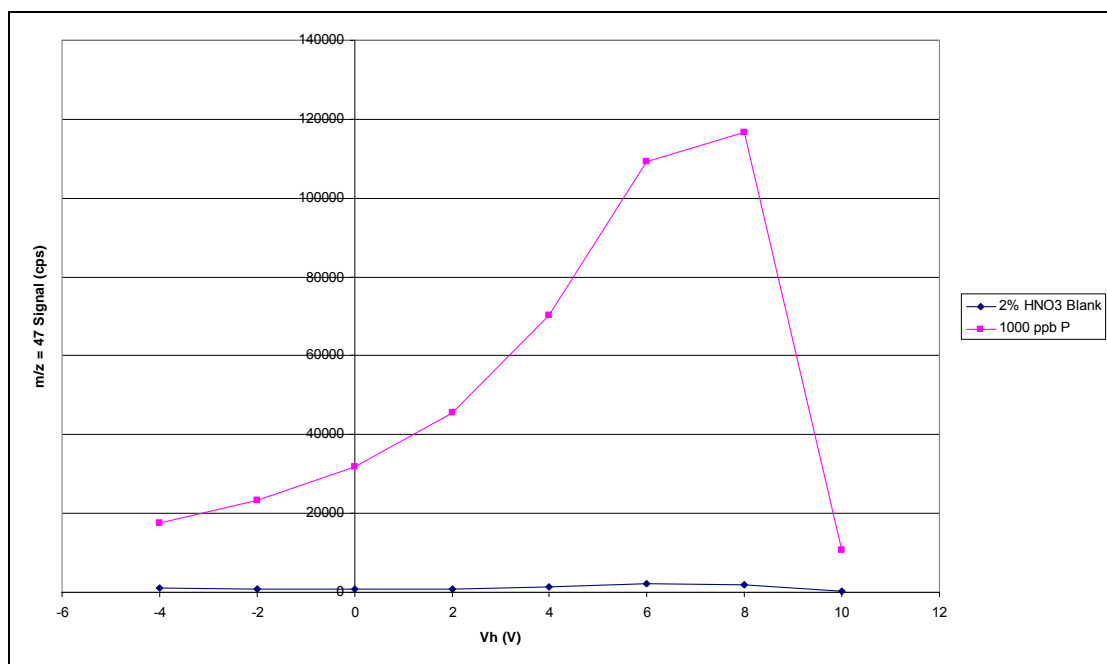


Figure 6. A Graph Comparing $m/z = 47$ Signal with V_h for the Analysis of 2% HNO₃ Blank and 1000 $\mu\text{g l}^{-1}$ P Solutions (Reaction Gases: He = 0.2 ml min⁻¹ and O₂ = 0.3 ml min⁻¹) ($V_q = +1$ V).

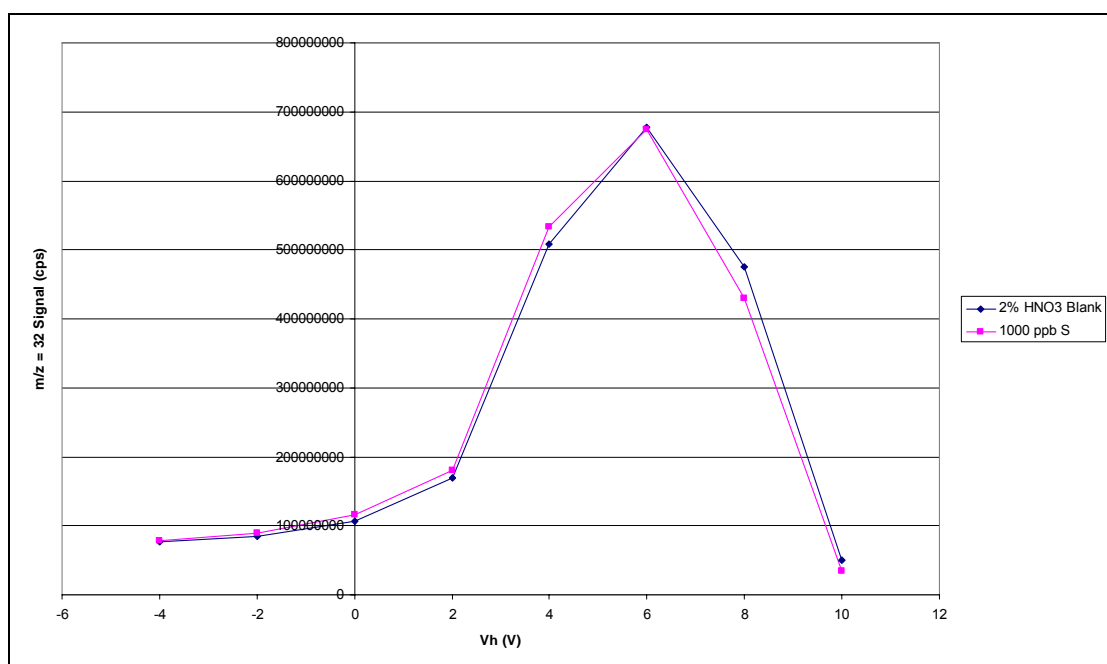


Figure 7. A Graph Comparing $m/z = 32$ Signal with V_h for the Analysis of 2% HNO₃ Blank and 1000 $\mu\text{g l}^{-1}$ S Solutions (Reaction Gases: He = 0.2 ml min⁻¹ and O₂ = 0.3 ml min⁻¹) ($V_q = +1$).

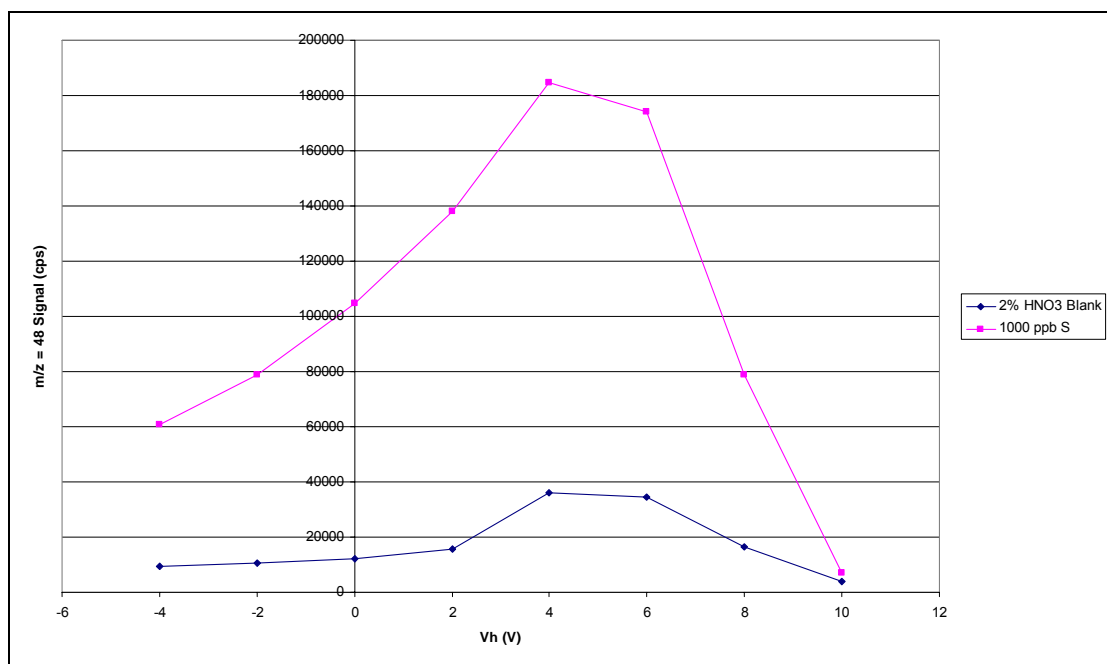


Figure 8. A Graph Comparing $m/z = 48$ Signal with V_h for the Analysis of 2% HNO₃ Blank and 1000 $\mu\text{g l}^{-1}$ S Solutions (Reaction Gases: He = 0.2 ml min⁻¹ and O₂ = 0.3 ml min⁻¹) ($V_q = +1$ V).

Figure 5 shows the variation of $m/z = 31$ signal with V_h during the analysis of 2 % HNO₃ blank and 1000 $\mu\text{g l}^{-1}$ P solutions. For both solutions analysed the $m/z = 31$ signal decreased as V_h tended towards a potential similar to that of the plasma potential ($\approx +9$ V). The intensity decrease of the $m/z = 31$ signal observed could be best described in the two following sections.

- The $m/z = 31$ decrease between $V_h = -4$ V and +8 V.
- The $m/z = 31$ decrease between $V_h = +8$ V and +10 V.

The signal decrease between $V_h = -4$ V and +8 V can be attributed to the loss of $^{31}\text{P}^+$ ions to the formation of $^{31}\text{P}^{16}\text{O}^+$, collisional scattering and the elimination of ions from the hexapole, via the vacuum pump, following sufficient collisions with the He and O₂ collision/reaction gases to reduce momentum. Beyond $V_h = +8$ V the signal plummeted, the reason for this was that the IKEE conditions were such that the majority of ions entering the hexapole were slowed sufficiently to result in full thermalisation and removal via the vacuum pump.

It should be noted here that there was a significant difference in signal intensity between the two samples, i.e. the presence of $1000 \mu\text{g l}^{-1}$ P produced a signal that was highly elevated above the $m/z = 31$ signal background. However, the mean background signal (arising from the 2 % HNO_3 blank solution) between $V_h = -4$ V and $+8$ V was approximately 15 000 ion counts per second (cps) which is very high compared to that observed at many other m/z 's.

Figure 6 shows the variation in $m/z = 47$ signal with V_h during the analysis of 2 % HNO_3 blank and $1000 \mu\text{g l}^{-1}$ P solutions. For both of these solutions analysed the $m/z = 47$ signal increased to an optimum value as V_h approached a potential similar to the plasma potential ($\approx +9$ V). Beyond this optimum value the $m/z = 47$ signal plummeted to approximately one tenth of the signal intensity. Similar to the $m/z = 31$ data in Figure 5, the $m/z = 47$ signal for the $1000 \mu\text{g l}^{-1}$ P solution was highly elevated above the $m/z = 47$ signal background (that is a more reasonable mean signal in the order of hundreds of ion counts per second). This experiment showed that IKEE can vary the degree of $^{31}\text{P}^{16}\text{O}^+$ ion formation enormously on the introduction of He and O_2 collision/reaction gases to the collision cell.

To describe the data in Figure 6 the graph can be divided into the following two sections.

- The $m/z = 47$ signal increase between $V_h = -2$ V and $+8$ V.
- The $m/z = 47$ signal decrease between $V_h = +8$ V and $+10$ V.

For both 2 % HNO_3 blank and $1000 \mu\text{g l}^{-1}$ P solutions, the signal increase between $V_h = -2$ V and $+8$ V was attributed to the formation of $^{31}\text{P}^{16}\text{O}^+$ ions. An increasing V_h resulted in the slowing of ions entering the cell leading to a greater number of collisions with the collision/reaction gases and therefore an increase in the formation of the $^{31}\text{P}^{16}\text{O}^+$ ion.⁸³ Similar to the graph in Figure 5, beyond $V_h = +8$ V there was a severe drop in $m/z = 47$ signal. Such a drop was attributed to the ions entering the hexapole becoming fully thermalised so they do not have the momentum to proceed and are removed via the vacuum pump.

Figures 5 and 6 show that with regard to IKEE the formation of $^{31}\text{P}^{16}\text{O}^+$ ($m/z = 47$) ions from $^{31}\text{P}^+$ and O_2 within a collision cell proceeded at an optimum V_h of +8 V with respect to V_p for an unshielded ICP torch. What should also be noted through the comparison of ion counts between Figures 5 and 6 is that comparatively little $^{31}\text{P}^{16}\text{O}^+$ was formed considering the concentration of $^{31}\text{P}^+$ ions available. It can be concluded from this data that the oxide ion formation resulting from collision cell ion-molecule reaction was particularly inefficient.

Figure 7 shows the variation in $m/z = 32$ signal with V_h during the analysis of 2 % HNO_3 and 1000 $\mu\text{g l}^{-1}$ S solutions. Three factors required consideration with regard to a description of this graph. The first factor was the intensity of signals generated during this analysis, being in the order of 10^8 cps. Secondly there was little difference in signal intensity over the V_h range studied between both sample solutions. Finally the shape of both plots in this graph required consideration.

The exceptionally high $m/z = 32$ signal for both solutions studied, well into the analogue range of the detector, implies that a very high number of ions were being transmitted through the hexapole and quadrupole. This suggests a very high level of spectroscopic interference, i.e. a large presence of the $^{16}\text{O}_2^+$ ion.^{90, 92, 100} The fact that the signal accrued from both sample solutions was very similar means that the presence of 1000 $\mu\text{g l}^{-1}$ S did not elevate the signal above the background. Therefore the $^{32}\text{S}^+$ ion did not dominate $m/z = 32$ at any point during the analysis.

For both solutions analysed the $m/z = 32$ signal data was best described by separating it into the following two sections.

- The $m/z = 32$ signal increase between $V_h = -4$ V and +6 V.
- The $m/z = 32$ signal decrease between $V_h = +6$ V and +10 V.

The $m/z = 32$ signal behaviour between $V_h = -4$ V and +10 V requires a more in depth discussion than previously in this section as there are two potential explanations that could lead to the optimum signal observed at $V_h = +6$ V. As the $m/z = 32$ signal over

the range of $V_h = -4$ V to $+6$ V is in the order of 100 million to 700 million cps, i.e. detected well into the analogue region of the detector, then it can be safely said that the dominant ion giving rise to these signals is $^{16}\text{O}_2^+$. With regard to this plot the question, therefore, is not what the ion species is but why its intensity increased and then decreased over the range.

One explanation for the signal enhancement in the first section of this graph is that the increase in V_h slowed certain ionic species, transmitted through the hexapole, resulting in charge transfer reactions with the O_2 reaction gas molecules that lead to their ionisation. However, this theory relies on a significant presence of an ionic charge donating species. To eliminate a charge transfer process with O_2 as an explanation for the enhancement in signal with V_h the mass spectrum survey data, taken at the time of the analysis, was studied (see Figure 9). As can be seen in Figure 9 there were no peaks in the background mass spectrum that indicate the presence of any species that are not typically observed (it should be recognised that the absence of peaks at $m/z = 40$ and 80 , i.e. $^{40}\text{Ar}^+$ and $^{40}\text{Ar}_2^+$ ion signals, is due to the restriction of measurement by the instrument software to prolong the detector lifetime). This can rule out a contamination issue so the only alternative, along this line of thinking, could be an interaction with a native polyatomic ion though this seems unlikely.

A more realistic explanation for the enhanced $m/z = 32$ signal with V_h is an optimisation of IKEE conditions with regard to transmission of the ICP formed $^{16}\text{O}_2^+$ ion. Slowing the $^{16}\text{O}_2^+$ ions entering the hexapole, by increasing V_h with respect to V_p , would lead to collisions with the collision cell species that are less energetic in nature. Such collisions would result in a lower degree of ion scattering than when ICP formed ions are introduced with a greater momentum.

As described previously, beyond $V_h = +6$ V the IKEE conditions are such that the ions entering the hexapole were fully thermalised and removed via the vacuum pump.

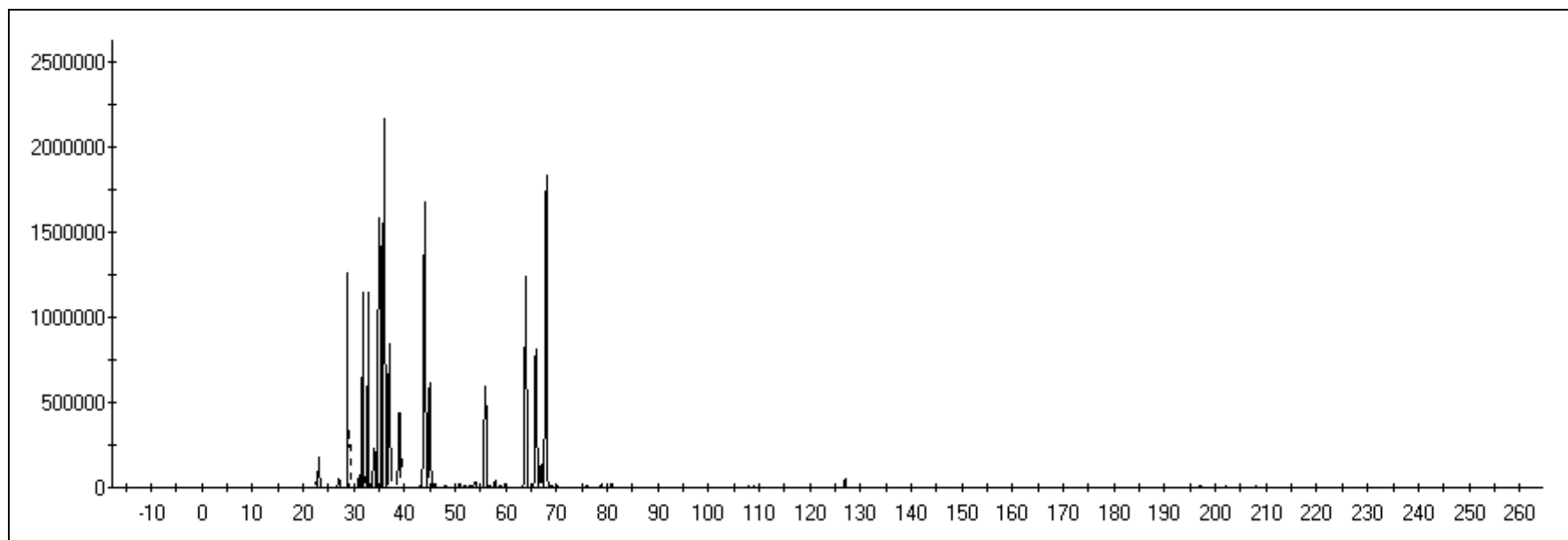


Figure 9. A Survey Data Mass Spectrum Generated During the Method 1 IKEE Experimental Work.

Figure 8 shows the variation in $m/z = 48$ signal with V_h during the analysis of 2 % HNO_3 blank and $1000 \mu\text{g l}^{-1}$ S solutions. For both solutions analysed the $m/z = 48$ signal increased to an optimum intensity, at $V_h = +4 \text{ V}$, and then decreased as V_h increased further. Here there was good separation between the signals of the two sample solutions allowing differentiation between background and $1000 \mu\text{g l}^{-1}$ S.

Similar to the graph concerning $^{31}\text{P}^{16}\text{O}^+$ ion formation the plots in Figure 8 can be split into the following two sections.

- The $m/z = 48$ signal increase between $V_h = -4 \text{ V}$ and $+4 \text{ V}$.
- The $m/z = 48$ signal decrease between $V_h = +4 \text{ V}$ and $+10 \text{ V}$.

In the case of the 2 % HNO_3 solution plot these sections can be described by the IKEE process, a positive slowing of the ions passing through the cell up to the point where they are slowed too much and then eliminated. However, there may be a complication in terms of the species that result in the enhanced $m/z = 48$ signal between $V_h = +2 \text{ V}$ and $+8 \text{ V}$. It is possible that the increase in signal in this V_h range is due to the oxidation of sulphur that was present in contaminated HNO_3 . What is more likely, however, is that the conditions in the hexapole are right for the formation of ozone ions ($^{16}\text{O}_3^+$, $m/z = 48$), this is an additional spectroscopic interference.

In the case of the $1000 \mu\text{g l}^{-1}$ S solution plot, again, the two sections can be described by IKEE in terms of the relative increase and decrease in signal. Here the optimum V_h range ($+4 \text{ V}$ to $+6 \text{ V}$) is the point at which the formation of $^{32}\text{S}^{16}\text{O}^+$ is enhanced. However, considering the trends recognised in the 2 % HNO_3 plot, there may be a contribution to the $m/z = 48$ signal in the form of interfering $^{16}\text{O}_3^+$.

It should be noted here that unlike the graphs for the $1000 \mu\text{g l}^{-1}$ P solution (Figures 5 and 6) a comparison of ion counts between Figures 7 and 8 cannot be commented on fairly, for the purpose of assessing reaction efficiency, as data for the determination of $^{32}\text{S}^+$ cannot be separated from that of $^{16}\text{O}_2^+$. Assuming that there is some similarity between the behaviour of ^{31}P and ^{32}S chemistries then it could be postulated that $^{32}\text{S}^{16}\text{O}^+$ ion formation by this method is also inefficient.

2.4.2. Method 2: The Determination of $^{31}\text{P}^{16}\text{O}^+$ and $^{32}\text{S}^{16}\text{O}^+$ Ions in a Collision Cell Incorporating O_2 Only Under IKEE Conditions

The work of section 2.4.1 was furthered through the study of the same samples under IKEE conditions but only incorporating an O_2 reaction gas. Such work would determine the necessity of an additional He collision gas flow to promote the thermalisation of ions and ion-molecule reaction. Again, the formation of the $^{31}\text{P}^{16}\text{O}^+$ and $^{32}\text{S}^{16}\text{O}^+$ ions was measured for the quantification of the ^{31}P and ^{32}S isotopes.

Experimental Details

An optimum O_2 reaction gas flow was determined at 0.3 ml min^{-1} for the formation of the ionic P and S oxide species. Mass spectrum signals at $m/z = 31, 32, 47$ and 48 were studied when varying V_h with respect to V_p whilst maintaining a constant V_q of $+1 \text{ V}$. General experimental conditions can be seen in Table 56 (Appendix 2).

Results and Discussion

The data generated are given in Table 57 (Appendix 2). This data was evaluated via a series of graphs constructed to establish the presence of trends. Plots for ^{31}P analysis are given in Figures 10 and 11 whilst plots for ^{32}S analysis can be seen in Figures 12 and 13.

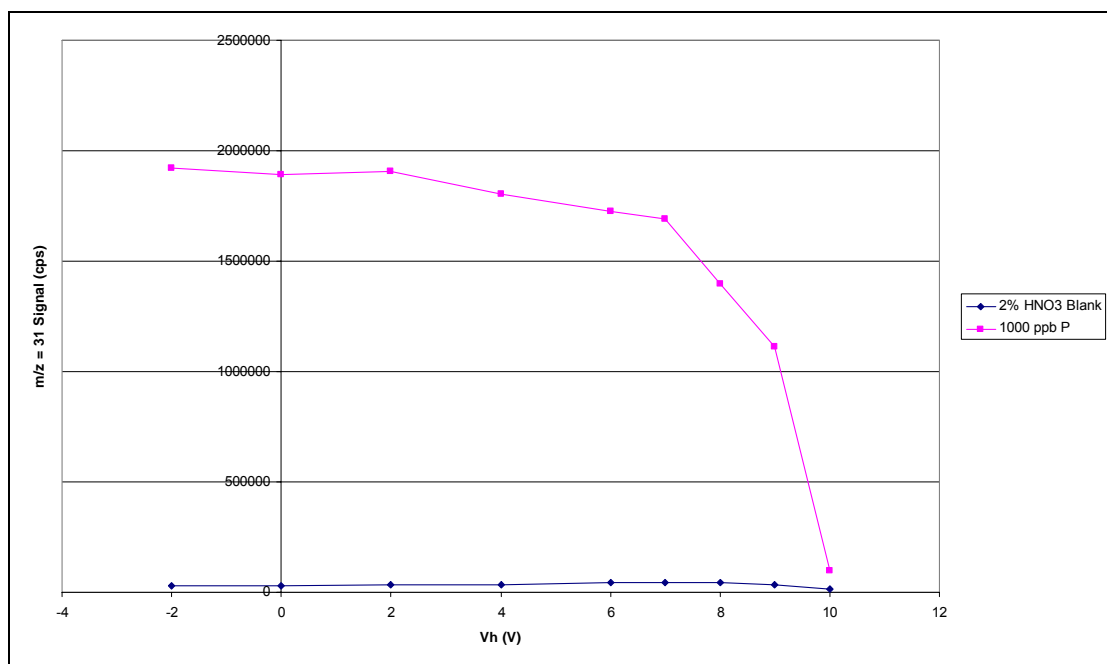


Figure 10. A Graph Comparing $m/z = 31$ Signal with V_h for the Analysis of 2% HNO₃ Blank and 1000 $\mu\text{g l}^{-1}$ P Solutions (Reaction Gas: O₂ = 0.3 ml min⁻¹) ($V_q = +1$ V).

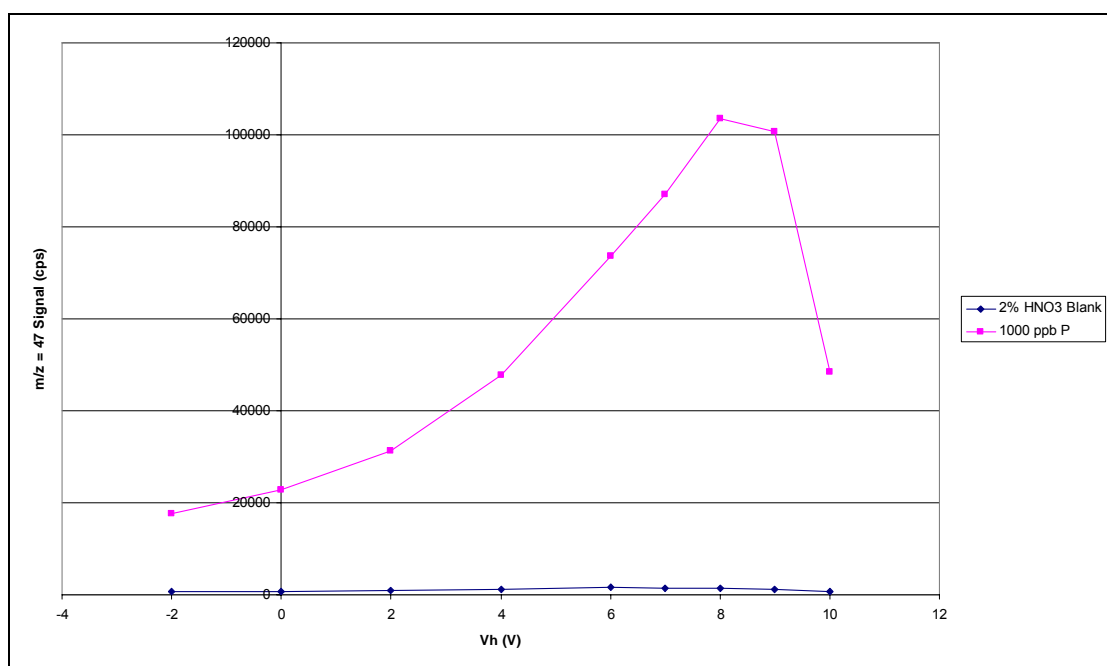


Figure 11. A Graph Comparing $m/z = 47$ Signal with V_h for the Analysis of 2% HNO₃ Blank and 1000 $\mu\text{g l}^{-1}$ P Solutions (Reaction Gas: O₂ = 0.3 ml min⁻¹) ($V_q = +1$ V).

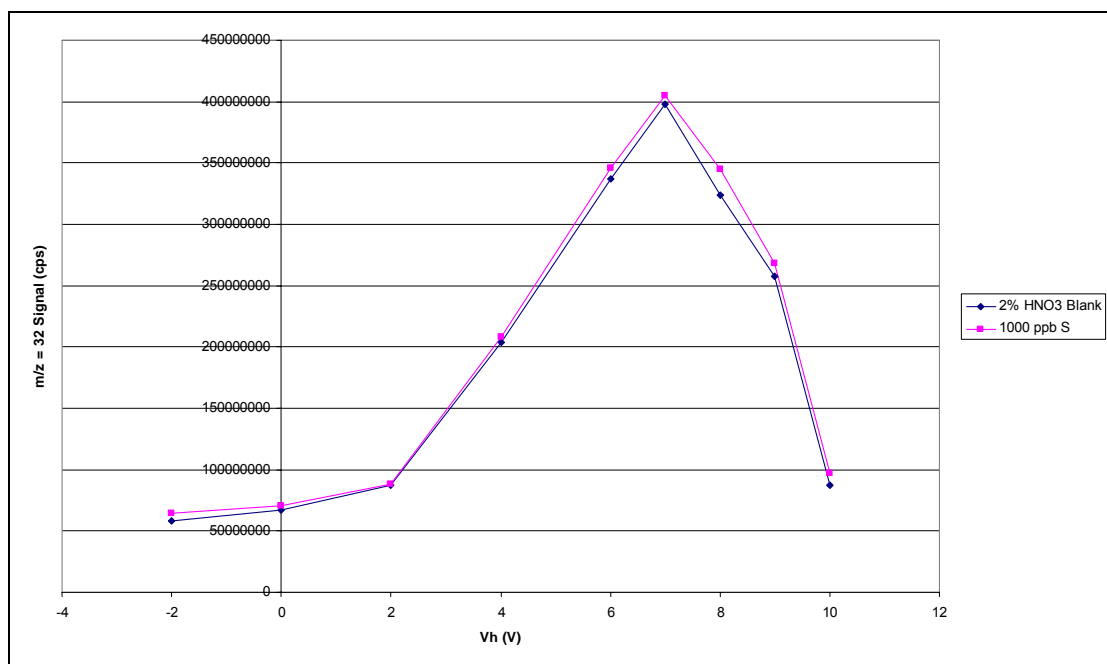


Figure 12. A Graph Comparing $m/z = 32$ Signal with V_h for the Analysis of 2% HNO₃ Blank and 1000 $\mu\text{g l}^{-1}$ S Solutions (Reaction Gas: O₂ = 0.3 ml min⁻¹) ($V_q = +1$ V).

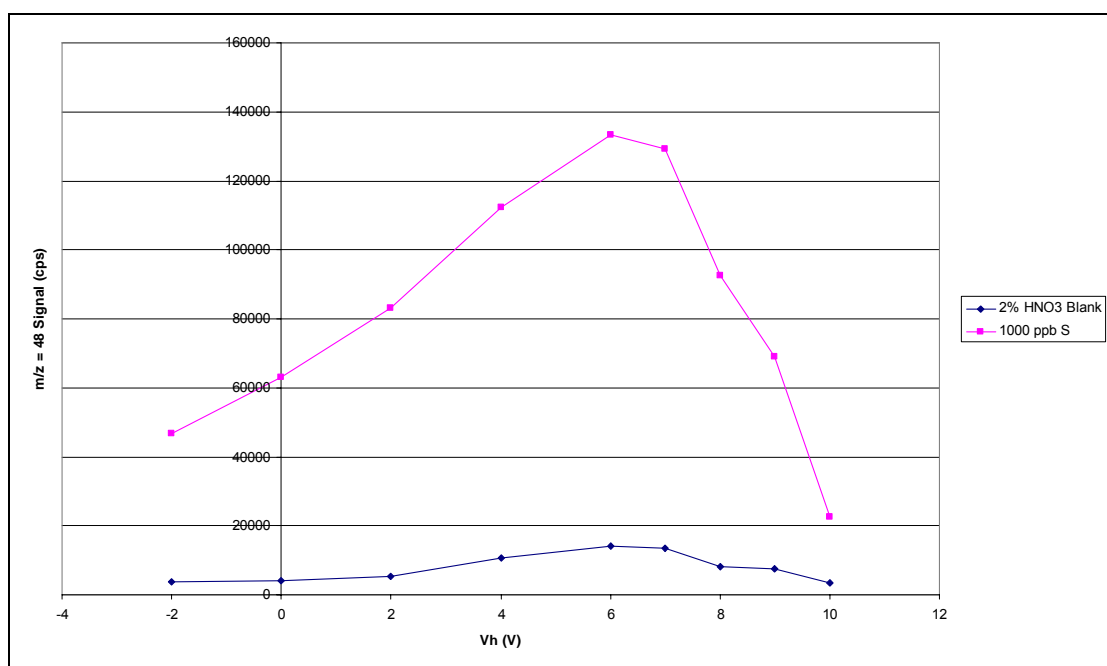


Figure 13. A Graph Comparing $m/z = 48$ Signal with V_h for the Analysis of 2% HNO₃ Blank and 1000 $\mu\text{g l}^{-1}$ S Solutions (Reaction Gas: O₂ = 0.3 ml min⁻¹) ($V_q = +1$ V).

Figure 10 shows the variation in $m/z = 31$ signal with V_h for the analysis of 2 % HNO_3 blank and 1000 $\mu\text{g l}^{-1}$ P solutions. For both solutions analysed the $m/z = 31$ signal decreased as V_h increased. Similar to Figure 5 (section 2.4.1) the $m/z = 31$ signal variation is best explained by reference to the following two sections:

- The $m/z = 31$ signal decrease between $V_h = -2$ V and +7 V.
- The $m/z = 31$ signal decrease between $V_h = +7$ V and +10 V.

The signal decrease between $V_h = -2$ V and +7 V was attributed to both the loss of $^{31}\text{P}^+$ to the formation of $^{31}\text{P}^{16}\text{O}^+$ ions and through collisional scattering as a result of collision with O_2 molecules within the hexapole and elimination following the reduction of momentum with thermalisation. After $V_h = +7$ V the signal dropped in two sections. Between $V_h = +7$ V and +9 V the signal was reduced to approximately half of its intensity at $V_h = +7$ V. Beyond $V_h = +9$ V the signal plummeted. The reason for this reduction beyond $V_h = +7$ V was that the vacuum pump elimination following full thermalisation of ions had become the dominant effect within the collision cell.

A significant difference existed between signals of the sample solutions, i.e. the presence of 1000 $\mu\text{g l}^{-1}$ P provided a signal significantly elevated above the background. Again, the background signal arising from analysis of the 2 % HNO_3 solution was approximately 35 000 cps which highlights the inability to measure ^{31}P at trace levels due to the presence of nitrogen, oxygen and hydrogen based polyatomic ions.

Figure 11 shows the variation in $m/z = 47$ signal with V_h for the analysis of the blank and P solutions. Showing an almost identical trend to that in Figure 6, both plots can be discussed in terms of two regions with the optimum $^{31}\text{P}^{16}\text{O}^+$ formation at $V_h = +8$ V, i.e:

- The $m/z = 47$ signal increase between $V_h = -2$ V and +8 V.
- The $m/z = 47$ signal decrease between $V_h = +8$ V and +10 V.

For both solutions, the signal increase between $V_h = -2$ V and $+8$ V was attributed to the formation of $^{31}\text{P}^{16}\text{O}^+$ ions. An increasing V_h was responsible for the slowing of ions entering the hexapole. This reduced ion momentum led to a greater number of collisions with the O_2 reaction gas molecules and therefore an increase in the formation of the $^{31}\text{P}^{16}\text{O}^+$ ion.⁸³ As described previously the severe signal reduction, beyond $V_h = +8$ V, was attributed to the thermalisation of ions within the hexapole. Again the signals generated from both samples are substantially different due to the vast difference in P concentration between sample solutions.

The data generated with the O_2 reaction gas alone is almost identical to the same analysis incorporating a combination of He and O_2 collision/reaction gases (see section 2.4.1). After studying the data associated with Figures 6 and 11 the necessity for He collision gas in the cell, in this case, could be questioned.

Figure 12 shows the variation of $m/z = 32$ signal with V_h for the study of 2 % HNO_3 and $1000 \mu\text{g l}^{-1}$ S solutions. Similar to the plot in Figure 7 (see section 2.4.1) the $m/z = 32$ signals for both solutions were abnormally high, increasing to an optimum, and then decreasing over the range of voltages applied to the hexapole collision cell.

Again, the signal intensity at each V_h value suggests a high degree of spectroscopic interference from the $^{16}\text{O}_2^+$ ion that dominates $m/z = 32$. In this case the optimum V_h value for both samples was $+7$ V, higher than for the same analysis incorporating He as well where the optimum was $+6$ V. As described in section 2.4.1, the most likely cause of the increase in signal up to $V_h = +7$ V was differing IKEE conditions that resulted in variations in the degree of ion scattering between species within the hexapole. Beyond $V_h = +7$ V the loss of signal was the result of vacuum pump elimination following ion thermalisation and reduction in momentum.

Figure 13 shows the variation of $m/z = 48$ signal with V_h for the analysis of 2 % HNO_3 blank and $1000 \mu\text{g l}^{-1}$ S solutions. This graph has almost identical features to that seen in Figure 8 where $m/z = 48$ signal increases with V_h to an optimum value

before decreasing. For the sake of this discussion the two plots were, again, considered as two regions, these being:

- The $m/z = 48$ signal increase between $V_h = -2$ V and $+6$ V.
- The $m/z = 48$ signal decrease between $V_h = +6$ V and $+10$ V.

Between $V_h = -2$ V and $+6$ V the signal increase arose due to the IKEE enhanced formation of the $^{32}\text{S}^{16}\text{O}^+$ ion. A slight signal reduction was observed between $V_h = +6$ V and $+7$ V, this was similar to that in Figure 8 where there was a short spread of optimum V_h values. As described previously, beyond $V_h = +7$ V the signal for both samples plummeted due to the reduced momentum of ions within the hexapole and their inability to exit.

From the data accrued during the work for this method, the maximised formation of analyte oxide ions by hexapole collision cell ICP-MS incorporating IKEE and O_2 alone as a reaction gas appeared to be a promising approach to the quantitative determination of ^{31}P and ^{32}S . At this point in the study the question of whether the presence of a He collision gas in the cell is beneficial to the analysis required an answer. It could be said that He is not required as the formation of analyte oxide ions is successful in its absence. However, close examination of the data revealed that a greater oxide ion signal, for both elements of interest, was being generated when He was present. In order to answer this question, and determine whether the difference in signal could be explained by day-to-day instrumental drift, ratios of analyte oxide ion signal to analyte ion signal were calculated for both ^{31}P and ^{32}S . These ratios are compared in Table 8.

Table 8. Analyte Oxide Ion Signal to Analyte Ion Signal Ratio for Data Generated During IKEE He/O₂ and O₂ Only ³¹P¹⁶O⁺ and ³²S¹⁶O⁺ Formation Maximisation Experiments.

Sample	V _h (V)	³¹ P ¹⁶ O ⁺ / ³¹ P ⁺ Ratio (He/O ₂)	³² S ¹⁶ O ⁺ / ³² S ⁺ Ratio (He/O ₂)	³¹ P ¹⁶ O ⁺ / ³¹ P ⁺ Ratio (O ₂)	³² S ¹⁶ O ⁺ / ³² S ⁺ Ratio (O ₂)
1000 µg I ⁻¹ P	8	0.098	-	0.074	-
1000 µg I ⁻¹ S	4	-	3.46 x 10 ⁻⁴	-	-
	6	-	-	-	3.86 x 10 ⁻⁴

From the data in Table 8 there seems to be very little difference in analyte oxide ion signal to analyte ion ratio between the two methods of differing gaseous composition for both ³¹P and ³²S analysis. The ratios calculated for ³¹P analysis are similar as are those calculated for ³²S analysis. As this is the case it can be said that the presence of the He collision gas in the cell was unnecessary.

Previously He has been employed as a collision gas in ICP-MS collision and dynamic reaction cells for two reasons. Firstly He has been used to aid the thermalisation of ions within a cell and bring about any desired ion-molecule reactions. Used in conjunction with H₂ and/or Xe, He can aid in promoting the attenuation of certain spectroscopic interferences.^{59, 91, 92} Secondly He has been used as the inert gas required to pressurise a collision cell when establishing a KED for the selective removal of certain unwanted cell formed polyatomic ion species.¹⁰⁴

In the former case the assumption is that He was required as a buffer gas to contribute a greater degree of pressure to the cell and promote thermalisation allowing the desired reaction processes to take place as efficiently as possible. The main reason, therefore, why the presence of He in the collision cell with O₂ is questionable is that it would appear that O₂ alone is sufficient to bring about thermalisation. If this is the case then the only question that remains is why there is a difference in signal between the analysis with an O₂ reaction gas and the same analysis with an O₂/He collision/reaction gas. As both series of analysis provide similar oxide ion to analyte ion ratios then the differences in signal between the two are most likely due to day to day instrumental drift. Instrumental drift is also reflected in the signal data for the

analysis of the 2 % HNO₃ solution where the background signal for the O₂ only analysis is twice that of the O₂/He analysis.

As the presence of He as a buffer gas was dismissed, of the two methods the O₂ gas only approach was further studied in order to determine the method LOD's for the two isotopes of interest. A series of P and S standard solutions were analysed employing the optimum conditions described in section 2.4.2. The data are given in Table 58 (Appendix 2) and graphs are presented in Figure 14.

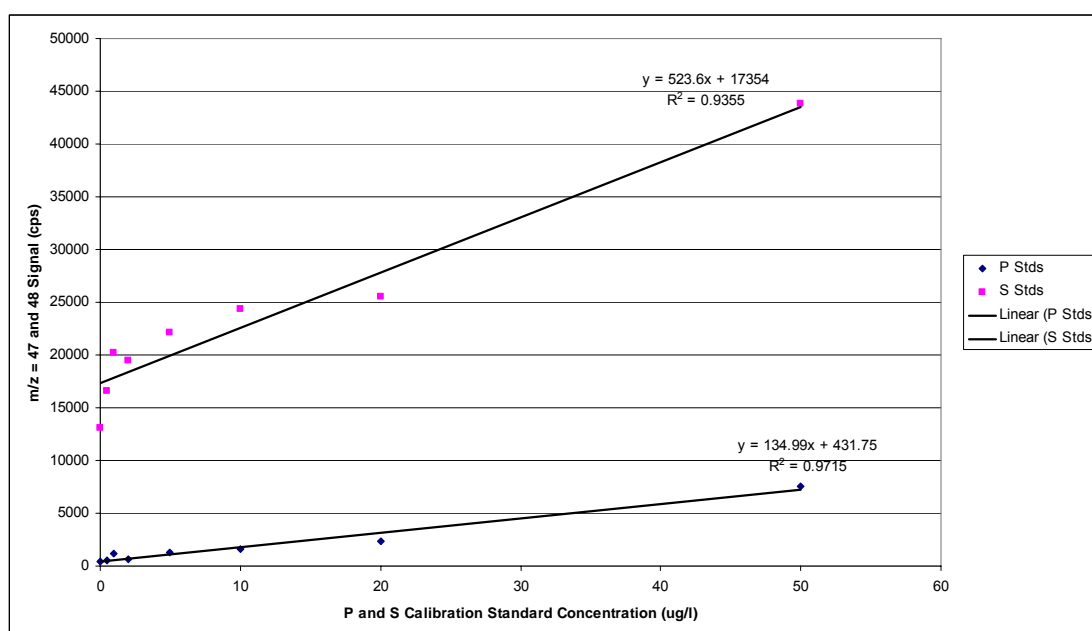


Figure 14. Graphs Exhibiting Signal Response as a Function of Concentration for the ³¹P and ³²S Isotopes Employing ‘Method 2’.

Linear curves were constructed for the isotopes of interest ($R^2 = 0.9715$ and 0.9355 for ³¹P and ³²S isotopes respectively). Two characteristics of these plots must be considered when evaluating this protocol for the determination of ³¹P and ³²S isotopes. Firstly the signal background for the 2 % HNO₃ blank solution and secondly the R^2 value of the curve itself.

The background signal at $m/z = 47$ is in the order of hundreds of ion counts per second. Such a background signal suggests the presence of a small degree of P contamination (or residual ^{47}Ti contamination), however, this is far more acceptable than the background signals typically observed at $m/z = 31$ (in the order of tens of thousands of ion counts per second). The R^2 value of the P curve (0.9715) describes a linear response over the range of P standard solutions studied. This suggests that the degree of formation of the $^{31}\text{P}^{16}\text{O}^+$ ion is consistent between standards and dependent on ^{31}P concentration. ^{31}P LOD's under method 2 conditions were calculated to be $0.69\ \mu\text{g l}^{-1}$ to $9.50\ \mu\text{g l}^{-1}$. These LOD calculations are fully described in section 2.5.

For the S standard solutions the background signal at $m/z = 48$ is approximately 13 000 cps. Such a signal suggests that there is a significant degree of S and/or ^{48}Ti contamination, a very different situation than that observed in the equivalent P calibration. As the background signal at $m/z = 47$ was so low in the P curve then ^{48}Ti contamination alone can be dismissed here for the following reasons. Firstly each of these P and S solutions were prepared with the same deionised water source so background data should be similar (which it is, see Table 58, Appendix 2). Secondly as the relative abundance of ^{47}Ti and ^{48}Ti is 7.3 % and 73.8 % respectively then a $m/z = 47$ signal of one tenth the intensity of that of the $m/z = 48$ signal, between the P and S calibrations, would be expected.⁶ The $m/z = 47$ and 48 signals measured for the 2 % HNO_3 solution were compared to see whether this was the case. For each measurement the $m/z = 47$ signal was far less than one tenth of that of the $m/z = 48$ signal. This data suggests that the main contribution to excessive ion counts at the $m/z = 48$ background will be the presence of contaminating ^{32}S that forms oxide ions in the collision cell.

However, 13 000 cps is a high background signal but could be described as miniscule on comparison to the typical background observed at $m/z = 32$. The R^2 value of the S curve (0.9355) describes a response for the S standard solutions analysed that is less linear than that observed in the P analysis. At first glance the gradient of the two curves could be commented on with regard to the efficiency of ^{31}P and ^{32}S oxidation within the hexapole. Based on the gradients of the two curves it could be said that the formation of the $^{32}\text{S}^{16}\text{O}^+$ ion is more efficient than the $^{31}\text{P}^{16}\text{O}^+$ ion. However, due to the more erratic response of the S standard solutions such a comparison is not

realistic. ^{32}S LOD's under method 2 conditions were calculated to be $1.43\ \mu\text{g l}^{-1}$ to $6.50\ \mu\text{g l}^{-1}$. These LOD calculations are fully described in section 2.5.

2.4.3. Method 3: Selective Removal of Polyatomic Ions in a Collision Cell Incorporating He Collision Gas Under KED Conditions

It has previously been demonstrated that the employment of a collision cell incorporating He gas under KED conditions can allow the attenuation of some high energy ICP or interface-formed polyatomic ion interferences.¹⁰⁴ The removal of such species occurs due to the selective loss of ion energy following collision between polyatomic ions and neutral He atoms. Within a collision cell, the possible occurrence of reactions between species aside, the presence of any gas has a severe effect on the transmission of ions due to variation of ion kinetic energy following collision. The frequency and effect of a collision is dependent on the physical and chemical characteristics (e.g. collisional cross section and bond strength) and initial kinetic energy of each species involved.^{33, 91}

Polyatomic ions exhibit a higher collisional cross section than that of monatomic analyte ions. Such ions collide more frequently with the He atoms present and therefore lose kinetic energy and momentum to a greater degree. This loss of energy can lead to the selective removal of polyatomic ions from the ion beam, along with low energy cell formed species, assuming that they have lost sufficient energy so cannot overcome the energy barrier established as a result of setting up KED conditions.^{83, 104}

It has been documented that the intensity of dominating polyatomic Ar based ions, such as $^{40}\text{Ar}^1\text{H}^+$, $^{40}\text{Ar}^{16}\text{O}^+$ and $^{40}\text{Ar}_2^+$, can be reduced by several orders of magnitude when KED conditions are established. The degree of metal oxide formation can also be limited.^{83, 104}

Experimental Details

For the determination of the problematic ^{31}P isotope it could be possible to favour the transmission of monatomic analyte ions, through the collision cell, over polyatomic ions at $m/z = 31$ (the most common being $^{14}\text{N}^{16}\text{O}^+\text{H}^+$, $^{15}\text{N}^{15}\text{N}^+\text{H}^+$, $^{15}\text{N}^{16}\text{O}^+$, $^{14}\text{N}^{17}\text{O}^+$, $^{13}\text{C}^{18}\text{O}^+$ and $^{12}\text{C}^{18}\text{O}^+\text{H}^+$) by incorporating He in the cell and establishing KED conditions. A series of experiments were carried out to establish whether or not such conditions could be beneficial to the determination of ^{31}P . For the analytical approach described in this section the ^{31}P isotope was studied rather than the ^{32}S isotope as the dominant interfering polyatomic ions, at $m/z = 31$, typically have a larger collisional cross section so any effects that can be observed should be greater.

Results and Discussion

Varying flows of He (0 to 4 ml min⁻¹) were incorporated and studied whilst employing KED voltage spreads (the difference between V_q and V_h) of +1 V, +2 V and +3 V. The data accrued for these experiments can be seen in Tables 60, 61 and 62 (Appendix 2) whilst general instrumental conditions can be seen in Table 59.

From this data a series of graphs were constructed to compare the blank subtracted data and sample : blank ratios that were calculated (see Figures 15, 16, 17, 18, 19 and 20). From the comparison of this data it could be determined whether polyatomic ions were being selectively removed and whether there were any optimum conditions to create such an effect.

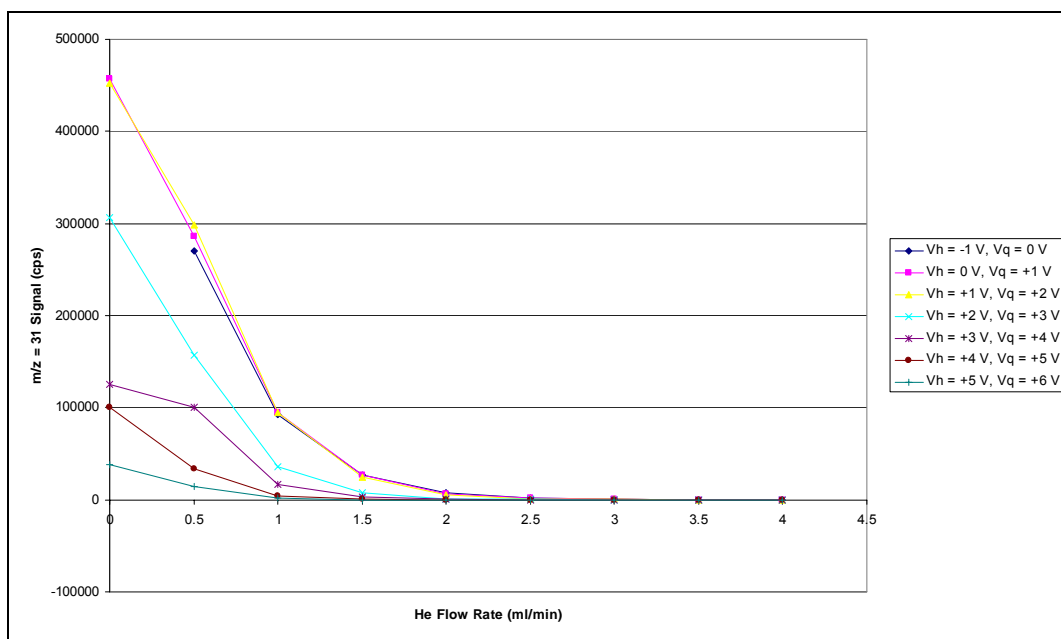


Figure 15. A Graph Comparing $m/z = 31$ Background Subtracted Signal for the Analysis of 2 % HNO_3 Blank and $200 \mu\text{g l}^{-1}$ P Solutions when Varying He Flow Rate (ml min^{-1}) Under Different KED Conditions (KED Spread = +1 V).

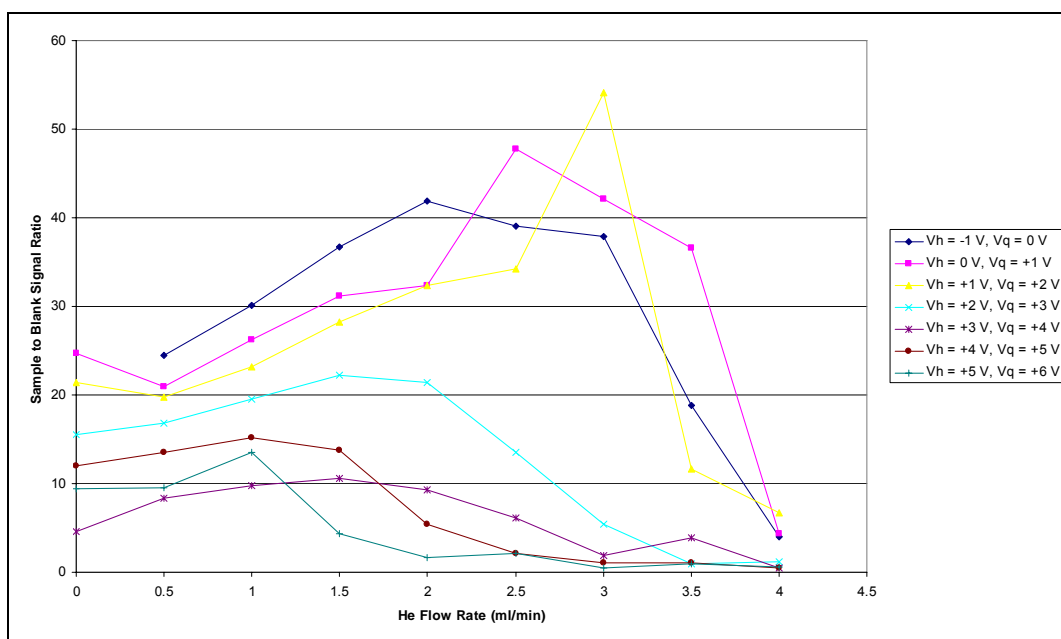


Figure 16. A Graph Comparing $m/z = 31$ Signal Sample : Blank Ratio for the Analysis of 2 % HNO_3 Blank and $200 \mu\text{g l}^{-1}$ P Solutions when Varying He Flow Rate (ml min^{-1}) Under Different KED Conditions (KED Spread = +1 V).

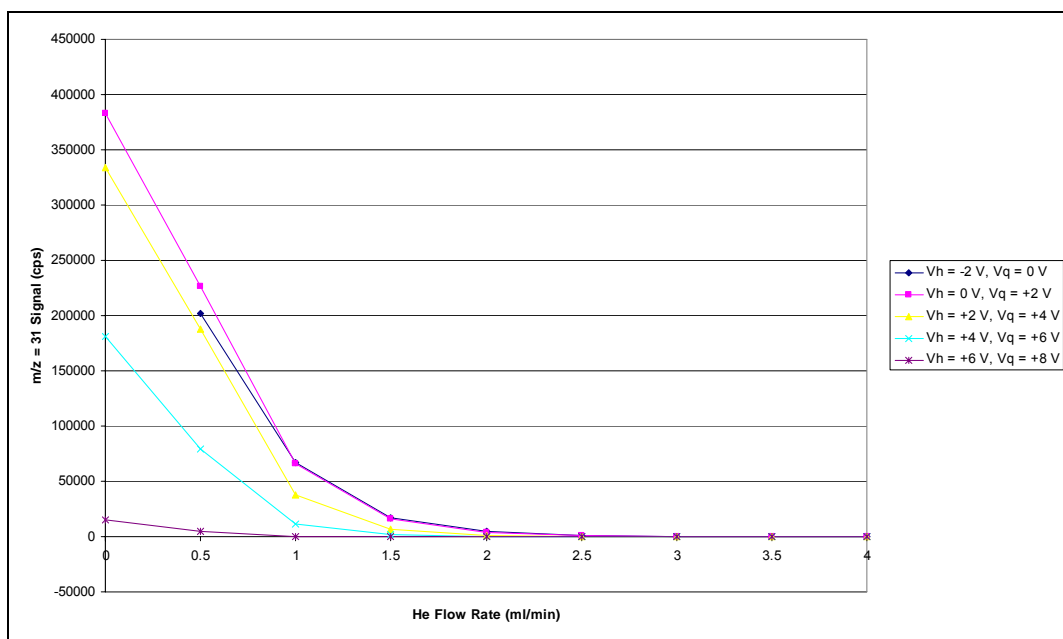


Figure 17. A Graph Comparing $m/z = 31$ Background Subtracted Signal for the Analysis of 2 % HNO_3 Blank and $200 \mu\text{g l}^{-1}$ P Solutions when Varying He Flow Rate (ml min^{-1}) Under Different KED Conditions (KED Spread = +2 V).

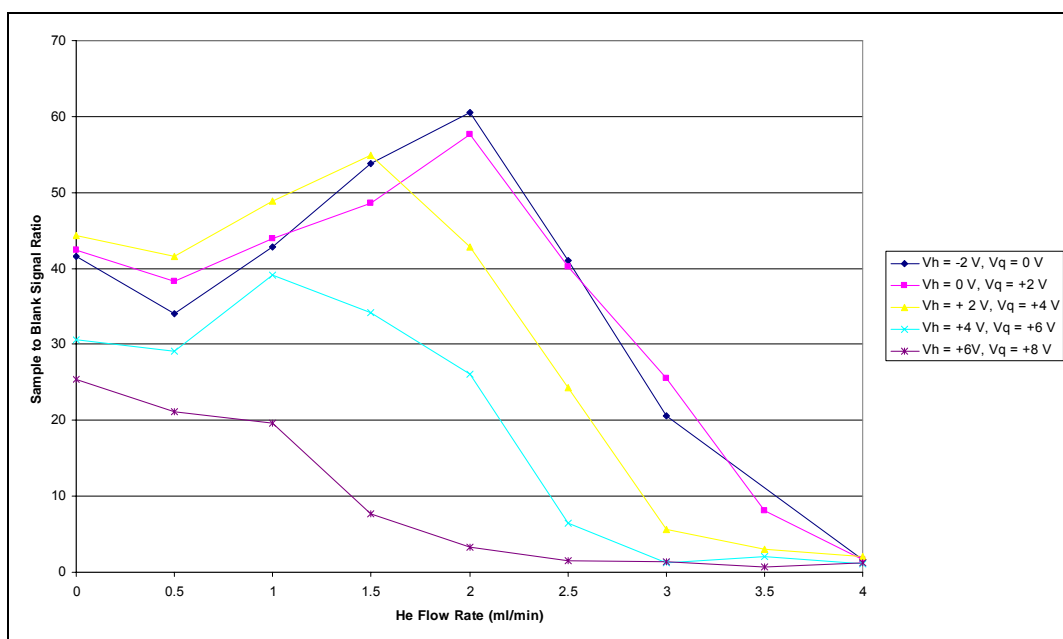


Figure 18. A Graph Comparing $m/z = 31$ Signal Sample : Blank Ratio for the Analysis of 2 % HNO_3 Blank and $200 \mu\text{g l}^{-1}$ P Solutions when Varying He Flow Rate (ml min^{-1}) Under Different KED Conditions (KED Spread = +2 V).

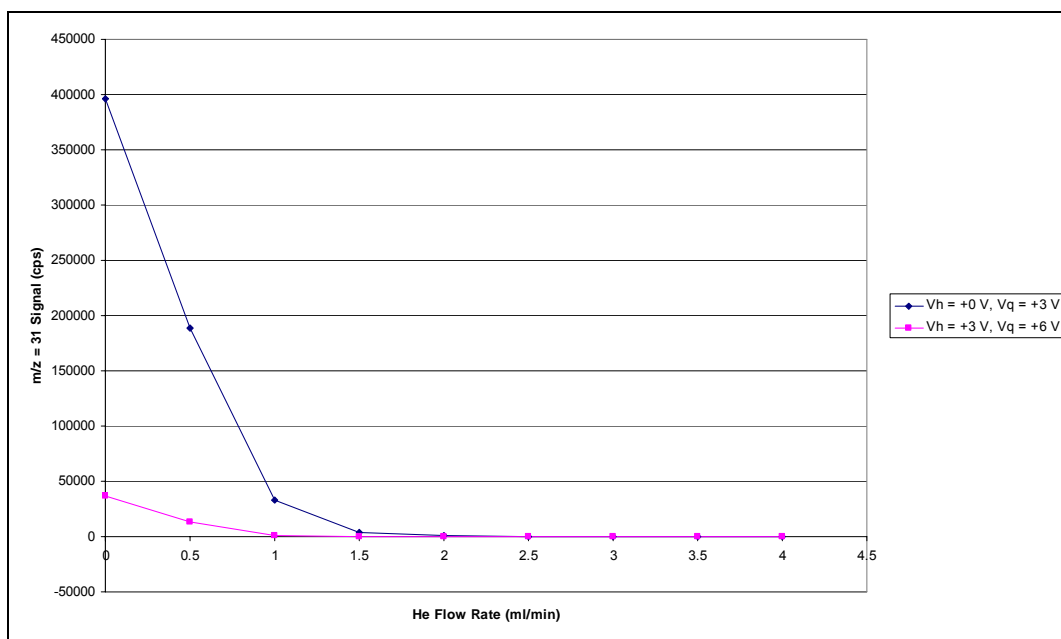


Figure 19. A Graph Comparing $m/z = 31$ Background Subtracted Signal for the Analysis of 2 % HNO_3 Blank and $200 \mu\text{g l}^{-1}$ P Solutions when Varying He Flow Rate (ml min^{-1}) Under Different KED Conditions (KED Spread = +3 V).

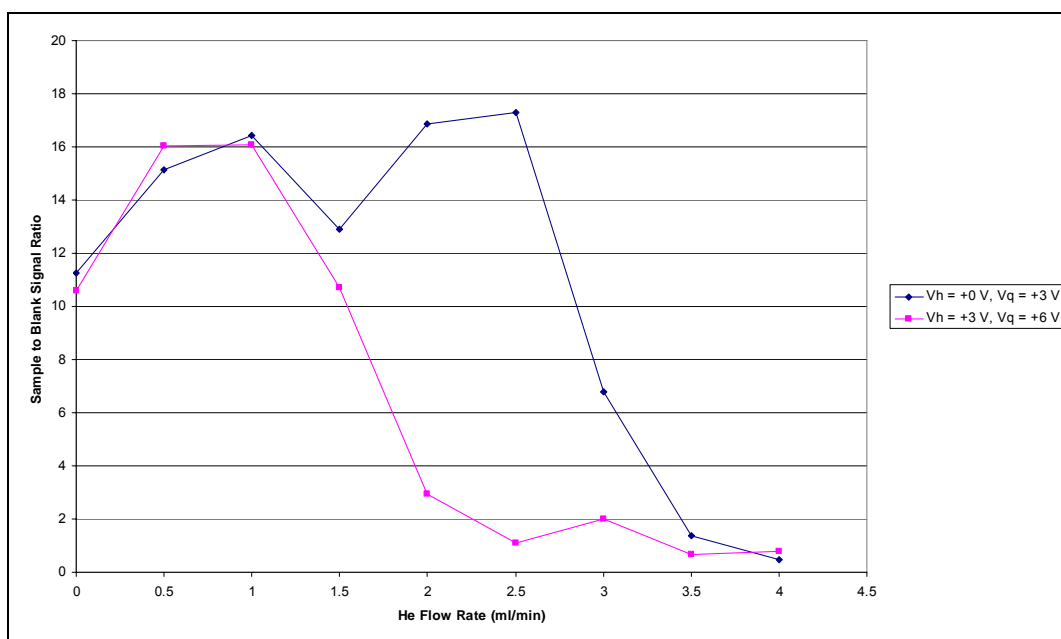


Figure 20. A Graph Comparing $m/z = 31$ Signal Sample : Blank Ratio for the Analysis of 2 % HNO_3 Blank and $200 \mu\text{g l}^{-1}$ P Solutions when Varying He Flow Rate (ml min^{-1}) Under Different KED Conditions (KED Spread = +3 V).

Figure 15 shows the effect of differing KED conditions (KED spread = +1 V) on the $m/z = 31$ signal when analysing 2 % HNO_3 blank and 200 $\mu\text{g l}^{-1}$ P solutions for various He flows to the collision cell. Generally, as the He flow increased the $m/z = 31$ signal decreased. For the first three KED conditions studied ($V_h = -1$ V, 0 V and +1 V) there was little difference in signal intensity at each He flow used. When V_h was increased, in line with V_q , beyond +1 V the $m/z = 31$ signal decreased severely for each He flow. Therefore there are two factors here that require discussion; the signal reduction dependency on the He flow and the signal reduction dependency on the increase in applied hexapole voltage (established in the various KED conditions).

The decreased signals arising from the increased He flow was the result of ion kinetic energy reduction following collision with He atoms. This energy reduction leads to a large elimination of ions from the hexapole as they cannot overcome the energy barrier established under the KED conditions. The reduction in signal that was generated when increasing the applied hexapole voltage can be described by IKEE. As V_h was increased, towards V_p , all species at $m/z = 31$ were slowed on entrance to the hexapole. The IKEE therefore contributed to a greater number of ions that were not capable of overcoming the energy barrier established under the KED conditions.

Figure 16 shows the effect of differing KED conditions (KED spread = +1 V) on the ratio of sample to blank signals at $m/z = 31$ when analysing 2 % HNO_3 blank and 200 $\mu\text{g l}^{-1}$ P solutions whilst using various He flows. Such a ratio can be used to determine the degree of polyatomic ion removal with regard to this m/z . For a KED spread of +1 V the greatest sample to blank signal ratio was found at a He flow of 3 ml min^{-1} and KED conditions of $V_h = +1$ V and $V_q = +2$ V, however, at such conditions the blank subtracted $m/z = 31$ signal was 265 cps which is completely unusable for analysis. Therefore, to achieve a realistic signal a lower He flow must be employed. Considering the data in Figure 15, a He flow of 1.5 ml min^{-1} cannot be exceeded in order to maintain a sensible signal. Because of this a compromise between He flow and KED voltages was struck to establish optimum, “working”, conditions. As a standard, between these experiments, it was decided that these optimum conditions would have the following requirements:

- A sample : blank signal ratio of >30 .

- A sample signal in the order of at least $\times 10^4$ cps.
- A blank signal in the order of <1000 cps.

For a KED spread of +1 V, the optimum working conditions were He flow rate = 1.5 ml min⁻¹, $V_h = -1$ V and $V_q = 0$ V.

Similar to Figure 15, Figure 17 shows the effect of differing KED conditions (KED spread = +2 V) on the $m/z = 31$ signal when analysing 2 % HNO₃ blank and 200 µg l⁻¹ P solutions at various He flows. As the He flow incorporated was increased the $m/z = 31$ signal decreased. Again, for the first three KED conditions studied ($V_h = -2$ V, 0 V and +2 V) there was little difference in signal intensity at each He flow rate. When V_h was increased beyond +2 V the $m/z = 31$ signal decreased significantly for each He flow, particularly at the lower flow rates (up to 1.5 ml min⁻¹). As with Figure 15, the signals of the graph in Figure 17 can be described by the ion kinetic energy reduction as the result of collision with increasing quantities of He and the loss of ion momentum due to the IKEE conditions becoming stronger.

Figure 18 is a graph comparing differing KED conditions (KED spread = +1 V) with the ratio of sample to blank signals at $m/z = 31$ when analysing 2 % HNO₃ blank and 200 µg l⁻¹ P solutions and introducing various He flows. Similar to Figure 16 at first glance the optimum set of conditions for selective removal of polyatomic ions would have been a He flow rate of 2 ml min⁻¹ and voltages of $V_h = -2$ V and $V_q = 0$ V. However, considering the low $m/z = 31$ signal that was obtained under these conditions (4526 cps for the P solution, see Figure 17) optimum working conditions were decided on at a He flow of 1.5 ml min⁻¹, $V_h = -2$ V and $V_q = 0$ V.

Figure 19 shows the effect of differing KED conditions (KED spread = +3 V) on the $m/z = 31$ signal when analysing 2 % HNO₃ blank and 200 µg l⁻¹ P solutions whilst using various He flows to the hexapole. The same general trends are observed in this graph as in those of Figures 15 and 17, as the He flow incorporated increased the $m/z = 31$ signal decreased. For both sets of conditions studied here the $m/z = 31$ signal drops to almost zero on the introduction of 1 ml min⁻¹ He. The two different sets of KED conditions generated very different data for the blank subtracted P standard

solution with the higher V_h value producing the lowest $m/z = 31$ signal. Again the reduced $m/z = 31$ signal arises due to the effects of collision with He atoms and the loss of momentum as V_h tends towards V_p .

Figure 20 shows the effect of differing KED conditions (KED spread = +3 V) on the ratio of sample to blank signals at $m/z = 31$ when analysing 2 % HNO_3 blank and 200 $\mu\text{g l}^{-1}$ P solutions whilst using various He flows. For a KED spread of +3 V there wasn't a clear optimum for either set of KED conditions studied, however, what should be recognised here is that the sample to blank signal ratios observed were much lower than those at KED spreads of +1 V and +2 V.

On comparison of the experiments carried out for this method, it appears that the optimum working conditions required to create a selective removal of polyatomic ions at $m/z = 31$ were He flow = 1.5 ml min^{-1} , $V_h = -1$ V and $V_q = 0$ V. As can be seen from the data generated from the experiments of this section the wider that the V_h to V_q range is then a poorer $m/z = 31$ signal is obtained. The reason for this is that a wider range produces a greater energy barrier that has to be overcome by ions transmitted through the cell. The optimum V_h/V_q range is a separation of +1 V.

Following the study of He flow and KED conditions on the $m/z = 31$ signal, a series of P standard solutions were studied under the optimum working conditions (He = 1.5 ml min^{-1} , $V_h = -1$ V and $V_q = 0$ V). The data accrued during this experiment can be seen in Table 63 and a graph comparing P concentration with $m/z = 31$ signal can be seen in Figure 21.

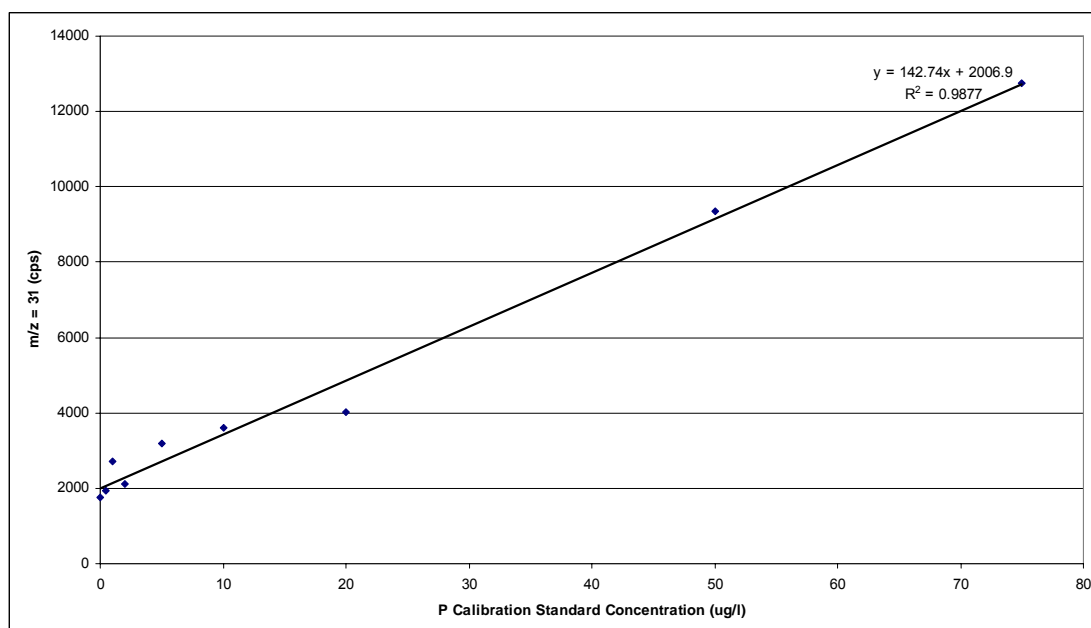


Figure 21. A Graph Exhibiting Signal Response as a Function of Concentration for the ^{31}P Isotope Employing ‘Method 3’.

As can be seen in the Figure 21 a linear graph was obtained ($R^2 = 0.9877$). On comparison to the study of P standards carried out under ‘method 2’ conditions (Figure 14) the background for the ^{31}P isotope here was higher, approximately 2000 ion counts per second. This will have a detrimental effect on the LOD calculated for this method. Considering that the same standard solutions were studied under method 2 and 3 conditions, it is more likely that the higher background for method 3 arises as the removal of interfering polyatomic ions is not 100 % efficient; ^{31}P contamination may also be an issue. ^{31}P LOD’s under method 3 conditions were calculated to be $1.48 \mu\text{g l}^{-1}$ to $7.78 \mu\text{g l}^{-1}$. These LOD calculations are fully described in section 2.5.

2.4.4. Method 4: The Determination of $^{31}\text{P}^{16}\text{O}^+$ and $^{32}\text{S}^{16}\text{O}^+$ Ions Formed Under ‘Cold/Cool Plasma’

During the work carried out by Wiedemann *et al.* and whilst optimising conditions for the measurements described in sections 2.4.1, 2.4.2 and 2.4.3 it was observed that

lowering the forward power of the ICP, from the typical 1350 W to approximately 800 W, when analysing P and S solutions resulted in enhancement of the $m/z = 47$ and 48 signals.¹³⁸ When employing a ‘cold/cool plasma’ for analysis the increased occurrence of measured oxide species is normally considered to be problematic. In this case, however, it can be advantageous by forming the $^{31}\text{P}^{16}\text{O}^+$ ($m/z = 47$) and $^{32}\text{S}^{16}\text{O}^+$ ($m/z = 48$) ions for the reasons described in sections 2.4.1 and 2.4.2. The work described in this section determines whether this method has potential for the determination of ^{31}P and ^{32}S isotopes.

Experimental Details

To fulfil the aim of establishing whether a ‘cold/cool plasma’ was a feasible approach to the measurement of P and S at trace levels, experiments were first carried out to determine the optimum forward power for the formation of these analyte oxide ions. A forward power range between 1700 W and 700 W was studied as this incorporates powers higher than normally employed down to those of the ‘cold plasma’ region. For forward power increments of this range $m/z = 31$, 32, 47 and 48 signals were measured for 2 % HNO_3 and 1000 $\mu\text{g l}^{-1}$ P and S solutions to determine optimum intensity and signal to background ratio.

Results and Discussion

General instrumental conditions employed during these experiments can be seen in Table 64 (Appendix 2) whilst the data generated can be seen in Tables 65, 66 and 67.

Manipulation of the data generated during these experiments has allowed construction of a series of graphs to determine the optimum ICP forward power for $^{31}\text{P}^{16}\text{O}^+$ and $^{32}\text{S}^{16}\text{O}^+$ ion formation, see Figures 22, 23, 24 and 25.

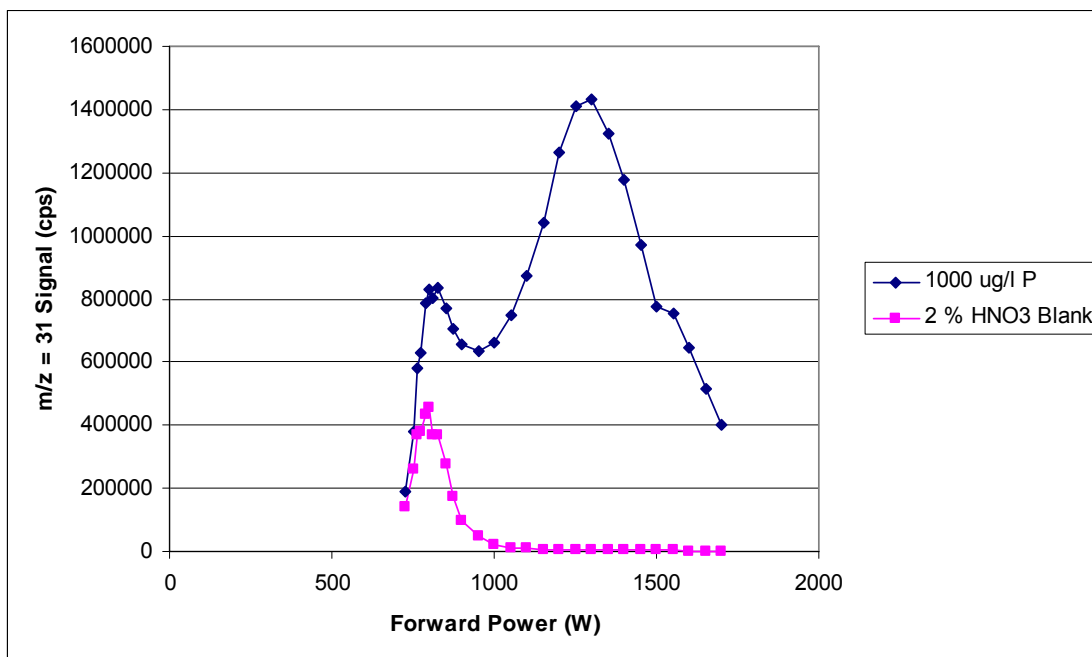


Figure 22. A Graph Comparing $m/z = 31$ Signal with Forward Power (W) for the Analysis of 2 % HNO₃ Blank and 1000 $\mu\text{g l}^{-1}$ P Solutions.

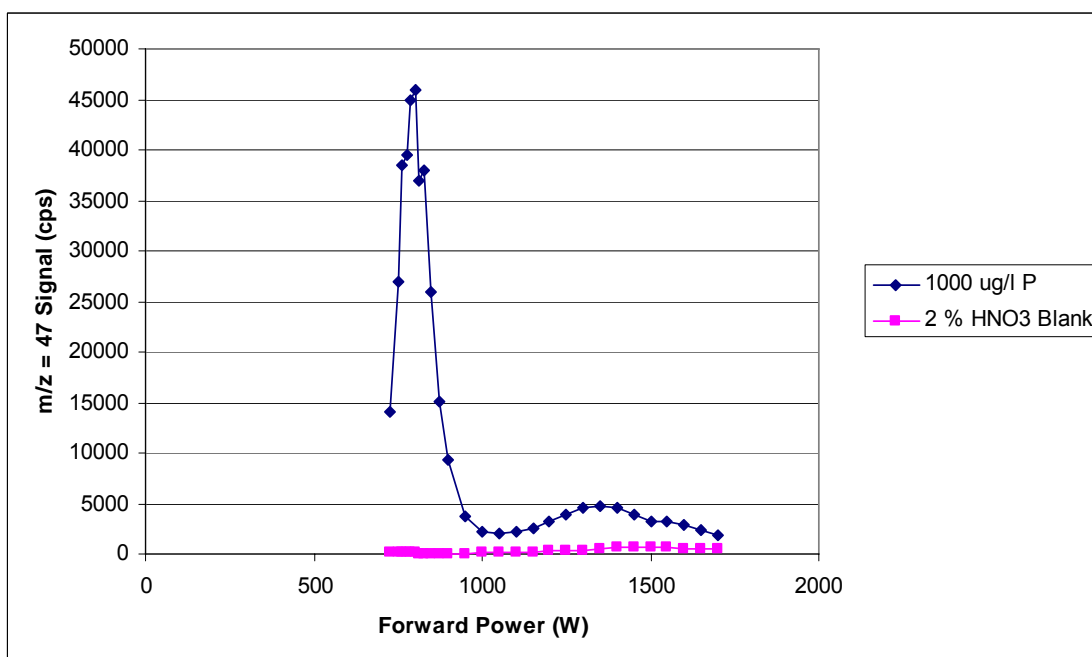


Figure 23. A Graph Comparing $m/z = 47$ Signal with Forward Power (W) for the Analysis of 2 % HNO₃ Blank and 1000 $\mu\text{g l}^{-1}$ P Solutions.

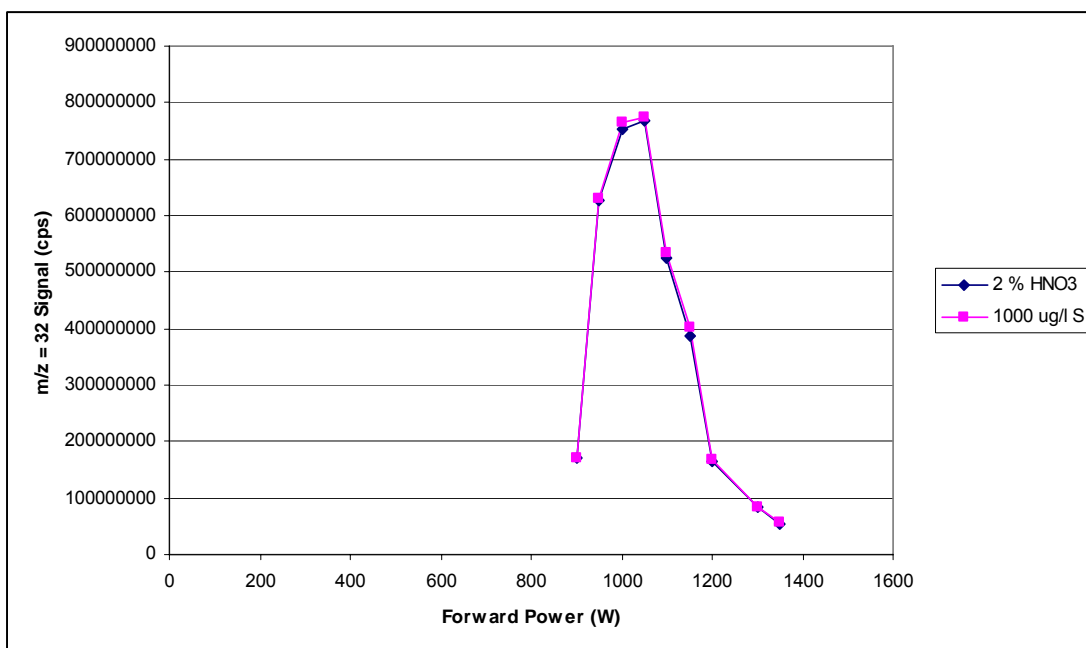


Figure 24. A Graph Comparing $m/z = 32$ Signal with Forward Power (W) for the Analysis of 2 % HNO_3 Blank and 1000 $\mu\text{g l}^{-1}$ S Solutions.

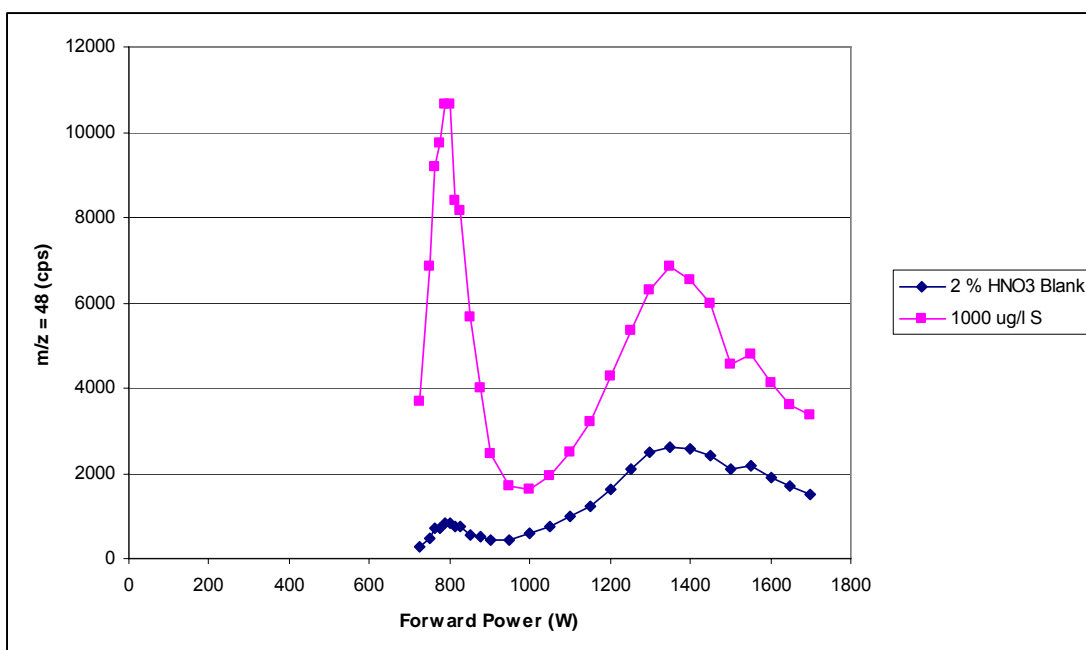


Figure 25. A Graph Comparing $m/z = 48$ Signal with Forward Power (W) for the Analysis of 2 % HNO_3 Blank and 1000 $\mu\text{g l}^{-1}$ S Solutions.

Figure 22 shows the variation of $m/z = 31$ signal with ICP forward power (W) during the analysis of 2 % HNO₃ blank and 1000 µg l⁻¹ P solutions. The 2 % HNO₃ solution plot exhibits a single peak, over the range of forward powers studied, at 800 W. This peak has arisen as at that particular forward power the conditions were ideal for the formation of N, O and H based polyatomic ions such as ¹⁴N¹⁶O¹H⁺. The 1000 µg l⁻¹ P solution plot shows a primary peak (1300 W) and a secondary peak (825 W). The primary peak has arisen due to the massive presence of ³¹P⁺ ions whilst the secondary peak is a polyatomic ion peak similar to that seen in the 2 % HNO₃ solution plot.

Figure 23 shows the variation of $m/z = 47$ signal with ICP forward power (W) for the analysis of 2 % HNO₃ blank and 1000 µg l⁻¹ P solutions. Over the range of forward powers studied the signal generated from the 2 % HNO₃ solution varied very little, only a slight elevation (up to approximately 600 cps) was observed in the region of 1500 W. For the signal from the 1000 µg l⁻¹ P solution primary (800 W) and secondary (1350 W) peaks were observed. The primary peak arose due to the formation of the ³¹P¹⁶O⁺ ($m/z = 47$) ion whilst the secondary peak was most likely present due to either a secondary optimum for the formation of ³¹P¹⁶O⁺ or background signal from ⁴⁷Ti contamination. At 800 W the signal : background ratio is 363 : 1 so this would be the optimum forward power for the formation of ³¹P¹⁶O⁺ ions in terms of both maximum signal and background.

Figure 24 shows the variation in $m/z = 32$ signal with ICP forward power (W) for the analysis of 2 % HNO₃ blank and 1000 µg l⁻¹ S solutions. Over the range of forward powers studied, the signals for both 2 % HNO₃ blank and 1000 µg l⁻¹ S solutions differ very little, again, highlighting the degree of interference at $m/z = 32$. A peak for both plots is seen at a forward power of 1050 W which suggests the optimum conditions for the ionisation of molecular oxygen.

Figure 25 shows the variation in $m/z = 48$ signal with ICP forward power (W) for the analysis of 2 % HNO₃ blank and 1000 µg l⁻¹ S solutions. Over the range of ICP forward powers studied primary and secondary signal peaks are exhibited for both solutions analysed. For the 2 % HNO₃ blank solution the primary signal peak (1350 W) appears due to the formation of either the ³¹P¹⁶O¹H⁺ ($m/z = 48$) polyatomic ion from contaminating ³¹P or the ¹⁶O₃⁺ ion. The secondary signal peak at 800 W is

present due to the formation of $^{32}\text{S}^{16}\text{O}^+$ from background ^{32}S . The primary peak (787 W) of the $1000\text{ }\mu\text{g l}^{-1}$ S solution arose due to the formation of the $^{32}\text{S}^{16}\text{O}^+$ ion whilst the secondary peak (1350 W), again, was present due to the formation of $^{31}\text{P}^{16}\text{O}^+\text{H}^+$ from contaminating ^{31}P or $^{16}\text{O}_3^+$. At 787 W the signal : background ratio is 12.8 : 1 so this is the optimum forward power for the formation of $^{32}\text{S}^{16}\text{O}^+$ ions in terms of maximum signal and background. However, on comparison to the ^{31}P experiments the measurement of ^{32}S by this approach is far less efficient.

Following study of the data accrued during the forward power experiments optimum formation of the $^{31}\text{P}^{16}\text{O}^+$ and $^{32}\text{S}^{16}\text{O}^+$ ions was observed at 800 W and 787 W respectively. On comparison of the $m/z = 31, 32, 47$ and 48 signals seen in the graphs of Figures 22, 23, 24 and 25 it can be said that, similar to the collision cell work of sections 2.4.1 and 2.4.2, the formation of analyte oxide ions by this method is particularly inefficient. Of the two isotopes ^{31}P oxidises, by this approach, to a greater degree within the ICP. As with the collision cell methods described in this thesis, the formation of $^{31}\text{P}^{16}\text{O}^+$ and $^{32}\text{S}^{16}\text{O}^+$ ions by ‘cold/cool plasma’ ICP-MS appears to be a promising approach to the determination of ^{31}P and ^{32}S isotopes.

Following optimisation, a series of P and S standard solutions were studied employing the ‘method 4’ conditions. The data generated during these measurements can be seen in Table 68 and graphs comparing standard concentration with $m/z = 47$ and 48 signal for both ^{31}P and ^{32}S isotopes can be seen in Figure 26.

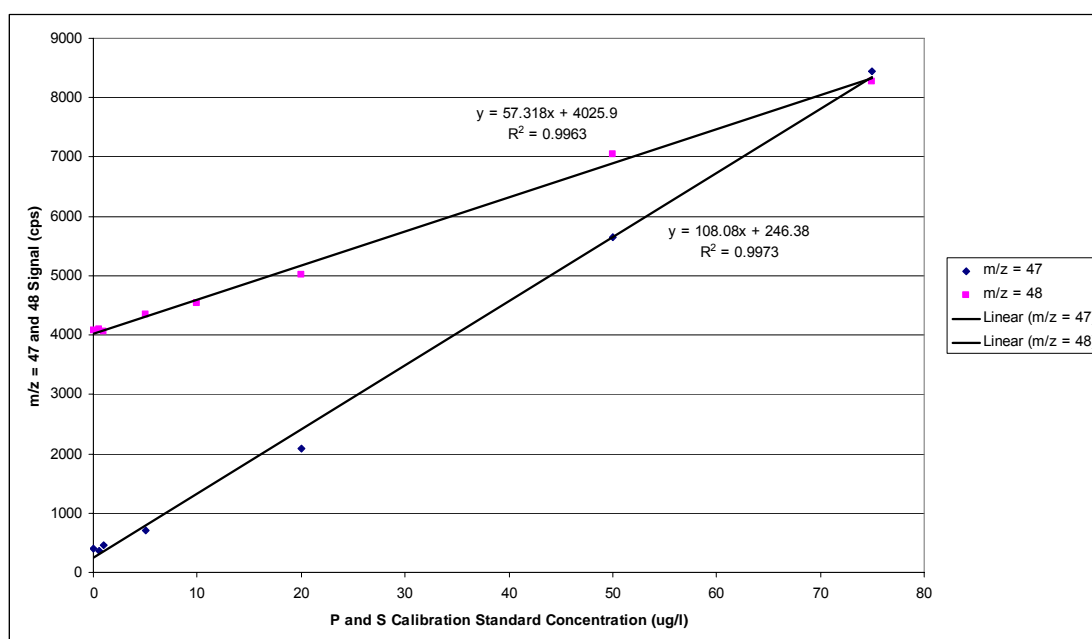


Figure 26. Graphs Exhibiting Signal Response as a Function of Concentration for the ^{31}P and ^{32}S Isotopes Under ‘Method 4’.

As can be seen in the Figure 26 two linear curves were constructed ($R^2 = 0.9973$ and 0.9963 for ^{31}P and ^{32}S isotopes respectively). What should be noted here is a comparison between the gradient of each line. If both curves were parallel then it could be argued that the oxidation reaction efficiency for ^{31}P and ^{32}S isotopes was similar. In Figure 26 the gradient data suggests that the formation of the $^{31}\text{P}^{16}\text{O}^+$ ion could be more prevalent than that of the $^{32}\text{S}^{16}\text{O}^+$ ion. The background signal for the $^{31}\text{P}^{16}\text{O}^+$ formation is desirably low, in the order of hundreds of ion counts per second, whilst the background for the $^{32}\text{S}^{16}\text{O}^+$ ion is comparatively high, of the order of thousands of counts. This is likely to be due to sulphur contamination of the deionised water used in preparation of the calibration standard solutions, a problem also highlighted during the work carried out towards methods 1 and 2. Under method 4 conditions ^{31}P and ^{32}S LOD's were calculated to be $0.89 \mu\text{g l}^{-1}$ to $6.56 \mu\text{g l}^{-1}$ and $6.84 \mu\text{g l}^{-1}$ to $25 \mu\text{g l}^{-1}$ respectively. These LOD calculations are fully described in section 2.5.

2.4.5. Method 5: The Determination of $^{31}\text{P}^{16}\text{O}^+$ and $^{32}\text{S}^{16}\text{O}^+$ Ions Formed by ‘Cold/Cool’ Plasma Incorporating an Additional O_2 Nebuliser Flow

Following the promising results evolved from the ‘cold/cool plasma’ work described in section 2.4.4, experiments were carried out to determine whether the degree of analyte oxide formation could be enhanced by the addition of an O_2 gas flow through the central channel of the ICP. By providing the ICP discharge with an additional source of O_2 it was hoped that oxidation of ^{31}P and ^{32}S could be maximised without causing any detrimental effect to the overall atomisation and ionisation capability of the plasma.

Experimental Details

Via a ‘Y-piece’ tube an O_2 gas flow was introduced into the nebuliser gas flow after sample passage through an external cyclonic spray chamber. Initial experiments were carried out to determine the effect of such a flow on the $^{31}\text{P}^{16}\text{O}^+$ and $^{32}\text{S}^{16}\text{O}^+$ ion formation whilst employing the optimum ‘cold/cool plasma’ conditions described in section 2.4.4.

Results and Discussion

The data generated during these experiments, see Table 70, was used to construct graphs to determine the effect of additional O_2 introduction (see Figures 27 and 28). General instrumental conditions employed during this work can be seen in Table 69 (Appendix 2).

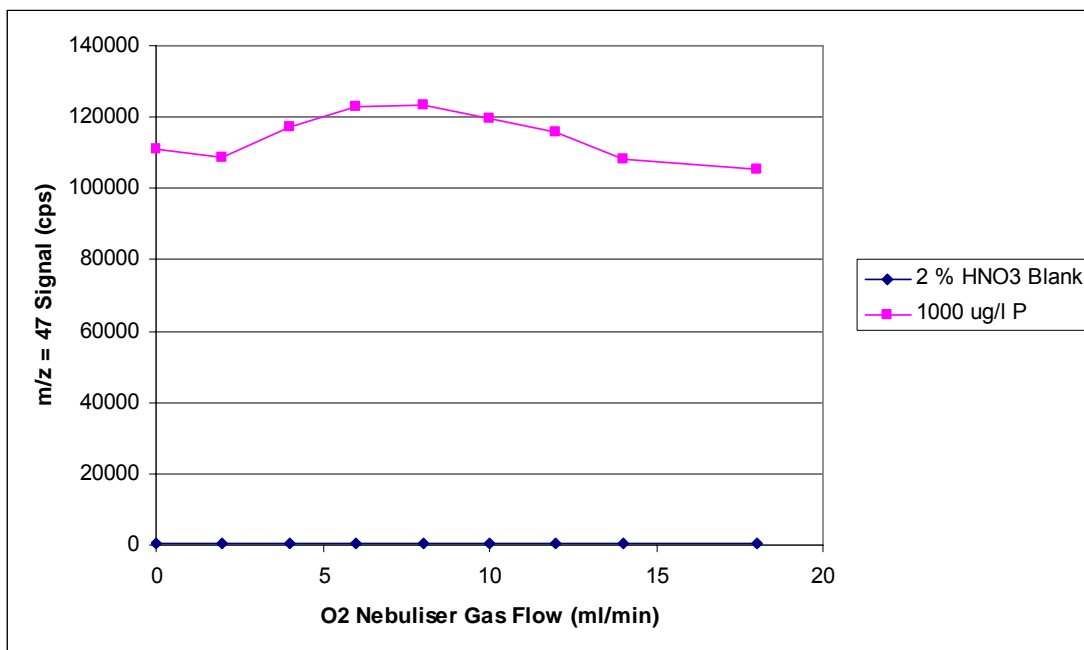


Figure 27. The Variation of $m/z = 47$ Signal with O_2 Nebuliser Gas Flow Introduction for the Analysis of 2 % HNO_3 Blank and 1000 $\mu g/l$ P Solutions.

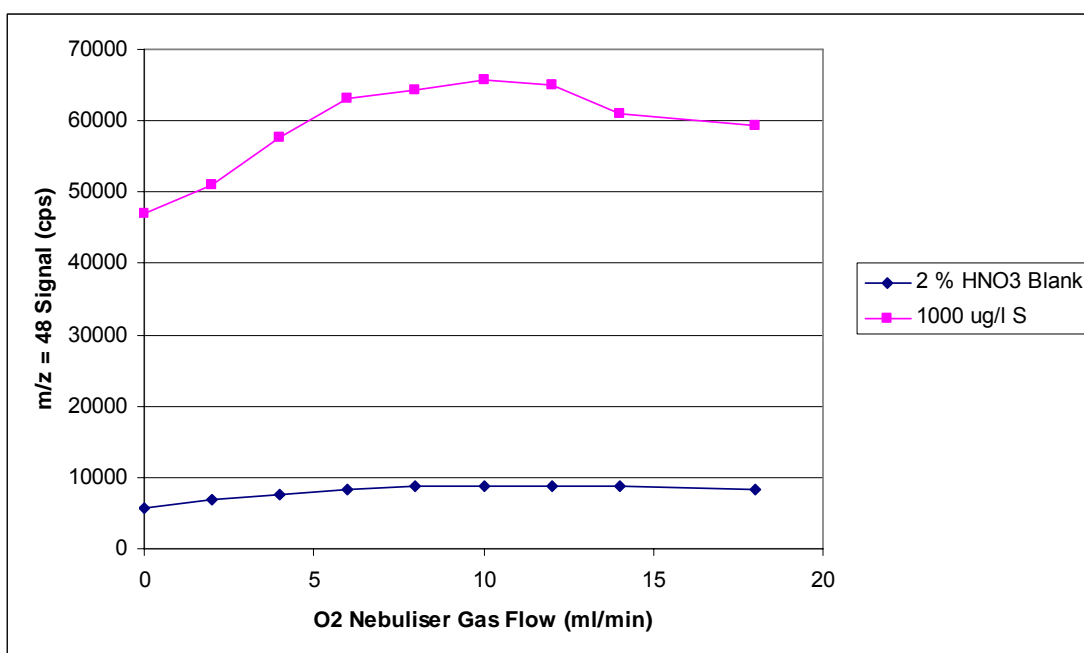


Figure 28. The Variation of $m/z = 48$ Signal with O_2 Nebuliser Gas Flow Introduction for the Analysis of 2 % HNO_3 Blank and 1000 $\mu g/l$ S Solutions.

Figure 27 is a graph comparing the variation in $m/z = 47$ signal with increasing introduction of an O₂ nebuliser gas flow for the analysis of 2 % HNO₃ blank and 1000 µg l⁻¹ P solutions under ‘cold/cool plasma’ conditions of 800 W forward power. For the 2 % HNO₃ blank solution signal there was no significant change between O₂ gas flows. However, for the 1000 µg l⁻¹ P solution, over the range of O₂ nebuliser flow rates studied there appeared to be a small degree of ³¹P¹⁶O⁺ ion enhancement at 8 ml min⁻¹. At this flow rate, for the 1000 µg l⁻¹ P solution, there was an enhancement of approximately 10 000 ion counts per second compared to the analysis of the same solution at 0 ml min⁻¹ O₂ introduction. This was an enhancement of approximately 10 %. As there was no significant change in the signal for the 2 % HNO₃ solution then it could be said that the majority of the signal enhancement was due to the formation of the ³¹P¹⁶O⁺ ion.

Figure 28 is a graph comparing variation in $m/z = 48$ signal with increasing O₂ nebuliser gas flow introduction for the analysis of 2 % HNO₃ blank and 1000 µg l⁻¹ S solutions under ‘cold/cool plasma’ conditions of 787 W forward power. For the 2 % HNO₃ blank solution there was a small degree of signal enhancement, in the region of 3000 ion counts per second at 10 ml min⁻¹ which probably has arisen due to the presence of contaminating S. Similar to the graph in Figure 27 for the P solution, between the 0 and 18 ml min⁻¹ O₂ nebuliser flow rate range studied there appears to be a small amount of ³²S¹⁶O⁺ ion enhancement at 10 ml min⁻¹. At this flow rate, for the 1000 µg l⁻¹ S solution, there was an ion count enhancement of approximately 20 000 cps compared to the same analysis at 0 ml min⁻¹ O₂ introduction. This was an enhancement of approximately 40 % which is a significant signal increase even considering the 3000 counts increase present in the background.

Following optimisation a series of P and S standards were studied under the optimum ‘method 5’ conditions. Data accrued and plots generated during this experiment can be seen in Table 71 and Figure 29.

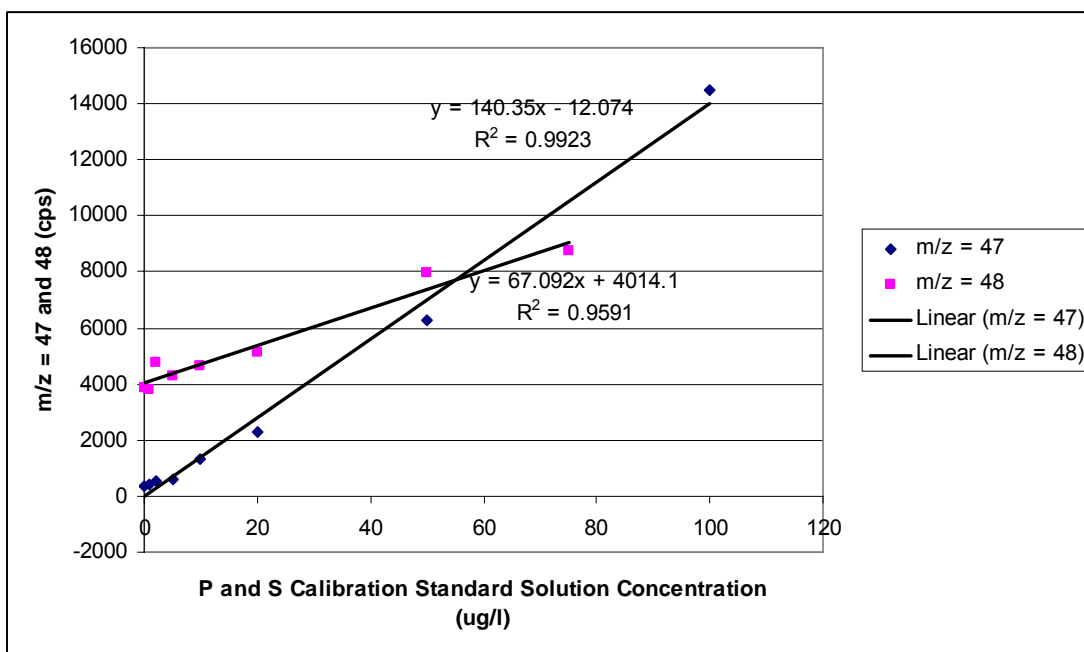


Figure 29. Graphs Exhibiting Signal Response as a Function of Concentration for the ^{31}P and ^{32}S Isotopes Employing Method 5 Conditions.

As can be seen in the graph of Figure 29, two linear curves were constructed ($R^2 = 0.9923$ and 0.9591 for ^{31}P and ^{32}S isotopes respectively). Similar to the concentration curves produced following ‘method 4’ optimisation (see Figure 26), what should be noted here is that these lines are not parallel, i.e. there is a significant difference in oxide formation efficiency between the ^{31}P and ^{32}S isotopes. Also similar to Figure 26 the background signal for the $^{31}\text{P}^{16}\text{O}^+$ formation is desirably low, in the order of hundreds of ion counts per second, whilst the background for the $^{32}\text{S}^{16}\text{O}^+$ ion is high, of the order of thousands of counts. This is due to the occurrence of the $^{16}\text{O}_3^+$ ion at $m/z = 48$. Under method 5 conditions ^{31}P and ^{32}S LOD’s were calculated to be $0.74 \mu\text{g l}^{-1}$ to $14 \mu\text{g l}^{-1}$ and $1.23 \mu\text{g l}^{-1}$ to $80 \mu\text{g l}^{-1}$ respectively. These LOD calculations are fully described in section 2.5.

2.4.6. Method 6 (Part 1): The Exclusion of Entrained Atmospheric Gases from the ICP

The formation of polyatomic ions within the ICP and the ICP-MS interface occurs due to the presence of elements originating from the plasma gas, entrained atmospheric gases and the sample matrix. To avoid spectroscopic interference due to the formation of these polyatomic ions certain measures can be taken, see sections 1.1.2 and 1.2.1.

Entrained atmospheric gases are responsible for a significant degree of spectroscopic interference, the most obvious examples being the presence of the $^{14}\text{N}_2^+$ and $^{16}\text{O}_2^+$ ions at $m/z = 28$ and 32 which arise due to atomisation survival of atmospheric N_2 and O_2 within the plasma. Previously it was recognised that an ICP discharge was more stable when enclosed with a flared torch extension.¹³⁴ Enclosed ICP ion sources have also been employed in ICP-OES for quite some time and it is now standard practise.^{142, 143}

The work in this section describes attempts made to limit the entrainment of atmospheric gases into the plasma to determine any analytical benefit. By limiting entrainment, the aim was to reduce spectroscopic interference. This limitation was attempted by enclosing the ICP within a ‘trumpet-end’ shaped torch bonnet positioned over the last 20 to 30 mm of the ICP torch and flush against the sample cone. This bonnet was held in place within the load coil.

By enclosing the ICP ion source it was believed that the surface area of the plasma open to the torch box atmosphere could be reduced, potentially limiting entrainment. Produced from silica, the bonnet design was composed of two sections; a tube of internal diameter (20.4 mm) slightly greater than that of the ICP torch and a widened ‘trumpet-end’ section to compensate for the lack of atmosphere at the sample cone that typically causes a compression at the tip of the plasma (see Figure 30).

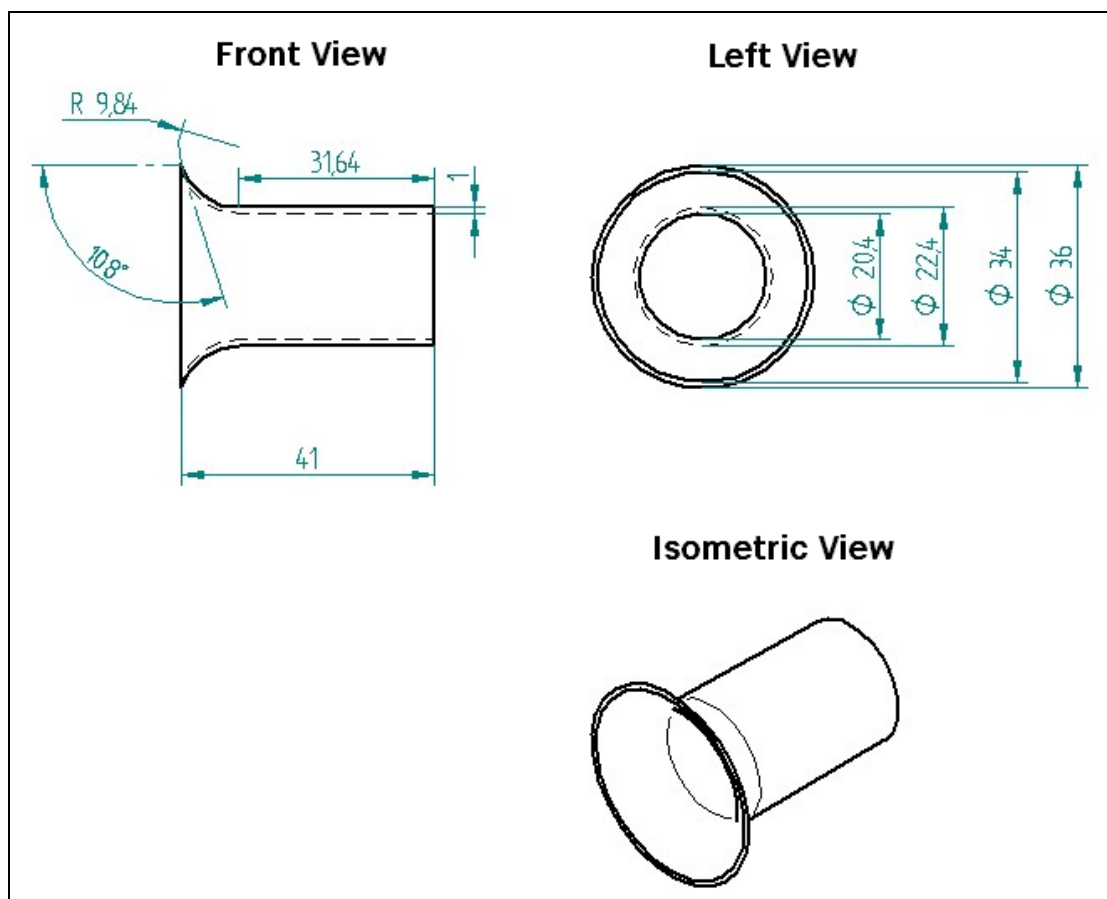


Figure 30. A Schematic of the Torch Bonnet Design (Dimensions Measured in mm).

Photographs of the torch bonnet, after its production, and its placement within the instrument torch box can be seen in Figures 91 and 92 (Appendix 2). There were initial concerns about carrying out this work with regard to whether the plasma generation would be affected by the presence of a second layer of silica from the torch bonnet and the tolerance of the silica with regard to its exposure to the high temperatures generated by the ICP. Initial experiments were cautiously carried out where an ICP was generated with the torch bonnet in place. On successful ICP generation, the bonnet was observed for periods of up to an hour after which, with no signs of deformity, the question of silica tolerance to plasma temperature was satisfactorily answered.

At this point experimentation was carried out to establish whether or not this approach would be beneficial with regard to tackling spectroscopic interferences.

Experimental Details

A series of P and S standard solutions, spiked with $1 \mu\text{g l}^{-1}$ In as an internal standard, were studied by ICP-MS both with and without the torch bonnet in position. Prior to analysis the ICP-MS instrument was stabilised and tuned as with the bonnet in place the torch box position could not be adjusted as the trumpet end sat closely against the sample cone. The general instrumental conditions employed during this study can be seen in Table 72 (Appendix 2) and the data generated can be seen in Table 73.

Results and Discussion

From the data generated three graphs were constructed that compare $m/z = 31$, 32 and 115 signals with and without the torch bonnet in position (see Figures 31, 32 and 33). It should be noted that under standard conditions the $m/z = 32$ signal for each standard solution was zero. This was because the number of ions being counted was so high, due to the presence of $^{16}\text{O}_2^+$, that the detector stops counting ions to preserve lifetime.

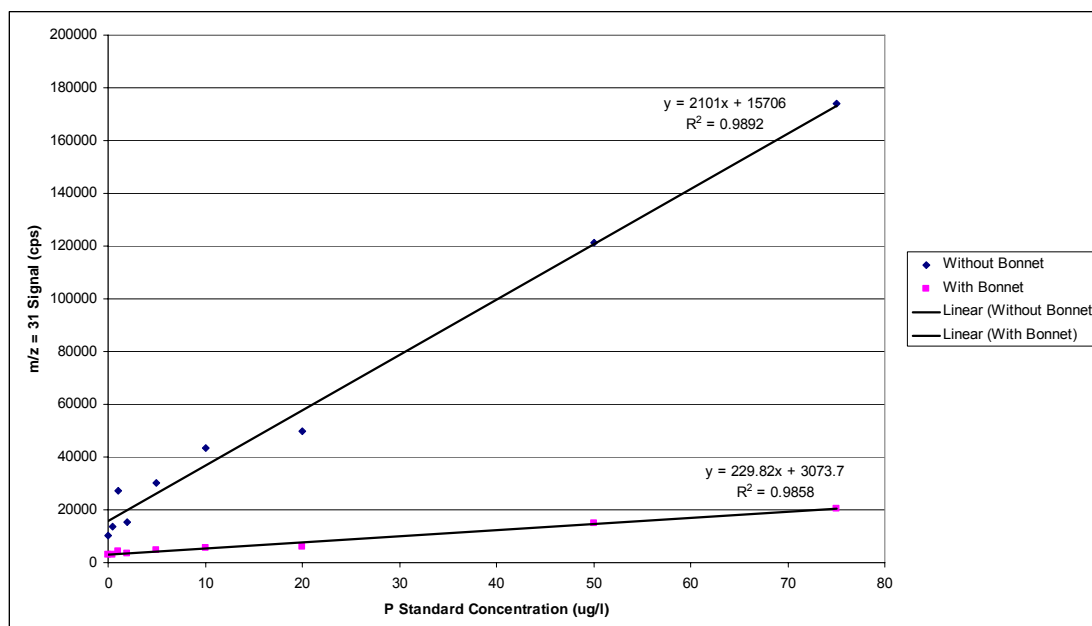


Figure 31. A Comparison of P Standard Concentration ($\mu\text{g l}^{-1}$) with $m/z = 31$ Signal (cps) for Analysis Under Standard Conditions and with the Torch Bonnet in Position.

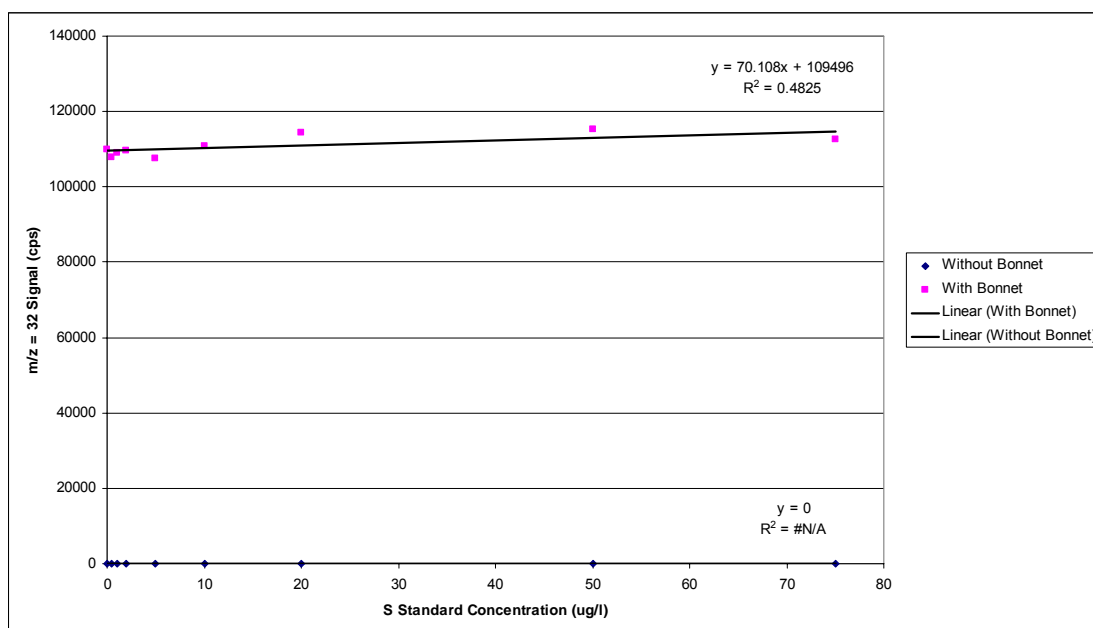


Figure 32. A Graph Comparing S Standard Concentration ($\mu\text{g l}^{-1}$) with $m/z = 32$ Signal (cps) for Analysis Under Standard Conditions and with the Torch Bonnet in Position.

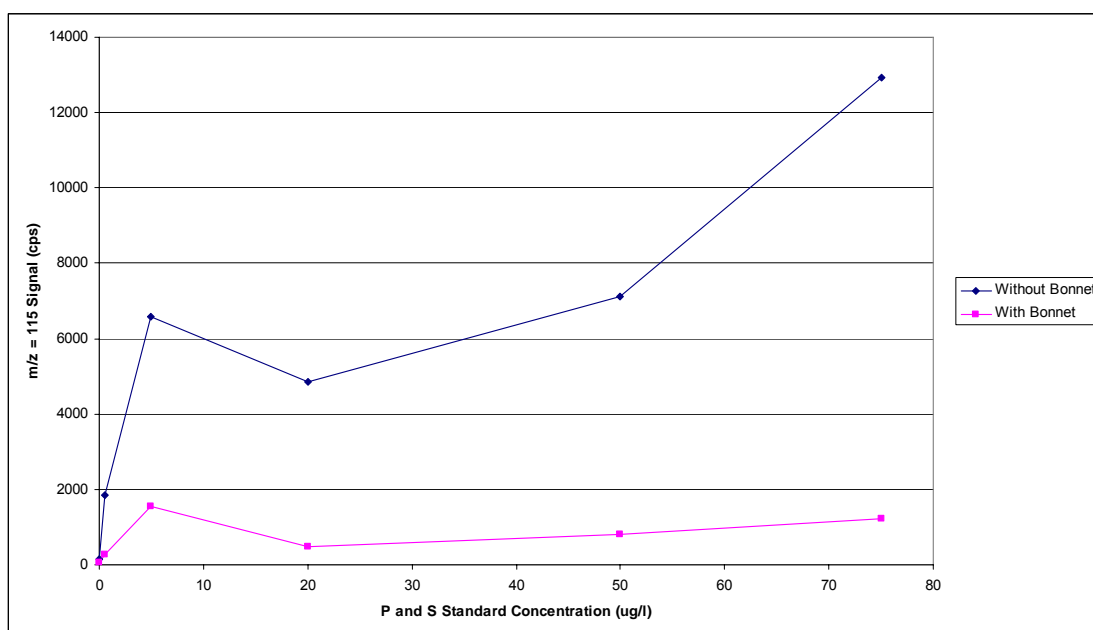


Figure 33. A Graph Comparing P and S Standard Concentration ($\mu\text{g l}^{-1}$) with $m/z = 115$ Signal (cps) for Analysis Under Standard Conditions and with the Torch Bonnet in Position.

As can be seen in Figure 31 when the torch bonnet was in position there was a reduction in signal, for each solution, compared to standard conditions. The $m/z = 31$ signal reduction for each solution studied was calculated and can be seen in Table 9.

Table 9. The $m/z = 31$ Signal Reduction Observed when the Torch Bonnet was in Position.

P Standard Concⁿ ($\mu\text{g l}^{-1}$)	$m/z = 31$ Signal Ratio (Standard Conditions : Torch Bonnet)
2 % HNO ₃ Blank	3.57
0.5	4.43
1	6.27
2	4.59
5	6.47
10	7.91
20	8.25
50	8.04
75	8.55

From the ratio data seen in Table 9 it would appear that there is not a uniform reduction of the $m/z = 31$ signal over the range of standard solutions studied. However, with the exception of three of the ratios calculated there is an approximate consistent reduction. The fact that the signal generated from the blank solution is reduced and that Figure 31 shows that with the torch bonnet in position the signal response for the range of solutions analysed maintains linearity suggests that the bonnet is in fact having a beneficial effect to a certain degree.

What should be understood, however, is that the enclosure of the ICP leads to a change in the discharge shape and length compared to the standard ICP-MS configuration whereby the last 20 to 30 mm of the plasma is open to the atmosphere of the torch box. Under the standard configuration, due to the incredibly high temperatures that the ICP reaches, as the discharge exits the torch it immediately contracts on contact with the lower temperature atmosphere of the torch box. When enclosed the ICP does not contract so technically should be longer and different in

shape (continuing in length rather than coming to a tip). Under the standard configuration the ICP ion source is very close to the sample cone so such changes to shape and length, when enclosed, would not be particularly noticeable. Under such an experimental approach to enclosing the ICP, drastically different signals compared to the standard data were to be expected.

As can be seen in the data of Table 73 and Figure 32 when the torch bonnet is in position there is a severe reduction in the $m/z = 32$ signal, from the region of hundreds of millions of ion counts per second to approximately 100 000 cps for each solution studied. Initially, this may sound as if the torch bonnet has been successful in excluding atmospheric O_2 from the plasma and limiting the generation of the $^{16}O_2^+$ ion. However, as the signals generated from each S sample solution studied are very similar then it is more likely that, in the case of $m/z = 32$, the bonnet is having a severe effect on ion sampling at the sample cone due to the change in characteristics of the ICP discharge.

As can be seen in Figure 33, similar to the $m/z = 31$ signal, when the torch bonnet was in position there was a reduction in $m/z = 115$ signal, for each solution, compared to standard conditions. Unfortunately this data confirmed that there was a blanket signal reduction rather than simply a reduction of polyatomic ion species that contribute to individual m/z signals. However, this reduction for each solution was still calculated and can be seen in Table 10.

Table 10. The $m/z = 115$ Signal Reduction Observed when the Torch Bonnet was in Position.

P and S Standard Concⁿ ($\mu\text{g l}^{-1}$) (1 $\mu\text{g l}^{-1}$ In Spike)	$m/z = 115$ Signal Ratio (Standard Conditions : Torch Bonnet)
2 % HNO ₃ Blank	2.40
0.5	6.91
1	11.25
2	11.13
5	4.25
10	12.14
20	10.08
50	8.69
75	10.57

Similar to the $m/z = 31$ data in Table 9 there is some consistency in signal reduction over the range of solutions studied but it is not uniform as would be desired.

It is possible that the signal reductions observed as a result of this work could be due to a hindrance of ion sampling as the plasma gases are being directed onto the sample cone with a limited possibility of exhaust into the main body of the torch box. Because this is a possibility and the data accrued was not particularly promising, a second torch bonnet was designed and manufactured to allow gas exhaust, see section 2.4.7.

2.4.7. Method 6 (Part 2): The Exclusion of Entrained Atmospheric Gases from the ICP

Following the sensitivity reduction observed when completely enclosing the ICP with the torch bonnet described in section 2.4.6 a second bonnet was designed with the aim of allowing the exhaust of plasma gases at the sample cone. This design was very similar to the first but differed with the incorporation of a series of spacers at the ‘trumpet’ end. Figure 34 shows a schematic of the second torch bonnet design that has been compared in appearance to a castle turret.

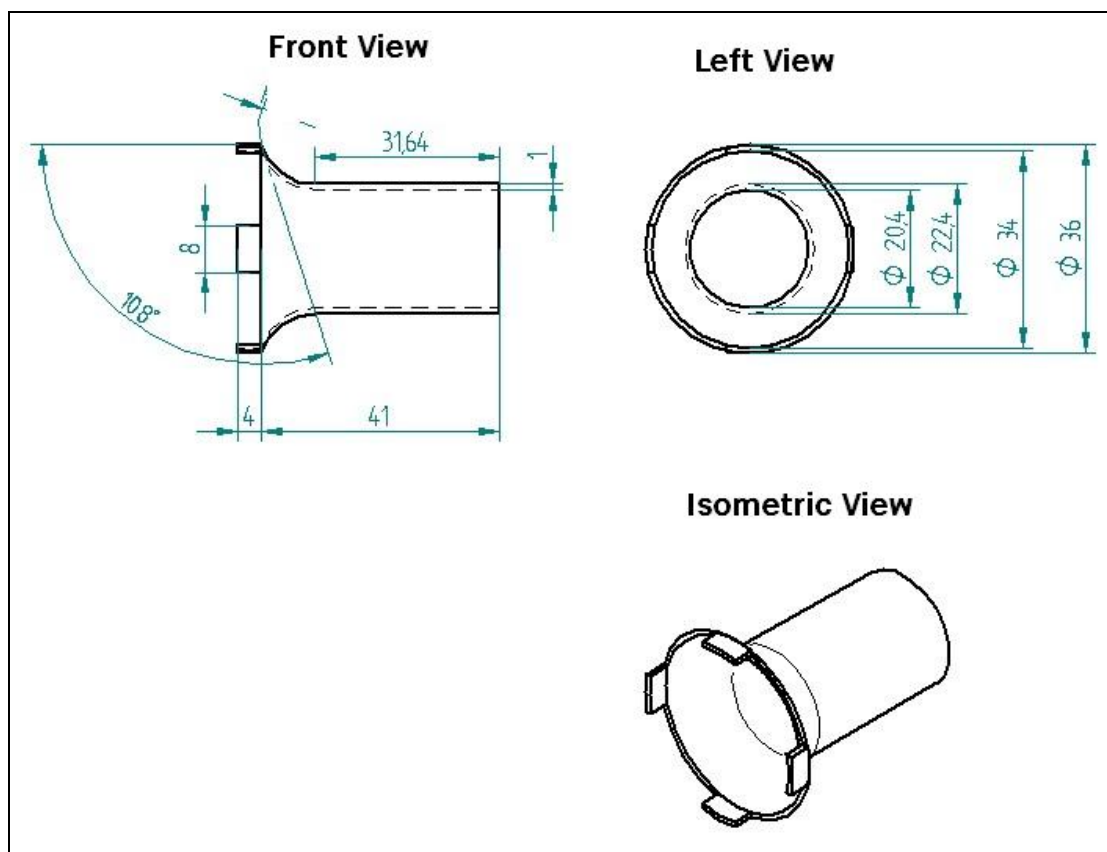


Figure 34. A Schematic of the Second Torch Bonnet Design (Dimensions Measured in mm).

Photographs of the second torch bonnet design, and its placement within the instrument torch box can be seen in Figures 91 and 93 (Appendix 2).

Experimental Details

As with the first torch bonnet design, a series of $1 \mu\text{g l}^{-1}$ In spiked P and S standard solutions, of increasing concentration, were studied with and without the second torch bonnet in position. Prior to this analysis the ICP-MS instrument was stabilised and tuned, for the reason that the torch box position could not be adjusted when the bonnet was in place. The general instrument conditions employed during this study can be seen in Table 74 (Appendix 2).

Results and Discussion

The data generated following study of the P and S solutions can be seen in Table 75 (Appendix 2). From the data generated during this study a series of graphs were constructed that compare $m/z = 31$, 32 and 115 signals with and without the torch bonnet in place (see Figures 35, 36 and 37).

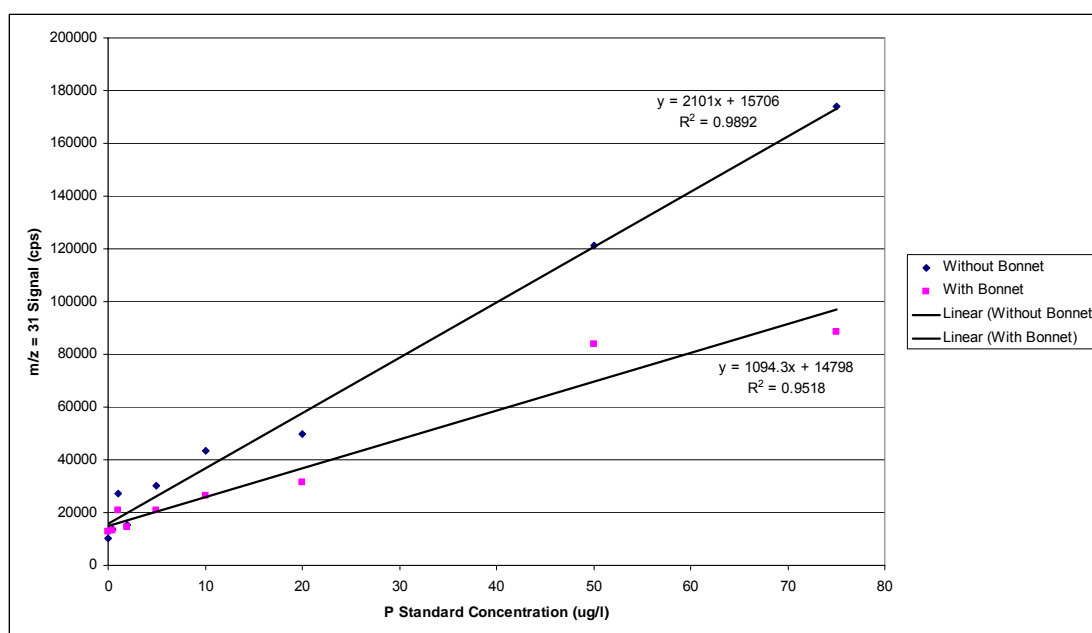


Figure 35. A Graph Comparing P Standard Concentration ($\mu\text{g l}^{-1}$) with $m/z = 31$ Signal (cps) for Analysis Under Standard Conditions and with the Second Torch Bonnet Design in Place.

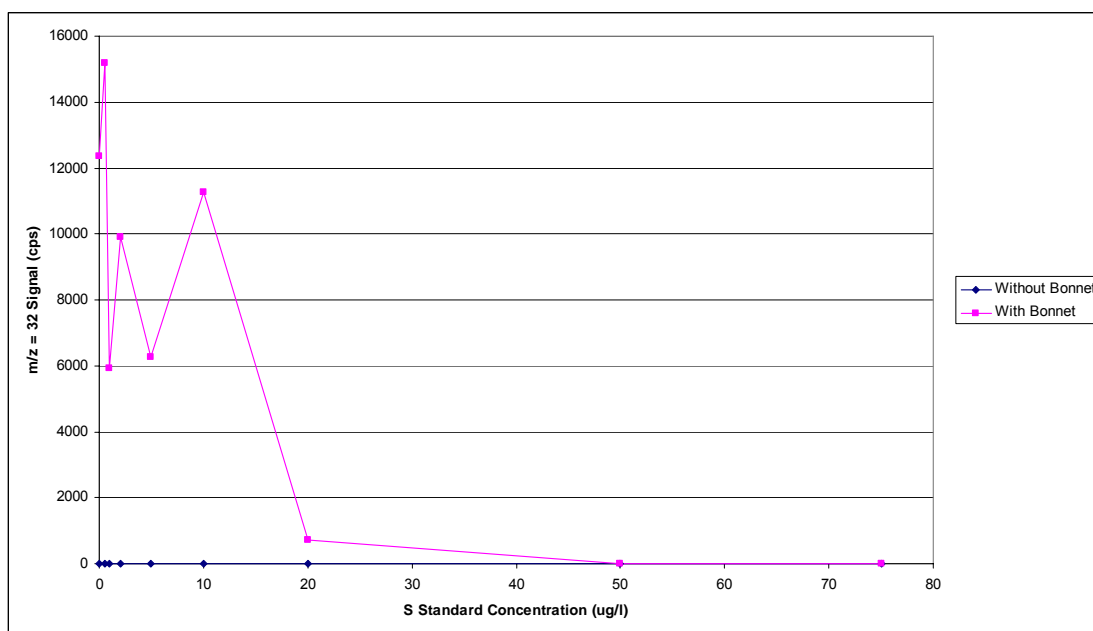


Figure 36. A Graph Comparing S Standard Concentration ($\mu\text{g l}^{-1}$) with $m/z = 32$ Signal (cps) for Analysis Under Standard Conditions and with the Second Torch Bonnet Design in Place.

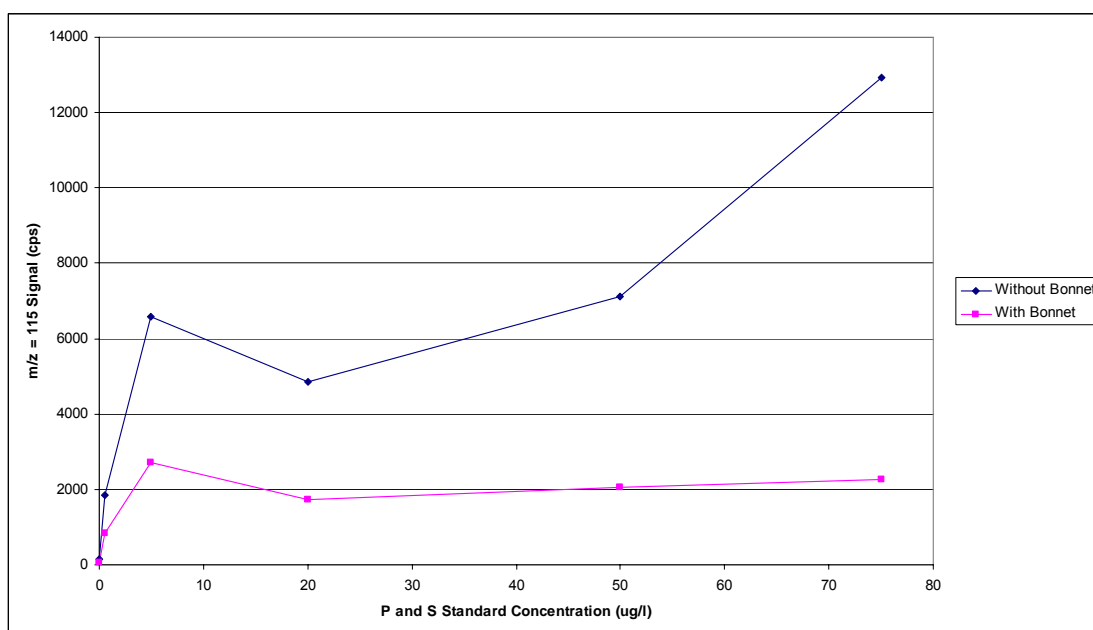


Figure 37. A Graph Comparing P and S Standard Concentration ($\mu\text{g l}^{-1}$) with $m/z = 115$ Signal (cps) for Analysis Under Standard Conditions and with the Second Torch Bonnet Design in Place.

As can be seen in Figure 35 when this second torch bonnet was in position there was a reduction in signal, for each solution, compared to standard conditions. The $m/z = 31$ signal reduction for each solution studied was calculated and can be seen in Table 11.

Table 11. The $m/z = 31$ Signal Reduction Observed when the Second Torch Bonnet was in Position.

P Standard Concⁿ ($\mu\text{g l}^{-1}$)	$m/z = 31$ Signal Ratio (Standard Conditions : Torch Bonnet)
2 % HNO ₃ Blank	0.81
0.5	1.04
1	1.31
2	1.06
5	1.43
10	1.65
20	1.59
50	1.44
75	1.96

Similar to the $m/z = 31$ ratio data associated with the first torch bonnet design (see Table 9), the data in Table 11 shows that with the second torch bonnet in position there was an approximate consistent signal reduction over the range of sample solutions studied. Again, this $m/z = 31$ data suggests that with the bonnet in position there may have been a beneficial effect taking place as the signal response maintains linearity.

As can be seen in the data of Table 75 and Figure 36 when this second design was in position, with the exception of the 50 and 75 $\mu\text{g l}^{-1}$ S solutions, there was a drastic reduction in $m/z = 32$ signal. In the case of this second bonnet design the signal reduction was far greater than that observed when the first was in position for each sample studied (to approximately 10 000 cps compared to approximately 100 000 cps). However, as the signal reduction for each sample resulted in a $m/z = 32$ response that did not represent any kind of gradual increase then there was obviously no selective species reduction taking place. This data suggests that the presence of the

bonnet was having a severe effect on ion sampling at the sample cone due to the change in characteristics of the ICP discharge.

Similar to the $m/z = 31$ signal, Figure 37 shows that when the second torch bonnet design was in position there was a reduction in $m/z = 115$ signal for each solution analysed when compared to standard conditions. The degree of signal reduction observed for each sample solution was calculated and can be seen in Table 12.

Table 12. The $m/z = 115$ Signal Reduction Observed when the Second Torch Bonnet was in Position.

P and S Standard Concⁿ ($\mu\text{g l}^{-1}$) (1 $\mu\text{g l}^{-1}$ In Spike)	$m/z = 115$ Signal Ratio (Standard Conditions : Torch Bonnet)
2 % HNO ₃ Blank	2.03
0.5	2.23
1	2.26
2	2.36
5	2.42
10	2.36
20	2.79
50	3.45
75	5.69

The signal reduction data in Table 12 shows that, with the exception of two samples (50 and 75 $\mu\text{g l}^{-1}$ P and S), the signal generated from each sample was reduced to a similar degree. Unfortunately this $m/z = 115$ data has confirmed that the presence of this second bonnet resulted in a blanket signal reduction rather than the desired selective polyatomic ion species reduction. The significant difference for $m/z = 115$ between the two bonnet designs was that the signals were suppressed to a slightly different degree. To the high hundreds and low thousands of ion counts for 1 $\mu\text{g l}^{-1}$ In for the first bonnet design and to thousands of ion counts for the second bonnet design.

As can be seen from the data accrued during study of both torch bonnet designs the sensitivity reduction observed applies to all m/z signals studied rather than those of specific isotopes. Although this is not the desired result such an approach shows promise with regard to the ^{31}P and ^{32}S isotopes as the $m/z = 31$ signal maintains linearity and the $m/z = 32$ signal was pulled into the detectable range. So far the work carried out in this area has shown promise, however, further study is required. With further modification and careful fabrication it may be possible to produce a torch bonnet that successfully limits atmospheric gas entrainment, and hence polyatomic ion formation, with minimal effect on the ion sampling process.

2.5. The Calculation of Method Limit of Detection (LOD)

The LOD for each method was calculated by two separate approaches. The reason for this was to provide fair LOD data for comparison with data already published by other research groups and instrument manufacturers. Although the more common approach to calculation of LOD (instrumental LOD) may provide a lower limit such a figure may not be realistic.

2.5.1. LOD Calculation 1

The most common method for LOD calculation incorporates the error associated with the blank solution only, i.e. an instrumental LOD. Here LOD was calculated using the equation in Figure 38 whereby the standard deviation of the 2 % HNO₃ blank ICP-MS signal and the slope of the calibration curve are manipulated.¹⁴⁴

$\text{Limit of Detection} = -3s_B / m$ <p>Where: s_B = Standard Deviation of the Blank Solution m = Slope of the Calibration Curve</p>

Figure 38. The Common Approach to the Calculation of Limit of Detection.

2.5.2. LOD Calculation 2

A more realistic approach to the calculation of LOD is to sum the ICP-MS signal corresponding to the blank solution with the standard error associated with the

calibration curve (multiplied by three) to produce a signal equivalent to LOD, i.e. a method LOD, see Figure 39.¹⁴⁴

$\text{Limit of Detection Signal} = y_B + 3s_{y/x}$ <p>Where: y_B = Blank Signal $s_{y/x}$ = Standard Error of the Calibration Curve</p>

Figure 39. The Equation used to Calculate Limit of Detection Signal (More Realistic Approach).

To determine standard error of the calibration curve a regression is carried out on the data generated during the calibration experiments. Following determination of the signal equivalent to the LOD the figure is fed back into the calibration curve equation to produce the limit.

2.5.3. A Comparison of LOD's

For the four successful approaches to ³¹P and ³²S measurement discussed in section 2.4 (methods 2, 3, 4 and 5) LOD was calculated via the above two approaches. These calculated limits can be seen in Table 13.

Table 13. LOD's Calculated by both Approaches for Methods 2, 3, 4 and 5.

Method Number	³¹P (Instrumental LOD) (µg l⁻¹)	³²S (Instrumental LOD) (µg l⁻¹)	³¹P (Method LOD) (µg l⁻¹)	³²S (Method LOD) (µg l⁻¹)
2	0.69	1.43	9.50	6.50
3	1.48	-	7.78	-
4	0.89	25	6.56	6.84
5	0.74	1.23	14	80

As can be seen in Table 13 the methods developed provide a range of LOD's for the ³¹P and ³²S isotopes.

For the ³¹P LOD by calculation 1 the limits obtained are very similar for methods 2, 4 and 5 (< 1 µg l⁻¹) whilst that for method 3 is slightly higher (1.48 µg l⁻¹) but not significantly. For ³²S LOD by calculation 1, methods 2 and 5 exhibit similar values of approximately 1 µg l⁻¹ whilst for method 4 the value is much higher at 25 µg l⁻¹. The reason for this is that the gradient of the calibration curve for method 4 is only 57.318 which is far more shallow than the other methods studied so results in a higher LOD. This suggests that the efficiency of formation of the ³²S¹⁶O⁺ ion by method 4 is lower than that of methods 2 and 5.

For the ³¹P LOD by calculation 2 the limits obtained are similar between the four calibrated methods. The limit calculated for method 5 is slightly higher but not greatly so. For ³²S LOD by calculation 2 methods 2 and 4 exhibit similar values (≈ 7 µg l⁻¹) whilst the value for method 5 is far higher at 80 µg l⁻¹.

2.6. Conclusions

As a result of the work carried out four methods, of six overall ideas, were successfully developed for the measurement of ^{31}P and ^{32}S isotopes by quadrupole based ICP-MS. Instrumental and method LOD's were calculated via two approaches, described in section 2.5, some of which are comparable to those quoted by other researchers whilst others are poorer (see Tables 13 and 14). However, an appraisal of the LOD data that has been calculated does not simply allow the selection of the best analytical method.

In this case the best LOD data was produced by methods 2, 4 and 5 (the collision cell oxygen reaction gas, the 'cold/cool plasma' and the 'cold/cool plasma' with additional oxygen nebuliser gas flow methods). Before selecting the most appropriate method for analysis other factors must be considered. The method precision and dynamic range require assessment and have not been considered during this work. Also, the application of the method is very important. Method 2 is very different from 4 and 5 in terms of the ICP power that was employed. Unfortunately, in the case of methods 4 and 5, there is a limit to the type of sample that the low power ICP can accept. Complex samples, containing a significant quantity of dissolved solids, would most likely extinguish the low power ICP. For this reason methods 4 and 5 would be limited to simple samples. A higher power plasma, like that employed in method 2, would accept more complex samples and efficiently atomise and ionise them. Therefore a choice of employment between these methods would be based on sample application. The use of a 'cold/cool plasma' for the measurement of the ^{31}P isotope has only been mentioned once (Wiedemann *et al.*¹³⁸) and has not been employed in the measurement of the ^{32}S isotope. On the other hand the use of a collision/reaction cell with an oxidising gas is a common approach to the measurement of these isotopes.

The enclosed ICP approach (method 3), although not fruitful, showed some promise with regard to the possible reduction of spectroscopic interferences. So far there has not been a torch bonnet successfully developed for this purpose, however, further

work on this idea and careful design of the enclosing bonnet may prove to be beneficial.

Although exhibiting slightly poorer LOD's than those quoted by the instrument manufacturer Perkin Elmer and in the method developed by Bandura *et al.*⁹⁰ (see section 2.1.1) it should be noted that the methods described were developed in a standard laboratory with standard reagents rather than under 'clean room' conditions with ultra pure reagents. Under such 'clean' conditions the methods described may be capable of superior LOD's for ^{31}P and ^{32}S . Many of the ICP-MS spectroscopic interferences that afflict the $m/z = 31$ and 32 ratios can be overcome or alleviated, however, during the course of this research it was appreciated that the ^{31}P and ^{32}S isotopes are at a significant disadvantage with regard to ionisation within the ICP, due to their primary ionisation potential. It is this disadvantage that dominates the determination of ^{31}P and ^{32}S isotopes at trace levels by ICP-MS regardless of the type of mass spectrometry in use.

To conclude this chapter, the merits and limitations of methods 2, 3, 4 and 5 and methods developed by other researchers are summarised and compared, see Table 14. Following the successful development work described in this chapter, methods 2, 3, 4 and 5 were each employed in the quantification of ^{31}P in DNA as an application in genomics, see Chapter 3.

Table 14. A Summary and Comparison of Methods Developed for the Measurement of ^{31}P and ^{32}S Isotopes by ICP-MS.

Method Identification	Method Authors	Reference	Method Description	Merits	Limitations
Method 2	P.D. Winship	-	The use of O_2 in a collision cell to oxidise ^{31}P and ^{32}S for alternative measurement at $m/z = 47$ and 48	LOD's of 0.7 to $9.50 \mu\text{g l}^{-1}$ and 1.43 to $6.50 \mu\text{g l}^{-1}$ for ^{31}P and ^{32}S respectively, normal ICP forward power	Specific for phosphorus and sulphur measurement
Method 3	P.D. Winship	-	The use of He and KED in a collision cell to remove polyatomic ions at $m/z = 31$	LOD's of 1.43 to $7.78 \mu\text{g l}^{-1}$ for ^{31}P , normal ICP forward power	Specific for phosphorus measurement
Method 4	P.D. Winship	-	The use of a low forward power ICP to promote ^{31}P and ^{32}S oxidation for measurement at $m/z = 47$ and 48	LOD's of 0.89 to $6.56 \mu\text{g l}^{-1}$ and 6.84 to $25 \mu\text{g l}^{-1}$ for ^{31}P and ^{32}S respectively, no collision/reaction cell requirement	Specific for phosphorus and sulphur measurement, less robust ICP
Method 5	P.D. Winship	-	The use of a low forward power ICP to promote ^{31}P and ^{32}S oxidation for measurement at $m/z = 47$ and 48	LOD's of 0.74 to $14 \mu\text{g l}^{-1}$ and 1.23 to $80 \mu\text{g l}^{-1}$ for ^{31}P and ^{32}S respectively, no collision/reaction cell requirement	Specific for phosphorus and sulphur measurement, less robust ICP
Hexapole Collision Cell ($\text{He}, \text{H}_2 + \text{Xe}$)	P. R. D. Mason <i>et al.</i>	<i>J. Anal. At. Spectrom.</i> , 1999, 14 , 1067-1074	The use of H_2 and Xe to remove polyatomic ions at $m/z = 32, 33$ and 34	LOD's of $20 - 50 \mu\text{g l}^{-1}$ for S isotope measurement, normal ICP forward power	Specific for sulphur measurement
Dynamic Reaction Cell (O_2)	D. R. Bandura <i>et al.</i>	<i>Anal Chem.</i> 2002, 74 , 1497-1502	The use of O_2 in a dynamic reaction cell to oxidise ^{31}P and ^{32}S for alternative measurement at $m/z = 47$ and 48	LOD's of $< 100 \text{ ng l}^{-1}$ and $< 200 \text{ ng l}^{-1}$ for ^{31}P and ^{32}S respectively, normal ICP forward power	Specific for phosphorus and sulphur measurement

Chapter 3

The Application of Methods Developed for the Determination of ^{31}P and ^{32}S and the Study of DNA and Related Material by ICP-MS

3.1. Genomics

Following the successful method development described in Chapter 2 it was decided to apply some of these methods to study within the field of genomics, i.e. the nucleic acids carrying genetic information, particularly DNA.¹³⁷ DNA was selected as an application of the methods developed as ^{31}P constitutes approximately 10 %, by mass, of the molecule. Table 15 compares the overall molecular mass of each nucleotide (base molecule and phosphate-sugar molecule) present in a DNA molecule and provides a mean mass to highlight how the 10 % ^{31}P component has been reached.

Table 15. The Overall Molecular Mass of Individual DNA Nucleotides.

Nucleotide Identification	Overall Molecular Mass
Adenine (A)	330
Guanine (G)	306
Cytosine (C)	346
Thymine (T)	321
Mean Nucleotide (Free State)	325.75
Mean Nucleotide (Bound State)	307.75

From the data in Table 15 it was calculated that the mean molecular mass of a DNA nucleotide in a free state is 325.75 and when bound in a helix 307.75. Therefore the ^{31}P content in the free state and bound state is 9.52 % and 10.07 % respectively.

An alternative application area, for these ICP-MS methods, could have been proteomics due to the prevalence of phosphorylation processes taking place as part of the biochemistry of the human body.¹³⁷ Such study could have involved the analysis of both ^{31}P and ^{32}S isotopes due to the presence of S in the cysteine and methionine amino acids. However, work is currently being carried out in this area by numerous research groups so the decision was to employ these ICP-MS methods in the lesser studied area of genomics.

Figure 40 is a structural diagram of the nucleotide sequences present in a DNA molecule. This diagram highlights the presence of ^{31}P within the structure of the molecule. P is the key element in the bridging structures that link the five membered ring sugar molecules providing a backbone to the base molecules adenine (A), guanine (G), cytosine (C) and thymine (T).^{137, 145}

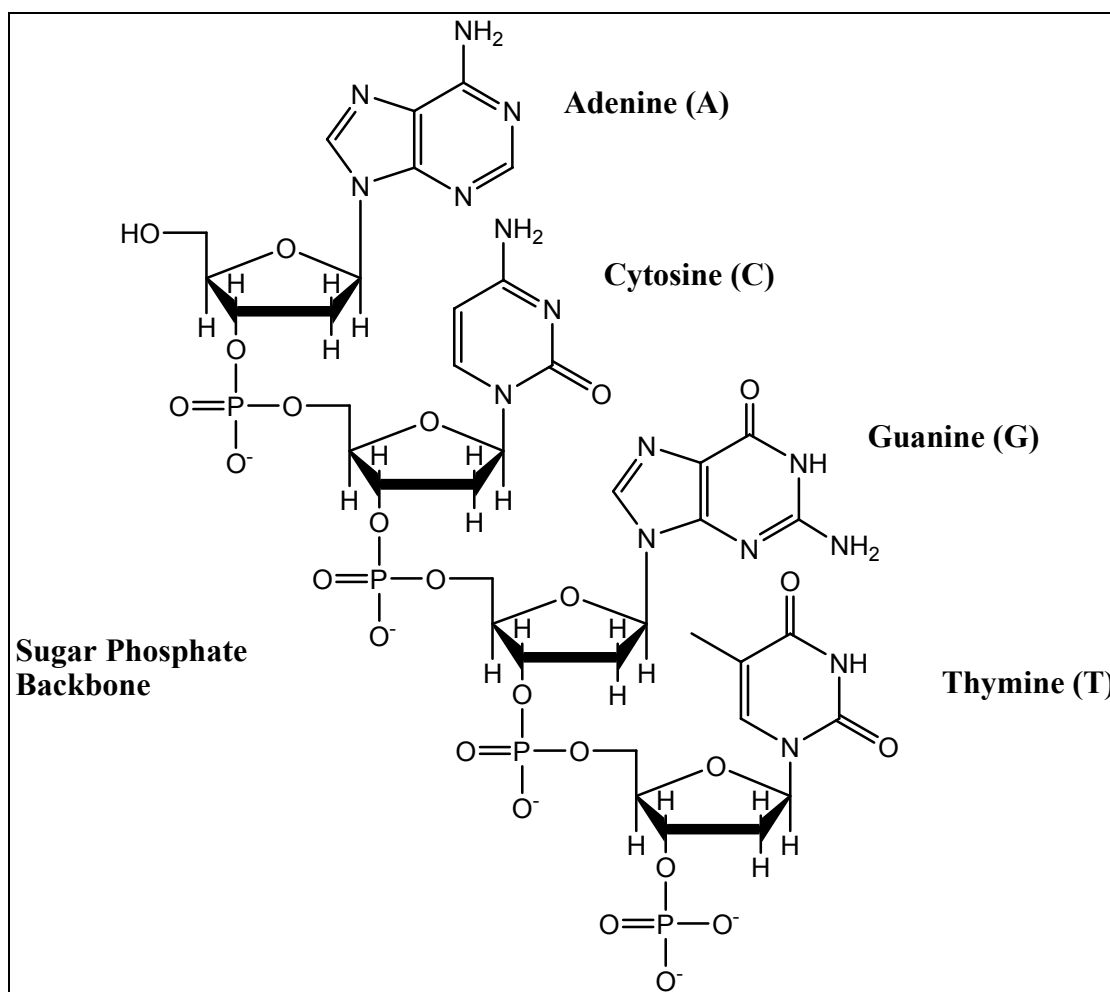


Figure 40. A Structural Diagram of Nucleotides That Make Up The DNA Molecule.

There has been very little work carried out on direct measurements of DNA by ICP-MS. Currently most work in the area of DNA study by ICP-MS can be divided into two types. Firstly the measurement of particular elements of species that interact with DNA, i.e. non direct study of the DNA molecule. For example the interaction

between DNA, or component nucleotides, and metal based therapeutic agents. Examples of such interactions are described in detail in Chapter 4. The second type of DNA study by ICP-MS involves the measurement of metal ‘tags’ that have been attached to DNA or DNA nucleotides. Nanoparticulate gold is one such tag and has been used in the determination of various nucleotide sequences by ICP-MS. This is an area of research that is being pursued by the Loughborough University atomic spectroscopy research group and shows great potential as an application of ICP-MS in the biological sciences.

3.2. Aims of Research

Currently DNA is commonly quantified by UV/Vis and fluorescence techniques that are well established and capable of the detection of single DNA molecules.¹⁴⁵ It was the aim of this work to determine the feasibility of quadrupole based ICP-MS as an alternative approach to the quantification of DNA via the measurement of the ³¹P isotope.

3.3. The Application of Developed Methods

Following the development work that was carried out (see Chapter 2) the four successful methods for the determination of ³¹P (methods 2, 3, 4 and 5) were applied to the quantification of DNA in solution via a standard additions approach. Beyond this method 2 was employed in the study of DNA separated within an agarose gel and sections of DNA amplified via a polymerase chain reaction (PCR). Methods 2 and 4 were also used in the analysis of single nucleotide polymorphisms (SNP’s) following separation by HPLC.

3.4. DNA Quantification by Methods 2, 3, 4 and 5

Initial experimentation was carried out to determine the capabilities of these ICP-MS methods with regard to the analysis of ‘real’ DNA samples in solution. Whilst evaluating the application of the methods developed the question of the effect of the DNA carbon content on the ICP was considered. Previous work has shown that the presence of a certain amount of carbon based material within a sample can have a beneficial effect on overall analytical sensitivity. Volatile carbon compounds in a sample, in certain quantities, can aid in the sample introduction process through a spray chamber and nebuliser.¹⁴⁶ However, the presence of a high level of carbon in a sample can have detrimental effects on an analysis, contributing increases in carbon based polyatomic ions and sample and skimmer cone deposition.⁴ The DNA molecular structure is predominantly composed of carbon so through these experiments the potential for spectroscopic and non-spectroscopic interference (i.e. presence of polyatomic ions and reduced sensitivity as a result of a lowering of plasma temperature and cone clogging) was monitored by the comparison of measured ³¹P concentration with the expected concentration. Concern was also raised with regard to the nebulisation efficiency of a DNA solution, this was also studied during initial experimentation.

Experimental Details

DNA samples were studied, under method 2, 3, 4 and 5 conditions, via a standard additions approach in order to quantify the concentration present and evaluate the occurrence of non-spectroscopic interference. In this case such interference may have originated from the presence of carbon originating from the DNA molecule or nebulisation problems. A series of DNA/³¹P and ³¹P standard solutions were prepared from calf thymus DNA (Sigma-Aldrich) and 1000 µg ml⁻¹ single element P standard solution (Fisher Chemicals, Loughborough, UK) and simultaneously analysed employing methods 2, 3, 4 and 5. As this work was carried out over a long period of time there was some variation between the application of these methods for the study of DNA. In the case of methods 2 and 4 2000 µg l⁻¹ DNA samples were studied

whereas $200 \mu\text{g l}^{-1}$ DNA samples were studied via methods 3 and 5. There is no data available for the analysis of standard solutions under method 2 as P standards were not simultaneously analysed. The general instrumental conditions under which this work was carried out can be seen in Tables 76 to 79 (Appendix 3).

Results and Discussion

The data for the analysis of the prepared DNA and ^{31}P solutions can be seen in Table 80 (Appendix 3). Using this data a series of graphs were constructed to compare the analysis of DNA via the four methods studied, see Figures 41, 42, 43 and 44.

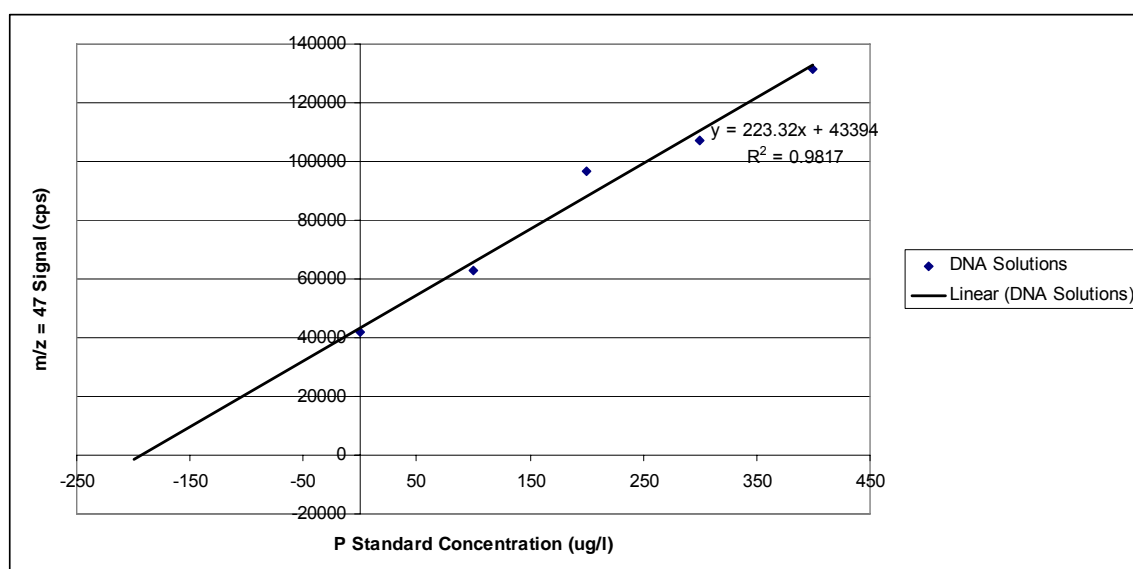


Figure 41. A Standard Additions Graph Comparing P Standard Concⁿ ($\mu\text{g l}^{-1}$) with $m/z = 47$ Signal (cps) for a Series of P Spiked $2000 \mu\text{g l}^{-1}$ DNA Solns Under Method 2 Conditions.

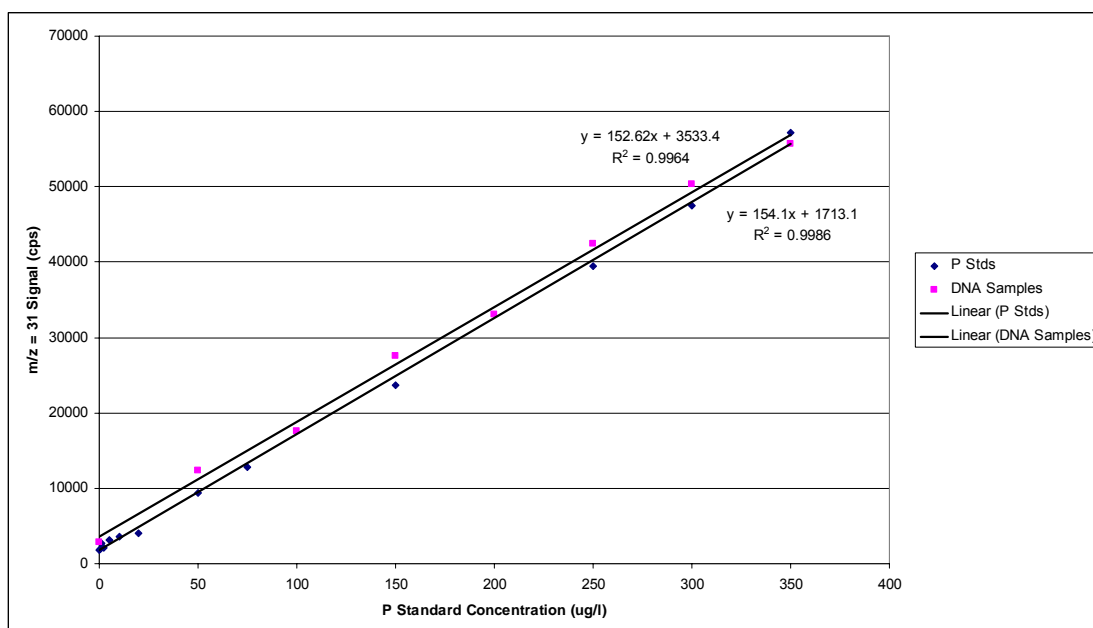


Figure 42. A Standard Additions Graph Comparing P Standard Concⁿ ($\mu\text{g l}^{-1}$) with $m/z = 31$ Signal (cps) for a Series of P Standard Solns and P Spiked $200 \mu\text{g l}^{-1}$ DNA Solns Under Method 3 Conditions.

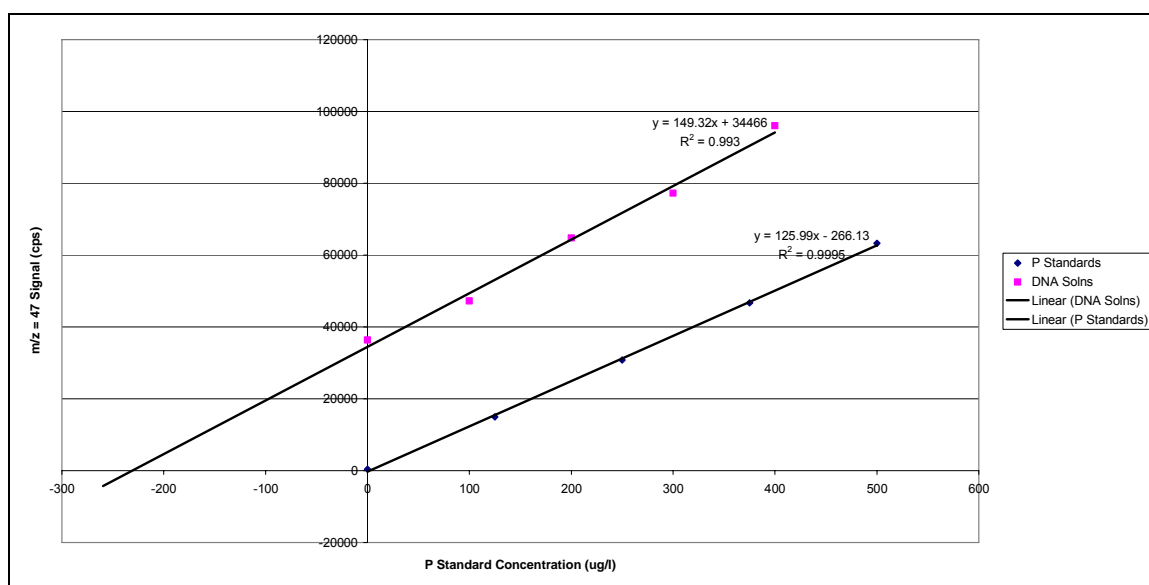


Figure 43. A Standard Additions Graph Comparing P Standard Concⁿ ($\mu\text{g l}^{-1}$) with $m/z = 47$ Signal (cps) for a Series of P Standard Solns and P Spiked $200 \mu\text{g l}^{-1}$ DNA Solns Under Method 4 Conditions.

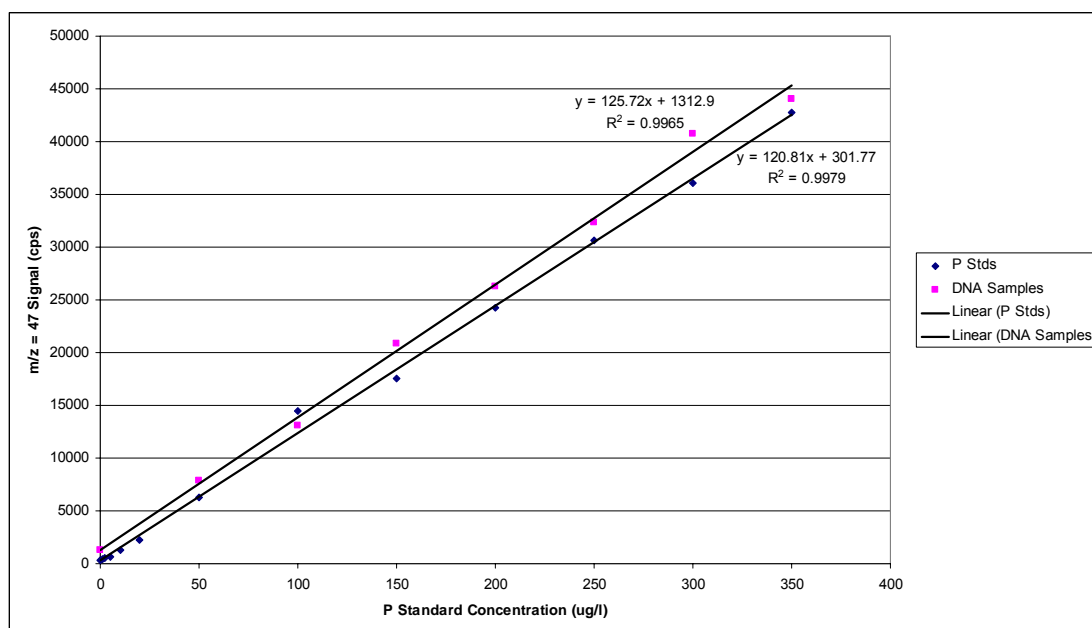


Figure 44. A Standard Additions Graph Comparing P Standard Concⁿ ($\mu\text{g l}^{-1}$) with $m/z = 47$ Signal (cps) for a Series of P Standard Solns and P Spiked $200 \mu\text{g l}^{-1}$ DNA Solns Under Method 5 Conditions.

Figures 41, 42, 43 and 44 are graphs comparing the $m/z = 31$ or 47 signal with the ^{31}P concentration of standard inorganic salt solutions and P spiked, 200 or $2000 \mu\text{g l}^{-1}$, DNA solutions for ICP-MS analysis by methods 2, 3, 4 and 5. Linearity of the points on each line amongst these graphs is very good. Extrapolation of the DNA solution line backwards allows quantification as the difference between the origin and the point at which the line intercepts the x-axis yields the ^{31}P concentration of the 200 or $2000 \mu\text{g l}^{-1}$ DNA solution.¹⁴⁷ The DNA quantification data for these standard addition studies can be seen in Table 16.

Table 16. Quantification Data for the Analysis of 200 and 2000 $\mu\text{g l}^{-1}$ DNA Solutions by Methods 2, 3, 4 and 5.

Method Number	Standard Additions Curve Equation	^{31}P Concⁿ Present in a 200 or 2000 $\mu\text{g l}^{-1}$ DNA Solution ($\mu\text{g l}^{-1}$)	^{31}P Composition of DNA Sample (%)
2	$y = 223.32x + 43394$	194.31	9.72
3	$y = 152.62x + 3533.4$	23.15	11.58
4	$y = 149.32x + 34466$	230.82	11.54
5	$y = 125.72x + 1312.9$	10.44	5.22

The data of Table 16 shows that all four methods are capable, to a certain degree, of the determination of DNA in a simple H_2O matrix. In the case of the 200 or 2000 $\mu\text{g l}^{-1}$ DNA solutions studied the ^{31}P content should be in the order of 20 or 200 $\mu\text{g l}^{-1}$ respectively and three methods (2, 3 and 4) provided a ^{31}P concentration close to what was expected. Method 5 exhibited a ^{31}P concentration approximately half of what was expected. It is possible in the case of this method that the atomisation of the DNA molecule and ionisation of the ^{31}P atom may not have been as efficient in the lower forward power Ar/O₂ mixed gas ICP as in the plasma run under the other three methods.

The most important information that has been obtained through the work described in this section is that, with the exception of the method 5 data, the DNA molecule in solution was successfully nebulised without difficulty and introduced to the ICP ion source. On comparison with P standard information the data accrued from methods 2, 3 and 4 has shown that non-spectroscopic interference was not a significant problem. Although this analysis was very simple in terms of the sample matrix it allowed the progression of the study of DNA by quadrupole based ICP-MS. It would appear, however, that at trace levels ICP-MS may struggle in the measurement of DNA compared to the capabilities of the robust UV/Vis and fluorescence techniques.

3.5. The Analysis of DNA Samples Separated on an Agarose Gel Plate by ICP-MS Employing Method 2

Following the successful analysis of DNA in solution employing three of the four methods developed, further study was carried out on DNA samples separated on agarose gel plates (2 % Agarose). Such a separation is commonly carried out to determine the presence of DNA polymorphisms during profiling experiments.¹⁴⁸ Again fluorescence techniques are normally employed in the determination of DNA present in such gels.¹⁴⁵ The aim of this section of work was to establish the feasibility of measuring DNA, via method 2 - ³¹P isotope analysis, within a gel following a digestion procedure. Method 2 was selected as, of the four, it was the most sensitive and robust, operating at a standard ICP forward power (see section 2.5.3).

Experimental Details

Agarose gel (2 %) was prepared by dissolving agarose (2 g) in tris-borate buffer, TBE, (100 ml) containing ethidium bromide (0.5 µg ml⁻¹) at 100 °C in a microwave. Following casting of the gel, DNA was separated through it with application of 125 V for a period of 1 hour. Sections of separated DNA were then identified under UV radiation and removed for ICP-MS study.

Digestion of the gel was originally attempted with a HNO₃/H₂O₂/H₂O digest solution, however, initial analysis revealed a problem. The blank solutions analysed appeared to contain significant quantities of ³¹P. The obvious explanation was that contamination of the HNO₃ and H₂O₂ solutions was the cause of this, but it was also possible that the digestion solution was leaching ³¹P from the pump tubing and sample introduction glassware before transport into the plasma. Even with thorough cleaning of the glassware and new pump tubing, this problem remained. Eventually a simple H₂O leachate was carried out to remove the DNA from the agarose gel whilst avoiding the contamination problems previously encountered.

Agarose gel (0.22 g, with an ensured quantity of DNA present determined by staining with ethidium bromide and observation under UV radiation) was transferred to a Nalgene bottle to which deionised H₂O was added giving the gel and H₂O a combined mass of 10 g. The bottle was sealed and incubated in a water bath at 80°C for a period of 3 hours. A similar bottle containing 10 g H₂O only was subjected to the same conditions to act as a crude blank (an ideal blank sample would have been a similarly treated agarose gel without DNA present).

Results and Discussion

Following the treatment described previously both solutions were analysed by ICP-MS employing method 2 conditions, see Table 81 (Appendix 3) for the general instrumental conditions employed. The data for this work can be seen in Table 17.

Table 17. Data Accrued During the Analysis of the Agarose Gel Leachate by ICP-MS Employing Method 2 Conditions.

Sample	³¹P⁺ (<i>m/z</i> = 31) Signal (cps)	³¹P¹⁶O⁺ (<i>m/z</i> = 47) Signal (cps)
Deionised H₂O Blank	62633	6979
Agarose/H₂O ‘Leachate’	107609	18762

Table 17 shows that the quantity of ³¹P present in the leachate sample was approximately twice that in the blank solution. Although the agarose was not being completely broken down it does appear that a significant quantity of DNA was being transferred into solution. A leachate or digestion process shows potential as an approach to the determination of the presence of DNA within an agarose gel band. It may be possible to carry out a quantitative analysis of a leached/digested agarose gel by the preparation of a series of agarose standards that have been impregnated with known concentrations of DNA.

The analysis of the agarose gel leachate by ICP-MS showed it to be a potentially useful tool in genomics as well as other biological fields. Although the trace measurement of the ^{31}P isotope by quadrupole based ICP-MS is not as straight forward as for many elements of the periodic table, considering the high concentration present in many biological samples such analyses might be a feasible approach for some samples. With further work the analysis of such gels, containing separated DNA, could prove to be an effective approach to quantitative determination of DNA. However, it is apparent that this cannot compete with the robustness of UV/Vis and the sensitivity of the fluorescence methods commonly employed for this analysis.

Alternatively it may be possible to approach agarose gel analysis by the use of laser ablation (LA-ICP-MS). By the ablation of a stained gel plate, impregnated with DNA, the sample could be transported into the ICP ion source without the need for a leachate or digestion treatment. Some initial experimentation was carried out using such an approach to determine validity, however, there were difficulties in sample introduction as the sample was desiccated under the heat and gas flows of the laser cell before ablation could be carried out. At this point the analysis was abandoned and it was decided that any further work pursued would involve DNA separated on polyacrylamide gel plates that would be more resistant to the heat and gas flows of the laser ablation cell.

3.6. The Study of DNA Replication by Polymerase Chain Reaction

Polymerase Chain Reaction (PCR) is an artificial process by which sections of DNA or RNA can be replicated. If a particular sequence of a nucleic acid is of interest it can be chemically synthesised by the PCR process for further study.¹⁴⁹

The PCR replication occurs through a series of sequences known as thermocycles whereby the DNA strands are denatured and separated on heating to a temperature of 94°C. The separated strands are then exposed to short chain nucleotide sections (primers), of complementary base pairing, that anneal to one end of each DNA strand. These primer molecules are required to flank the region of interest that is to be amplified to control the process. From these primer molecules deoxynucleotidetriphosphate (dNTP) molecules polymerise along the length of the strand (at 72°C over a period of 2 minutes), catalysed by the enzyme DNA polymerase. The result of this process is the formation of two new DNA sequences formed from the original sequence. At this point the thermocycling process continues until the source of primers and dNTP's is exhausted.¹⁴⁹

Typically the progression of a PCR process is determined by separation on an agarose gel plate, staining with ethidium bromide and study by fluorescence which is a very sensitive analytical method, having the capability of studying single DNA molecules.¹⁴⁵ Similar to section 4.5. the aim behind this work was to establish whether ICP-MS is a feasible alternative, to the well established fluorescence methods commonly in use, for PCR monitoring and quantification.

Experimental Details

A PCR experiment was carried out on a DNA sequence 490 base pairs in length. This PCR process employed 25 µl reactions incorporating genomic DNA (0.5 µg), primers (200 pmol of each), deoxy-ATP, GTP, CTP and TTP (0.5 mM each), MgCl₂ (3 mM), Taq DNA polymerase (1 unit), gelatine (0.001 %) and Tris-HCl (10 mM, pH 8.3).

Two sets of ten separate PCR mixture solutions were prepared, nine of each ten were allowed through the process whilst the remaining two were kept as control solutions. The purpose of preparing two sets in this way was to double up the volume of sample solution available so to make ICP-MS analysis easier in terms of sample introduction. During the replication process, one of these sample mixtures was removed after every four thermocycles. The idea behind this removal was the preparation of a series of DNA solutions that had undergone different degrees of amplification.

A third set of sample solutions was also prepared, similarly amplified employing the PCR process, and separated on 2 % agarose gel containing ethidium bromide to confirm amplification via UV/Vis fluorescence. This agarose gel separation revealed successful DNA amplification that should also be observed during ICP-MS analysis.

Following completion of the PCR process the problem faced was that each sample solution contained quantities of each of the four main PCR components. Therefore, prior to analysis the amplified DNA sequences required separation from the remaining ^{31}P containing components, i.e. the sequence primers and the dNTP's. Separation of these components was attempted through a centrifugation process whereby the sample solutions (50 μl , due to the combination of the two sample sets) were centrifuged in microcon centrifugal filter tubes (Micon Bioseparations) of 100 000 molecular weight cut-off (MWCO) for 5 minutes at 800 RPM. Such filter tubes separate molecules of a molecular weight less than 100 000 from those of a higher molecular weight, therefore the amplified DNA sequences could be removed from the smaller primer and dNTP molecules. The amplified DNA sequences remaining on the filters following centrifugation were resuspended in deionised water (100 μl).

Results and Discussion

The DNA solutions obtained following the PCR and centrifugation processes were analysed by ICP-MS employing method 2 for the ^{31}P isotope content. For this analysis a Micromist 100 $\mu\text{l min}^{-1}$ concentric nebuliser was used in conjunction with an impact bead spray chamber. The general instrumental conditions employed during this work can be seen in Table 82 (Appendix 3) and the data generated during the

study of these amplified DNA solutions can be seen in Table 83. From the data in Table 83 a graph was constructed charting the progress of the PCR amplification via determination of the $^{31}\text{P}^{16}\text{O}^+$ ion ($m/z = 47$), see Figure 45.

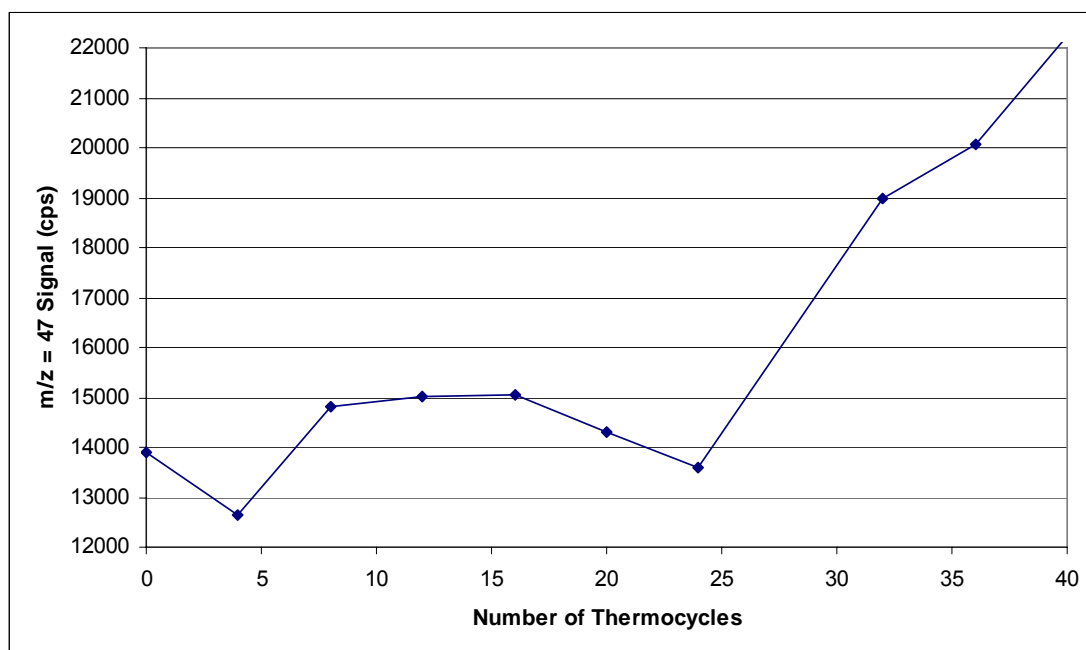


Figure 45. A Graph Comparing Number of Thermocycles with $m/z = 47$ Signal for the Analysis of a PCR Process Employing ICP-MS Method 2.

Figure 45 compares the $m/z = 47$ signal with the number of thermocycles that the DNA solutions under study were passed through. PCR has been described as an exponential amplification so, theoretically, what should be observed is an exponential increase in $m/z = 47$ signal. Such an increase was not observed in the ICP-MS data as a significant increase in $m/z = 47$ signal did not appear until beyond thermocycle 20. This suggests that either the method in place was not sensitive enough to detect smaller changes in amplification or that the separation of amplified sequences, primers and dNTP's was not particularly efficient.

It should be noted that PCR is an artificial process, whereby the DNA strands are initially separated as a result of exposure to a high temperature (94°C), compared to replication processes that take place in cells at body temperature. Therefore, DNA

replication carried out by PCR cannot be compared fairly to that which takes place in the body where enzymes separate the strands. However, recently Vincent *et al.*¹⁵⁰ published a new approach to artificial DNA replication that is more comparable to that taking place in the human body. Helicase enzymes were employed to separate DNA strands and lower temperatures were employed during the replication.

Following this study it can be concluded that ICP-MS does not appear to be a successful approach to monitoring the PCR process. However it is believed that, in conjunction with PCR, ICP-MS may be a useful tool in the study of metal interaction in DNA replication processes. The exposure of cells, either accidentally (through occupation for example) or intentionally (i.e. through medication) to complexes of As, Cr, Cd, Ni and Pt can lead to nucleic acid interaction causing disruption to replication processes. A similar exposure to nucleic acid fragments in a PCR process, which is monitored by ICP-MS, may provide useful information. Such information could be related, to a certain degree, to the inhibition of DNA replication processes in the human body on exposure to such metals. Further work in this area could be fruitful in anti-cancer research.

3.7. The Study of Single Nucleotide Polymorphisms by HPLC-ICP-MS

The cause and progression of a disease in humans is mostly influenced by environmental factors and lifestyle as well as genetics. The “genetic background” of an individual is responsible for susceptibility to infectious or auto-immune diseases so changes in nucleic acid sequence can have far reaching effects and it is thought that certain changes can influence the manifestation and course of a disease.¹⁴⁸ In the case of the work described in this section the potential of an individual to develop a disease based on the genetic background, i.e. nucleic acid sequences, is the issue of importance. The ability to determine changes, or mutations, in nucleic acid sequences is, therefore, one of the most important tools available in genetic research.¹⁵¹

The majority of these changes are in the form of a single nucleotide polymorphism (SNP). SNP is a small genetic variation that can occur within a nucleic acid sequence whereby one nucleotide base is substituted for another (for example an A base could be changed to a G, T or C base), a base is deleted from the sequence or a base is inserted into the sequence. Because genetic background is linked to certain diseases it is believed that certain SNP's can predispose an individual to a disease and possibly influence drug efficacy. For these reasons it is desirable to be able to determine changes in nucleic acid sequence and research into this area is fruitful with regard to forecasting illness.

A popular approach to the detection of SNP's is polymerase chain reaction single strand confirmation polymorphism (PCR-SSCP) which has so far proved to be an effective method.¹⁴⁸ PCR-SSCP involves amplification of nucleotide sequences followed by separation via electrophoresis and detection by autoradiography or ethidium bromide or silver staining.¹⁴⁸ HPLC has also been employed in the study of SNPs.¹⁵² The aim of the work in this section was to employ the ³¹P methods developed in sections 2.4.2 to 2.4.5 to the study of SNP's. The development of an *in vitro* method to separate and detect specific nucleotide sequences that differ according to variations in single, or a small number of, bases by HPLC-ICP-MS may reveal an

alternative approach to the analysis of SNP's. Such a method may be faster than PCR-SSCP and allow a higher throughput of samples.

Experimental Details

Two oligonucleotide molecules (25 bases in length, see Table 18) differing by one base were separated using on-line anion exchange HPLC-ICP-MS. Such a coupling has been extensively employed in the analysis of nucleic acids. From such an analysis both UV data (via presence of chromophore groups) and mass spectrometric data (via measurement of the ^{31}P isotope content) was obtained during detection.

Table 18. The Oligonucleotide Sequences Studied by HPLC-ICP-MS.

Oligonucleotide Identification Number	Oligonucleotide Sequence (5' to 3')	Molecular Mass
2	TGA AGA AAT TCA GTT CAT AGC TTG T	7696
3	TGA AGA AAT TCA GTT CAT AGC TTG G	7721

A HP 1090 series 2 HPLC instrument (Agilent) in conjunction with a TSKgel-DNA-NPR anion exchange column (Tosoh Bioscience, Germany. 7.5 cm x 4.6 mm, 2.5 μm particle size) was employed in the separation of the oligonucleotides. This instrument was directly coupled to the PQ ExCell ICP-MS (operated under time resolved analysis (TRA) mode) which employed methods 2 and 4 for the detection of ^{31}P during two separate analyses, see Tables 84 and 85 (Appendix 3) for general instrument parameters. Chromatographic conditions employed can be seen in Table 19. The separation of oligonucleotides used here was developed by Miss S. L. Kerr of the Loughborough University atomic spectroscopy research group.

Table 19. Chromatographic Conditions Employed During the Study of Oligonucleotide Sequences by HPLC-ICP-MS.

Parameter	Description	
Mobile Phase Composition	A = 20 mM Tris-HCl, pH 9 B = 20 mM Tris + 0.3 M Citrate + 0.1 M NH ₄ Cl, pH 9	
Mobile Phase Flow Rate (ml min ⁻¹)	0.7	
Sample Injection Volume (μl)	5	
UV Detector Wavelength (nm)	257	
Mobile Phase Gradient	Time (min)	% B
	0	40
	15	100
Stop Time (min)	17	
Post Time (min)	4	

Prior to analysis oligonucleotide samples (Invitrogen, Paisley) were diluted in 20 mM Tris-HCL buffer (pH 9) to a concentration of 10 μM.

Results and Discussion

Of the two analyses carried out the first, employing method 2, was successful (with regard to both UV and ICP-MS detection) with complete resolution of the two peaks well above the background. For the second analysis, that employing method 4, the UV detection was successful but neither of the emerging peaks was visible above the background signal for the ICP-MS detection. It would appear that in this case the formation of the ³¹P¹⁶O⁺ ion was being suppressed due to the introduction of the mobile phase into such a low forward power plasma. Over the time period studied for this separation, for both analyses, the background signal rose with the increasing concentration of mobile phase B introduced to the anion exchange column. The reason for this was an increase in the formation of interfering polyatomic ions, present at $m/z = 47$, as a result of an increasing contribution of N and O isotopes from the mobile phase. For the first analysis, employing method 2, the UV and ICP-MS chromatograms can be seen in Figures 46 and 47.

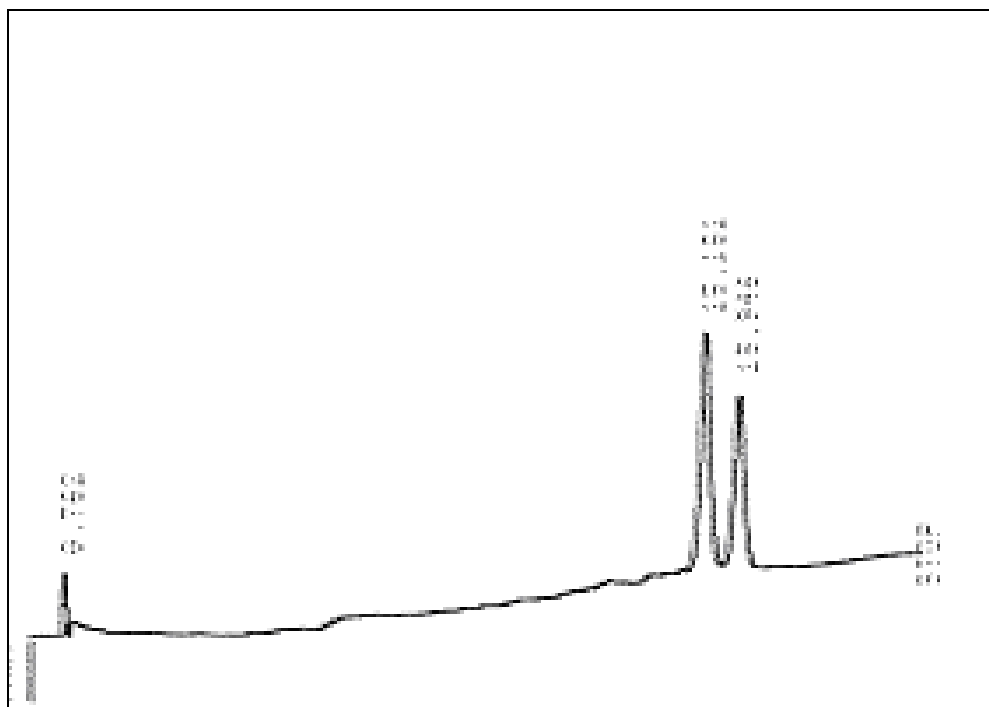


Figure 46. The UV Chromatogram of Oligonucleotides 2 and 3 Separated and Detected by HPLC-ICP-MS (Absorbance Versus Retention Time (Minutes)).

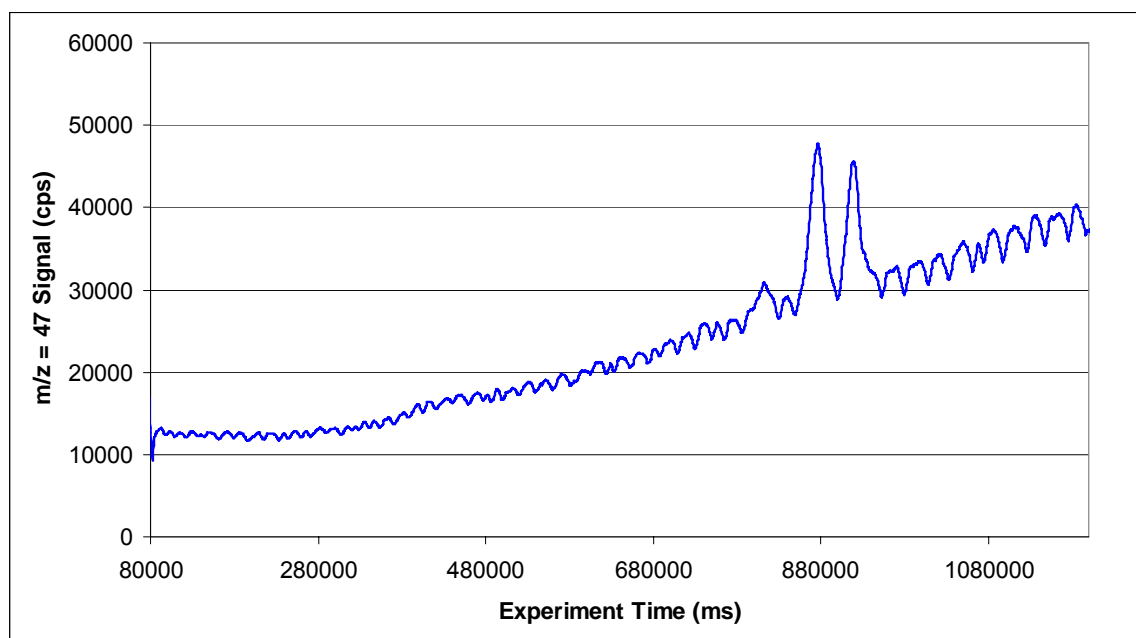


Figure 47. The ICP-MS Chromatogram of Oligonucleotides 2 and 3 Separated and Detected by HPLC-ICP-MS.

The retention times and resolution of peaks for the two separated oligonucleotides, from UV and ICP-MS data, are highlighted in Table 20. There is an additional effect that should be noted here. The ripple of the $m/z = 47$ signal trace of Figure 47 is due to the fluctuation of sample introduction via the peristaltic pump. This effect becomes more noticeable as the experiment time increases.

Table 20. Retention Times Acquired Following the Study of Oligonucleotides by HPLC-ICP-MS Employing Method 2.

Oligonucleotide Identity Number	Retention Time (min)	
	Method 2 UV	Method 2 ICP-MS
2	15.18	15.12
3	15.95	15.90
Resolution	0.96	1.03

As can be seen in Table 20 the UV and ICP-MS data acquired following this analysis agree with regard to the retention time of each oligonucleotide passed through the anion exchange column. This analysis is a good example of the application of one of the methods developed and described in Chapter 2. Again, however, the success of this analysis was based on the prevalence of ^{31}P in the sample and, considering the background signals observed during this work, ultra-trace levels of the oligonucleotides would not be compatible with the method conditions.

Of the two analyses carried out that employing method 2 showed promise with regard to the analysis of SNP's. Although this was a simple experiment studying short chain nucleotides, with appropriate pre-treatment and separation processes in place HPLC-ICP-MS could be a useful tool in the study of SNP's *in vivo*.

3.8. Conclusions for the Application of ^{31}P and ^{32}S ICP-MS

Methods

It has been shown through the work described in this chapter that quadrupole based ICP-MS is promising with regard to the analysis of DNA via the measurement of the ^{31}P isotope.

The simple analysis of DNA in a water matrix revealed that such a biological molecule can be studied without any problematic non-spectroscopic interferences. However, when considering ‘real’ biological samples, containing DNA, the matrix involved would be far more complicated so such interferences would be a significant issue. Either DNA would be analysed as a sample close to that of its native form or as a component following a separation approach. Either way the molecule of interest would be present within a sample rich in elements that would cause problems. For the sample close to its native form such elements may be Na or K which could cause signal degradation via blockage of the skimmer cone. ^{31}P contamination would also be an issue in such a sample from a number of sources, for example proteins. For the sample prepared following a separation process, such as HPLC, the DNA molecule may be present in a mobile phase or other eluent containing a high concentration of C, N and O containing species that would contribute to a high level of interfering polyatomic ions.

For the latter type of sample (that within a mobile phase or eluent) the background signals associated with the analysis carried out into the DNA within an agarose gel and the SNP’s analysis demonstrated that such ‘real’ samples may be problematic. However, given a sufficient concentration of ^{31}P within such a sample then ICP-MS analysis would be satisfactory due to the elevated signal to background ratio. Difficulties may arise if the requirement of the sample was measurement of ^{31}P at trace levels specifically.

Overall, through the work described in Chapter 2 and this applications chapter and previous research carried out by other groups, it can be said that ICP-MS has the potential to provide useful data from the analysis of the nucleic acids and associated

biological species containing ^{31}P . Although the matrix of such samples may be problematic on introduction to the ICP ion source, and with regard to sample and skimmer cone deposition, such elemental data would be valuable to the genomics field.

Chapter 4

The Measurement of Platinum Based Anti-Cancer Drugs and DNA by ICP- MS

4.1. Disease and Metal Based Complexes

Over the past seventy years studies have been carried out relating the chemical structure and therapeutic efficacy, or toxicity, of metal based complexes with regard to various diseases.¹⁵³ Amongst other elements, complexes of Au,¹⁵⁴⁻¹⁵⁶ Cu,¹⁵⁶ Fe,¹⁵⁷ Ga,¹⁵⁷ Pd,^{153, 158-160} Pt,^{153-156, 158, 159, 161-163} Rh,¹⁶⁴ Ru,^{153, 156, 164-166} Sn,^{167, 168} Ti¹⁵⁵ and Zn¹⁵⁶ have been studied for therapeutic benefit particularly in the fields of alzheimer's disease, arthritis, cancer diseases and malaria. There are many examples of metal based complexes that are employed in the treatment of cancers, of these there are several based on Pt employed in cancer chemotherapies. ICP-MS is therefore an ideal analytical technique that can be, and has been, employed in the qualitative and quantitative measurement of such metal based complexes in numerous types of sample matrix.

4.2. Cancer and Cancer Treatments

Although loosely defined as the growth of cells without the restraints that regulate normal tissue growth, a cancer is a disease not easily categorised.¹⁶⁹ A cancer can evolve in any organ of the body initiated by various factors. Interaction with carcinogenic chemicals, industrial pollutants, radiation, oncogenic viruses and parasitic infection can be the cause of uncontrolled growth as can dietary factors, genetic predisposition and the aging process.¹⁶⁹

Surgery, radiotherapy and chemotherapy have all proved to be effective treatments for cancer being used either individually or in combination depending on the type of the disease and on how far it has progressed. However, such treatments can be particularly difficult for the patient with radiotherapy and chemotherapy, particularly, exhibiting some harsh side effects. Although such approaches can be successful in the treatment of tumours they cannot guarantee the total eradication of a cancer as, in theory, if one cancer cell survives then uncontrolled growth can continue through the replication of that single cell. Metastasis (the spreading of a tumour resulting in the

formation of secondary tumours in other parts of the body) is also a significant problem that makes tackling the occurrence of a cancer far more complex.¹⁶⁹

The ultimate requirement of an anticancer drug (chemotherapy) is that it eliminates tumour cells at doses that allow the survival of a sufficient number of healthy cells in critical tissues, such as bone marrow and the gastrointestinal tract.¹⁶⁹ The search for drugs that are capable of either destroying a greater number of tumour cells than healthy cells, or differentiating between the two completely, is ongoing and for many types of cancer the survival rate following diagnosis is steadily improving. With regard to chemotherapies, currently there are several approaches to the limitation of tumour growth or the termination of tumour cells. Alkylating agents, antimetabolites, antibiotics and hormones have all proved to be beneficial treatments with their success dependent on the properties of a tumour and its location.

Prior to the discussion of the research carried out for this chapter, what follows is a description of two Pt based anti-cancer complexes that are in common use today as well as a summary of some of the previous work by other researchers that has been carried out into them.

4.2.1. Cisplatin

Approved for clinical use by the Food and Drug Administration (FDA) in 1978 *cis*-diamminedichloroplatinum (II), or cisplatin, is described as a first generation anti-cancer drug that is still used regularly today. Successful use of this drug has been observed in the treatment of testicular, cervical, ovarian, head, neck and oesophageal cancers.^{155, 156, 164, 170-173} Composed of a Pt atom, two amine groups and two Cl atoms in the *cis* isomer configuration (see Figure 48), cisplatin is a simple molecule. The success of this drug lies in its binding to nucleic acid molecules within cancer cells, particularly DNA, followed by the inhibition of replication and transcription processes, cell cycle arrest and apoptosis.^{156, 164, 170, 174}

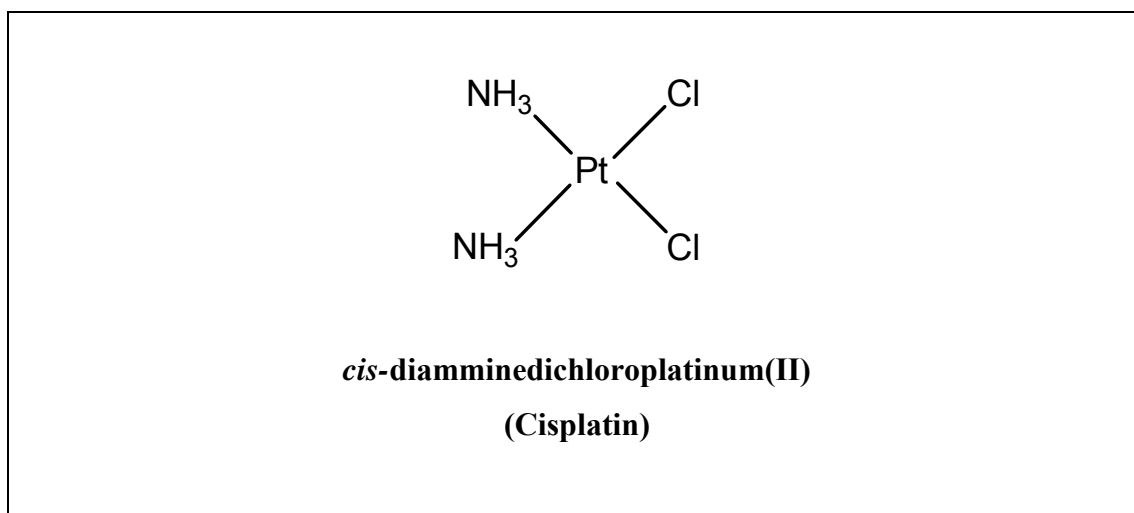


Figure 48. A Structural Diagram of Cisplatin.

Despite its successes, cisplatin suffers limitations in that it binds to many biological cell components not just the nucleic acid target. The drug is known to react with cellular proteins, cell membrane phospholipids and cytoskeleton microfilaments.¹⁶² Cisplatin treatment is also hindered by resistance problems, see section 4.2.5. The result of these limitations is that a patient must be exposed to high drug doses in order to obtain the desired effect, such that $\mu\text{g l}^{-1}$ levels of cisplatin are typically observed in patient blood samples following treatment.¹⁷¹ There are further limitations, however, in that the administration of high doses can lead to neurotoxicity. Due to this, large numbers of patients are unable to complete a full cisplatin therapy.¹⁷²

The result of this is a very difficult experience for the patient. The reaction of the human body to such a treatment includes nausea, vomiting and elevations in blood urea nitrogen and creatine levels. Renal toxicity is common in many patients but this can be overcome with hydration therapy followed by diuresis. These physical problems limit the dose of cisplatin, that can be received by a patient, which is typically an intravenous injection of $50 - 120 \text{ mg/m}^2$ every three to four weeks for the duration of the treatment.^{162, 171} Not only is the use of cisplatin limited by the side effects that it inflicts but the development of an acquired resistance, by the patient, to the drug can be problematic.

4.2.2. Oxaliplatin

trans-L-diaminocyclohexaneoxalatoplatinum (II), or oxaliplatin, is a third generation anticancer drug that is successfully used in the treatment of colorectal cancers.¹⁷⁵⁻¹⁷⁸ An analogue of cisplatin, oxaliplatin is a slightly more complex molecule being composed of a Pt atom linking an oxalic group with a cyclohexane ring and two amine groups, see Figure 49.^{162, 164, 173, 176} Similar to cisplatin, the success of oxaliplatin lies in the binding of the drug molecule to nucleic acid molecules of cancer cells leading to the inhibition of cellular replication processes and apoptosis.¹⁷³

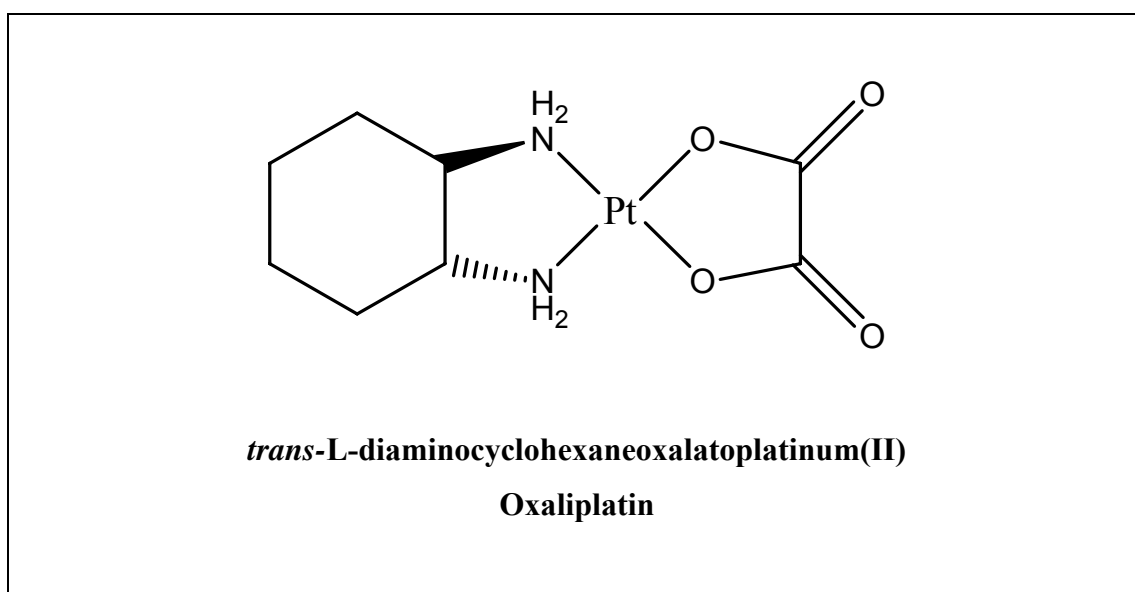


Figure 49. A Structural Diagram of Oxaliplatin.

For some types of cancer, oxaliplatin treatment has proved to be an excellent alternative to that of cisplatin as it exhibits a broad spectrum of antitumour activity in tumours that are intrinsically cisplatin resistant.^{173, 175-177} With regard to clinical toxicity, oxaliplatin is a less severe drug than cisplatin so for certain types of tumour its use would be preferential for the patient.¹⁷⁸ Previous study has shown that oxaliplatin is at least as successful as cisplatin in the instigation of apoptosis, however, recent data suggests that fewer drug-DNA adducts are formed by oxaliplatin and that it is simply more efficient at inducing cell death.^{175, 176} For this reason, drug

doses (lower than those for cisplatin) can be administered to patients to obtain a beneficial effect. Following the success of oxaliplatin as an alternative therapeutic agent the search has continued for analogues that could provide a greater degree of efficacy with a reduction in side effects. So far a number of promising molecules have been synthesised and tested, a number of these exhibiting additional side chains to the cyclohexane ring. However, an analogue exhibiting vastly superior efficacy and safety to the patient is yet to be discovered.¹⁷⁹

4.2.3. Types of Drug-Target Interaction Exhibited by Cisplatin and Oxaliplatin and Other Metal Based Drug Complexes

As mentioned in sections 4.2.1 and 4.2.2, the primary target for both cisplatin and oxaliplatin drugs is DNA, this is also the primary target of many other metal based drug complexes. The interaction between these drug and target species results in the formation of adducts that are known to disrupt the DNA transcription and translation processes and it is widely believed, without repair, can therefore bring about apoptosis (programmed cell death).^{162, 176} The main type of interaction that can take place between these drug and target species is that of a covalent binding or cross linking. There are two types of such binding and these are described shortly. Other, minority, types of binding are also considered.

Covalent binding, or cross linking, between metal based drugs and the constituent base molecules of their DNA target is a very important process and certainly in the case of cisplatin and oxaliplatin such binding is believed to be the dominant interaction between the species. As metal centres are positively charged they favour binding to biomolecules that are negatively charged. Sections of proteins and nucleic acids, for example, act as ideal binding targets.¹⁵⁶ Such binding involves a chemical change of the drug molecule following passage into the cell, during which the environmental chloride concentration drops.¹⁶² In the case of cisplatin, once inside the cell, the molecule undergoes hydrolysis resulting in the formation of the activated *cis*-[Pt(NH₃)₂Cl(OH₂)]⁺ ion which is more readily capable of reaction with the DNA

target.¹⁶² For the oxaliplatin drug molecule it is believed that, once inside the cell, the oxalic group is replaced by two Cl atoms that are then, themselves, replaced by H₂O molecules.¹⁷⁶ Therefore it is suggested that the activated form of oxaliplatin, within the cell, is $[\text{Pt}(\text{H}_2\text{O})_2(\text{NH}_2)_2\text{C}_6\text{H}_8]^{2+}$.¹⁷⁶

Such adducts can form between bases on the same DNA strand (intrastrand binding) or bridging from one strand to another (interstrand binding).¹⁶² It has previously been shown (via enzymatic digestion of cisplatin treated salmon sperm DNA, chromatographic separation of the digested components and ¹H NMR analysis) that the most common forms of cisplatin-DNA and oxaliplatin-DNA adduct are that whereby the Pt atom binds between two guanine (G) bases or one guanine and one adenine (A) base, i.e. the purine bases, within the same DNA strand (intrastrand).^{156, 162, 173, 175, 180} Such binding can be seen in the diagrams of Figures 50 and 51.^{173, 180, 181}

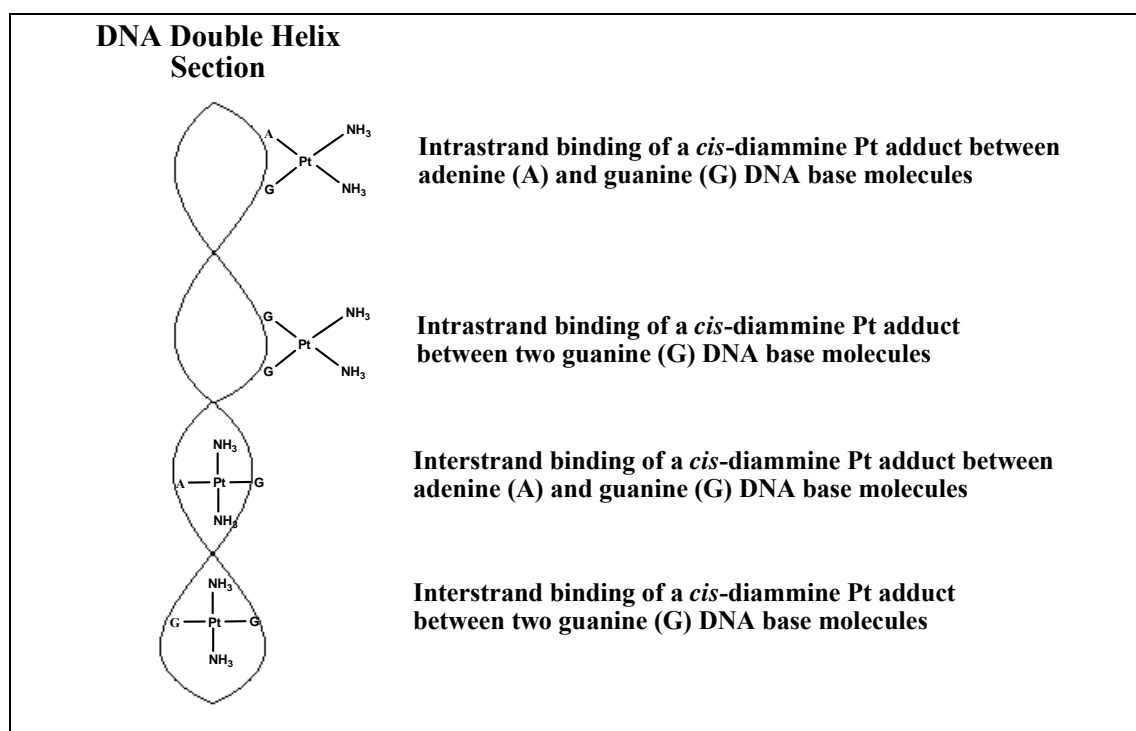


Figure 50. A Diagram of the Most Common Binding Interactions between *cis*-diammine Pt Adducts and the Purine Molecular Bases of a DNA Strand (Not to Scale).

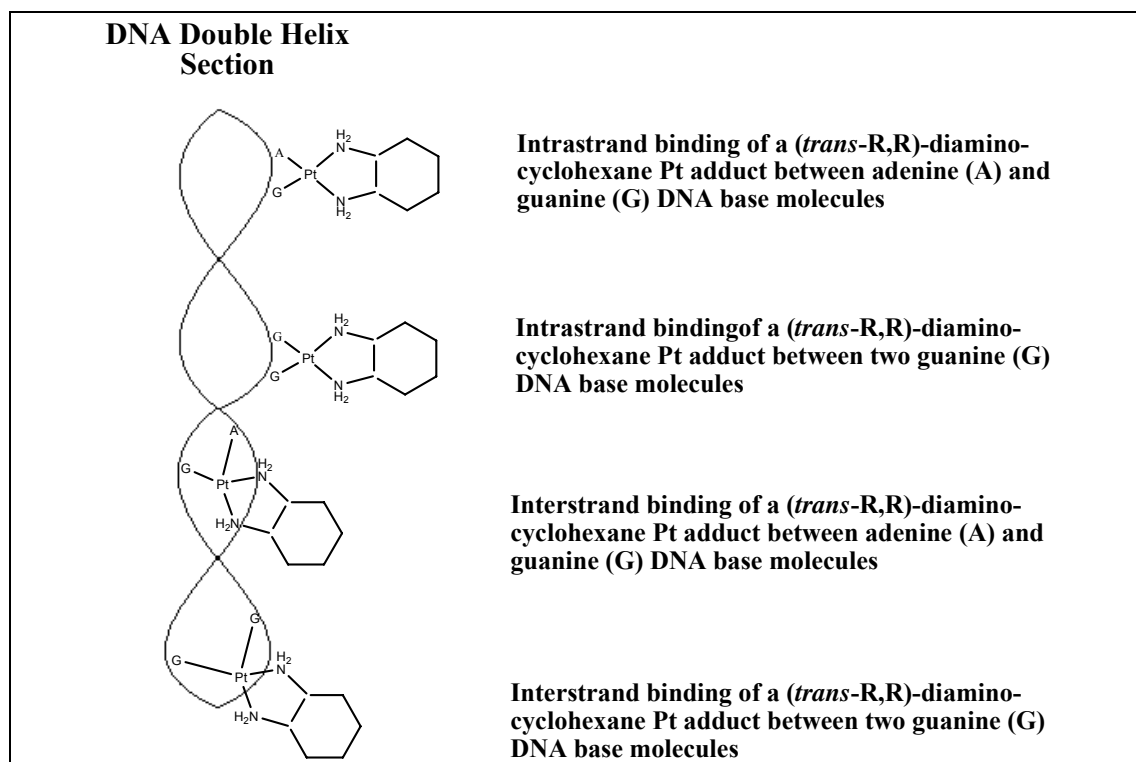


Figure 51. A Diagram of the Most Common Binding Interactions between (*trans*-R,R)-diamino-cyclohexane Pt Adducts and the Purine Molecular Bases of a DNA Strand (Not to Scale).

Intercalation between a drug and its DNA target has proved to be a highly successful approach to the formation of drug-target adducts that can lead to interference with cellular replication processes. A large number of intercalating agents have been identified (e.g. proflavin, ethidium, actinomycin D, daunomycin and adriamycin) that exhibit a common structural characteristic, the presence of a planar polycyclic aromatic chromophore.^{164, 182} It is this polycyclic aromatic structure that can be inserted between adjacent base pairs of the target DNA helix, acting as the initial component for the interaction which takes place between the molecule and adjacent base pairs via van der Waals forces and electrostatic stabilisation.^{182, 183} Further chemical components that reside within the drug molecule are also influential with regard to the degree of interaction between drug and target by this approach.¹⁸² The study of intercalating agents that include a metal atom(s) as part of their structure is ongoing. Researchers have proposed and developed a number of metal based molecules exhibiting intercalating structures that interact with the DNA target.¹⁸² Neither cisplatin nor oxaliplatin molecules exhibit a polycyclic aromatic structure so their ability to interact with DNA by this intercalative approach would be nil, however

some Pt based intercalating drugs have been developed that exhibit enhanced antitumour activity.¹⁵⁶

Intercalation is an example of a non-covalent binding between drug and DNA target. Other types of drug are available that interact with the DNA target in a different way but do not bind covalently, such interactions take place via hydrogen bonding with base pairs.¹⁸³

4.2.4. The Effect of Cisplatin and Oxaliplatin Binding on DNA Structure

The formation of drug-DNA adducts, following cisplatin or oxaliplatin treatment, has been shown by NMR and X-ray crystallography to lead to the distortion of sections of the DNA molecule.¹⁶² Such distortion can exist in the form of either bending of the helix molecule or a change in the degree of twisting, or untwisting, of the DNA strands (or both).^{156, 162, 164, 180} Such distortions contribute a rigidity to these affected sections that, it is believed, lead to the hindrance of the DNA strand winding and unwinding involved in the replication processes.

4.2.5. DNA Repair Mechanisms and Drug Resistance

Similar to many pharmaceutical compounds, one of the main reasons for the failure of a cisplatin or oxaliplatin treatment is the resistance of cancer cells to the action of the drug molecules. Resistance to cisplatin or oxaliplatin by cancer cells can be either inherent or acquired following initial exposure (such as in the case of ovarian cancer).^{162, 173} The degree of resistance of a cell to the drug treatment is best described in terms of that cell's ability to repair itself following exposure or to detoxify itself. The recognition of the problem of cisplatin resistance spurred the study of the cytotoxicity of molecular analogues in order to develop different Pt based

drugs without such a limitation. Oxaliplatin is one such analogue and does not exhibit treatment resistance to such a degree.

As mentioned in section 4.2.4, when a cisplatin-DNA or oxaliplatin-DNA adduct is formed the structure of that section of the DNA molecule is changed. Although such structural changes are desired with regard to inhibition of cellular processes, to bring about cell death, they also provide a site for the action of repair mechanisms.¹⁷³ Previous studies on yeast and mammalian cells have shown that the drug-DNA adducts formed following exposure can be recognised and acted on by nucleotide excision repair, recombination repair and translesion DNA synthesis pathways that can lead to the removal of adducts and the restoration of the DNA molecule.^{156, 170, 173} Cells have a degree of ability to detoxify themselves following penetration by foreign molecules. In the case of Pt based drug molecules this can be mediated by glutathione or metallothionein.¹⁷⁵

The progress and efficiency of these pathways is dependant on the type of DNA bound drug molecule, hence the difference in degree of resistance between cisplatin and oxaliplatin.

4.2.6. Cancer Treatments and Drug Efficacy

The treatment of a patient with any kind of drug will result in side effects. For many drugs such side effects are not noticeable but in the case of certain cancer treatments they can be very severe. Therefore, when treating cancers by chemotherapy, drug efficacy must be weighed up against potential negative effects. There are two significant issues that must be considered when deciding to expose a harsh anticancer drug (such as cisplatin or oxaliplatin) to a patient, these are drug efficacy and drug resistance. The drug efficacy of cisplatin and oxaliplatin varies considerably from patient to patient though it remains very low. The reason for such variation lies in physiological differences, i.e. the person to person differences in DNA sequence (the drug molecule target). Drug efficacy is also significantly affected by the second issue of drug resistance (see section 4.2.5). It would therefore be very useful to the

clinician to have drug efficacy data for an individual patient prior to, or soon after, exposure to establish the best course of tackling a cancer that would typically be treated by cisplatin or oxaliplatin. However, a fast and low cost test to establish such data for individual patients is currently not available.

4.2.7. Previous Studies of Cisplatin and Oxaliplatin Exposure to DNA

A number of researchers have conducted studies into the destination and modes of action of both cisplatin and oxaliplatin following drug administration. Research has also been carried out to study the problem of resistance to these drugs and to establish how much of each drug species is required to bring about apoptosis. One of the results of this type of research has been the further study of cisplatin and oxaliplatin analogues, the aim of which being the development of drug molecules that are just as efficient in causing apoptosis but with a reduced degree of cellular resistance and side effects. Such research has made good use of a wide range of analytical techniques, some of which is described as follows.

As was mentioned in section 4.2.3 there are a number of ways in which the cisplatin and oxaliplatin drugs, as well as their analogues, can interact with the primary target DNA. To confirm that the formation of drug-DNA adducts takes place following exposure elemental analytical techniques such as atomic absorption spectrometry (AAS), inductively coupled plasma mass spectrometry (ICP-MS) and inductively coupled plasma optical emission spectrometry (ICP-OES) have all been employed via the measurement of Pt isotopes.^{158, 159, 175, 184}

The types of drug-DNA binding and the resulting adduct structures have previously been established via NMR and X-ray crystallography.^{159, 161, 162, 173, 185} The data accrued from such work has allowed researchers to associate cytotoxicity with both drug and adduct structures allowing the comparison of cisplatin and oxaliplatin and their analogues. The interactions between cisplatin and some cellular components

have previously been quantified by radiochemical methods. ¹⁹⁵Pt-radiolabeled cisplatin was exposed to HeLa cells at the mean lethal concentration during studies by Akaboshi *et al.*¹⁸⁶ After exposure periods of 1, 2 and 3 hours the distribution of the radiolabeled cisplatin was determined in DNA, RNA and protein components by scintillation counting. From the data accrued during this analysis it was determined that at the mean lethal concentration approximately 9 Pt atoms bind to each DNA molecule. Similar data has also been published by Harder *et al* and Howle *et al* stating that approximately 22 Pt atoms bind to each DNA molecule.¹⁶²

When considering the treatment of patients with cisplatin or oxaliplatin, at the molecular level, there are two major factors that must be appreciated. The first of these factors considers how the drug molecules pass through the cell membrane to reach their binding target. This passage takes place via passive diffusion rather than some type of active transport involving the use of energy.^{156, 184} Therefore, there must be a limit to the quantity of drug species that can pass into a cell according to the equilibrium of a diffusion process. This is one reason for the requirement of high doses of cisplatin and oxaliplatin being administered to patients.

The second factor that must be considered is that these foreign drug molecules do not simply seek out their DNA binding target without interaction with other intra- and extra-cellular species. Following study by various analytical techniques, it has been shown that these drug molecules also have an affinity for numerous intra- and extra-cellular species that are encountered prior to meeting the cell nucleus, following exposure.^{174, 186} Phospholipids, peptides, oligosaccharides and cholesterol are just some of the biomolecules that can offer potential binding sites to metal based drug species.¹⁷⁴ Cisplatin and oxaliplatin are also known to interact with haemoglobin causing structural changes which can result in severe side effects for the patient, such as anemia.^{171, 187}

The issue of drug resistance in molecules of the type discussed in this chapter is one of great importance. Analytical techniques have been employed in the identification of cancerous cell lines that do not respond to drug treatment as efficiently as others. Such work allows the evaluation of certain pharmaceuticals with regard to their efficacy. Previously the degree of drug accumulation and binding has been

established in numerous types of cell line (some drug resistant and others drug sensitive) via elemental analysis techniques such as AAS.¹⁷⁵ Cisplatin and oxaliplatin resistance and repair mechanisms have been investigated via the study of elevations in certain cellular species. It has recently been suggested that the cellular repair mechanisms for cisplatin and oxaliplatin are very similar, although they differ in their degree of cytotoxicity.¹⁷⁵

4.3. Aims of Research

Researchers at Leicester University are investigating the interaction between the Pt based complexes cisplatin and oxaliplatin and their biological target DNA. The overall aim of their work is to establish a clinical test to determine the efficacy of these drugs for individual patients. Such a test would prevent the unnecessary exposure of these drugs to patients that would not benefit significantly.

The study of metal based drugs in cancer chemotherapies is an area of research that can take advantage of the low limits of detection in analysis by ICP-MS with or without the use of radiolabels. Previous study by ICP-MS has shown that biological samples, such as whole DNA molecules, may be analysed without difficulty via nebuliser and spray chamber sample introduction. In collaboration with researchers at Leicester University, it was proposed that ICP-MS could be employed in the study of the drug/target interaction. If, following such study, it was determined that ICP-MS was sensitive enough to measure the presence of Pt in a sample at clinical levels then the degree of binding could then be calculated and a clinical test established.

Prior to the commencement of work towards this aim, the idea of separating drug exposed DNA by electrophoresis followed by LA-ICP-MS was floated. Although such an approach may allow a fast analysis time for an established test, it was decided that for initial work there would be too many complications. Therefore the work carried out to meet the aims described above was based on the interaction between drug and target in solution. The simultaneous measurement of ^{31}P (via the methods established in Chapter 2) and $^{190,192,194,195,196,198}\text{Pt}$ isotopes would allow their signal ratios to be used in a calculation to determine a binding constant. Such a binding constant may be used as the basis of a clinical efficacy test.

4.4. The Study of DNA and Pt Based Drug Interactions *In Vitro* by ICP-QMS

A significant degree of experimentation was carried out on determining the interaction of cisplatin and oxaliplatin with their DNA target by measurement of the ^{31}P and $^{190,192,194,195,196,198}\text{Pt}$ isotopes by ICP-QMS. Divided into five studies, this experimentation is described as follows.

4.4.1. Study 1

Initial experiments were carried out to determine the ^{31}P and $^{190,192,194,195,196,198}\text{Pt}$ isotope content of a series of DNA samples exposed to varying concentrations of cisplatin (*in vitro*) by ICP-QMS. The main aim of this initial experimentation was to evaluate the capability of the PQ ExCell ICP-QMS instrument with regard to the analysis of such samples. A concentration of 0.5 mg ml^{-1} was originally agreed, on between researchers of both Leicester and Loughborough Universities, as being appropriate for the DNA samples studied during this work with regard to both drug/target binding and ICP-MS analysis. Typically, such a sample concentration would be considered as high for routine ICP-MS analysis so this initial work would establish the presence of any matrix effects.

Experimental Details

For this study of Pt based drug and DNA target interaction the experimental detail is very extensive. These experimental details could be considered in two parts, the first describing sample preparation (carried out by researchers at both Leicester and Loughborough Universities) and the second describing instrumental analysis (carried out at Loughborough University).

Prior to sample preparation certain information obtained by calculation was required. Firstly, the binding between drug and DNA was based on the mean molecular weight of a nucleotide. This mean molecular weight has, initially, been calculated to be 325.61 after multiplying nucleotide molecular weight with nucleotide abundance for each and dividing the total obtained by 100. This mean nucleotide molecular weight assumes that the majority of nucleotides that are being studied are in a free state. In this work however, this is not the case. The bulk of our DNA nucleotides are bound in a polymer form and if nucleotides were to polymerise via the combination of one nucleotide at the three prime end and the phosphate linking group attached to the five prime end of another then the result would be the elimination of a water molecule (molecular weight equal to 18). So, a molecular weight of 18 is subtracted from 325.61 to give a final mean molecular weight of a DNA nucleotide as **307.61**.

As genetic variation ensures that DNA sequence is different between individuals there is no accepted molecular weight for a DNA molecule. So, for the sake of this work DNA is described in terms of constituent nucleotides of which molecular weight is known. It is believed that the therapeutic region for these types of Pt based drugs, with respect to their DNA target, is one drug molecule to 400 000 DNA nucleotides (this therapeutic level is set out and discussed in *Carcinogenesis*, 1997, **18**, 9, 1767-1774). To assess the capability of the ICP-QMS a series of samples were prepared for analysis with the aim of achieving ratios of drug molecule to nucleotide approximately equivalent to a range of 1 : 100 to 1 : 1 000 000 to buffer the therapeutic region. Details of the preparation of these samples are in Table 21.

Table 21. Preparation Details for the Samples Investigated During Study 1.

Solution Number	Solution Description	Procedure	Nucleotide Conc ⁿ (μM)	Cisplatin Conc ⁿ (μM)	Drug : Nucleotide Ratio
Stock Solutions					
1	DNA Stock Solution	DNA (1 mg in 1 ml)	3250	-	-
2	Cisplatin Stock Solution	Cisplatin (1 mg in 1 ml)	-	3330	-
Cisplatin Preparative Solutions					
3	Serial Dilution of Cisplatin Stock Solution	10 Fold Dilution of Soln 2 with H ₂ O	-	333	-
4		10 Fold Dilution of Soln 3 with H ₂ O	-	33.3	-
5		10 Fold Dilution of Soln 4 with H ₂ O	-	3.33	-
6		10 Fold Dilution of Soln 5 with H ₂ O	-	0.333	-
7		10 Fold Dilution of Soln 6 with H ₂ O	-	0.033	-
Final Sample Solutions					
8	Final Sample Preparation, Exposure of Solution 1 to Solutions 3 to 7	Soln 1 (2600 μl) + Phosphate Buffer (100 μl) + H ₂ O (2300 μl)	-	-	Control
9		Soln 1 (2600 μl) + Phosphate Buffer (100 μl) + Soln 3 (300 μl) + H ₂ O (2000 μl)	-	-	1 : 100
10		Soln 1 (2600 μl) + Phosphate Buffer (100 μl) + Soln 4 (600 μl) + H ₂ O (1700 μl)	-	-	1 : 500
11		Soln 1 (2600 μl) + Phosphate Buffer (100 μl) + Soln 4 (300 μl) + H ₂ O (2000 μl)	-	-	1 : 1 000
12		Soln 1 (2600 μl) + Phosphate Buffer (100 μl) + Soln 5 (600 μl) + H ₂ O (1700 μl)	-	-	1 : 5 000
13		Soln 1 (2600 μl) + Phosphate Buffer (100 μl) + Soln 5 (300 μl) + H ₂ O (2000 μl)	-	-	1 : 10 000
14		Soln 1 (2600 μl) + Phosphate Buffer (100 μl) + Soln 6 (600 μl) + H ₂ O (1700 μl)	-	-	1 : 50 000
15		Soln 1 (2600 μl) + Phosphate Buffer (100 μl) + Soln 6 (300 μl) + H ₂ O (2000 μl)	-	-	1 : 100 000
16		Soln 1 (2600 μl) + Phosphate Buffer (100 μl) + Soln 7 (600 μl) + H ₂ O (1700 μl)	-	-	1 : 500 000
17		Soln 1 (2600 μl) + Phosphate Buffer (100 μl) + Soln 7 (300 μl) + H ₂ O (2000 μl)	-	-	1 : 1 000 000

As described in Table 21 a DNA solution was used as the basis for exposure of nucleotides to varying concentrations of cisplatin. DNA nucleotide samples (3250 μM) were exposed to the cisplatin solutions at Leicester University by Dr Rachel Le Pla and transported to Loughborough University for study. Calf thymus DNA (Sigma Aldrich) was dissolved in deionised water and exposed to the cisplatin, of varying concentration, for a period of 24 hours. Different volumes of the cisplatin solutions were used in order to prepare the desired exposed DNA nucleotide samples. The exposed DNA was then precipitated and washed twice with ethanol to remove unbound drug molecules prior to being redissolved in deionised water (≈ 5 ml). Each sample was prepared in duplicate. Following preparation the amount of recovered DNA was calculated using OD_{260} . The details of sample preparation and DNA recovery are seen in Table 87. From the original exposed DNA sample solutions, a series of P and Pt spiked samples were prepared in order to study the interaction between drug and target via a standard additions approach (see Table 87 for spiked sample details). Five solutions were evolved for each sample duplicate at this point incorporating a one hundred fold dilution, see Table 87 (Appendix 4), with a deionised water diluent.

The instrument used in analysis of the samples was as described previously in this thesis, see sections Chapters 2 and 3. A Micromist ($100 \mu\text{l min}^{-1}$) nebuliser and a silica impact bead spray chamber were used. ICP-MS ^{31}P determination Method 2, as described in section 2.4.2, was employed in the analysis of the DNA/Cisplatin samples prepared for the study of the ^{31}P and $^{190,192,194,195,196,198}\text{Pt}$ isotopes. External standards of P and Pt were prepared from $1000 \mu\text{g ml}^{-1}$ single element standard solutions (Fisher Chemicals, Loughborough, UK) by sequential dilution with high purity deionised water produced using a Maxima Ultra (Elga) water purification system. Measurements were conducted using a peristaltic pump to introduce sample solutions into the plasma via the nebuliser and spray chamber arrangement. The ICP-MS was optimised to produce standard operating conditions (see Table 88, Appendix 4), from which adjustments were made to accommodate the additional ‘method 2’ conditions required. When the required ICP-MS instrument conditions were established the prepared samples were analysed for ^{31}P and $^{190,192,194,195,196,198}\text{Pt}$ isotope content. Data for each of these isotopes was collected by the software of the PQ ExCell (Thermo Plasmalab). Three replicate readings were taken for each isotope

measurement allowing mean, standard deviation and relative standard deviation data to be established. Results of the analysis of the samples are given in the next section.

Results and Discussion

The mean data generated during the ICP-MS analysis of the DNA/Cisplatin samples discussed previously can be seen in Table 89. From this data a series of standard addition graphs were constructed, with a graph for each of the $m/z = 47$, 194 and 195 signals per sample. Due to the large number of graphs produced, examples of graphs for each signal are shown in Figures 52 to 54. The remaining graphs are shown in Figures 94 to 141 (Appendix 4). The curve equations were used to calculate the ^{31}P , ^{194}Pt and ^{195}Pt concentration associated with each of the samples prepared. Quantification of the ^{31}P isotope was carried out via measurement of the $^{31}\text{P}^{16}\text{O}^+$ ion at $m/z = 47$ and the $^{194,195}\text{Pt}$ isotopes were looked at specifically as they are the most abundant.

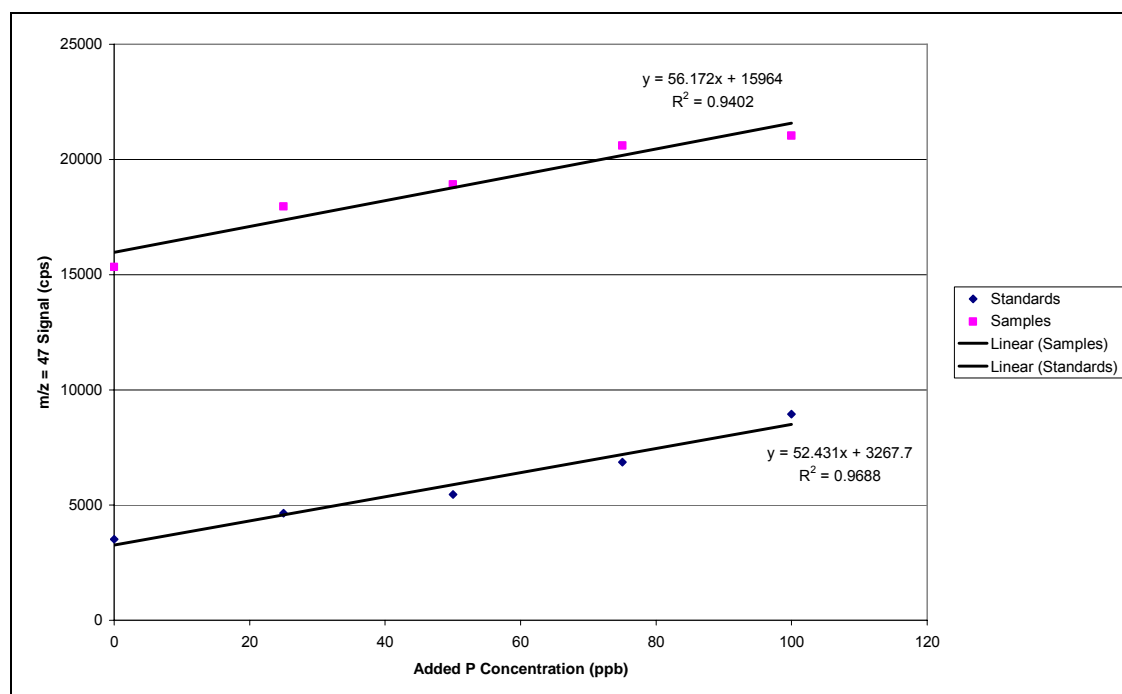


Figure 52. A Graph Comparing P Spike Concentration ($\mu\text{g l}^{-1}$) with $m/z = 47$ Signal (cps) for Sample 1 : 1 000 000 and External Standards.

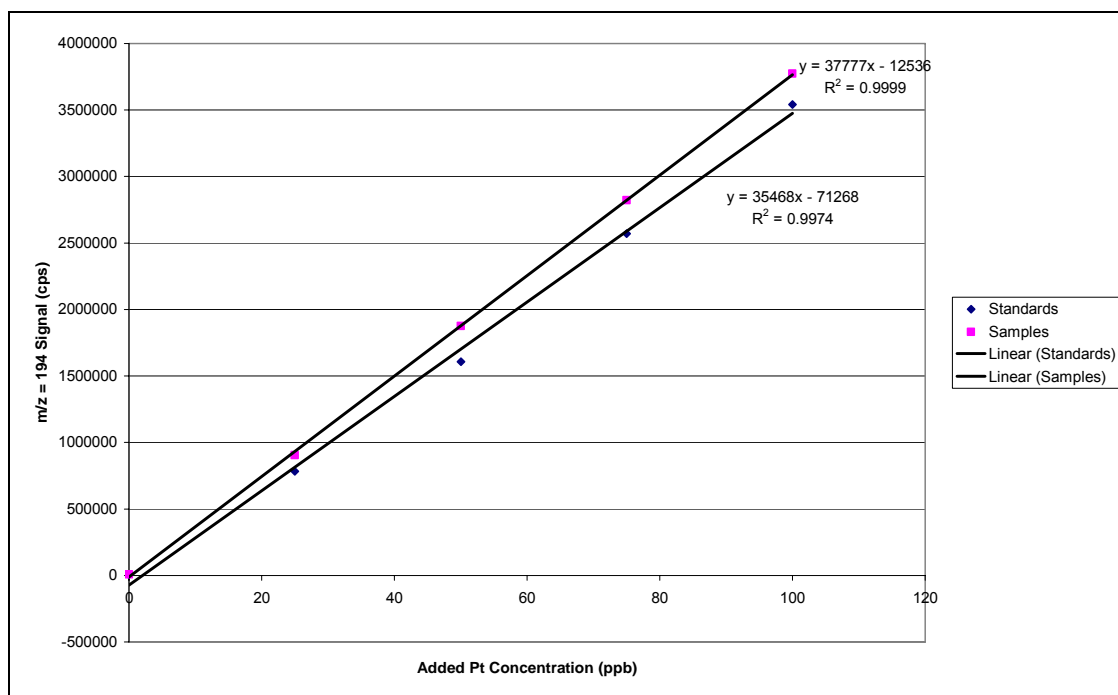


Figure 53. A Graph Comparing Pt Spike Concentration ($\mu\text{g l}^{-1}$) with $m/z = 194$ Signal (cps) for Sample 1 : 1 000 000 and External Standards.

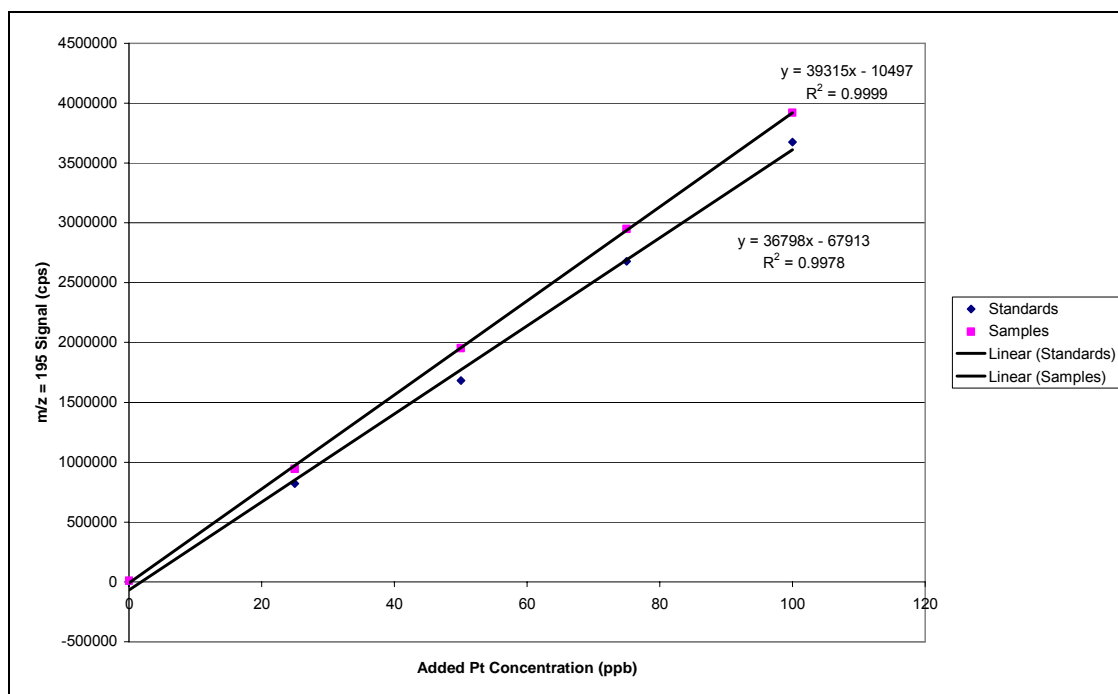


Figure 54. A Graph Comparing Pt Spike Concentration ($\mu\text{g l}^{-1}$) with $m/z = 195$ Signal (cps) for Sample 1 : 1 000 000 and External Standards.

Following construction of the graphs in Figures 52 to 54 and 94 to 141 it was clear that there were significant quantities of ^{31}P detected in each sample whilst there was very little, if any, Pt detected. Manipulation of the data generated following analysis of the prepared samples, by use of the equations associated with the $m/z = 47$, 194 and 195 graphs constructed previously, determined the ^{31}P , ^{194}Pt and ^{195}Pt isotope content. In the case of a standard additions graph, for the $y = mx + c$ equation, when assuming that the y value is equal to zero the resulting negative x value provided the parameter of interest. Here the x value is the desired isotope concentration data. An alternative external calibration approach for the determination of isotope concentration was also carried out. Using these methods the ^{31}P , ^{194}Pt and ^{195}Pt isotope content of each sample studied was calculated and can be seen in Tables 22, 23 and 24.

Table 22. ^{31}P Isotope Content of the DNA/Cisplatin Samples Studied by ICP-MS.

Sample Identity	Graph Figure N^o	Sample Curve Equation	^{31}P Concⁿ, $\mu\text{g l}^{-1}$	Stds Curve Equation	^{31}P Concⁿ, $\mu\text{g l}^{-1}$
			$m/z = 47$ Measurement (Std Add)		$m/z = 47$ Measurement (Ext Cal)
1:1 000 000	52	$y = 56.172x + 15964$	284	$y = 52.431x + 3267.7$	230
1:1 000 000 (2)	97	$y = 84.589x + 15051$	178	$y = 52.431x + 3267.7$	211
1:500 000	100	$y = 102.48x + 21651$	211	$y = 47.008x + 3858.6$	359
1:500 000 (2)	103	$y = 70.529x + 23945$	340	$y = 47.008x + 3858.6$	410
1:100 000	106	$y = 101.81x + 25273$	248	$y = 48.354x + 3730.7$	430
1:100 000 (2)	109	$y = 54.731x + 28762$	526	$y = 48.354x + 3730.7$	514
1:50 000	112	$y = 73.687x + 23839$	324	$y = 45.916x + 3788.5$	451
1:50 000 (2)	115	$y = 53.23x + 25345$	476	$y = 45.916x + 3788.5$	475
1:10 000	118	$y = 86.551x + 31556$	365	$y = 49.297x + 3648.6$	591
1:10 000 (2)	121	$y = 235.17x + 29746$	126	$y = 49.297x + 3648.6$	614
1:5 000	124	$y = 89.018x + 33153$	372	$y = 51.908x + 3714.6$	577
1:5 000 (2)	127	$y = 94.161x + 31183$	331	$y = 51.908x + 3714.6$	496
1:1 000	130	$y = 113.2x + 34475$	305	$y = 50.664x + 3747$	552
1:1 000 (2)	133	$y = 132.3x + 35711$	270	$y = 50.664x + 3747$	602
Control	136	$y = 157.28x + 33357$	212	$y = 47.179x + 3477.2$	590
Control (2)	139	$y = 54.692x + 39836$	728	$y = 47.179x + 3477.2$	777

Table 23. ¹⁹⁴Pt Isotope Content of the DNA/Cisplatin Samples Studied by ICP-MS.

Sample Identity	Graph Figure N°	Sample Curve Equation	¹⁹⁴Pt Concⁿ, µg l⁻¹	Stds Curve Equation	¹⁹⁴Pt Concⁿ, µg l⁻¹
			<i>m/z = 47</i> Measurement (Std Add)		<i>m/z = 47</i> Measurement (Ext Cal)
1:1 000 000	53	y = 37777x - 12536	-	y = 35468x - 71268	2.26
1:1 000 000 (2)	98	y = 39207x - 3936.6	-	y = 35468x - 71268	2.24
1:500 000	101	y = 40041x - 28533	-	y = 39446x - 12578	0.64
1:500 000 (2)	104	y = 39198x + 21095	0.54	y = 39446x - 12578	0.63
1:100 000	107	y = 39586x - 33284	-	y = 38263x + 23519	-
1:100 000 (2)	110	y = 38687x + 39574	1.03	y = 38263x + 23519	-
1:50 000	113	y = 38788x - 35786	-	y = 38731x - 48454	1.57
1:50 000 (2)	116	y = 38702x - 25568	-	y = 38731x - 48454	1.45
1:10 000	119	y = 38518x - 49974	-	y = 37094x - 32754	1.34
1:10 000 (2)	122	y = 38978x - 55141	-	y = 37094x - 32754	1.23
1:5 000	125	y = 35984x - 4085	-	y = 36164x - 25204	0.98
1:5 000 (2)	128	y = 35910x - 12934	-	y = 36164x - 25204	1.21
1:1 000	131	y = 36324x - 24926	-	y = 34899x - 22944	1.27
1:1 000 (2)	134	y = 35019x - 27275	-	y = 34899x - 22944	1.15
Control	137	y = 32496x - 7259.5	-	y = 32049x + 9507.1	0.28
Control (2)	140	y = 32146x - 17847	-	y = 32049x + 9507.1	-

Table 24. ¹⁹⁵Pt Isotope Content of the DNA/Cisplatin Samples Studied by ICP-MS.

Sample Identity	Graph Figure N°	Sample Curve Equation	¹⁹⁵Pt Concⁿ, µg l⁻¹	Stds Curve Equation	¹⁹⁵Pt Concⁿ, µg l⁻¹
			<i>m/z</i> = 47 Measurement (Std Add)		<i>m/z</i> = 47 Measurement (Ext Cal)
1:1 000 000	54	y = 39315x - 10497	-	y = 36798x - 67913	2.10
1:1 000 000 (2)	99	y = 40661x + 735.3	0.02	y = 36798x - 67913	2.07
1:500 000	102	y = 41710x - 28805	-	y = 40993x - 7950.5	0.52
1:500 000 (2)	105	y = 40797x + 25640	0.63	y = 40993x - 7950.5	0.51
1:100 000	108	y = 41185x - 31431	-	y = 39754x + 28424	-
1:100 000 (2)	111	y = 40290x + 42108	1.05	y = 39754x + 28424	-
1:50 000	114	y = 40416x - 36083	-	y = 40315x - 47456	1.50
1:50 000 (2)	117	y = 40265x - 23436	-	y = 40315x - 47456	1.38
1:10 000	120	y = 39991x - 50533	-	y = 38472x - 27041	1.16
1:10 000 (2)	123	y = 40400x - 51315	-	y = 38472x - 27041	1.05
1:5 000	126	y = 37380x - 291.01	-	y = 37655x - 23798	0.91
1:5 000 (2)	129	y = 37391x - 11624	-	y = 37655x - 23798	1.15
1:1 000	132	y = 37602x - 18083	-	y = 36203x - 16885	1.09
1:1 000 (2)	135	y = 36509x - 31351	-	y = 36203x - 16885	0.96
Control	138	y = 33887x - 5543.7	-	y = 33518x + 9065.1	0.31
Control (2)	141	y = 33615x - 19251	-	y = 33518x + 9065.1	0.02

As can be seen from the concentrations of ³¹P and ^{194,195}Pt present in the samples studied there is an abundance of ³¹P (in each case the concentration measured is approximately one tenth of the concentration of DNA present which shows agreement with known content) whilst there is no, or little, ^{194,195}Pt. At first glance the initial conclusions are that there were large quantities of DNA present in each solution but no Pt based drug, i.e. the suggestion that either no drug binding took place. However, it is more likely that the measurement of Pt isotopes was not compatible with the instrument conditions established for the formation of ³¹P¹⁶O⁺ in the collision cell. It is likely that the majority of Pt ions being transmitted through the hexapole collision cell are slowed, destabilised and eliminated following collision with O₂ molecules under IKEE conditions.

Due to this absence of Pt in the samples that are expected to be Pt rich aliquots of the original most concentrated samples (1 : 1 000 000 and 1 : 500 000) were diluted, this time only ten fold, and analysed again. These measurements revealed no significant difference compared to the quantities of Pt present in the hundred fold diluted samples originally studied showing that the degree of dilution is not the cause of this issue.

4.4.2. Study 2

Following the initial failure of the ICP-MS study of cisplatin exposed DNA samples a second attempt at the analysis was carried out. This time however, with similarly prepared samples, an answer was required as to whether the absence of Pt isotopes in study 1 was the result of a lack of drug/target binding or the use of instrumental conditions that were not appropriate. In order to try and answer at least one aspect of this question the approach to study of these samples was changed.

For this repeat of the study, however, the measurement of the ^{31}P isotope was reconsidered. As the employment of the collision cell and an O_2 reaction gas, for the measurement of the $^{31}\text{P}^{16}\text{O}^+$ ion, raised a question mark with regard to simultaneous determination of Pt isotopes the ICP-MS method was changed. As, prior to arrival at Loughborough University, the concentration of DNA present in each sample was determined by UV/Vis analysis it was decided to concentrate on the study of the Pt isotopes. This being the case, to simplify the analysis and limit any non-spectroscopic interference arising from the C-based structure of DNA and degree of dissolved material, for this repeat analysis the sample treatment following preparation was also approached differently. It was decided to chemically cleave the Pt based drug molecules from the target DNA molecules and analyse the drug component alone.

Experimental Details

A new series of drug exposed DNA samples, similar to that of study 1, were prepared by Dr R. Le Pla at Leicester University and transported to Loughborough University

for analysis. For this second attempt the analysis was again limited to the study of cisplatin only. As with section 4.4.1 the experimental details are discussed in terms of sample preparation and instrumental analysis.

A 1 mg ml^{-1} DNA solution (3.25 mM DNA nucleotide) was exposed to a series of three cisplatin solutions of various concentrations, prepared from a 1 mg ml^{-1} cisplatin stock solution (3.33 mM). Different volumes of the three cisplatin solutions were added to 4.223 ml of the 1 mg ml^{-1} DNA solution (3.25 mM) to prepare a series of DNA/cisplatin samples similar to those described in Study 1. Similar to the previous preparation the exposed DNA samples were incubated at 37°C for 24 hours. The exposed DNA was precipitated, washed with ethanol to remove excess drug molecules and the precipitated DNA was then redissolved in deionised water. The final sample volume was approximately 5 ml and for this preparation there was no duplication of samples. Details of the full preparation of the samples investigated during this second study are in Table 25.

Table 25. Preparation Details for the Samples Investigated During Study 2.

Solution Number	Solution Description	Procedure	Nucleotide Conc ⁿ (μM)	Cisplatin Conc ⁿ (μM)	Drug : Nucleotide Ratio
Stock Solutions					
1	DNA Stock Solution	DNA (1 mg in 1 ml)	3250	-	-
2	Cisplatin Stock Solution	Cisplatin (1 mg in 1 ml)	-	3330	-
Cisplatin Preparative Solutions					
3	Serial Dilution of Cisplatin Stock Solution	1000 Fold Dilution of Soln 2 with H ₂ O	-	3.077	-
4		100 Fold Dilution of Soln 3 with H ₂ O	-	0.0308	-
5		100 Fold Dilution of Soln 4 with H ₂ O	-	0.0003	-
Final Sample Solutions					
6	Final Sample Preparation, Exposure of Solution 1 to Solutions 3 to 5	Soln 1 (4223 μl) + H ₂ O (777 μl)	-	-	Control
7		Soln 1 (4223 μl) + Soln 3 (500 μl) + H ₂ O (277 μl)	-	-	1 : 10 000
8		Soln 1 (4223 μl) + Soln 3 (100 μl) + H ₂ O (677 μl)	-	-	1 : 50 000
9		Soln 1 (4223 μl) + Soln 3 (50 μl) + H ₂ O (727 μl)	-	-	1 : 100 000
10		Soln 1 (4223 μl) + Soln 3 (10 μl) + H ₂ O (767 μl)	-	-	1 : 500 000
11		Soln 1 (4223 μl) + Soln 4 (500 μl) + H ₂ O (277 μl)	-	-	1 : 1 000 000
12		Soln 1 (4223 μl) + Soln 4 (100 μl) + H ₂ O (677 μl)	-	-	1 : 5 000 000
13		Soln 1 (4223 μl) + Soln 4 (50 μl) + H ₂ O (727 μl)	-	-	1 : 10 000 000
14		Soln 1 (4223 μl) + Soln 4 (10 μl) + H ₂ O (767 μl)	-	-	1 : 50 000 000
15		Soln 1 (4223 μl) + Soln 5 (500 μl) + H ₂ O (277 μl)	-	-	1 : 100 000 000
16		Soln 1 (4223 μl) + Soln 5 (100 μl) + H ₂ O (677 μl)			1 : 500 000 000
17		Soln 1 (4223 μl) + Soln 5 (50 μl) + H ₂ O (727 μl)			1 : 1 000 000 000

Following this preparation, aliquots (5 μ l) of each sample were diluted (to 195 μ l in H₂O) and analysed by UV spectroscopy to determine final DNA concentration, see Table 90.

Following preparation, at Leicester University, the samples were subject to further pre-analysis treatment for the separation of the bound drug molecule from the target DNA. Each sample (\approx 500 μ l) was treated one to one with 25% NH₃ (\approx 500 μ l) in sealed 1 ml centrifuge tubes and heated to 70°C in a water bath for 48 hours. As this initial step incorporated a two fold dilution, and the resulting 12.5% NH₃ solution would prove difficult to analyse by ICP-MS, a volume reduction step was employed. The caps of each centrifuge tube were removed and each tube was heated at 40°C in a water bath until the volume was reduced to approximately 500 μ l. The aim of this step was to evaporate the ammonia and concentrate the samples taking them back to close to the original concentration prior to dilution.

The resulting, reduced, solution would contain whole DNA and the cleaved drug molecules, these two species therefore required separation prior to ICP-MS analysis. Separation was carried out via a centrifuge method. 3 ml VectaSpin 3 centrifuge tubes containing a 100 000 MWCO filter were employed, the aim here being to retain the large DNA molecules on the filter and allow the cleaved drug molecules to reach the tube space beneath during centrifugation. The approximate 500 μ l (accurately weighed) of each sample was transferred to a tube and centrifuged at 8000 RPM for 2 hours. The solution that passed through the filter of each tube was weighed and transferred to a sample vial for analysis. Details of the pre-treatment carried out on each sample can be seen in Tables 91 and 92 and final details, including correction factors, can be seen in Table 93. In this case the samples, which should only contain the cleaved drug molecules, were analysed by ICP-MS in standard mode, i.e. without the use of a collision cell or the presence of any reaction gas.

The instrument used in analysis of these samples was as described previously in this chapter as was the sample introduction apparatus. As the measurement of the ³¹P isotope was not required for this second study the DNA/cisplatin samples were analysed by ICP-MS under standard mode for the presence of ^{190,192,194,195,196,198}Pt isotopes, i.e. without the use of specific conditions such as collision cell or cold

plasma. However, to provide additional information, the $m/z = 31$ and 47 signals (i.e. $^{31}\text{P}^+$ and $^{31}\text{P}^{16}\text{O}^+$ ions) were also monitored to establish, qualitatively, whether significant quantities of ^{31}P based components penetrated the filter of the centrifuge tubes. External standards of Pt were prepared from a $1000\ \mu\text{g ml}^{-1}$ single element standard solution (Fisher Chemicals, Loughborough, UK) by sequential dilution with high purity deionised water produced using a Maxima Ultra (Elga) water purification system. Prior to carrying out these measurements, the ICP-MS instrument was optimised to produce standard operating conditions (see Table 94, Appendix 4).

When the optimum ICP-MS conditions were established the prepared samples together with a series of Pt standard solutions for external calibration were analysed for $^{190,192,194,195,196,198}\text{Pt}$ isotope content. Data for each of these isotopes was collected by the software of the PQ ExCell (Thermo Plasmalab) and, as with study 1, three replicate readings were taken for each isotope measurement allowing mean, standard deviation and relative standard deviation data to be established. Results of the analysis of the samples are given in the next section.

Results and Discussion

The mean data generated during the ICP-MS analysis of the DNA/cisplatin samples for this second study can be seen in Table 95. This mean data was then corrected to account for variations in volume, i.e. concentration variation, following the reduction step, see Table 96. All data were corrected in relation to $500\ \mu\text{l}$. From this corrected data Figure 55 was constructed to establish the concentration of $^{194,195}\text{Pt}$ isotopes and the degree of linearity over the sample range. The data accrued from analysis of the Pt standard solutions can be seen in Table 97 and calibration curves constructed from this data can be seen in Figure 56. A bar chart was also constructed from the ^{31}P data to highlight the presence of any significant ^{31}P based components in the sample analysed, see Figure 57. Figure 57 is a qualitative comparison of $m/z = 31$ signal between samples, the blank sample signal provides data to account for the presence of background polyatomic ions to which other samples can be compared.

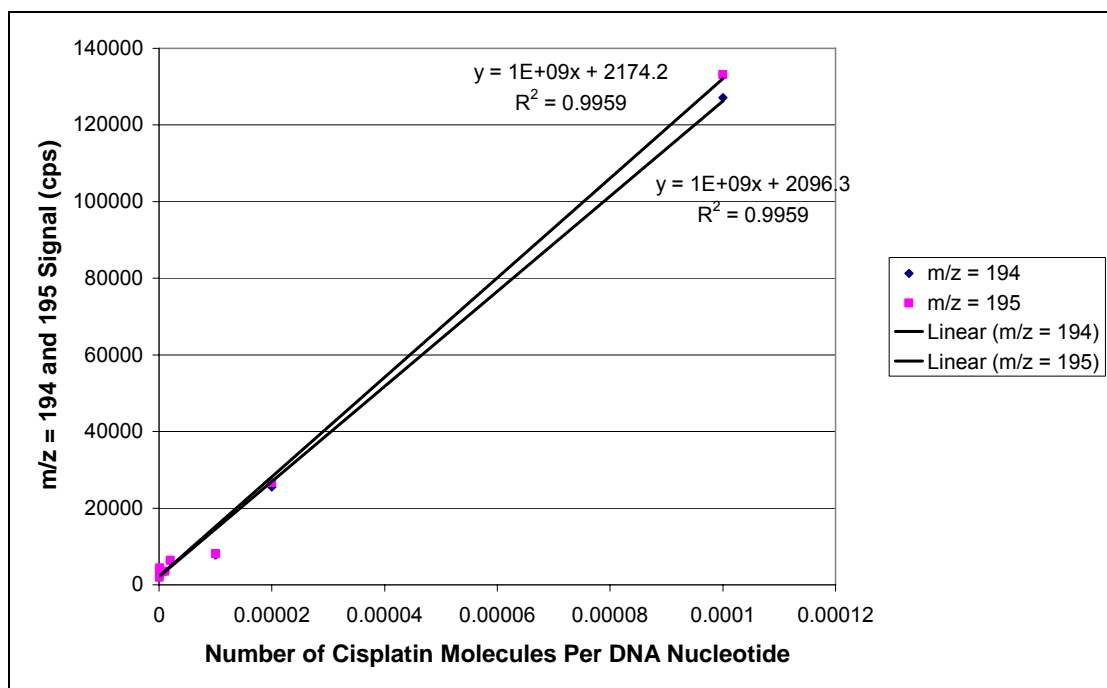


Figure 55. A Graph Comparing Number of Cisplatin Molecules Per DNA Nucleotide with Corrected $m/z = 194$ and 195 Signal (cps).

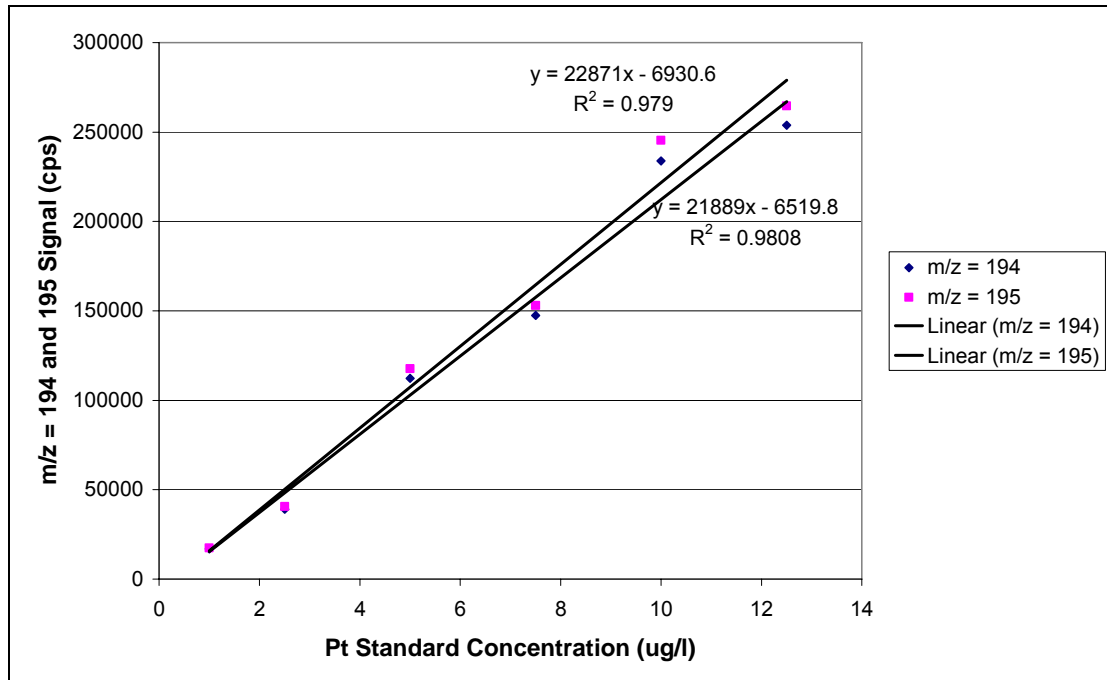


Figure 56. A Graph Comparing Pt Standard Concentration ($\mu\text{g l}^{-1}$) with $m/z = 194$ and 195 Signal (cps).

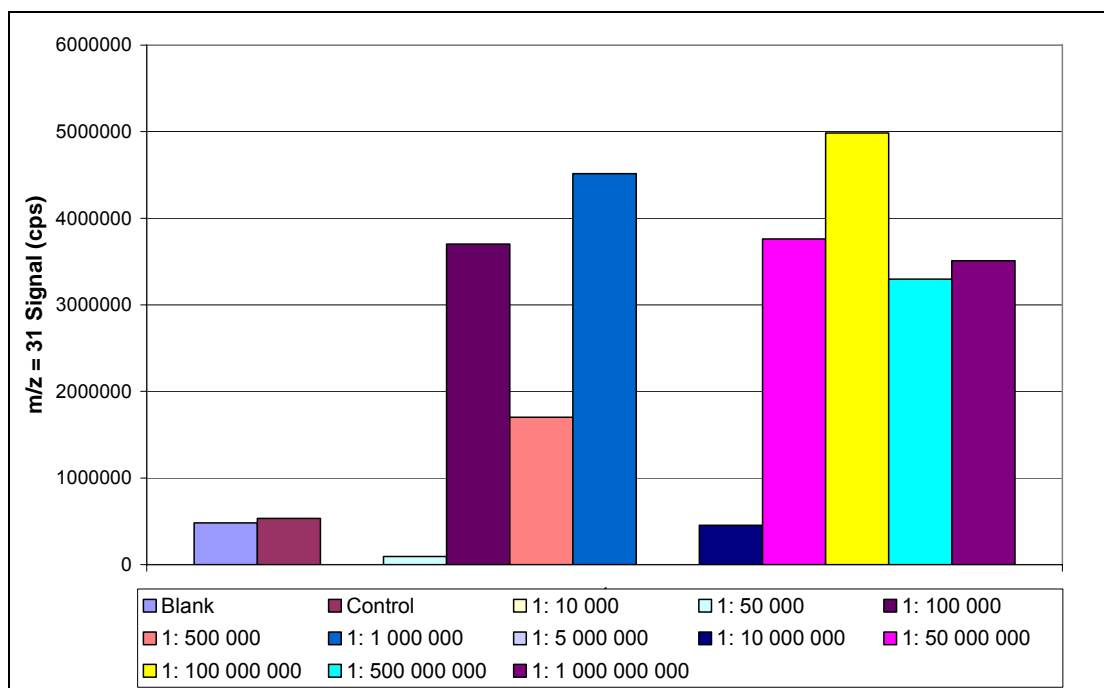


Figure 57. A Bar Chart Comparing $m/z = 31$ Signals (cps) Between DNA/Cisplatin Samples Studied During Study 2.

Following study of the data accrued, from analysis of the DNA/Cisplatin sample solutions, and construction of the graph in Figure 55 and bar chart in Figure 57 a number of issues became apparent.

Firstly in each cisplatin exposed DNA sample studied there were significant quantities of the Pt isotopes. As can be seen in Figure 55 a linear response was observed between the number of cisplatin molecules per DNA nucleotide and the $m/z = 194$ and 195 signal. Such a relationship is what would have been expected at the beginning of this work, this suggests that the absence of Pt in the samples analysed in study 1 was due to the employment of instrument conditions not conducive to the determination of Pt isotopes. Secondly, the ion counts generated through analysis of the sample series show that the limit of measurement by this method with regard to the study of platinum associated with these samples lies within the region of 100 000 to 500 000 nucleotides per cisplatin molecule. This is the equivalent of 2 to 10 $\mu\text{g l}^{-1}$, however, the limit of detection of Pt by ICP-MS is less than 1 ng l^{-1} which suggests that there may be suppression of the Pt signal. Although this may be the case, this is the desired analytical range as for therapeutic activity it is believed that a cisplatin molecule

bound every 400 000 DNA nucleotides is required to inhibit replication processes. Here the ion counts generated from the 100 000 nucleotides sample is significantly elevated above that of the blank and control solutions, however, the ion counts for the 500 000 nucleotides sample were not. The concentration of each sample analysed was established via the external calibration equations of Figure 56. The calculated concentration values can be seen in Tables 26 and 27.

Table 26. ^{194}Pt Isotope Content of the DNA/Cisplatin Samples Analysed During Study 2.

N° of DNA Nucleotides Per Cisplatin	N° of Cisplatins Per DNA Nucleotide	^{194}Pt Stds Curve Equation	$m/z = 194$ Sample Signal (cps)	^{194}Pt Concⁿ ($\mu\text{g l}^{-1}$)
Blank	Blank	$y = 21889x - 6519.8$	2952	0.43
Control	Control	$y = 21889x - 6519.8$	1225	0.35
10 000	0.0001	$y = 21889x - 6519.8$	116226	5.61
50 000	0.0005	$y = 21889x - 6519.8$	23095	1.35
100 000	0.00001	$y = 21889x - 6519.8$	8465	0.68
500 000	0.00005	$y = 21889x - 6519.8$	3863	0.47
1 000 000	0.000001	$y = 21889x - 6519.8$	3082	0.44
5 000 000	0.000005	$y = 21889x - 6519.8$	3461	0.46
10 000 000	0.0000001	$y = 21889x - 6519.8$	4299	0.49
50 000 000	0.0000005	$y = 21889x - 6519.8$	3096	0.44
100 000 000	0.00000001	$y = 21889x - 6519.8$	2485	0.41
500 000 000	0.00000005	$y = 21889x - 6519.8$	2382	0.41
1 000 000 000	0.000000001	$y = 21889x - 6519.8$	2307	0.40

Table 27. ¹⁹⁵Pt Isotope Content of the DNA/Cisplatin Samples Analysed During Study 2.

N° of DNA Nucleotides Per Cisplatin	N° of Cisplatins Per DNA Nucleotide	¹⁹⁵Pt Stds Curve Equation	<i>m/z</i> = 195 Sample Signal (cps)	¹⁹⁵Pt Concⁿ (µg l⁻¹)
Blank	Blank	$y = 22871x - 6930.6$	3128	0.44
Control	Control	$y = 22871x - 6930.6$	1238	0.36
10 000	0.0001	$y = 22871x - 6930.6$	121648	5.62
50 000	0.0005	$y = 22871x - 6930.6$	24142	1.36
100 000	0.00001	$y = 22871x - 6930.6$	8832	0.69
500 000	0.00005	$y = 22871x - 6930.6$	4045	0.48
1 000 000	0.000001	$y = 22871x - 6930.6$	3171	0.44
5 000 000	0.000005	$y = 22871x - 6930.6$	3613	0.46
10 000 000	0.0000001	$y = 22871x - 6930.6$	4479	0.50
50 000 000	0.0000005	$y = 22871x - 6930.6$	3261	0.45
100 000 000	0.00000001	$y = 22871x - 6930.6$	2598	0.42
500 000 000	0.00000005	$y = 22871x - 6930.6$	2478	0.41
1 000 000 000	0.000000001	$y = 22871x - 6930.6$	2412	0.41

As can be seen in Tables 26 and 27 the background concentration of Pt present appears to be in the order of 0.40 µg l⁻¹. From this background it can be said that, as mentioned previously, the method LOD could be found between 100 000 and 500 000 DNA nucleotides per cisplatin molecule. This background concentration is quite high for Pt so it could confidently be said that there is a likely source of Pt contamination affecting the analysis. Leaching from the peristaltic pump tubing and centrifuge tubes used would be a likely source of such contamination. Finally, as can be seen in the bar chart of Figure 57, there are large quantities of ³¹P present in a majority of the final sample solutions analysed. The presence of such ³¹P implies that ³¹P based fragments of DNA are passing through the centrifuge filter during the separation procedure. As ³¹P appears in large quantities in most of the samples studied then it could be said that either these centrifuge filters were not as efficient as desired or that the NH₃ treatment was too harsh resulting in DNA fragmentation allowing passage through the two tube compartments.

As this second study of the interaction between DNA and cisplatin (*in vitro*) was successful, with regard to producing data that described an increased degree of

binding with increasing drug exposure, work could then commence on establishing binding constant data that could be used as the basis of a clinical test for cisplatin efficacy for individual patients. The calculation of binding constants and ratios is described in detail in section 4.5 and compared to constants and ratios determined following further studies to establish the viability of a clinical test. Unfortunately, due to the preparation error, the sample series analysed during this second study was flawed slightly as many of the samples were out of the range of detection of the ICP-QMS. At this point it was intended to repeat the work with a more realistic sample series to establish a greater amount of data. However, the more important point that this study has established is that the lack of Pt data in study 1 was not the result of binding failure but instead the result of instrumental conditions that were suitable for ^{31}P measurement only.

4.4.3. Studies 3 and 4

Following the success of the second study of DNA and Pt based drug interaction the binding of drug to target and subsequent measurement of $^{194,195}\text{Pt}$ isotopes was repeated with both cisplatin and oxaliplatin drugs. Such further study (studies 3 and 4) should determine both the repeatability of data and establish a better understanding of the limits of the ICP-QMS for this work. A third and fourth study of this drug/target binding were conducted. The third study was a simple repeat of study 2 with a more realistic sample series whilst the fourth study involved the analysis of a wider range of samples that would allow the limits of the ICP-QMS to be tested.

Experimental Details

For studies 3 and 4 DNA samples were prepared and exposed to both cisplatin and oxaliplatin in a similar fashion to that described previously. For studies 3 and 4, exposed DNA samples were prepared based on the mean molecular weight of a DNA nucleotide, bound in the helix, being 307.61 and the molecular weight of cisplatin and

oxaliplatin being 300 and 397, respectively. Details of the full preparation of the samples investigated during these studies are in Tables 28, 29, 30 and 31.

Table 28. Preparation Details for the Cisplatin Samples Investigated During Study 3.

Solution Number	Solution Description	Procedure	Nucleotide Concⁿ (μM)	Cisplatin Concⁿ (μM)	Drug : Nucleotide Ratio
Stock Solutions					
1	DNA Stock Solution	DNA (1 mg in 1 ml)	3250	-	-
2	Cisplatin Stock Solution	Cisplatin (1 mg in 1 ml)	-	3330	-
Cisplatin Preparative Solutions					
3	Serial Dilution of	1.023 Fold Dilution of Soln 2 with H ₂ O	-	3250	-
4	Cisplatin Stock Solution	1000 Fold Dilution of Soln 3 with H ₂ O	-	3.25	-
Final Sample Solutions					
5	Final Sample Preparation, Exposure of Solution 1 to Solutions 3 and 4	Soln 1 (3000 μl) + H ₂ O (3000 μl)	-	-	Control
6		Soln 1 (3000 μl) + Soln 3 (60 μl) + H ₂ O (2940 μl)	-	-	1 : 50
7		Soln 1 (3000 μl) + Soln 3 (30 μl) + H ₂ O (2970 μl)	-	-	1 : 100
8		Soln 1 (3000 μl) + Soln 3 (6 μl) + H ₂ O (2994 μl)	-	-	1 : 500
9		Soln 1 (3000 μl) + Soln 4 (3000 μl)	-	-	1 : 1 000
10		Soln 1 (3000 μl) + Soln 4 (600 μl) + H ₂ O (2400 μl)	-	-	1 : 5 000
11		Soln 1 (3000 μl) + Soln 4 (300 μl) + H ₂ O (2700 μl)	-	-	1 : 10 000
12		Soln 1 (3000 μl) + Soln 4 (60 μl) + H ₂ O (2940 μl)	-	-	1 : 50 000
13		Soln 1 (3000 μl) + Soln 4 (30 μl) + H ₂ O (2970 μl)	-	-	1 : 100 000
14		Soln 1 (3000 μl) + Soln 4 (6 μl) + H ₂ O (2994 μl)	-	-	1 : 500 000
15		Soln 1 (3000 μl) + Soln 4 (3 μl) + H ₂ O (2997 μl)			1 : 1 000 000

Table 29. Preparation Details for the Oxaliplatin Samples Investigated During Study 3.

Solution Number	Solution Description	Procedure	Nucleotide Concⁿ (μM)	Oxaliplatin Concⁿ (μM)	Drug : Nucleotide Ratio
Stock Solutions					
1	DNA Stock Solution	DNA (1 mg in 1 ml)	3250	-	-
2	Oxaliplatin Stock Solution	Oxaliplatin (2 mg in 1 ml)	-	5040	-
Cisplatin Preparative Solutions					
3	Serial Dilution of	1.550 Fold Dilution of Soln 2 with H ₂ O	-	3250	-
4	Oxaliplatin Stock Solution	100 Fold Dilution of Soln 3 with H ₂ O	-	3.25	-
Final Sample Solutions					
5	Final Sample Preparation, Exposure of Solution 1 to Solutions 3 and 4	Soln 1 (3000 μl) + H ₂ O (3000 μl)	-	-	Control
6		Soln 1 (3000 μl) + Soln 3 (60 μl) + H ₂ O (2940 μl)	-	-	1 : 50
7		Soln 1 (3000 μl) + Soln 3 (30 μl) + H ₂ O (2970 μl)	-	-	1 : 100
12		Soln 1 (3000 μl) + Soln 3 (6 μl) + H ₂ O (2994 μl)	-	-	1 : 500
13		Soln 1 (3000 μl) + Soln 4 (3000 μl)	-	-	1 : 1 000
14		Soln 1 (3000 μl) + Soln 4 (600 μl) + H ₂ O (2400 μl)	-	-	1 : 5 000
15		Soln 1 (3000 μl) + Soln 4 (300 μl) + H ₂ O (2700 μl)	-	-	1 : 10 000
16		Soln 1 (3000 μl) + Soln 4 (60 μl) + H ₂ O (2940 μl)	-	-	1 : 50 000
17		Soln 1 (3000 μl) + Soln 4 (30 μl) + H ₂ O (2970 μl)	-	-	1 : 100 000
18		Soln 1 (3000 μl) + Soln 4 (6 μl) + H ₂ O (2994 μl)	-	-	1 : 500 000
19		Soln 1 (3000 μl) + Soln 4 (3 μl) + H ₂ O (2997 μl)			1 : 1 000 000

Table 30. Preparation Details for the Cisplatin Samples Investigated During Study 4.

Solution Number	Solution Description	Procedure	Nucleotide Concⁿ (μM)	Cisplatin Concⁿ (μM)	Drug : Nucleotide Ratio
Stock Solutions					
1	DNA Stock Solution	DNA (1 mg in 1 ml)	3250	-	-
2	Cisplatin Stock Solution	Cisplatin (1 mg in 1 ml)	-	3330	-
Cisplatin Preparative Solutions					
3	Serial Dilution of	1.023 Fold Dilution of Soln 2 with H ₂ O	-	3250	-
4	Cisplatin Stock Solution	1000 Fold Dilution of Soln 3 with H ₂ O	-	3.25	-
Final Sample Solutions					
5	Final Sample Preparation, Exposure of Solution 1 to Solutions 3 and 4	Soln 1 (3000 μl) + H ₂ O (3000 μl)	-	-	Control
6		Soln 1 (3000 μl) + Soln 3 (30 μl) + H ₂ O (2970 μl)	-	-	1 : 100
7		Soln 1 (3000 μl) + Soln 3 (20 μl) + H ₂ O (2980 μl)	-	-	1 : 150
8		Soln 1 (3000 μl) + Soln 3 (10 μl) + H ₂ O (2990 μl)	-	-	1 : 300
9		Soln 1 (3000 μl) + Soln 4 (6 μl) + H ₂ O (2994 μl)	-	-	1 : 500
10		Soln 1 (3000 μl) + Soln 4 (3000 μl)	-	-	1 : 1 000
11		Soln 1 (3000 μl) + Soln 4 (600 μl) + H ₂ O (2400 μl)	-	-	1 : 5 000
12		Soln 1 (3000 μl) + Soln 4 (300 μl) + H ₂ O (2700 μl)	-	-	1 : 10 000
13		Soln 1 (3000 μl) + Soln 4 (60 μl) + H ₂ O (2940 μl)	-	-	1 : 50 000
14		Soln 1 (3000 μl) + Soln 4 (30 μl) + H ₂ O (2970 μl)	-	-	1 : 100 000
15		Soln 1 (3000 μl) + Soln 4 (12 μl) + H ₂ O (2988 μl)			1 : 250 000
16		Soln 1 (3000 μl) + Soln 4 (6 μl) + H ₂ O (2994 μl)			1 : 500 000

Table 31. Preparation Details for the Oxaliplatin Samples Investigated During Study 4.

Solution Number	Solution Description	Procedure	Nucleotide Concⁿ (μM)	Oxaliplatin Concⁿ (μM)	Drug : Nucleotide Ratio
Stock Solutions					
1	DNA Stock Solution	DNA (1 mg in 1 ml)	3250	-	-
2	Oxaliplatin Stock Solution	Oxaliplatin (2 mg in 1 ml)	-	5040	-
Cisplatin Preparative Solutions					
3	Serial Dilution of	1.550 Fold Dilution of Soln 2 with H ₂ O	-	3250	-
4	Oxaliplatin Stock Solution	100 Fold Dilution of Soln 3 with H ₂ O	-	3.25	-
Final Sample Solutions					
5	Final Sample Preparation, Exposure of Solution 1 to Solutions 3 and 4	Soln 1 (3000 μl) + H ₂ O (3000 μl)	-	-	Control
6		Soln 1 (3000 μl) + Soln 3 (30 μl) + H ₂ O (2970 μl)	-	-	1 : 100
7		Soln 1 (3000 μl) + Soln 3 (20 μl) + H ₂ O (2980 μl)	-	-	1 : 150
8		Soln 1 (3000 μl) + Soln 3 (10 μl) + H ₂ O (2990 μl)	-	-	1 : 300
9		Soln 1 (3000 μl) + Soln 4 (6 μl) + H ₂ O (2994 μl)	-	-	1 : 500
10		Soln 1 (3000 μl) + Soln 4 (3000 μl)	-	-	1 : 1 000
11		Soln 1 (3000 μl) + Soln 4 (600 μl) + H ₂ O (2400 μl)	-	-	1 : 5 000
12		Soln 1 (3000 μl) + Soln 4 (300 μl) + H ₂ O (2700 μl)	-	-	1 : 10 000
13		Soln 1 (3000 μl) + Soln 4 (60 μl) + H ₂ O (2940 μl)	-	-	1 : 50 000
14		Soln 1 (3000 μl) + Soln 4 (30 μl) + H ₂ O (2970 μl)	-	-	1 : 100 000
15		Soln 1 (3000 μl) + Soln 4 (12 μl) + H ₂ O (2988 μl)			1 : 250 000
16		Soln 1 (3000 μl) + Soln 4 (6 μl) + H ₂ O (2994 μl)			1 : 500 000

As with previous studies the final DNA concentration of each sample was determined by UV spectroscopy, see Tables 98, 99, 100 and 101. Following preparation the samples were treated further, as described in Study 2. Compared to previous analysis there was twice as much sample available so a two-fold preconcentration was carried out with the aim of measuring lower drug molecule : nucleotide ratios. Details of the pre-treatment carried out on each sample, for both studies, can be seen in Tables 102 to 107 and final details, including correction factors, can be seen in Tables 108, 109 and 110. The final sample solutions, as well as Pt standard solutions, were then analysed by ICP-QMS under standard mode. Instrumental conditions employed during this analysis can be seen in Tables 111, 117 and 118 (Appendix 4). Results of the sample analysis are in the next section.

Results and Discussion

Data generated during the ICP-MS analysis of these DNA/cisplatin and DNA/oxaliplatin samples, of study 3 and 4, as well as Pt standard solutions can be seen in Tables 112 to 116 and 119 to 124. It should be noted that two sets of standard Pt solutions were measured for external calibration data for Study 4 as cisplatin and oxaliplatin samples were analysed on different days. From this data a series of graphs were constructed comparing the number of cisplatin and oxaliplatin molecules per DNA nucleotide versus the Pt isotope signal in order to determine the presence of the major Pt isotopes ($^{194,195}\text{Pt}$) in each sample prepared (see Figures 58, 59, 63 and 64). Calibration graphs were also constructed from the standard solution data to determine the Pt concentration of each sample via external quantification (see Figures 60, 65 and 66).

As in Study 2 the $m/z = 31$ data for each sample analysed was also used to construct bar charts to ascertain the degree of passage of ^{31}P based DNA fragments through the centrifuge filter tubes used, see Figures 61, 62, 67 and 68.

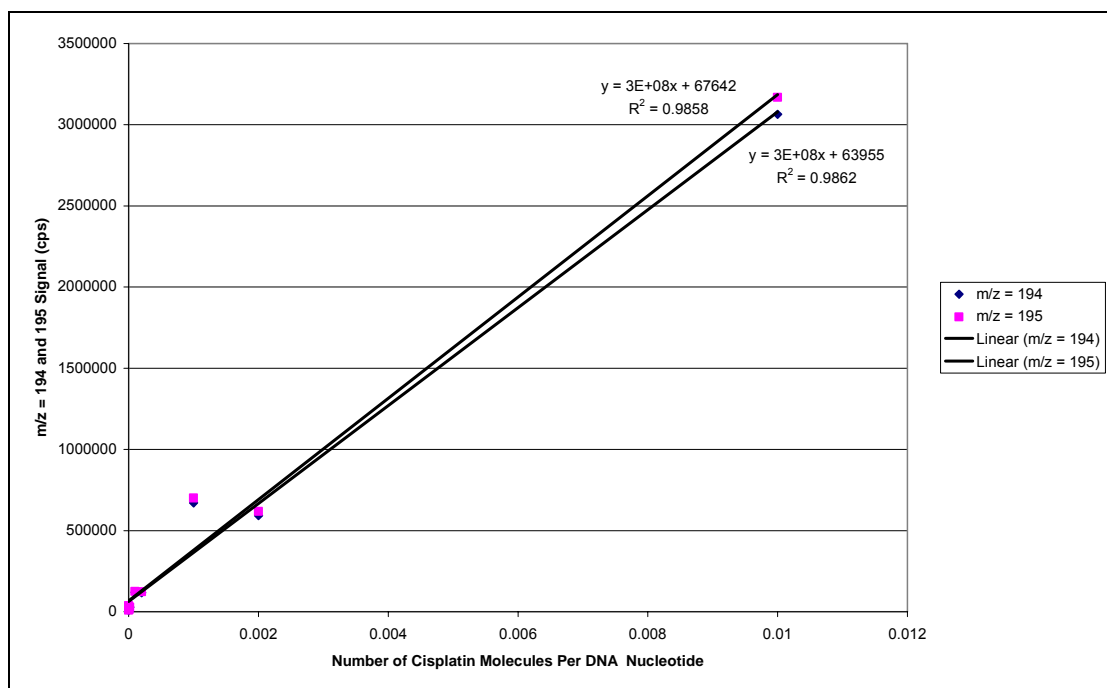


Figure 58. A Graph Comparing Number of Cisplatin Molecules Per DNA Nucleotide with Corrected $m/z = 194$ and 195 Signal (cps) for Study 3.

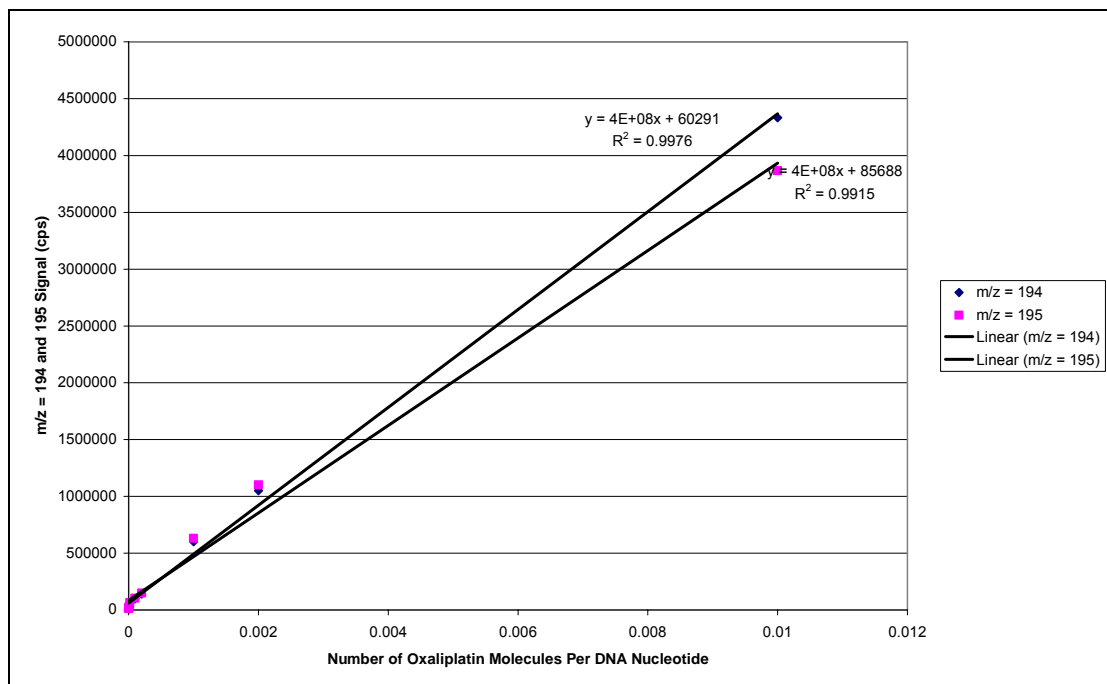


Figure 59. A Graph Comparing Number of Oxaliplatin Molecules Per DNA Nucleotide with Corrected $m/z = 194$ and 195 Signal (cps) for Study 3.

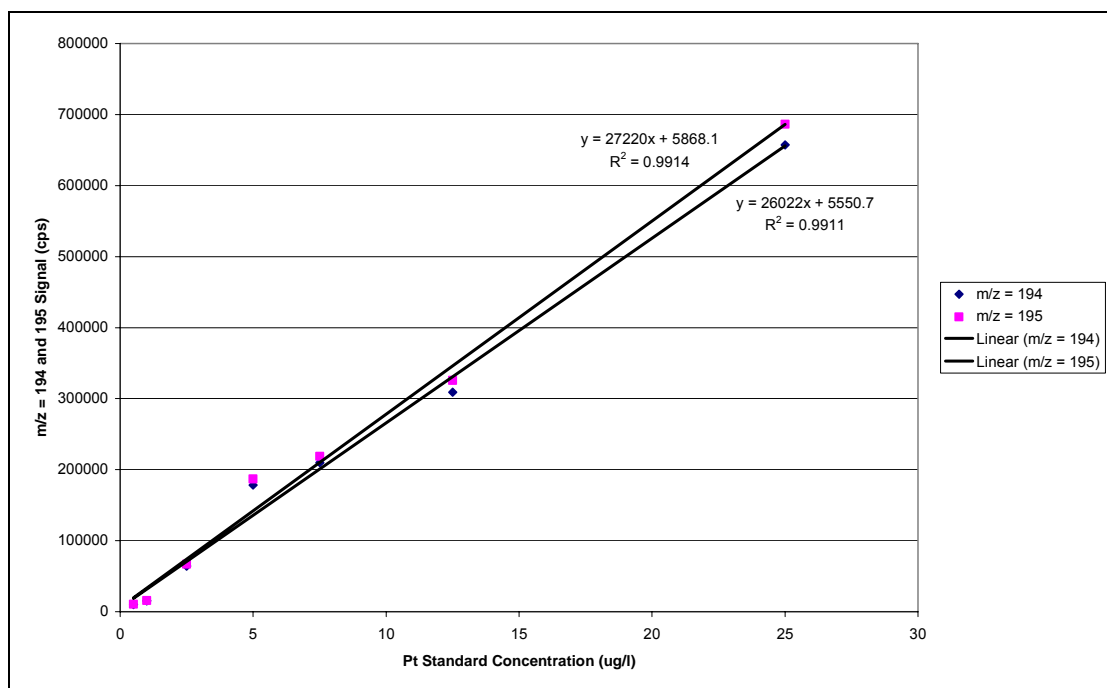


Figure 60. An External Calibration Graph Comparing Pt Standard Concentration ($\mu\text{g l}^{-1}$) with $m/z = 194$ and 195 Signal (cps) for both DNA/Cisplatin and DNA/Oxaliplatin Samples Studied During Study 3.

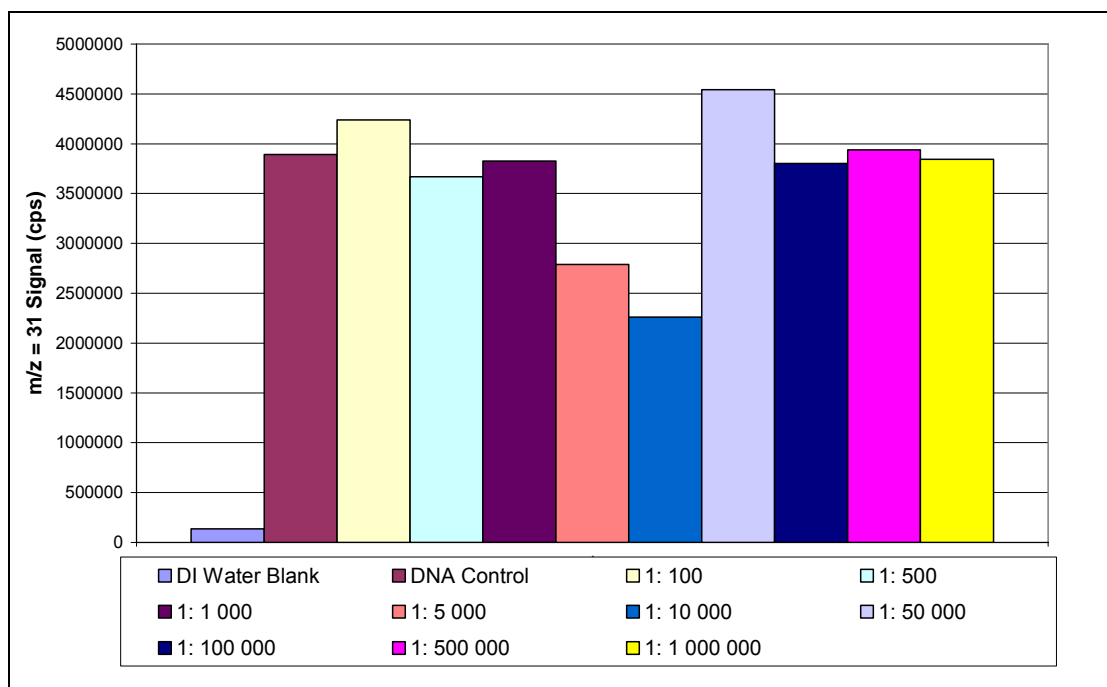


Figure 61. A Bar Chart Comparing $m/z = 31$ Signals (cps) Between DNA/Cisplatin Samples Studied During Study 3.

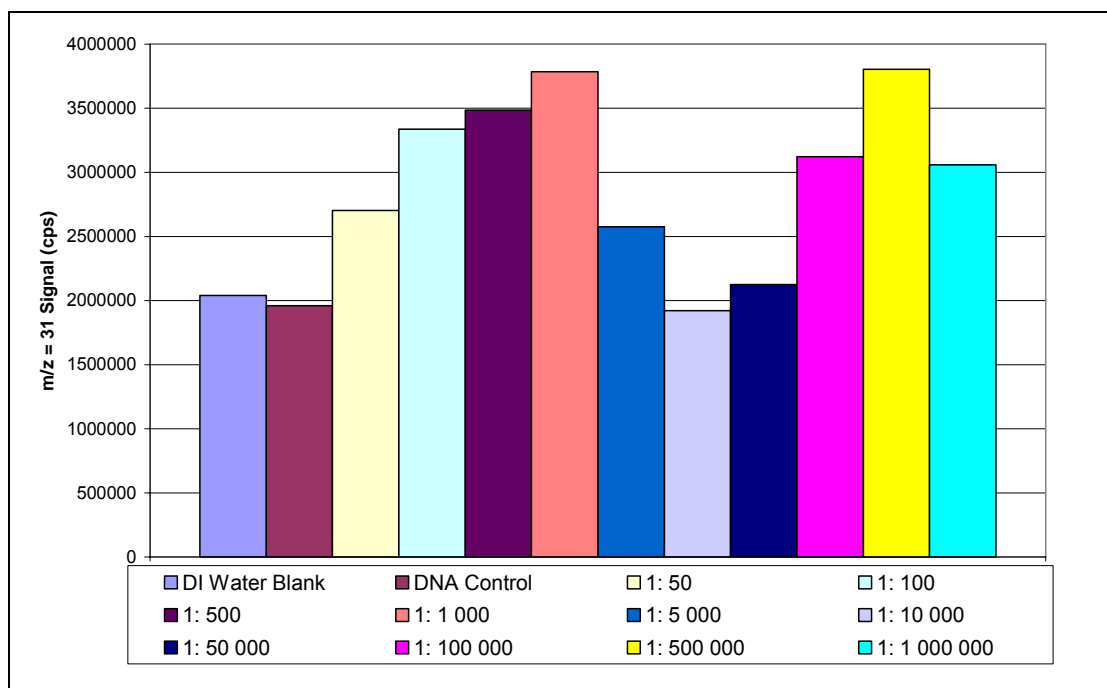


Figure 62. A Bar Chart Comparing $m/z = 31$ Signals (cps) Between DNA/Oxaliplatin Samples Studied During Study 3.

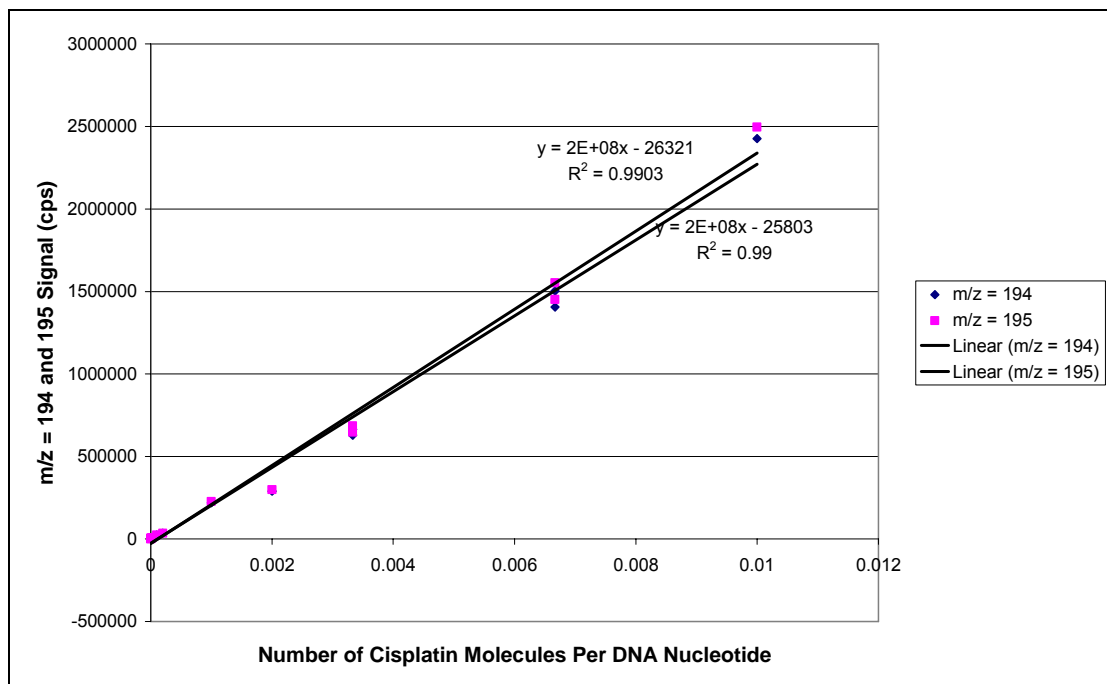


Figure 63. A Graph Comparing Number of Cisplatin Molecules Per DNA Nucleotide with Corrected $m/z = 194$ and 195 Signal (cps) for Study 4.

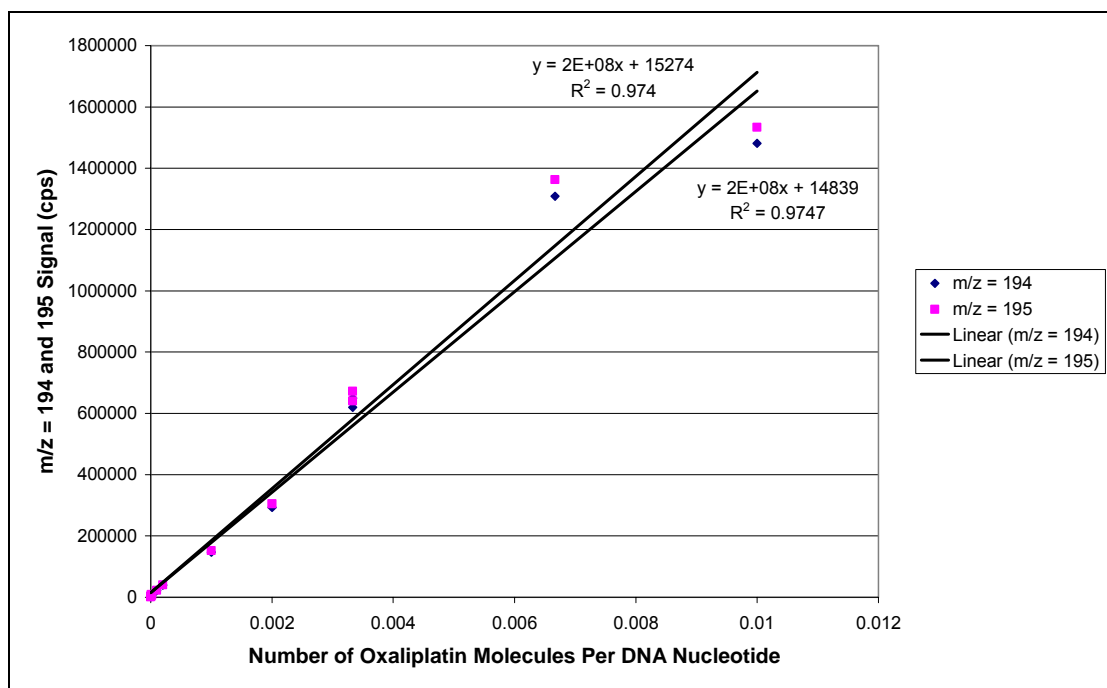


Figure 64. A Graph Comparing Number of Oxaliplatin Molecules Per DNA Nucleotide with Corrected $m/z = 194$ and 195 Signal (cps) for Study 4.

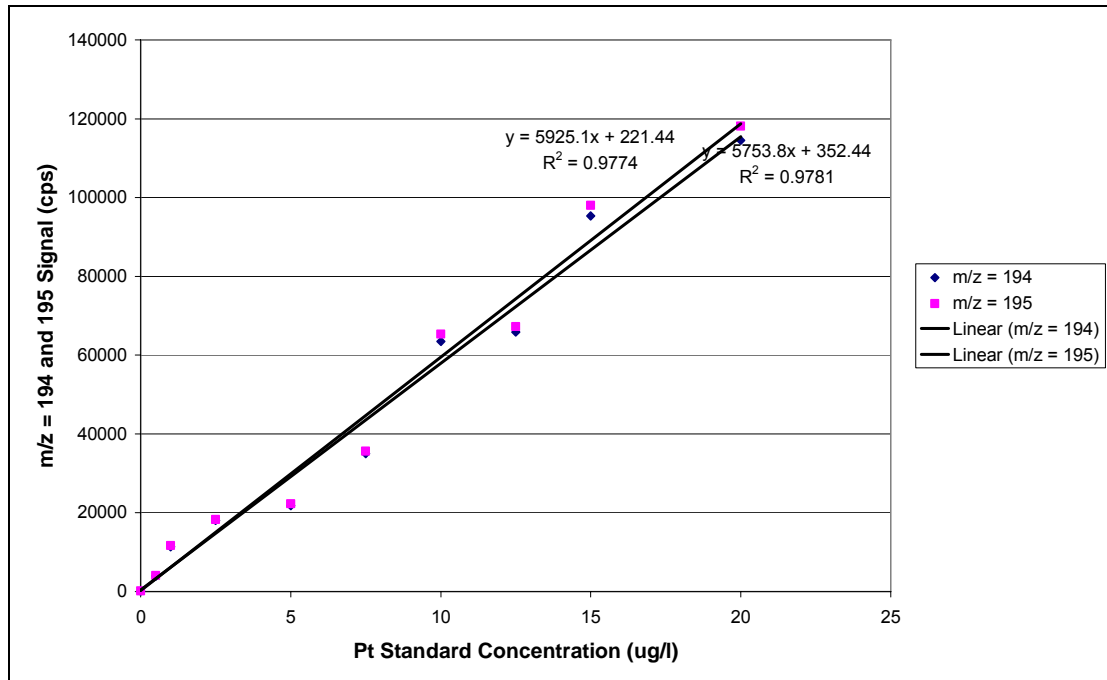


Figure 65. An External Calibration Graph Comparing Pt Standard Concentration ($\mu\text{g l}^{-1}$) with $m/z = 194$ and 195 Signal (cps) for DNA/Cisplatin Samples Studied During Study 4.

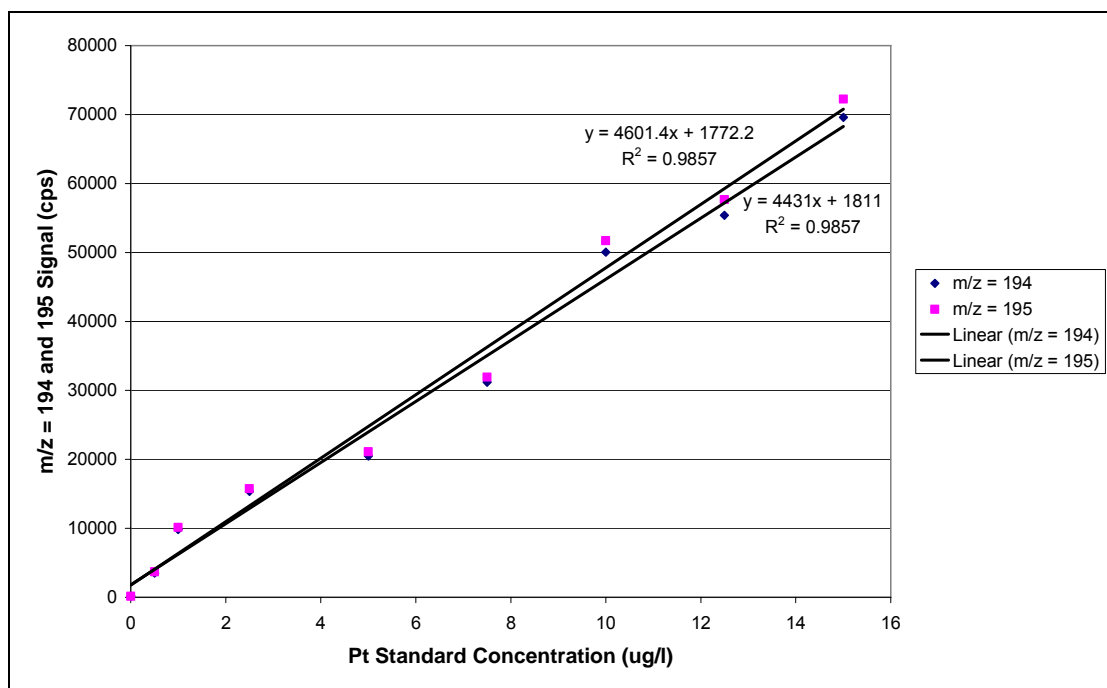


Figure 66. An External Calibration Graph Comparing Pt Standard Concentration ($\mu\text{g l}^{-1}$) with $m/z = 194$ and 195 Signal (cps) for DNA/Oxaliplatin Samples Studied During Study 4.

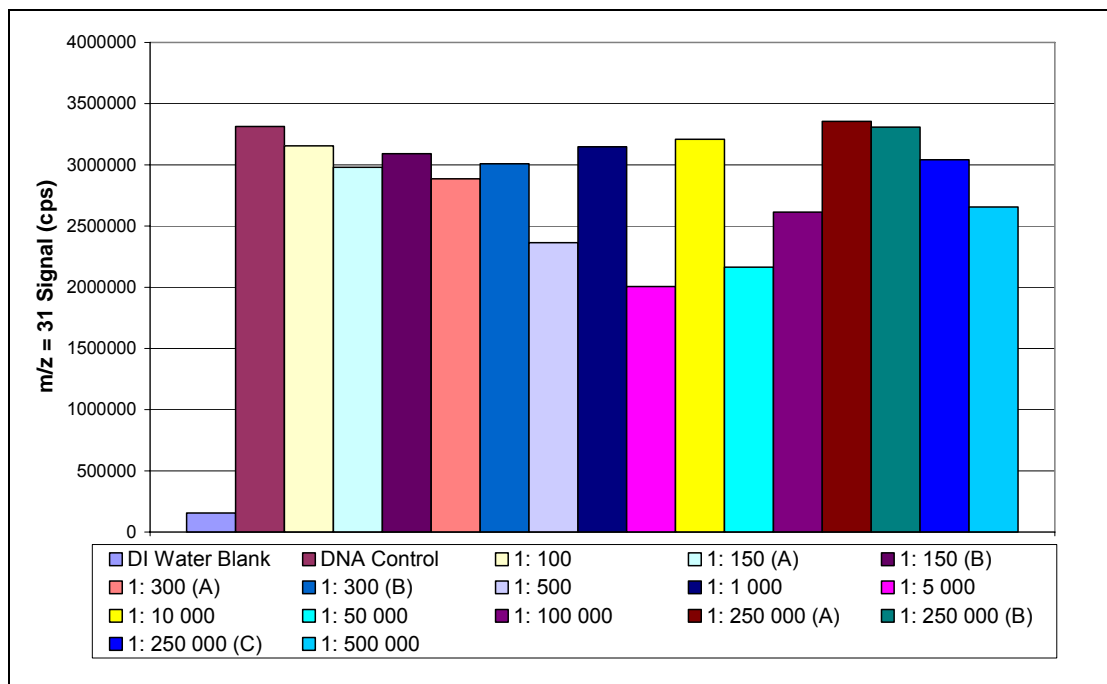


Figure 67. A Bar Chart Comparing $m/z = 31$ Signals (cps) Between DNA/Cisplatin Samples Studied During Study 4.

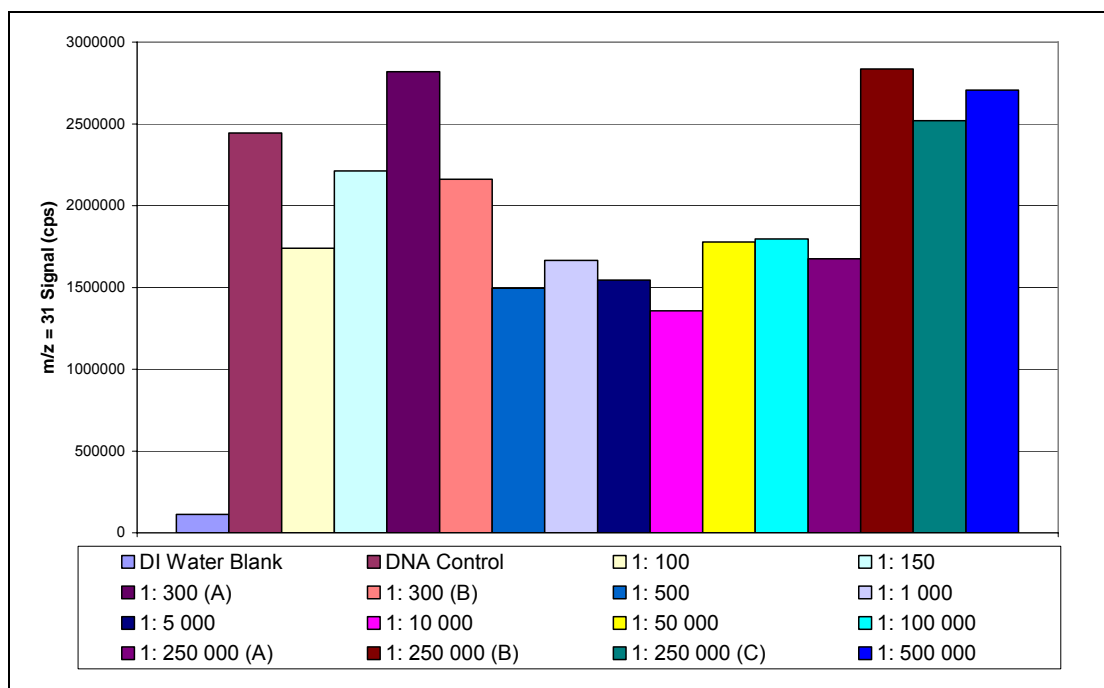


Figure 68. A Bar Chart Comparing $m/z = 31$ Signals (cps) Between DNA/Oxaliplatin Samples Studied During Study 4.

Following study of the data generated, from analysis of the DNA/Cisplatin and DNA/Oxaliplatin sample solutions (studies 3 and 4), and construction of the graphs in Figures 58, 59, 60, 63, 64, 65 and 66 and bar charts in Figures 61, 62, 67 and 68 a number of issues became apparent. These issues are described as follows:

Study 3

The first issue is that in each cisplatin and oxaliplatin exposed DNA sample analysed there were significant quantities of the Pt isotopes present. As can be seen in Figure 59 a linear response was observed between the number of oxaliplatin molecules per DNA nucleotide and the $m/z = 194$ and 195 signal. Although a similar response was seen in the analysis of DNA/cisplatin samples the graph linearity of Figure 58 was determined by the dominating signal of the most concentrated sample. As mentioned during the discussion of study 2 (see section 4.4.2) such trends were as expected but the successful repetition of this work shows the reproducibility of the exposure and separation methods employed during these last two studies. Such method

reproducibility confirms that the analytical failure observed during study 1 was due to the incompatibility of instrument conditions with Pt isotope measurement.

Secondly, the ion counts for the samples in study 3 show that, as in study 2, a limit of measurement for cisplatin exposed DNA lies in the region of 1 cisplatin per 100 000 DNA nucleotides to 1 cisplatin to 500 000 DNA nucleotides. A limit of measurement for the oxaliplatin exposed DNA samples was seen to be slightly different, tending more towards the region of 1 oxaliplatin molecule per 500 000 DNA nucleotides. This is in the desired range for therapeutic activity so this third study has, again, shown that ICP-MS is a promising approach to the analysis of these Pt based anti-cancer complexes. For both cisplatin and oxaliplatin the ion counts generated from the 1 drug to 100 000 DNA nucleotides sample are significantly elevated above that of the blank and control solutions, however, the ion counts for the 1: 500 000 nucleotides were not elevated sufficiently to confidently say state that it could be differentiated from the background. The concentration of each sample analysed was established via the external calibration equations of the graphs in Figure 60. The calculated concentration values can be seen in Tables 32 to 35.

Table 32. ¹⁹⁴Pt Isotope Content of the DNA/Cisplatin Samples Analysed During Study 3.

N° of DNA Nucleotides Per Cisplatin	N° of Cisplatins Per DNA Nucleotide	¹⁹⁴Pt Stds Curve Equation	<i>m/z</i> = 194 Sample Signal (cps)	¹⁹⁴Pt Concⁿ (µg l⁻¹)
Blank	Blank	$y = 26022x + 5550.7$	3071.78	<0.17
Control	Control	$y = 26022x + 5550.7$	10064.1	0.17
50	0.02	$y = 26022x + 5550.7$	0 ↑	>117.52
100	0.01	$y = 26022x + 5550.7$	3063635	117.52
500	0.002	$y = 26022x + 5550.7$	592193	22.54
1 000	0.001	$y = 26022x + 5550.7$	670908	25.57
5 000	0.0002	$y = 26022x + 5550.7$	117662	4.31
10 000	0.0001	$y = 26022x + 5550.7$	119239	4.37
50 000	0.00002	$y = 26022x + 5550.7$	27843.3	0.86
100 000	0.00001	$y = 26022x + 5550.7$	12310.0	0.26
500 000	0.000002	$y = 26022x + 5550.7$	10554.3	0.19
1 000 000	0.000001	$y = 26022x + 5550.7$	35341.7	1.14

Table 33. ¹⁹⁵Pt Isotope Content of the DNA/Cisplatin Samples Analysed During Study 3.

N° of DNA Nucleotides Per Cisplatin	N° of Cisplatins Per DNA Nucleotide	¹⁹⁵Pt Stds Curve Equation	<i>m/z</i> = 195 Sample Signal (cps)	¹⁹⁵Pt Concⁿ (µg l⁻¹)
Blank	Blank	$y = 27220x + 5868.1$	3189.49	<0.17
Control	Control	$y = 27220x + 5868.1$	10408.1	0.17
50	0.02	$y = 27220x + 5868.1$	0 ↑	>116.16
100	0.01	$y = 27220x + 5868.1$	3167829	116.16
500	0.002	$y = 27220x + 5868.1$	618678	22.51
1 000	0.001	$y = 27220x + 5868.1$	699919	25.50
5 000	0.0002	$y = 27220x + 5868.1$	122543	4.29
10 000	0.0001	$y = 27220x + 5868.1$	124226	4.35
50 000	0.00002	$y = 27220x + 5868.1$	28870.0	0.85
100 000	0.00001	$y = 27220x + 5868.1$	12802.3	0.25
500 000	0.000002	$y = 27220x + 5868.1$	11066.9	0.19
1 000 000	0.000001	$y = 27220x + 5868.1$	36880.0	1.14

Table 34. ¹⁹⁴Pt Isotope Content of the DNA/Oxaliplatin Samples Analysed During Study 3.

N° of DNA Nucleotides Per Oxaliplatin	N° of Oxaliplatins Per DNA Nucleotide	¹⁹⁴Pt Stds Curve Equation	<i>m/z</i> = 194 Sample Signal (cps)	¹⁹⁴Pt Concⁿ (µg l⁻¹)
Blank	Blank	$y = 26022x + 5550.7$	4038.34	<0.05
Control	Control	$y = 26022x + 5550.7$	6828.81	0.05
50	0.02	$y = 26022x + 5550.7$	0 ↑	>166.23
100	0.01	$y = 26022x + 5550.7$	4331231	166.23
500	0.002	$y = 26022x + 5550.7$	1051619	40.20
1 000	0.001	$y = 26022x + 5550.7$	601475	22.90
5 000	0.0002	$y = 26022x + 5550.7$	141180	5.21
10 000	0.0001	$y = 26022x + 5550.7$	99130.8	3.60
50 000	0.00002	$y = 26022x + 5550.7$	61830.6	2.16
100 000	0.00001	$y = 26022x + 5550.7$	20252.1	0.56
500 000	0.000002	$y = 26022x + 5550.7$	16939.9	0.44
1 000 000	0.000001	$y = 26022x + 5550.7$	15902.8	0.40

Table 35. ¹⁹⁵Pt Isotope Content of the DNA/Oxaliplatin Samples Analysed During Study 3.

N° of DNA Nucleotides Per Oxaliplatin	N° of Oxaliplatins Per DNA Nucleotide	¹⁹⁵Pt Stds Curve Equation	<i>m/z</i> = 195 Sample Signal (cps)	¹⁹⁵Pt Concⁿ (µg l⁻¹)
Blank	Blank	$y = 27220x + 5868.1$	4202.82	<0.30
Control	Control	$y = 27220x + 5868.1$	14103.4	0.30
50	0.02	$y = 27220x + 5868.1$	0 ↑	>141.87
100	0.01	$y = 27220x + 5868.1$	3867462	141.87
500	0.002	$y = 27220x + 5868.1$	1100346	40.21
1 000	0.001	$y = 27220x + 5868.1$	630667	22.95
5 000	0.0002	$y = 27220x + 5868.1$	148305	5.23
10 000	0.0001	$y = 27220x + 5868.1$	103905	3.60
50 000	0.00002	$y = 27220x + 5868.1$	65132.5	2.18
100 000	0.00001	$y = 27220x + 5868.1$	21021.0	0.56
500 000	0.000002	$y = 27220x + 5868.1$	17646.3	0.43
1 000 000	0.000001	$y = 27220x + 5868.1$	16508.0	0.39

As can be seen in Tables 32 to 35 the background concentration of Pt present over the sample ranges for both cisplatin and oxaliplatin drugs was of the order of 0.20 to 0.30 µg l⁻¹. From these established backgrounds and the spurious data for the lowest level samples (1 drug molecule per 1 000 000 DNA nucleotides) it can be said that, again, the limit of measurement for this analytical approach could be found between 100 000 and 500 000 DNA nucleotides per drug molecule for both cisplatin and oxaliplatin. As mentioned in Section 4.4.2 the limit of detection capability of ICP-MS is less than 1 ng l⁻¹. Again the background concentrations are relatively high for Pt so it could be confidently said that there was a source of contamination present within the system or samples affecting the analysis. Leaching from the peristaltic pump tubing or centrifuge tubes could be a source of such contamination.

There are two points to be made considering this limit for both drugs. Firstly, in the case of cisplatin, this work has shown to be repeatable on comparison with the data of study 2. Secondly, however, the data for study 3 has shown very similar limits for both cisplatin and oxaliplatin. Although this work was carried out *in vitro*, it contradicts with previous research that has shown that there is a significant difference

in the degree of binding between cisplatin and oxaliplatin *in vivo*.¹⁷⁶ So, either the interaction between drug and target *in vitro* is very different to that *in vivo* or there one or more aspects of the analytical method that is establishing contradictory data.

Finally, as can be seen in the bar charts of Figures 61 and 62, and similar to the bar chart constructed for study 2 (see Figure 57) there were large quantities of ³¹P present in a majority of the final sample solutions analysed. Such quantities in most of these samples suggests that ³¹P based fragments of DNA (of <100 000 molecular weight) were passing through the centrifuge filter during the separation procedure, most likely due to an over-harsh NH₃ treatment for separation of drug and target.

In general a linear response was observed between drug exposure concentration and Pt signal response, the R² value of the graphs comparing these two parameters (see Figures 58 and 59) are dictated by the most concentrated sample. The reason for this is that the exposure concentrations described in the sample list increase in an almost exponential way. For this reason a fourth study into these interactions was undertaken with a revised sample list to confirm the linearity between drug exposure and binding (i.e. ICP-MS signal) without relying on such a concentrated sample. The sample list was also expanded at the lower end to provide more accurate data for the method limit of measurement.

Study 4

The reasons behind carrying out a fourth study into these cisplatin/DNA and oxaliplatin/DNA interactions were two-fold. Firstly the analysis of the oxaliplatin drug interactions required repeating to ensure consistency with the data of study 3. Secondly, and more importantly, a revised sample list was needed to study linearity between exposure concentration and binding (i.e. ICP-MS signal).

As with study 3 the first issue for discussion, with regard to the study 4 data, is that in each cisplatin and oxaliplatin exposed DNA sample analysed there were significant quantities of the Pt isotopes present. As can be seen in the graphs of Figures 63 and 64 there was a clear linear response between the number of cisplatin and oxaliplatin

molecules per DNA nucleotide and the $m/z = 194$ and 195 signals. Although such trends have always been expected it has not been until this fourth study that they have been confirmed during this work. The data of this fourth study has, again, shown reproducibility of this analytical method and that the failure seen during study 1 was the result of incompatibility of instrumental conditions.

The second issue is that the ion counts accrued during the analysis of samples during study 4 show that a limit for the measurement of cisplatin exposed DNA lies in the region of 1 drug molecule per 250 000 DNA nucleotides whilst that for the oxaliplatin exposed samples leans more towards 1 drug molecule per 500 000 DNA nucleotides. Again, these limits are in the desired range for therapeutic activity and show the potential of ICP-MS for this type of work. The Pt concentration of each sample analysed was established via the external calibration equations of the graphs in Figures 65 and 66. The calculated Pt concentrations can be seen in Tables 36 to 39.

Table 36. ^{194}Pt Isotope Content of the DNA/Cisplatin Samples Analysed During Study 4.

N° of DNA Nucleotides Per Cisplatin	N° of Cisplatins Per DNA Nucleotide	^{194}Pt Stds Curve Equation	$m/z = 194$ Sample Signal (cps)	^{194}Pt Concⁿ ($\mu\text{g l}^{-1}$)
Blank 2	Blank 2	$y = 5753.8x + 352.44$	594.554	0.04
Control 2	Control 2	$y = 5753.8x + 352.44$	966.139	0.11
100	0.01	$y = 5753.8x + 352.44$	2426296	421.62
150 A	0.00667	$y = 5753.8x + 352.44$	1503598	261.26
150 B	0.00667	$y = 5753.8x + 352.44$	1405440	244.20
300 A	0.00333	$y = 5753.8x + 352.44$	628084	109.10
300 B	0.00333	$y = 5753.8x + 352.44$	664254	115.38
500	0.002	$y = 5753.8x + 352.44$	289479	50.25
1 000	0.001	$y = 5753.8x + 352.44$	220257	38.22
5 000	0.0002	$y = 5753.8x + 352.44$	34650.2	5.96
10 000	0.0001	$y = 5753.8x + 352.44$	23200.5	3.97
50 000	0.00002	$y = 5753.8x + 352.44$	6722.20	1.11
100 000	0.00001	$y = 5753.8x + 352.44$	4796.61	0.77
250 000 A	0.000004	$y = 5753.8x + 352.44$	1352.15	0.17
250 000 B	0.000004	$y = 5753.8x + 352.44$	1433.90	0.19
250 000 C	0.000004	$y = 5753.8x + 352.44$	1318.33	0.17
500 000	0.000002	$y = 5753.8x + 352.44$	3080.78	0.47

Table 37. ¹⁹⁵Pt Isotope Content of the DNA/Cisplatin Samples Analysed During Study 4.

N° of DNA Nucleotides Per Cisplatin	N° of Cisplatins Per DNA Nucleotide	¹⁹⁵Pt Stds Curve Equation	<i>m/z</i> = 195 Sample Signal (cps)	¹⁹⁵Pt Concⁿ (µg l⁻¹)
Blank 2	Blank 2	$y = 5925.1x + 221.44$	612.659	0.07
Control 2	Control 2	$y = 5925.1x + 221.44$	1001.29	0.13
100	0.01	$y = 5925.1x + 221.44$	2495780	421.18
150 A	0.00667	$y = 5925.1x + 221.44$	1551885	261.88
150 B	0.00667	$y = 5925.1x + 221.44$	1450669	244.80
300 A	0.00333	$y = 5925.1x + 221.44$	647716	109.28
300 B	0.00333	$y = 5925.1x + 221.44$	685725	115.69
500	0.002	$y = 5925.1x + 221.44$	298307	50.31
1 000	0.001	$y = 5925.1x + 221.44$	226771	38.24
5 000	0.0002	$y = 5925.1x + 221.44$	35828.5	6.01
10 000	0.0001	$y = 5925.1x + 221.44$	24159.3	4.04
50 000	0.00002	$y = 5925.1x + 221.44$	6931.36	1.13
100 000	0.00001	$y = 5925.1x + 221.44$	4896.41	0.79
250 000 A	0.000004	$y = 5925.1x + 221.44$	1382.56	0.20
250 000 B	0.000004	$y = 5925.1x + 221.44$	1459.02	0.21
250 000 C	0.000004	$y = 5925.1x + 221.44$	1382.55	0.20
500 000	0.000002	$y = 5925.1x + 221.44$	3126.73	0.49

Table 38. ^{194}Pt Isotope Content of the DNA/Oxaliplatin Samples Analysed During Study 4.

N° of DNA Nucleotides Per Oxaliplatin	N° of Oxaliplatins Per DNA Nucleotide	^{194}Pt Stds Curve Equation	$m/z = 194$ Sample Signal (cps)	^{194}Pt Concⁿ ($\mu\text{g l}^{-1}$)
Blank 2	Blank 2	$y = 4431x + 1811$	2413.36	0.14
Control 2	Control 2	$y = 4431x + 1811$	1333.38	<0.14
100	0.01	$y = 4431x + 1811$	1480804	333.78
150 A	0.00667	$y = 4431x + 1811$	1308963	295.00
150 B	0.00667	$y = 4431x + 1811$	2360702	547.18
300 A	0.00333	$y = 4431x + 1811$	649510	146.17
300 B	0.00333	$y = 4431x + 1811$	619977	139.51
500	0.002	$y = 4431x + 1811$	293269	65.78
1 000	0.001	$y = 4431x + 1811$	147249	32.82
5 000	0.0002	$y = 4431x + 1811$	39277.4	8.46
10 000	0.0001	$y = 4431x + 1811$	21993.0	4.55
50 000	0.00002	$y = 4431x + 1811$	7105.54	1.19
100 000	0.00001	$y = 4431x + 1811$	8433.38	1.49
250 000 A	0.000004	$y = 4431x + 1811$	2855.42	0.24
250 000 B	0.000004	$y = 4431x + 1811$	3325.83	0.34
250 000 C	0.000004	$y = 4431x + 1811$	4256.99	0.55
500 000	0.000002	$y = 4431x + 1811$	1966.78	0.04

Table 39. ¹⁹⁵Pt Isotope Content of the DNA/Oxaliplatin Samples Analysed During Study 4.

N° of DNA Nucleotides Per Oxaliplatin	N° of Oxaliplatins Per DNA Nucleotide	¹⁹⁵Pt Stds Curve Equation	<i>m/z</i> = 195 Sample Signal (cps)	¹⁹⁵Pt Concⁿ (µg l⁻¹)
Blank 2	Blank 2	y = 4601.4 + 1772.2	2433.32	0.14
Control 2	Control 2	y = 4601.4 + 1772.2	1335.33	<0.14
100	0.01	y = 4601.4 + 1772.2	1533310	332.84
150 A	0.00667	y = 4601.4 + 1772.2	1363158	295.86
150 B	0.00667	y = 4601.4 + 1772.2	2453064	532.73
300 A	0.00333	y = 4601.4 + 1772.2	671724	145.60
300 B	0.00333	y = 4601.4 + 1772.2	640683	138.85
500	0.002	y = 4601.4 + 1772.2	304659	65.82
1 000	0.001	y = 4601.4 + 1772.2	152257	32.70
5 000	0.0002	y = 4601.4 + 1772.2	40829.2	8.49
10 000	0.0001	y = 4601.4 + 1772.2	22713.1	4.55
50 000	0.00002	y = 4601.4 + 1772.2	7275.23	1.20
100 000	0.00001	y = 4601.4 + 1772.2	8690.51	1.50
250 000 A	0.000004	y = 4601.4 + 1772.2	2967.49	0.26
250 000 B	0.000004	y = 4601.4 + 1772.2	3422.16	0.36
250 000 C	0.000004	y = 4601.4 + 1772.2	4356.50	0.56
500 000	0.000002	y = 4601.4 + 1772.2	1969.50	0.04

Similar to the data of study 3, Tables 36 to 39 show the background concentration of Pt for both cisplatin and oxaliplatin exposures were of the order of 0.10 to 0.20 µg l⁻¹ which translates to an equivalent of 1 drug molecule per 250 000 DNA nucleotides. Slightly elevated background counts at *m/z* = 194 and 195 suggest the presence of a small degree of Pt contamination.

Again the analysis of study 4 has shown repeatability with previous work, this includes the contradiction described previously in this section regarding the similar degree of binding between cisplatin and oxaliplatin drugs and their target. The bar charts of Figures 67 and 68 again show that the fragmentation of the DNA target (and passage through the centrifuge filters) was significant during the species separation process. This is most likely due to the NH₃ treatment being overly aggressive. The data for this fourth study has shown that the relationship between drug exposure

concentration and ICP-MS signal is in fact a linear one, with R^2 values in the order of 0.99 for cisplatin and 0.97 for oxaliplatin. With the limit of measurement, via this method, being in the region of 1 drug molecule per 250 000 DNA nucleotides, ICP-MS appears to have a lot of potential for this kind of biological analysis.

Following the success of the third and fourth studies, and similar to the second study, work was commenced on establishing binding constant data that could be used as the basis of a clinical test for the determination of drug efficacy of cisplatin and oxaliplatin in individual patients, see section 4.5.

At this stage during the work on these drugs, to cover as many unknowns as possible, it was decided to carry out further analysis on the centrifuge filters used during one of the studies (in this case it was study 4) to establish whether any Pt based species were being retained. It was also decided to carry out one final study, on another sample series for each drug, without separating drug and target to establish the degree of any loss of Pt species during the preparation and treatment procedures and to determine the degree of any matrix effects from the quantity of DNA present.

4.4.4. The Analysis of Study 4 Centrifuge Filters

To establish the efficiency of the drug and target separation method employed during this work, the centrifuge filters used in the final stages were leached to remove any material retained on the filter. The study of such leachate solutions would establish whether any Pt based species were being kept behind and determine whether this separation of species is the best approach to ICP-MS study of these samples.

Experimental Details

Following the analysis of study 4 samples the 100 000 molecular weight centrifuge tubes, that were used during the separation process, were broken to remove the filter

at the base of the inner tube. These filters were then leached, in deionised water, to remove any material on them to provide solutions that could be analysed by ICP-MS.

The filter and surrounding material, removed from the bottom section of the inner tube of each centrifuge tube was accurately weighed and suspended in approximately 2 ml of deionised water (again accurately weighed) in sealed tubes that were then incubated in a water bath at 75 °C for 24 hours. Following incubation the leachate solution was then analysed by ICP-MS. The details of sample preparation can be seen in Tables 125 and 126. From the measurements taken for these leachate solutions correction factors can be calculated and applied when establishing concentration data from the ICP-MS analysis and external calibration (see the results and discussion section).

The instrument used in analysis of the samples was as described previously. Leachate solutions and Pt standards were analysed under standard mode for the presence of $^{190,192,194,195,196,198}\text{Pt}$ and ^{31}P isotopes. The optimised operating conditions employed during this work are in Table 127. Results of the sample analysis can be seen in the next section.

Results and Discussion

The data generated following the ICP-MS study of these centrifuge filter leachate solutions and Pt external standards can be seen in Tables 128, 129 and 130 (Appendix 4). From this data six bar charts were constructed, four describing the Pt data (see Figures 69 to 72) and a further two for the ^{31}P data (see Figures 73 and 74). An external calibration graph for the $^{194,195}\text{Pt}$ isotopes can be seen in Figure 75. The reason that bar charts have been drawn up to qualitatively compare the Pt present in each leachate solution rather than calculating concentration by the external calibration is that the signals measured were far out of the calibration range that was expected.

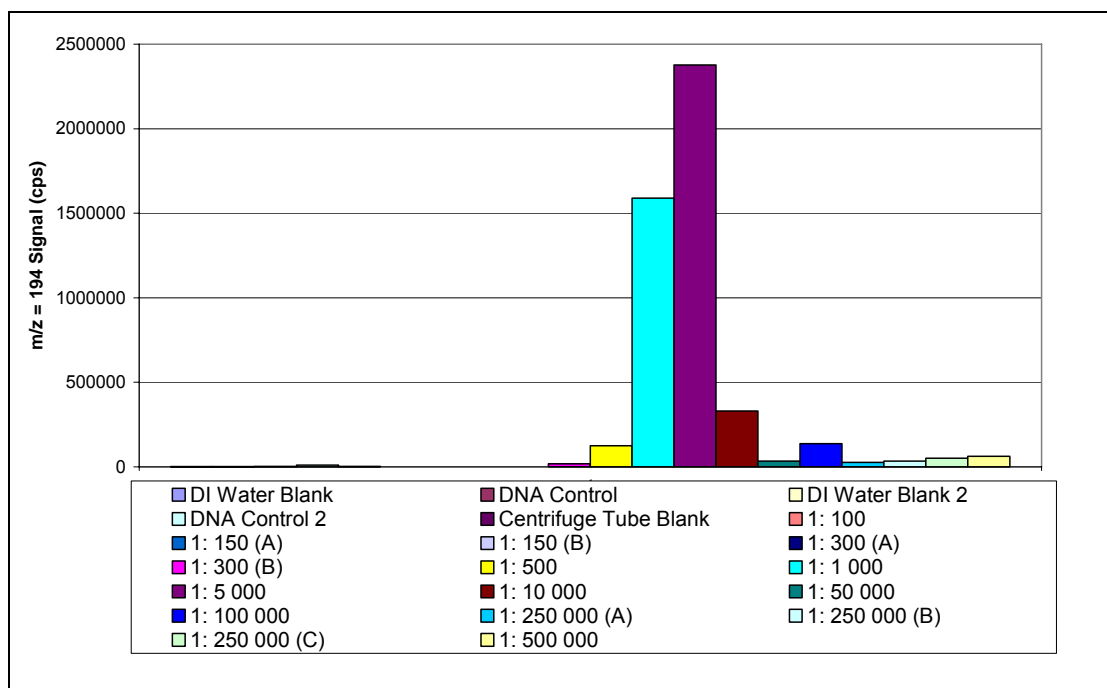


Figure 69. A Bar Chart Comparing $m/z = 194$ Signals (cps) Between Centrifuge Filter Leachate Solutions of the DNA/Cisplatin Samples Studied for Study 4.

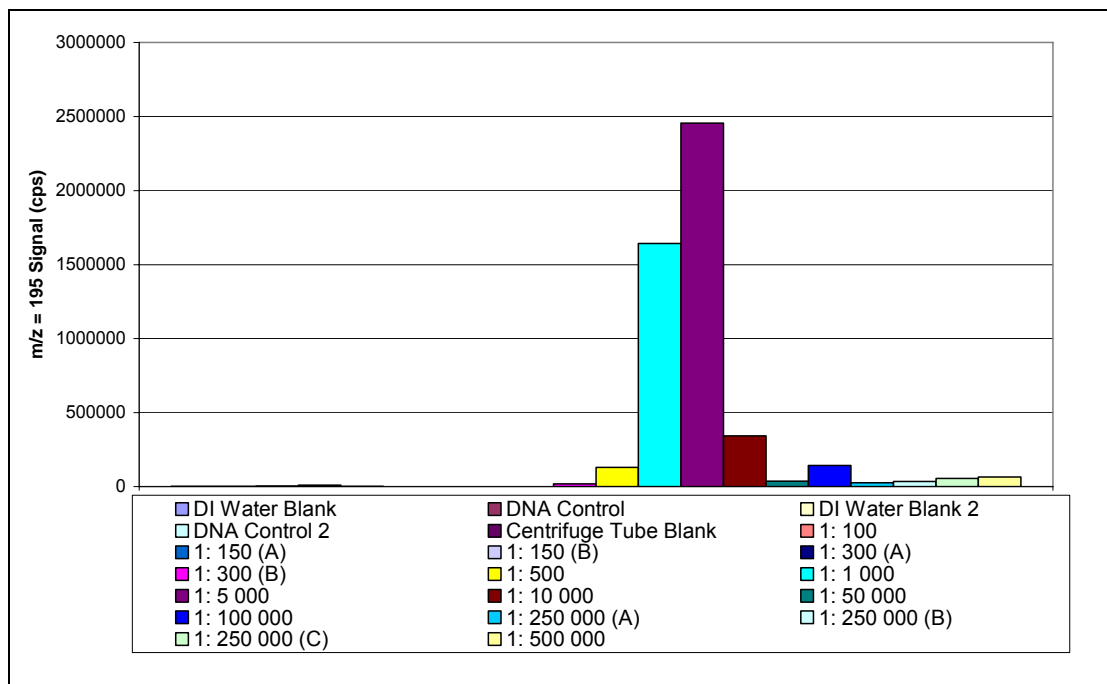


Figure 70. A Bar Chart Comparing $m/z = 195$ Signals (cps) Between Centrifuge Filter Leachate Solutions of the DNA/Cisplatin Samples Studied for Study 4.

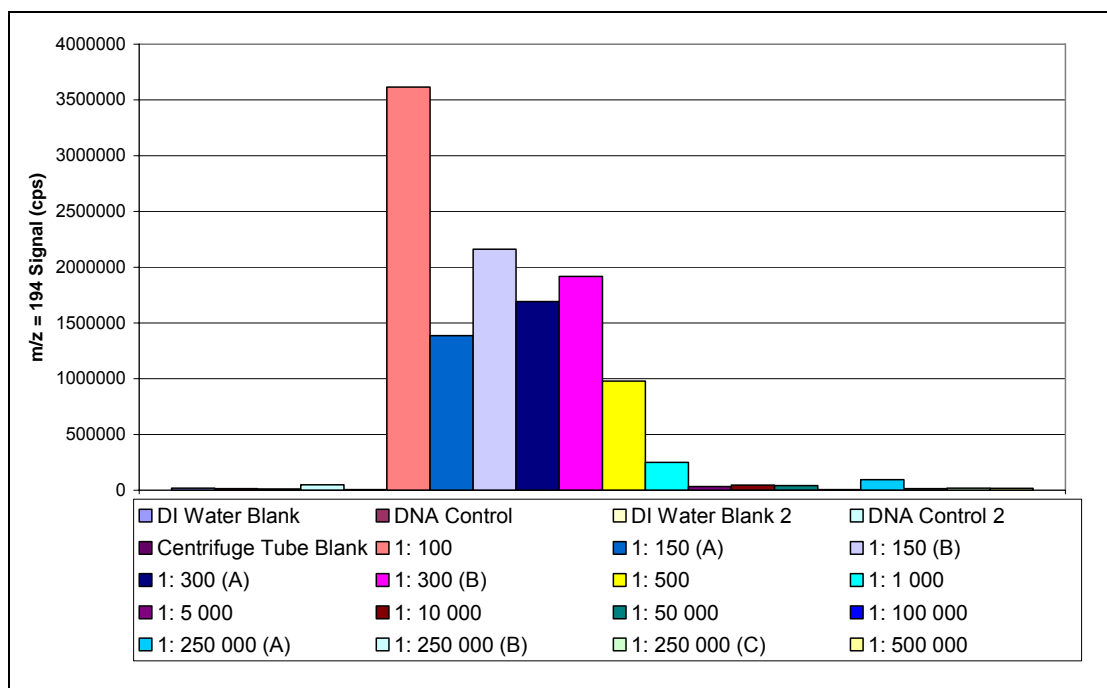


Figure 71. A Bar Chart Comparing $m/z = 194$ Signals (cps) Between Centrifuge Filter Leachate Solutions of the DNA/Oxaliplatin Samples Studied for Study 4.

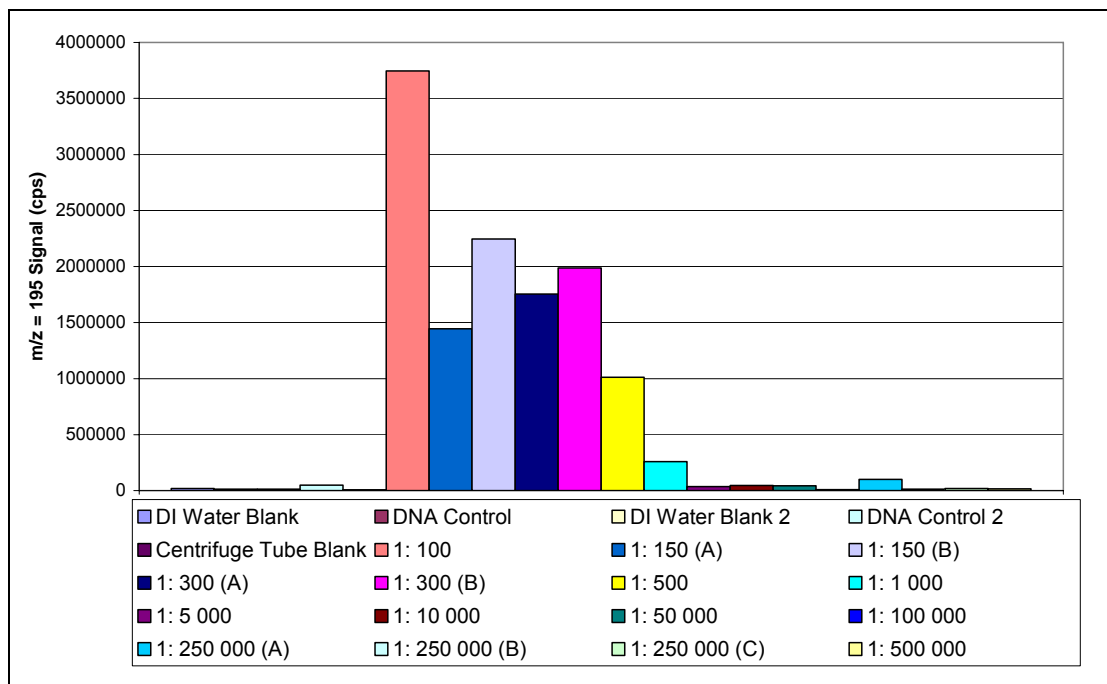


Figure 72. A Bar Chart Comparing $m/z = 195$ Signals (cps) Between Centrifuge Filter Leachate Solutions of the DNA/Oxaliplatin Samples Studied for Study 4.

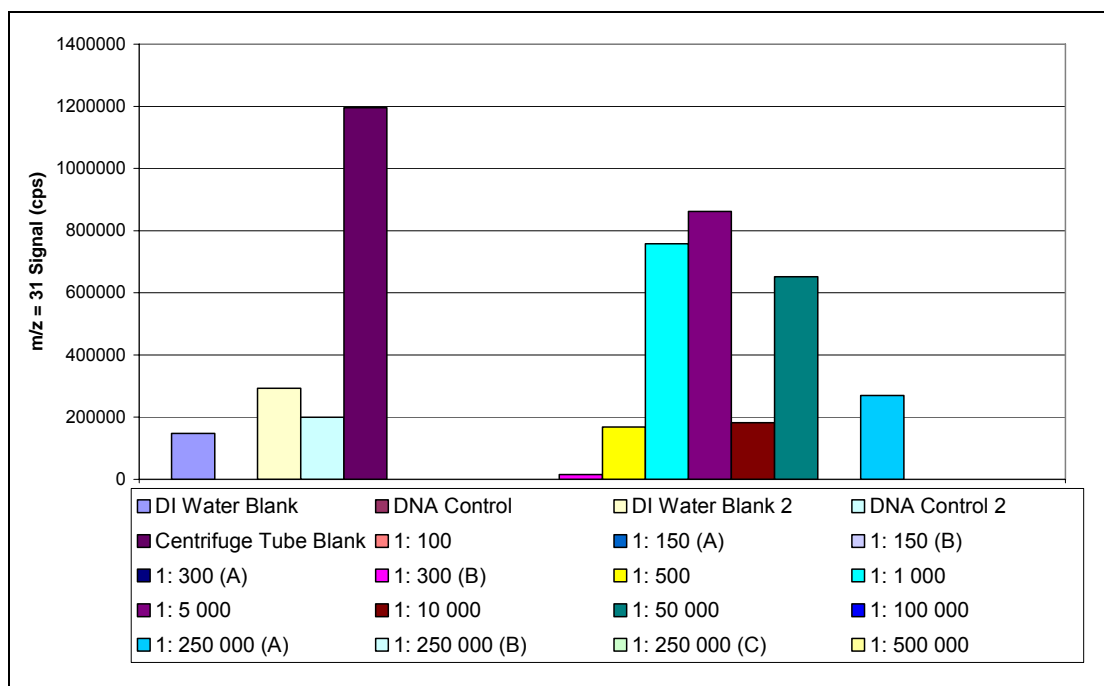


Figure 73. A Bar Chart Comparing $m/z = 31$ Signals (cps) Between Centrifuge Filter Leachate Solutions of the DNA/Cisplatin Samples Studied for Study 4.

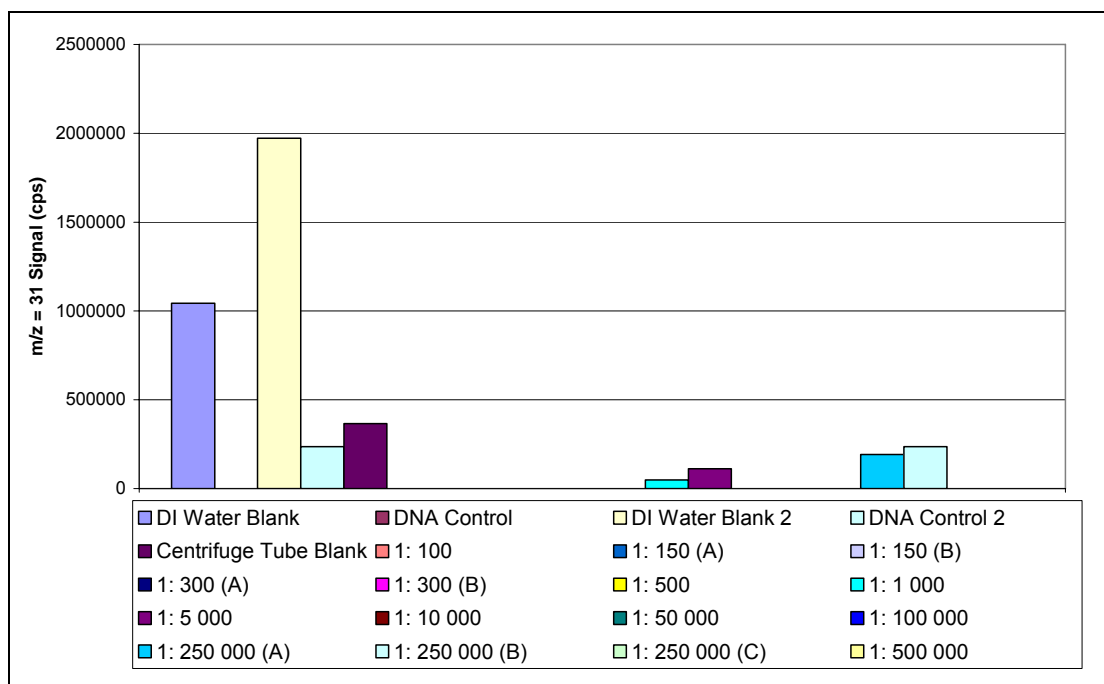


Figure 74. A Bar Chart Comparing $m/z = 31$ Signals (cps) Between Centrifuge Filter Leachate Solutions of the DNA/Oxaliplatin Samples Studied for Study 4.

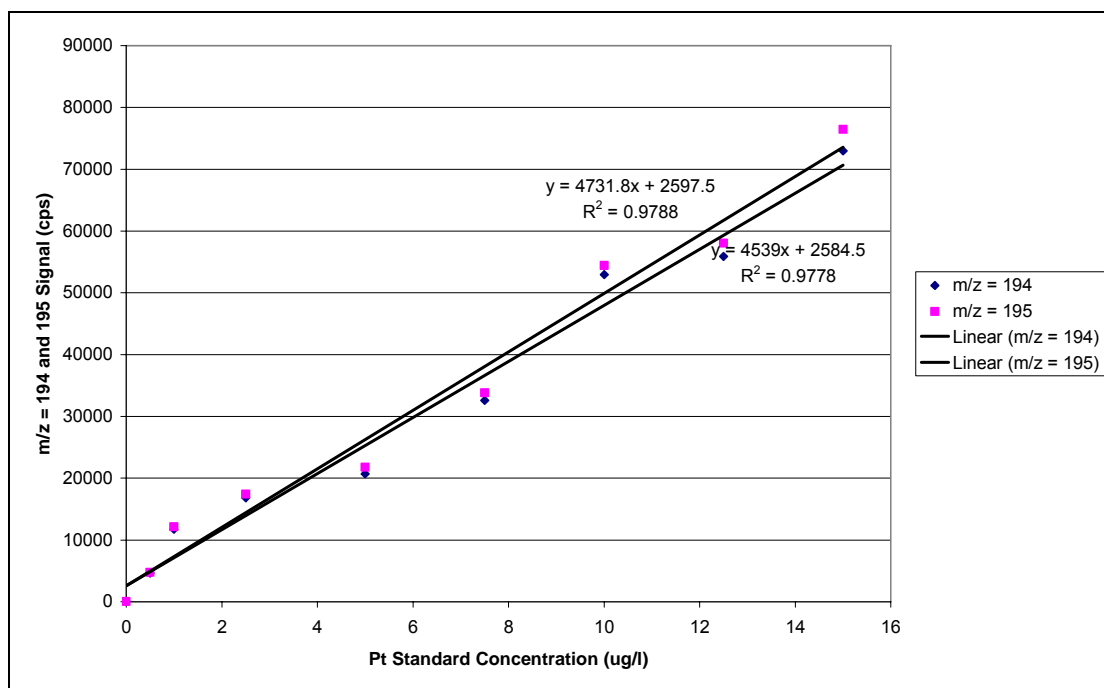


Figure 75. An External Calibration Graph Comparing Pt Standard Concentration ($\mu\text{g l}^{-1}$) with $m/z = 194$ and 195 Signal (cps) for the Centrifuge Filter Leachate Solutions of the DNA/Cisplatin and DNA/Oxaliplatin Samples Studied for Study 4.

The data accrued during the study of these centrifuge filter leachate solutions has proved to be very interesting and has provided some contradicting information compared to that of the previous studies (studies 2 to 4). Two major issues have been raised as a result of study of the data produced. It should be noted that in the data tables and bar charts, a signal of 0 ion counts per second represents a signal of such great intensity that it exceeded the capability of the electron multiplier detector. Although an external calibration was carried out during the analysis of the leachate solutions, the calibration range was not compatible with the Pt signals obtained from the samples (most such signals exceeded that of the top standard of $15 \mu\text{g l}^{-1}$ so can be described as being in excess of this particular concentration). For this reason the work cannot be discussed in terms of quantification. Instead, analytical signals are compared in a qualitative fashion.

On comparison of the Pt signals between sample solutions it can be seen that there is very little Pt present in either the deionised water blank, DNA control or centrifuge tube blank solutions (for both the cisplatin and oxaliplatin sample series) compared to

the drug exposed sample tube leachates. So, from this information, the first issue for discussion is that each centrifuge filter leachate solution contains large quantities of Pt. In most cases those quantities of Pt seem to exceed those measured in previous solutions, obtained following separation of the drug and DNA target species, and are assumed to be in the $\mu\text{g l}^{-1}$ (ppb) to mg l^{-1} (ppm) range. One conclusion that could be drawn from this data is that in previous sample solutions (obtained following the separation), during the sample treatment there was one or more problematic procedural stages that resulted in such quantities of Pt being left behind. Such stages could either have been associated with the separation of species (i.e. the NH_3 treatment did not efficiently remove drug species or caused fragmentation of the DNA strands such that fragments containing the Pt were in excess of 10 000 molecular weight so were not allowed through the filter) or the filtering process (i.e. the filters were not particularly efficient). Another conclusion, however, far less likely is that there could be a contamination issue associated with these centrifuge filter tubes that results in erroneous data. On comparison of the data accrued from the cisplatin and oxaliplatin filter leachate solutions there appears to be a significant difference. For the oxaliplatin leachates several of the more concentrated sample signals are very high (in the region of 3 million to 4 million cps) but none exceed the capability of the detector unlike many of the cisplatin leachates. This comparison could highlight a difference between these two drugs with regard to the interaction between drug and target species.

The second issue to consider is that of the ^{31}P measurements. The study of the ^{31}P bar charts for both cisplatin and oxaliplatin samples series studied has shown that very large quantities of DNA molecules and fragments are retained on the filter during the separation process. Comparing the ^{31}P signals obtained from these leachates with those from the separated samples analysed during studies 2 to 4 shows that far more ^{31}P containing components are retained on the centrifuge filters than are allowed through. This suggests that the NH_3 treatment caused some fragmentation of the DNA target molecule during the separation processes but that breakdown was not complete.

At this stage it could be argued that the centrifuge filter leachate data suggests that the previous studies, involving the separation of drug and target, were not carried out as

efficiently as they could have been and that the unwanted retention of Pt species has a significant effect on the limit of measurement and possibly the calculated binding constant (see Section 4.5). However, it appears that there may be a complication to this idea and this is the third issue for consideration. There is contradictory information from the previous studies (particularly study 4) in the form of the linear relationship between drug exposure concentration and ICP-MS signal ($m/z = 194$ and 195) seen following analysis of the separated solutions. This linear relationship on its own would suggest an efficient separation and analysis of a majority of the Pt species, however, from the leachate data, it is known that this is not the case. This conflicting information leads to the idea that the Pt species measured in the separated solutions and the leachate solutions could differ in terms of the type of binding interaction with the DNA target. As described in Section 4.2.3 there are two major types of binding interaction between the cisplatin and oxaliplatin drugs and DNA (inter- and intra-strand covalent binding) as well as far less significant non-covalent groove binding interactions.^{156, 162, 173, 175, 180} Armed with this information, conclusions can be drawn from the qualitative comparison of data between the studies carried out and the investigation of centrifuge tube filters. From the data that has been accrued during the first studies (studies 2 to 4) as well as the investigation into the centrifuge tube filters of study 4 it can be said that there are two significant sources of Pt being measured; the Pt being removed from the DNA via NH_3 treatment and the Pt being left behind on the filters. A qualitative comparison of the order of signal derived from these two Pt sources suggests that the larger quantity of Pt, that being left behind on the filters, was in the form of covalently bound interstrand DNA adducts (that could not be removed under the NH_3 treatment due to the steric conditions) whilst the smaller Pt quantity, measured following the separation process, was in the form of covalently bound intrastrand DNA adducts.

This qualitative comparison suggests differences in binding strength, between the two types, on exposure to the NH_3 treatment. To confirm these conclusions other analytical techniques would be required to establish the number of types of adduct species present and their structure. HPLC-MS and NMR would provide invaluable, additional, information in this case.

The data generated during the investigation of the centrifuge tube filters, employed during study 4, has provided information that allows better understanding of the data provided by the studies that preceded it. Although structural information would be required to confirm this the experiments carried out for this investigation have suggested that the cisplatin and oxaliplatin drugs are forming adducts with the DNA target via both covalent inter- and intra-strand forms of binding. It would appear that following an NH_3 treatment the majority of covalently bound interstrand Pt based adducts were not removed and were retained on the filter whilst the majority of covalently bound intrastrand DNA adducts were removed and allowed through during the centrifugation process.

As a final experiment it was decided that an analysis of drug exposed DNA samples, without incorporating the separation process, was required in order to measure the total quantity of Pt based drug associated with the DNA target (and hence produce more realistic K_f and adduct ratio data). Although this was originally believed to be problematic, with regard to the introduction of such large quantities of DNA into the plasma, it was decided to attempt to analyse exposed samples with little, or no, pre-treatment.

4.4.5. Study 5

Although it was originally believed to be problematic, it was decided to analyse a series of DNA samples exposed to each drug without any further treatment by ICP-MS. If such a study was successful it was hoped that the data would provide an improved limit of measurement as well as comparable, if not better, binding constant data (compared to those established during studies 2 to 4).

Experimental Details

For this final study DNA samples were prepared and exposed to both drugs (cisplatin and oxaliplatin) by the same method as that described for the previous studies (see

Tables 28 and 29 in section 4.4.3). Following preparation, aliquots of each sample were diluted approximately forty fold and analysed by UV spectroscopy to establish the final DNA concentration, see Tables 131 and 132. Samples were studied for Pt and P isotope content under optimum conditions (see Table 133, Appendix 4). Due to limitations of the prepared Pt standard range several of the more concentrated sample solutions, between both cisplatin and oxaliplatin drugs, were diluted prior to analysis to allow quantification. Results of the sample analysis described can be seen in the next section.

Results and Discussion

The data generated following the ICP-QMS study of these drug exposed whole DNA solutions and DNA based Pt external standards can be seen in Tables 134, 135 and 136. From the data accrued from the standard solutions a calibration curve was generated to allow the calculation of Pt concentration of each sample solution to be established (see Figure 76). As some sample dilutions were undertaken during analysis, graphs to show linearity between drug exposure and ICP-QMS signal can be seen in Figures 77 and 78 following the establishment of sample concentration.

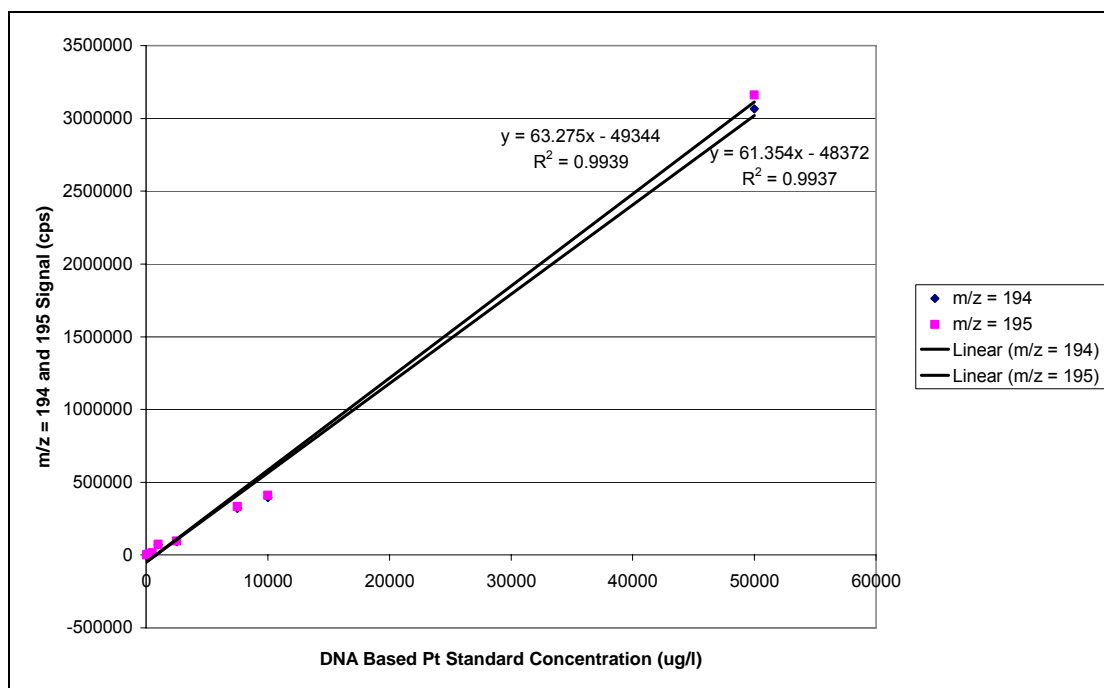


Figure 76. An External Calibration Graph Comparing DNA Based Pt Standard Concentration (ng l^{-1}) with $m/z = 194$ and 195 Signal (cps) for the Untreated DNA/Cisplatin and DNA/Oxaliplatin Samples Solutions Studied During Study 5.

Following interpretation of the data accrued during this study several issues came to light, some of which have implications with regard to the conclusions drawn from previous studies. The first obvious issue for discussion is that of the overall successful ICP-MS analysis of both untreated DNA/drug sample series. Originally it was believed that a DNA solution of a concentration of 1 mg ml^{-1} would yield significant matrix effects to an analysis (if indeed it could be analysed without extinguishing the ICP). It is clear from the mean raw data of this study (see Tables 135 and 136) that the significant quantities of Pt present in each sample solution could be measured reliably based on matrix matched standard solutions indicating that the separation of drug and target species need not be necessary when considering such samples.

Secondly, the ion intensity for Pt shows a limit of measurement of both drugs to be below the region of 1 drug molecule per 500 000 DNA nucleotides, i.e. the $m/z = 194$ and 195 signals for that lowest exposure concentration was significantly elevated above that of the blank and control solutions. Such LOD's are far superior to those

calculated in previous studies and show that ICP-MS is capable of measurement of these Pt based drugs below the desired therapeutic range. During studies 2 to 4 there seemed to be very little difference in ICP-MS signal and LOD between the two drugs, however, in this fifth study this does not appear to be the case. The $m/z = 194$ and 195 signal measured for each cisplatin exposed sample appears to be of a greater intensity than that of the equivalent oxaliplatin exposed sample. The concentration of each sample analysed was established via the external calibration equations of Figure 76. The calculated concentration values can be seen in Tables 40 to 43 (which include dilution factors and corrections made during this analysis).

To highlight the linearity between drug exposure concentration and ICP-MS signal (in this case the measured and calculated Pt concentration), two graphs were constructed to compare these two parameters, see Figures 77 and 78.

Table 40. ^{194}Pt Isotope Content of the Untreated DNA/Cisplatin Sample Solutions Analysed During Study 5.

N° of DNA Nucleotides Per Cisplatin	N° of Cisplatins Per DNA Nucleotide	^{194}Pt Stds Curve Equation	$m/z = 194$ Sample Signal (cps)	$^{194}\text{Pt Conc}^n$ (ng l⁻¹)
DI Water Blank	DI Water Blank	$y = 61.354x - 48372$	141.001	790.7
Control	Control	$y = 61.354x - 48372$	295.67	793.2
100 (Dil ⁿ x 25)	0.01	$y = 61.354x - 48372$	2685407	44557 (1113925)
500 (Dil ⁿ x 20)	0.002	$y = 61.354x - 48372$	543279	9643 (192860)
1 000 (Dil ⁿ x 5)	0.001	$y = 61.354x - 48372$	1058457	18040 (90200)
5 000	0.0002	$y = 61.354x - 48372$	864789	14883
10 000	0.0001	$y = 61.354x - 48372$	488285	8747
50 000	0.00002	$y = 61.354x - 48372$	91931.4	2287
100 000	0.00001	$y = 61.354x - 48372$	44915.8	1520
250 000	0.000004	$y = 61.354x - 48372$	17035.8	1066
500 000	0.000002	$y = 61.354x - 48372$	10975.2	967.3

Table 41. ^{194}Pt Isotope Content of the Untreated DNA/Oxaliplatin Sample Solutions Analysed During Study 5.

N° of DNA Nucleotides Per Oxaliplatin	N° of Oxaliplatins Per DNA Nucleotide	^{194}Pt Stds Curve Equation	$m/z = 194$ Sample Signal (cps)	^{194}Pt Concⁿ (ng l⁻¹)
DI Water Blank	DI Water Blank	$y = 61.354x - 48372$	141.001	790.7
Control	Control	$y = 61.354x - 48372$	270.003	792.8
100 (DiI ⁿ x 25)	0.01	$y = 61.354x - 48372$	244942	4781 (119525)
500	0.002	$y = 61.354x - 48372$	1655373	27769
1 000	0.001	$y = 61.354x - 48372$	427880	7762
5 000	0.0002	$y = 61.354x - 48372$	122725	2789
10 000	0.0001	$y = 61.354x - 48372$	68308.6	1902
50 000	0.00002	$y = 61.354x - 48372$	16262.9	1053
100 000	0.00001	$y = 61.354x - 48372$	7834.82	916.1
250 000	0.000004	$y = 61.354x - 48372$	4335.33	859.1
500 000	0.000002	$y = 61.354x - 48372$	2083.15	822.4

Table 42. ^{195}Pt Isotope Content of the Untreated DNA/Cisplatin Sample Solutions Analysed During Study 5.

N° of DNA Nucleotides Per Cisplatin	N° of Cisplatins Per DNA Nucleotide	^{195}Pt Stds Curve Equation	$m/z = 195$ Sample Signal (cps)	^{195}Pt Concⁿ (ng l⁻¹)
DI Water Blank	DI Water Blank	$y = 63.275x - 49344$	157.001	782.3
Control	Control	$y = 63.275x - 49344$	297.67	784.5
100 (DiI ⁿ x 25)	0.01	$y = 63.275x - 49344$	2788651	44852 (1121300)
500 (DiI ⁿ x 20)	0.002	$y = 63.275x - 49344$	564077	9695 (193900)
1 000 (DiI ⁿ x 5)	0.001	$y = 63.275x - 49344$	1097030	18117 (90585)
5 000	0.0002	$y = 63.275x - 49344$	905806	15095
10 000	0.0001	$y = 63.275x - 49344$	506702	8788
50 000	0.00002	$y = 63.275x - 49344$	95442.2	2288
100 000	0.00001	$y = 63.275x - 49344$	46091.9	1508
250 000	0.000004	$y = 63.275x - 49344$	17787.4	1061
500 000	0.000002	$y = 63.275x - 49344$	11304.8	958.5

Table 43. ^{195}Pt Isotope Content of the Untreated DNA/Oxaliplatin Sample Solutions Analysed During Study 5.

N° of DNA Nucleotides Per Oxaliplatin	N° of Oxaliplatins Per DNA Nucleotide	^{195}Pt Stds Curve Equation	$m/z = 195$ Sample Signal (cps)	^{195}Pt Conc ⁿ (ng l ⁻¹)
DI Water Blank	DI Water Blank	$y = 63.275x - 49344$	157.001	782.3
Control	Control	$y = 63.275x - 49344$	290.336	784.4
100 (Dil ⁿ x 25)	0.01	$y = 63.275x - 49344$	254474	4802 (120050)
500	0.002	$y = 63.275x - 49344$	1708544	27782
1 000	0.001	$y = 63.275x - 49344$	442770	7777
5 000	0.0002	$y = 63.275x - 49344$	127394	2793
10 000	0.0001	$y = 63.275x - 49344$	70903.2	1900
50 000	0.00002	$y = 63.275x - 49344$	16965.7	1048
100 000	0.00001	$y = 63.275x - 49344$	8213.03	909.6
250 000	0.000004	$y = 63.275x - 49344$	4575.73	852.1
500 000	0.000002	$y = 63.275x - 49344$	2160.83	814.0

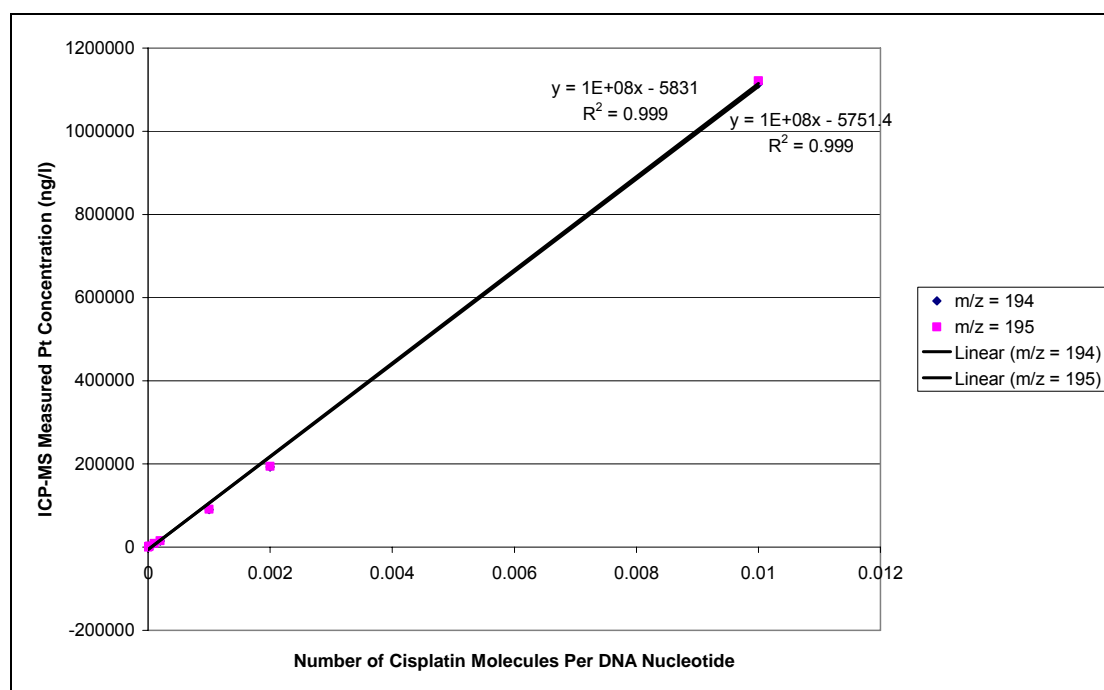


Figure 77. A Graph Comparing Number of Drug Molecules Per Nucleotide with the ICP-MS Measured Pt Concentration for the Study of Cisplatin Exposed DNA Samples (Study 5).

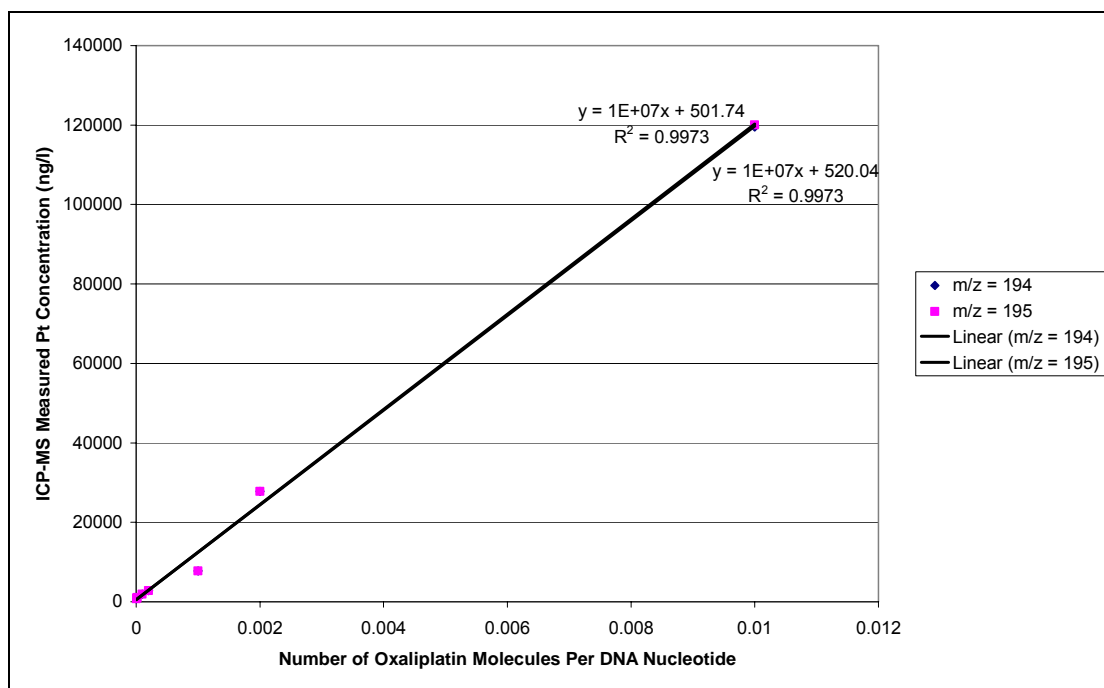


Figure 78. A Graph Comparing Number of Drug Molecules Per Nucleotide with the ICP-MS Measured Pt Concentration for the Study of Oxaliplatin Exposed DNA Samples (Study 5).

Figures 77 and 78 show that there is very good linearity between drug exposure (number of drug molecules per DNA nucleotide) and the measured Pt concentration for both cisplatin and oxaliplatin. Such linearity is far superior to that of the previous studies involving the separation of drug and target.

As can be seen in Tables 135 and 136, for a majority of the drug sample solutions studied the $m/z = 31$ signals were in excess of the detector capability. For some of the samples exhibiting higher drug exposure concentrations the measurement of the $^{31}\text{P}^+$ ion appears to be reduced such that data of the order of 1 to 3 million cps is observed. There are two potential reasons for this, the first being the presence of a lower quantity of DNA in these samples and the second being that the increased presence of Pt (which has slightly lower ionisation potential, 9 eV compared to 10.5 eV of P) was preferentially forming ions over ^{31}P .

This study was carried out with the aim of establishing the necessity for the separation of the drug and target species by gauging the degree of potential matrix effects that could originate from the high concentration of DNA. Not only did this fifth study

show that the separation was not required but it also revealed that direct analysis of the sample solutions allows the measurement of Pt at concentrations below that of the therapeutic region of these drugs. This work, as well as conclusions drawn from the previous studies, has also highlighted a possible difference in the degree of interaction strength between the two types of covalent binding that is possible between the drug and target molecules (inter- and intra-strand binding). Direct comparison between the data associated with cisplatin and that of oxaliplatin has shown that there were significant differences in the degree of binding. Such differences were not observed following the separation of drug and target during studies 2 to 4.

Following the success of this fifth study (and the provision of some information that contradicts that of studies 2 to 4), similar to studies 2 to 4, work was commenced on establishing binding constant data for use as the basis of a clinical test for the determination of drug efficacy of cisplatin and oxaliplatin in individual patients, see section 4.5.

4.5. The Calculation of DNA and Pt Based Drug Formation Constants (K_f) and Adduct Ratios

Using the data accrued during studies 2 to 5, the calculation of a formation constant (K_f) for the cisplatin-nucleotide and oxaliplatin-nucleotide species can be attempted as well as that of the number of drug-target adducts actually being formed per DNA nucleotide. Such K_f and adduct data would provide information considering the efficiency of binding between these Pt based drug molecules and the nucleotides of a DNA strand.

4.5.1. Formation Constant (K_f) Theory

To determine a K_f value in the case of the species involved in these studies the exposure reaction between reactant (the Pt drug and nucleotide) molecules must be considered, see the equation in Figure 79.

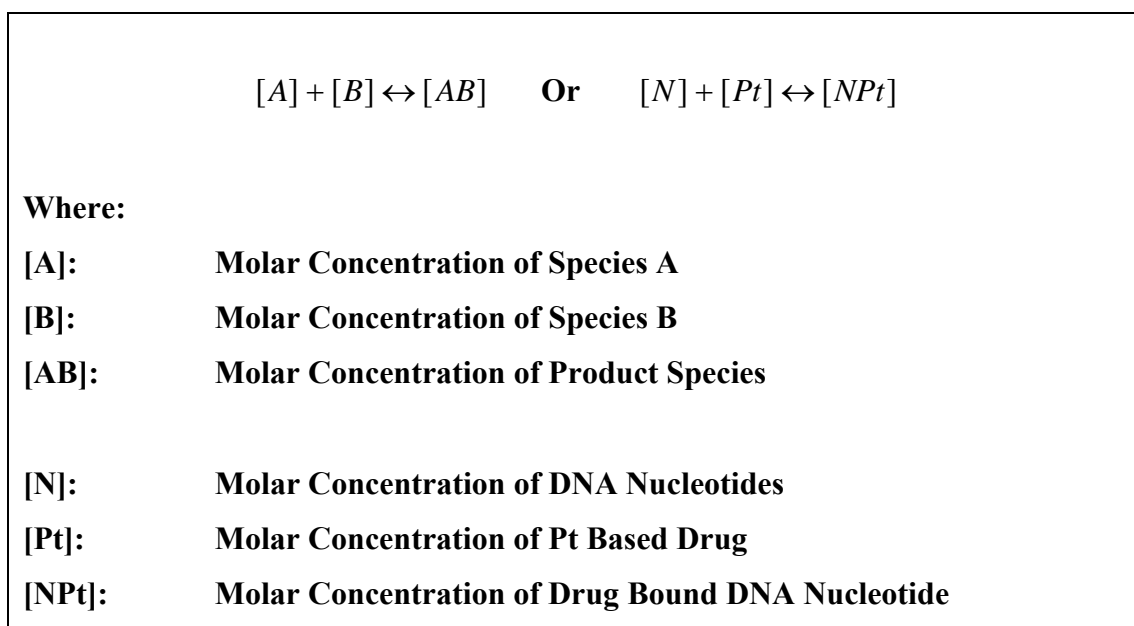


Figure 79. The Equilibrium Reaction between DNA Nucleotides and Pt Based Drug Molecules.

As can be seen in Figure 79 the interaction between reactant species, in this case the DNA nucleotide and Pt based drug molecules, is described in terms of an equilibrium process involving the formation of a product, ‘adduct’, species. Normally, when considering such a reaction the equation in Figure 80 would be appropriate for the calculation of a formation constant (K_f).

$K_f = \frac{[AB]}{[A][B]} \qquad \text{Or} \qquad K_f = \frac{[NPt]}{[N][Pt]}$	
<p>Where:</p> <p>K_f: Formation Constant</p> <p>$[A]$: Molar Concentration of Species A</p> <p>$[B]$: Molar Concentration of Species B</p> <p>$[AB]$: Molar Concentration of Product Species</p> <p>$[N]$: Molar Concentration of DNA Nucleotides</p> <p>$[Pt]$: Molar Concentration of Pt Based Drug</p> <p>$[NPt]$: Molar Concentration of Drug Bound DNA Nucleotide</p>	

Figure 80. The Equation Required for the Determination of a Formation Constant (K_f).

When normally describing such an equilibrium the reactant and product species are considered in terms of molar concentrations. However, in this case such concentrations are not available as DNA does not have a standard molecular weight due to variation between individuals. Therefore, to successfully calculate a K_f value the equation in Figure 80 must be altered, this is to be carried out for two reasons. Firstly, in this case, the K_f will be calculated in terms of ‘numbers of species’ (i.e. number of atoms or molecules) present during the interaction and secondly the equation in Figure 80 does not represent an equilibrium with regard to such numbers. To balance the equation in Figure 80 for equilibrium, the number concentration of the

drug bound nucleotide must be subtracted from the number concentrations of the DNA nucleotides and the Pt based drug molecules, respectively. The result of this is the equation seen in Figure 81.

$$K_f = \frac{[AB]}{([A_i] - [AB]) ([B_i] - [AB])}$$

Or

$$K_f = \frac{[NPt]}{([N_i] - [NPt]) ([Pt_i] - [NPt])}$$

Where:

K_f:	Formation Constant
[A_i]:	Initial Number Concentration of Species A
[B_i]:	Initial Number Concentration of Species B
[AB]:	Number Concentration of Product Species
[N_i]:	Initial Number Concentration of DNA Nucleotides
[Pt_i]:	Initial Number Concentration of Pt Based Drug
[NPt]:	Number Concentration of Drug Bound DNA Nucleotide

Figure 81. The Altered Equation Required for the Determination of a Formation Constant (K_f).

In order to establish K_f and adduct information for the samples analysed during studies 2 to 4 the data obtained must be converted into forms compatible with the components of the altered equation in Figure 81. To convert this data the following equations were utilised and all parameters were converted to standard international (SI) units (see Figure 82).

a)

$$N^{\circ} \text{ of Nucleotide s Per Litre} = \left(\left(\frac{([DNA] \times 0.001)}{\text{Mean Nucleotide RMM}} \right) \times \text{Avagadro 's Number} \right) \times 1000$$

b)

$$N^{\circ} \text{ of Pt Atoms Exposed Per Litre} = \frac{N^{\circ} \text{ of Nucleotide s Per Litre}}{N^{\circ} \text{ of Drug Molecules Exposed Per DNA Nucleotide}}$$

c)

$$N^{\circ} \text{ of Drug - Target Adducts Formed Per Litre} = \left(\frac{([Pt] \times 0.001)}{\text{Pt RAM}} \right) \times \text{Avagadro 's Number}$$

d)

$$N^{\circ} \text{ of Adducts Formed Per DNA Nucleotide} = \frac{N^{\circ} \text{ of Drug - Target Adducts Formed Per Litre}}{N^{\circ} \text{ of Nucleotide s Per Litre}}$$

Where:

[DNA]: Concentration of DNA

RMM: Relative Molecular Mass

RAM: Relative Atomic Mass

Figure 82. Additional Equations Used During the Conversion of Study Data to Components Required for the Calculation of K_f and Number of Adducts Formed.
a) An Equation for the Calculation of the Number of Nucleotides Per Litre. b) An Equation for the Calculation of the Number of Pt Atoms Exposed Per Litre. c) An Equation for the Calculation of the Number of Drug-Target Adducts Formed Per Litre. d) An Equation for the Calculation of the Number of Adducts formed Per DNA Nucleotide.

4.5.2. Formation Constant (K_f) and Adduct Ratios: Calculations

Formation constants and ratios were calculated for each drug exposed DNA sample analysed between studies 2 and 5. The data used for these calculations and the resultant values themselves can be seen in Tables 44 to 50.

Table 44. Further Data Generated During the Calculation of K_f and the Ratio of Number of Adducts Per DNA Nucleotide for the Cisplatin Exposed DNA Samples Analysed During Study 2.

Sample Identity							Final Data	
(Number of DNA Nucleotides Per Cisplatin Molecule)	(Number of Cisplatin Molecules Per DNA Nucleotide)	DNA Conc ⁿ (mg ml ⁻¹)	Number of DNA Nucleotides Per Litre	Number of Pt Atoms Exposed Per Litre	Conc ⁿ of ¹⁹⁵ Pt (mg l ⁻¹): Established by ICP-QMS	Number of Drug-Nucleotide Adducts Formed Per Litre	K_f (Per Number Litre)	Number of Drug-Nucleotide Adducts Formed Per DNA Nucleotide
Blank	0	0	0	-	0.00044	1.36×10^{15}	-	-
Control	0	1	1.96×10^{21}	-	0.00036	1.11×10^{15}	-	-
10 000	0.0001	1	1.96×10^{21}	1.96×10^{17}	0.00562	1.74×10^{16}	4.97×10^{-23}	8.86×10^{-06}
50 000	0.00002	1	1.96×10^{21}	3.92×10^{16}	0.00136	4.20×10^{15}	6.14×10^{-23}	2.14×10^{-06}
100 000	0.00001	1	1.96×10^{21}	1.96×10^{16}	0.00069	2.13×10^{15}	6.24×10^{-23}	1.09×10^{-06}
500 000	0.000002	1	1.96×10^{21}	3.92×10^{15}	0.00048	1.48×10^{15}	3.11×10^{-22}	7.57×10^{-07}
1 000 000	0.000001	1	1.96×10^{21}	1.96×10^{15}	0.00044	1.36×10^{15}	1.16×10^{-21}	6.94×10^{-07}
5 000 000	0.0000002	1	1.96×10^{21}	3.92×10^{14}	0.00046	1.42×10^{15}	-7.05×10^{-22}	7.25×10^{-07}
10 000 000	0.0000001	1	1.96×10^{21}	1.96×10^{14}	0.0005	1.54×10^{15}	-5.85×10^{-22}	7.88×10^{-07}
50 000 000	0.00000002	1	1.96×10^{21}	3.92×10^{13}	0.00045	1.39×10^{15}	-5.26×10^{-22}	7.10×10^{-07}
100 000 000	0.00000001	1	1.96×10^{21}	1.96×10^{13}	0.00042	1.30×10^{15}	-5.19×10^{-22}	6.62×10^{-07}
500 000 000	0.000000002	1	1.96×10^{21}	3.92×10^{12}	0.00041	1.27×10^{15}	-5.12×10^{-22}	6.47×10^{-07}
1 000 000 000	0.000000001	1	1.96×10^{21}	1.96×10^{12}	0.00041	1.27×10^{15}	-5.12×10^{-22}	6.47×10^{-07}

Table 45. Further Data Generated During the Calculation of K_f and the Ratio of Number of Adducts Per DNA Nucleotide for the Cisplatin Exposed DNA Samples Analysed During Study 3.

Sample Identity							Final Data	
(Number of DNA Nucleotides Per Cisplatin Molecule)	(Number of Cisplatin Molecules Per DNA Nucleotide)	DNA Concⁿ (mg ml⁻¹)	Number of DNA Nucleotides Per Litre	Number of Pt Atoms Exposed Per Litre	Concⁿ of ¹⁹⁵Pt (mg l⁻¹): Established by ICP-QMS	Number of Drug-Nucleotide Adducts Formed Per Litre	K_f (Per Number Litre)	Number of Drug-Nucleotide Adducts Formed Per DNA Nucleotide
Blank	0	0	0	-	-	-	-	-
Control	0	1	1.96×10^{21}	-	0.00017	5.25×10^{14}	-	2.68×10^{-07}
50	0.02	1	1.96×10^{21}	3.92×10^{19}	-	-	-	-
100	0.01	1	1.96×10^{21}	1.96×10^{19}	0.11616	3.59×10^{17}	9.53×10^{-24}	1.83×10^{-04}
500	0.002	1	1.96×10^{21}	3.92×10^{18}	0.02251	6.95×10^{16}	9.23×10^{-24}	3.55×10^{-05}
1 000	0.001	1	1.96×10^{21}	1.96×10^{18}	0.0255	7.87×10^{16}	2.14×10^{-23}	4.02×10^{-05}
5 000	0.0002	1	1.96×10^{21}	3.92×10^{17}	0.00429	1.32×10^{16}	1.79×10^{-23}	6.77×10^{-06}
10 000	0.0001	1	1.96×10^{21}	1.96×10^{17}	0.00435	1.34×10^{16}	3.76×10^{-23}	6.86×10^{-06}
50 000	0.00002	1	1.96×10^{21}	3.92×10^{16}	0.00085	2.62×10^{15}	3.67×10^{-23}	1.34×10^{-06}
100 000	0.00001	1	1.96×10^{21}	1.96×10^{16}	0.00025	7.72×10^{14}	2.10×10^{-23}	3.94×10^{-07}
500 000	0.000002	1	1.96×10^{21}	3.92×10^{15}	0.00019	5.87×10^{14}	9.00×10^{-23}	3.00×10^{-07}
1 000 000	0.000001	1	1.96×10^{21}	1.96×10^{15}	0.00114	3.52×10^{15}	-1.15×10^{-21}	1.80×10^{-06}

Table 46. Further Data Generated During the Calculation of K_f and the Ratio of Number of Adducts Per DNA Nucleotide for the Oxaliplatin Exposed DNA Samples Analysed During Study 3.

Sample Identity							Final Data	
(Number of DNA Nucleotides Per Cisplatin Molecule)	(Number of Cisplatin Molecules Per DNA Nucleotide)	DNA Concⁿ (mg ml⁻¹)	Number of DNA Nucleotides Per Litre	Number of Pt Atoms Exposed Per Litre	Concⁿ of ¹⁹⁵Pt (mg l⁻¹): Established by ICP-QMS	Number of Drug-Nucleotide Adducts Formed Per Litre	K_f (Per Number Litre)	Number of Drug-Nucleotide Adducts Formed Per DNA Nucleotide
Blank	0	0	0	-	< 0.0003	-	-	-
Control	0	1	1.96×10^{21}	-	0.0003	9.26×10^{14}	-	4.73×10^{-07}
50	0.02	1	1.96×10^{21}	3.92×10^{19}	> 0.14187	-	-	-
100	0.01	1	1.96×10^{21}	1.96×10^{19}	0.14187	4.38×10^{17}	1.17×10^{-23}	2.24×10^{-04}
500	0.002	1	1.96×10^{21}	3.92×10^{18}	0.04021	1.24×10^{17}	1.67×10^{-23}	6.34×10^{-05}
1 000	0.001	1	1.96×10^{21}	1.96×10^{18}	0.02295	7.08×10^{16}	1.92×10^{-23}	3.62×10^{-05}
5 000	0.0002	1	1.96×10^{21}	3.92×10^{17}	0.00523	1.61×10^{16}	2.20×10^{-23}	8.25×10^{-06}
10 000	0.0001	1	1.96×10^{21}	1.96×10^{17}	0.0036	1.11×10^{16}	3.07×10^{-23}	5.68×10^{-06}
50 000	0.00002	1	1.96×10^{21}	3.92×10^{16}	0.00218	6.73×10^{15}	1.06×10^{-22}	3.44×10^{-06}
100 000	0.00001	1	1.96×10^{21}	1.96×10^{16}	0.00056	1.73×10^{15}	4.95×10^{-23}	8.83×10^{-07}
500 000	0.000002	1	1.96×10^{21}	3.92×10^{15}	0.00043	1.33×10^{15}	2.62×10^{-22}	6.78×10^{-07}
1 000 000	0.000001	1	1.96×10^{21}	1.96×10^{15}	0.00039	1.20×10^{15}	8.16×10^{-22}	6.15×10^{-07}

Table 47. Further Data Generated During the Calculation of K_f and the Ratio of Number of Adducts Per DNA Nucleotide for the Cisplatin Exposed DNA Samples Analysed During Study 4.

Sample Identity							Final Data	
(Number of DNA Nucleotides Per Cisplatin Molecule)	(Number of Cisplatin Molecules Per DNA Nucleotide)	DNA Concⁿ (mg ml⁻¹)	Number of DNA Nucleotides Per Litre	Number of Pt Atoms Exposed Per Litre	Concⁿ of ¹⁹⁵Pt (mg l⁻¹): Established by ICP-QMS	Number of Drug-Nucleotide Adducts Formed Per Litre	K_f (Per Number Litre)	Number of Drug-Nucleotide Adducts Formed Per DNA Nucleotide
Blank 2	0	0	0	-	0.00007	2.16×10^{14}	-	-
Control 2	0	1	1.96×10^{21}	-	0.00013	4.01×10^{14}	-	2.05×10^{-07}
100	0.01	1	1.96×10^{21}	1.96×10^{19}	0.42118	1.3×10^{18}	3.64×10^{-23}	6.64×10^{-04}
150 A	0.006666667	1	1.96×10^{21}	1.31×10^{19}	0.26188	8.08×10^{17}	3.37×10^{-23}	4.13×10^{-04}
150 B	0.006666667	1	1.96×10^{21}	1.31×10^{19}	0.2448	7.56×10^{17}	3.14×10^{-23}	3.86×10^{-04}
300 A	0.003333333	1	1.96×10^{21}	6.53×10^{18}	0.10928	3.37×10^{17}	2.79×10^{-23}	1.72×10^{-04}
300 B	0.003333333	1	1.96×10^{21}	6.53×10^{18}	0.11569	3.57×10^{17}	2.96×10^{-23}	1.82×10^{-04}
500	0.002	1	1.96×10^{21}	3.92×10^{18}	0.05031	1.55×10^{17}	2.11×10^{-23}	7.93×10^{-05}
1 000	0.001	1	1.96×10^{21}	1.96×10^{18}	0.03824	1.18×10^{17}	3.28×10^{-23}	6.03×10^{-05}
5 000	0.0002	1	1.96×10^{21}	3.92×10^{17}	0.00601	1.86×10^{16}	2.54×10^{-23}	9.48×10^{-06}
10 000	0.0001	1	1.96×10^{21}	1.96×10^{17}	0.00404	1.25×10^{16}	3.48×10^{-23}	6.37×10^{-06}
50 000	0.00002	1	1.96×10^{21}	3.92×10^{16}	0.00113	3.49×10^{15}	5.00×10^{-23}	1.78×10^{-06}
100 000	0.00001	1	1.96×10^{21}	1.96×10^{16}	0.00079	2.44×10^{15}	7.27×10^{-23}	1.25×10^{-06}
250 000 A	0.000004	1	1.96×10^{21}	7.83×10^{15}	0.0002	6.17×10^{14}	4.37×10^{-23}	3.15×10^{-07}
250 000 B	0.000004	1	1.96×10^{21}	7.83×10^{15}	0.00021	6.48×10^{14}	4.61×10^{-23}	3.31×10^{-07}
250 000 C	0.000004	1	1.96×10^{21}	7.83×10^{15}	0.0002	6.17×10^{14}	4.37×10^{-23}	3.15×10^{-07}
500 000	0.000002	1	1.96×10^{21}	3.92×10^{15}	0.00049	1.51×10^{15}	3.22×10^{-22}	7.73×10^{-07}

Table 48. Further Data Generated During the Calculation of K_f and the Ratio of Number of Adducts Per DNA Nucleotide for the Oxaliplatin Exposed DNA Samples Analysed During Study 4.

Sample Identity							Final Data	
(Number of DNA Nucleotides Per Oxaliplatin Molecule)	(Number of Oxaliplatin Molecules Per DNA Nucleotide)	DNA Conc ⁿ (mg ml ⁻¹)	Number of DNA Nucleotides Per Litre	Number of Pt Atoms Exposed Per Litre	Conc ⁿ of ¹⁹⁵ Pt (mg l ⁻¹): Established by ICP-QMS	Number of Drug-Nucleotide Adducts Formed Per Litre	K_f (Per Number Litre)	Number of Drug-Nucleotide Adducts Formed Per DNA Nucleotide
Blank 2	0	0	0	-	0.00014	4.32×10^{14}	-	-
Control 2	0	1	1.96×10^{21}	-	-	-	-	-
100	0.01	1	1.96×10^{21}	1.96×10^{19}	0.33284	1.03×10^{18}	2.83×10^{-23}	5.25×10^{-04}
150 A	0.006666667	1	1.96×10^{21}	1.31×10^{19}	0.29586	9.13×10^{17}	3.85×10^{-23}	4.67×10^{-04}
150 B	0.006666667	1	1.96×10^{21}	1.31×10^{19}	0.53273	1.64×10^{18}	7.37×10^{-23}	8.40×10^{-04}
300 A	0.003333333	1	1.96×10^{21}	6.53×10^{18}	0.1456	4.49×10^{17}	3.78×10^{-23}	2.30×10^{-04}
300 B	0.003333333	1	1.96×10^{21}	6.53×10^{18}	0.13885	4.29×10^{17}	3.59×10^{-23}	2.19×10^{-04}
500	0.002	1	1.96×10^{21}	3.92×10^{18}	0.06582	2.03×10^{17}	2.80×10^{-23}	1.04×10^{-04}
1 000	0.001	1	1.96×10^{21}	1.96×10^{18}	0.0327	1.01×10^{17}	2.78×10^{-23}	5.16×10^{-05}
5 000	0.0002	1	1.96×10^{21}	3.92×10^{17}	0.00849	2.62×10^{16}	3.66×10^{-23}	1.34×10^{-05}
10 000	0.0001	1	1.96×10^{21}	1.96×10^{17}	0.00455	1.40×10^{16}	3.95×10^{-23}	7.17×10^{-06}
50 000	0.00002	1	1.96×10^{21}	3.92×10^{16}	0.0012	3.70×10^{15}	5.34×10^{-23}	1.89×10^{-06}
100 000	0.00001	1	1.96×10^{21}	1.96×10^{16}	0.0015	4.63×10^{15}	1.58×10^{-22}	2.37×10^{-06}
250 000 A	0.000004	1	1.96×10^{21}	7.83×10^{15}	0.00026	8.03×10^{14}	5.83×10^{-23}	4.10×10^{-07}
250 000 B	0.000004	1	1.96×10^{21}	7.83×10^{15}	0.00036	1.11×10^{15}	8.45×10^{-23}	5.68×10^{-07}
250 000 C	0.000004	1	1.96×10^{21}	7.83×10^{15}	0.00056	1.73×10^{15}	1.45×10^{-22}	8.83×10^{-07}
500 000	0.000002	1	1.96×10^{21}	3.92×10^{15}	0.00004	1.23×10^{14}	1.66×10^{-23}	6.31×10^{-08}

Table 49. Further Data Generated During the Calculation of K_f and the Ratio of Number of Adducts Per DNA Nucleotide for the Cisplatin Exposed DNA Samples Analysed During Study 5.

Sample Identity							Final Data	
(Number of DNA Nucleotides Per Cisplatin Molecule)	(Number of Cisplatin Molecules Per DNA Nucleotide)	DNA Concⁿ (mg ml⁻¹)	Number of DNA Nucleotides Per Litre	Number of Pt Atoms Exposed Per Litre	Concⁿ of ¹⁹⁵Pt (mg l⁻¹): Established by ICP-QMS	Number of Drug-Nucleotide Adducts Formed Per Litre	K_f (Per Number Litre)	Number of Drug-Nucleotide Adducts Formed Per DNA Nucleotide
Blank	0	0	0	-	0.0007823	2.42×10^{15}	-	-
Control	0	1	1.96×10^{21}	-	0.0007845	2.42×10^{15}	-	1.23×10^{-06}
100	0.01	1	1.96×10^{21}	1.96×10^{19}	1.1213	3.46×10^{18}	1.10×10^{-22}	1.77×10^{-03}
500	0.002	1	1.96×10^{21}	3.92×10^{18}	0.1939	5.99×10^{17}	9.22×10^{-23}	3.06×10^{-04}
1 000	0.001	1	1.96×10^{21}	1.96×10^{18}	0.090585	2.80×10^{17}	8.51×10^{-23}	1.43×10^{-04}
5 000	0.0002	1	1.96×10^{21}	3.92×10^{17}	0.015095	4.66×10^{16}	6.90×10^{-23}	2.38×10^{-05}
10 000	0.0001	1	1.96×10^{21}	1.96×10^{17}	0.008788	2.71×10^{16}	8.22×10^{-23}	1.39×10^{-05}
50 000	0.00002	1	1.96×10^{21}	3.92×10^{16}	0.002288	7.06×10^{15}	1.12×10^{-22}	3.61×10^{-06}
100 000	0.00001	1	1.96×10^{21}	1.96×10^{16}	0.001508	4.66×10^{15}	1.59×10^{-22}	2.38×10^{-06}
250 000	0.000004	1	1.96×10^{21}	7.83×10^{15}	0.001061	3.28×10^{15}	3.67×10^{-22}	1.67×10^{-06}
500 000	0.000002	1	1.96×10^{21}	3.92×10^{15}	0.0009585	2.96×10^{15}	1.58×10^{-21}	1.51×10^{-06}

Table 50. Further Data Generated During the Calculation of K_f and the Ratio of Number of Adducts Per DNA Nucleotide for the Oxaliplatin Exposed DNA Samples Analysed During Study 5.

Sample Identity							Final Data	
(Number of DNA Nucleotides Per Oxaliplatin Molecule)	(Number of Oxaliplatin Molecules Per DNA Nucleotide)	DNA Concⁿ (mg ml⁻¹)	Number of DNA Nucleotides Per Litre	Number of Pt Atoms Exposed Per Litre	Concⁿ of ¹⁹⁵Pt (mg l⁻¹): Established by ICP-QMS	Number of Drug-Nucleotide Adducts Formed Per Litre	K_f (Per Number Litre)	Number of Drug-Nucleotide Adducts Formed Per DNA Nucleotide
Blank	0	0	0	-	0.0007823	2.41×10^{15}	-	-
Control	0	1	1.96×10^{21}	-	0.0007844	2.42×10^{15}	-	1.24×10^{-06}
100	0.01	1	1.96×10^{21}	1.96×10^{19}	0.12005	3.71×10^{17}	9.86×10^{-24}	1.89×10^{-04}
500	0.002	1	1.96×10^{21}	3.92×10^{18}	0.027782	8.58×10^{16}	1.14×10^{-23}	4.38×10^{-05}
1 000	0.001	1	1.96×10^{21}	1.96×10^{18}	0.007777	2.40×10^{16}	6.34×10^{-24}	1.23×10^{-05}
5 000	0.0002	1	1.96×10^{21}	3.92×10^{17}	0.002793	8.62×10^{15}	1.15×10^{-23}	4.40×10^{-06}
10 000	0.0001	1	1.96×10^{21}	1.96×10^{17}	0.0019	5.87×10^{15}	1.58×10^{-23}	3.00×10^{-06}
50 000	0.00002	1	1.96×10^{21}	3.92×10^{16}	0.001048	3.24×10^{15}	4.60×10^{-23}	1.65×10^{-06}
100 000	0.00001	1	1.96×10^{21}	1.96×10^{16}	0.0009096	2.81×10^{15}	8.55×10^{-23}	1.43×10^{-06}
250 000	0.000004	1	1.96×10^{21}	7.83×10^{15}	0.0008521	2.63×10^{15}	2.58×10^{-22}	1.34×10^{-06}
500 000	0.000002	1	1.96×10^{21}	3.92×10^{15}	0.000814	2.51×10^{15}	9.15×10^{-22}	1.28×10^{-06}

4.5.3. Formation Constant (K_f) and Adduct Ratios: Discussion and Conclusions

Following analysis of the numerous Pt based drug exposed DNA samples during studies 2 to 5, K_f data and the number of adducts formed per DNA nucleotide were successfully calculated. Table 51 compares the parameter value ranges obtained between the four successful studies.

Table 51. A General Comparison of K_f Values and Numbers of Drug-Nucleotide Adducts Formed Per DNA Nucleotide Between Studies 2 to 5.

Study Number	Pt Based Drug Identity	K_f (Per Number Litre)	Number of Drug-Nucleotide Adducts Formed Per DNA Nucleotide
2	Cisplatin	10^{-21} to 10^{-23}	10^{-06} to 10^{-07}
3	Cisplatin	10^{-21} to 10^{-24}	10^{-04} to 10^{-07}
	Oxaliplatin	10^{-22} to 10^{-23}	10^{-04} to 10^{-07}
4	Cisplatin	10^{-22} to 10^{-23}	10^{-04} to 10^{-07}
	Oxaliplatin	10^{-22} to 10^{-23}	10^{-04} to 10^{-07}
5	Cisplatin	10^{-21} to 10^{-23}	10^{-03} to 10^{-06}
	Oxaliplatin	10^{-22} to 10^{-24}	10^{-04} to 10^{-06}

Between studies 2 to 5 the values calculated, for both of the final parameters, appeared to fall within the same ranges. For the K_f parameter all of the calculated values for both cisplatin and oxaliplatin drugs were in the range of 10^{-21} to 10^{-24} , such values were very low. For the number of adducts formed per DNA nucleotide parameter all of the calculated values for both drugs were of the order of 10^{-03} to 10^{-07} , such values would appear to be the equivalent of the numbers of drug molecules per DNA molecule stated by Akaboshi *et al* and Jamieson *et al*.^{162, 186}

This information gives rise to three issues that require discussion. Firstly the calculated data backs up previous research suggesting that the binding between these

drugs and their DNA target is particularly inefficient.^{162, 186} As mentioned previously the binding of drug to DNA target was different between cisplatin and oxaliplatin *in vivo*,^{177, 178, 188} however, this work has shown similarities between the degree of binding that took place (via the calculation of K_f and the number of adducts formed parameters) during *in vitro* experiments. The reason for this was that a huge environmental difference exists between *in vivo* and *in vitro* experiments. If this difference is simplified slightly to compare the condition in which DNA exists within a cell to naked DNA in the *in vitro* experiment then a gulf can be seen in terms of the target exposure area, chemical conditions and the presence of alternate binding sites. Therefore, with the two drugs being structurally different, a difference in the degree of binding *in vivo* would be expected. For the interaction between naked DNA and these drugs, *in vitro*, these environmental differences would be minimised and binding would be similar.

Secondly, there appears to be no significant difference in the K_f and number of adducts per nucleotide parameters between the initial studies (2 to 4) and the final study (5). The data, however, is not the best approach to comparing the studies with regard to how these two drugs respond as the degree of difference is rather small. If the components of the equations used to calculate the two final parameters are considered then it can be seen that the final Pt concentrations of the samples are incorporated. Therefore, if there is no significant difference in the two parameters between the initial and final studies then the concentration component must be being masked, to a certain degree, by the other components. The best approach to a comparison is, therefore, to consider the Pt isotope instrument signals, at $m/z = 194$ and 195, and concentrations of each sample between drugs.

Finally, to describe the K_f data a range of values to cover the samples studied has been quoted rather than a single figure. This shows that the calculated K_f values are varying according to the drug exposure concentration which implies that the calculated data cannot be truly described as a constant. Although the data discussed in this section are adequate for describing the drug-target interaction, the original calculation needs to be revisited to develop an equation that can better describe a binding constant parameter. With regard to using data as the basis of an efficacy test

the number of drug-nucleotide adducts formed data is probably more meaningful at this stage.

4.6. Conclusions and Further Work

The overall result of the work described in this chapter is that it appears that a low resolution quadrupole based ICP-MS instrument is more than capable of measuring Pt isotopes at the desired concentrations when analysing highly concentrated, drug exposed, DNA samples. Therefore, such an instrument would be a viable option in the development of a clinical test for drug efficacy determination for blood samples from individual patients. However, the overall aim of such a test is to establish the quantity of DNA bound drug molecules within the cell so the analyst must be able to appreciate the different types of drug-DNA interactions and the final distribution of drug molecules within a cell.

A greater amount of work is required on the development of K_f equations that can better describe the interactions between drug and target. Improved equations would lead to an easier interpretation of data generated following the analysis of patient DNA during an efficacy test.

Further work must be carried out in this area prior to the establishment of a final test. Following the work that was carried out it became apparent that the separation of drug and target molecules to avoid potential matrix effects was not necessary. However, such work has provided some very interesting data with regard to appreciating inter- and intra strand DNA binding and, potentially, the difference in 'binding strength' according to steric conditions. This work has also shown that the analysis of a 1 mg ml⁻¹ DNA solution (what would be considered a highly concentrated solution) via the usual nebuliser and spray chamber arrangement is not problematic with regard to the presence of non-spectroscopic interferences. The direct introduction of such a sample, without further treatment, maintains a simple ICP-MS analysis. The next step for this work is the study of blood samples taken from patients and untreated volunteers to establish the limitations of this approach *in vivo*. With regard to the observed differences between inter- and intra-strand drug binding, it would be interesting to continue this work and quantitatively determine a ratio between the two types. It may then be possible to relate the type of covalent binding with drug efficacy.

Chapter 5

The Development of ICP-MS Interface Structures

5.1. The ICP-MS Interface

Without doubt the most important, and in many ways problematic, region of an ICP-MS instrument is the interface between the atmospheric pressure plasma ion source and the mass analyser operating at vacuum conditions. Although the design of this interface has been very successful, it has changed very little in the twenty years of commercially available instruments. The main reason for this lack of design development is that the smallest change made can have a dramatic detrimental affect on instrument sensitivity, even the same design built with the same materials but from different manufacturers can produce vastly different analytical performances.¹⁸⁹

Although little has changed with regard to the interface design, research into the processes that take place within the region has been ongoing. A significant degree of research has been carried out to establish the fate of plasma species as they pass into the vacuum interface region. Over the past ten years measurements have been carried out to determine the temperature and pressure environments of the interface region and to establish the velocity and trajectory of ions passing through. The overall conclusions of such measurements have been that the physical behaviour is as would be expected of a gaseous flow through an orifice and into a low-pressure region. However, there are some departures from what would be expected and currently the expressions used to describe the region are too simple. The ICP-MS interface region remains to be an area of very interesting research that is not yet fully understood. A complete knowledge of the processes that take place in this region is required before any significant changes in its construction can be carried out for the improved sampling of ions from the ICP ion source.^{101, 190-193}

ICP-MS can be described as a “flow into” technique whereby the ions generated are transported from the ICP, through the interface region and the mass analyser and into the detector. This is the opposite of what can be described as a “flow by” technique, such as ICP-OES, where the ions generated in the plasma are detected by their photon emission without passage into any instrumental regions. Due to this instrument configuration the ICP-MS technique exhibits some significant analytical problems,

not observed in ICP-OES, originating within the current interface design region. These problems are described as follows.

5.1.1. Deposition problems within the ICP-MS Interface

As the ions generated are transported between extreme pressure and temperature environments and through the cone orifices the deposition of ions, particularly matrix ions, on and within the sample and skimmer cones can lead to blockage which results in a degradation, and sometimes complete loss, of analyte sensitivity. This problem is a limiting factor in the analysis of samples containing a high concentration of matrix, during the analysis of some of which the cones have been known to block completely within a short period of time (see section 1.2.2).

5.1.2. Ion Kinetic Energy Spread Associated with the ICP-MS Interface

The current standard ICP-MS interface design carries ions through a step-down in pressure from atmospheric conditions at the ICP ion source (≈ 1 Bar) to a low pressure in an expansion chamber (≈ 2 mBar) and then to vacuum conditions in the mass analyser ($\approx 1.33 \times 10^{-9}$ Bar). As previously described in section 1.3, ions passing through the interface, from the ICP ion source to the mass analyser, are subject to a number of influential factors that can cause a wide ion kinetic energy spread for an individual ion species. Such a wide ion energy spread leads to some ions of the same element having a greater or lesser stable trajectory in the mass analyser, or the multipole of a collision/reaction cell, hence such a spread has an effect on overall sensitivity.⁴

Any development of the ICP-MS interface region that can result in the restriction of ion kinetic energy spread would be a welcome evolution of the technique. One such approach to achieving this restriction could lie in the transport of ions between the

different ICP ion source and the mass analyser environments whilst limiting ions to sub-sonic velocities.

5.2. Previous Approaches to Tackling ICP-MS Interface Problems

Various approaches have been made to the improvement of ion transport through the ICP-MS interface. Skimmer cone geometry, sample/skimmer cone separation and a greater number of pressure reduction steps have all been studied as potential avenues for transport improvement. Such approaches to the development of the ICP-MS interface design are described as follows. When considering such variations in interface design it should be appreciated that even changes that may be considered insignificant can have drastic effects on instrument sensitivity.¹⁸⁹ The smallest of variations in the construction of an ICP-MS have led to significant differences in sensitivity capability between instruments.

5.2.1. Skimmer Cone Geometry

The geometry, i.e. size and shape, of the skimmer cone is an important parameter in the ICP-MS interface region. As the skimmer cone samples ions for analysis from the barrel shock region of the expansion chamber its shape is important with regard to the temperature that it reaches, the quantity of ions that it allows through and the point at which it skims from the zone of silence.

Various designs of skimmer cone are commercially available with differing dimensions of the tip and base of the cone as well as a variable orifice diameter. Jarvis *et al.*¹⁹⁴ compared three commercially available skimmers (mini, micro and polyskim skimmers) in ICP-MS analysis with the aim of reducing interferences. This work showed that the magnitude of polyatomic ions, oxide ions and doubly charged ions entering the mass analyser was dependent, to a certain degree, on the type of skimmer in use. Therefore, skimmer geometry is critical in the reduction of some interferences originating from such ions.

5.2.2. Sample and Skimmer Cone Separation

Similar to certain aspects of the skimmer cone geometry, the separation distance between sample and skimmer cones is a significant parameter with regard to the extraction of ions. Typically the sample and skimmer cones in the interface are separated by approximately 5 mm, this yields the maximum ion beam intensity on the opposite side of the skimmer cone which samples ions from the zone of silence.

Lam and Horlick studied the effects of the separation distance between the sample and skimmer cones during the analysis of Cu in a HNO₃ matrix employing both an Ar based ICP and a N₂/Ar mixed gas ICP.¹⁹⁵ By adjusting the separation distance between the two cones and the nebuliser flow, for both types of plasma, some common polyatomic Ar based ions could be attenuated with respect to the Cu analyte signal. For example, in the Ar only ICP at a cone separation of 2.3 mm the $^{40}\text{Ar}^{16}\text{O}^1\text{H}^+$ ($m/z = 57$) and $^{40}\text{Ar}_2^1\text{H}^+$ ($m/z = 81$) polyatomic ions were observed to be attenuated whilst in the N₂/Ar mixed gas ICP at the same cone separation the $^{40}\text{Ar}^{16}\text{O}^1\text{H}^+$ ($m/z = 57$) and $^{40}\text{Ar}^{14}\text{N}^+$ ($m/z = 54$) polyatomic ions were attenuated.

Lam and Horlick also observed the effects of sample cone-skimmer separation on signal suppression associated with matrix effects.¹⁹⁵ Lam and Horlick studied the Mn signal ($m/z = 55$) of a 0.2 µg ml⁻¹ Mn solution and observed a maximum signal at a cone separation of 6 mm. The $m/z = 55$ signal was then seen to be suppressed linearly to 20 % of its original value when the separation was increased to 12 mm. By spiking another 0.2 µg ml⁻¹ Mn solution with 1000 µg ml⁻¹ U and then another with a similar level of Na further experiments were carried out. At a cone separation of 6 mm the Mn ($m/z = 55$) signal of the U spiked solution was suppressed to approximately 10 % whilst for the Na spiked solution a suppression to 40 % was observed. As the cone separation distance was increased a change in the degree of Mn suppression for both spiked solutions was observed. At a separation of 12 mm the Mn signal suppression was improved to 50 % and 60 % for the U and Na spiked solutions, respectively.

5.2.3. Three Cone Interface

Tanner *et al.*⁷² studied the effects of a more gradual reduction in pressure environment between the ICP ion source and the mass analyser in an ICP-MS instrument. An extra pressure reduction region was incorporated into the typical interface design in the form of a third cone situated between the skimmer cone and the extraction lens. In this case a reduction in pressure was observed from 1 Bar (at the plasma ion source) to approximately 4 mBar (between the sampler and skimmer cones) then to 0.4 mBar (in the new region between the skimmer cone and the third cone) and finally to 1.33×10^{-5} mBar (at the extraction lens).

Analytical sensitivity employing the instrument containing this three cone interface was comparable to a typical commercial instrument. There was significant benefit observed, using such an interface, in the form of a reduction in signal suppression previously seen due to the presence of high mass matrix elements. It was thought that the acceleration of electrons due to supersonic expansion, in this interface, would be reduced hence charge separation and space charge effects may have occurred to a lesser degree.

5.3. The Development of an Adapted ICP-MS Interface for the Reduction of Ion Deposition

An adaptation to the current Thermo Electron PQ ExCell ICP-MS interface region was considered with the aim of improving the extraction of ions into the mass analyser for the analysis of samples composed of a highly concentrated matrix. As mentioned previously in this chapter one of the major problems of analysing such samples by ICP-MS is the issue of ion deposition on the skimmer cone.

The idea behind such an adaptation is the manipulation of the interaction between the shockwave generated within the expansion chamber and the skimmer cone. Such an interaction can be compared to that between a shockwave and a conical surface as a skimmer cone tip is essentially conical in shape. On the meeting between a shockwave and a conical surface a curved shape deflected shock emanates from the tip of the cone, the degree of this deflection being dependent on the angle of the conical tip at the point of meeting.¹⁹⁶ Within the ICP-MS interface as this shock deflection takes place a small quantity of ions are skimmed to form the ion beam, in the state ready for detection, behind the skimmer cone whilst the bulk of ions in the shock are carried down the sides of the cone. During the analysis of a sample based on a highly concentrated matrix, this deflected bulk flow of ions typically results in deposition at and around the skimmer orifice which has a detrimental effect on instrument sensitivity. On the meeting of the adiabatic shock and the tip of the skimmer cone, the larger the angle of the tip then the further the shock is deflected around the tip itself and, in theory, less deposition should occur, see Figures 83 and 84.¹⁹⁶

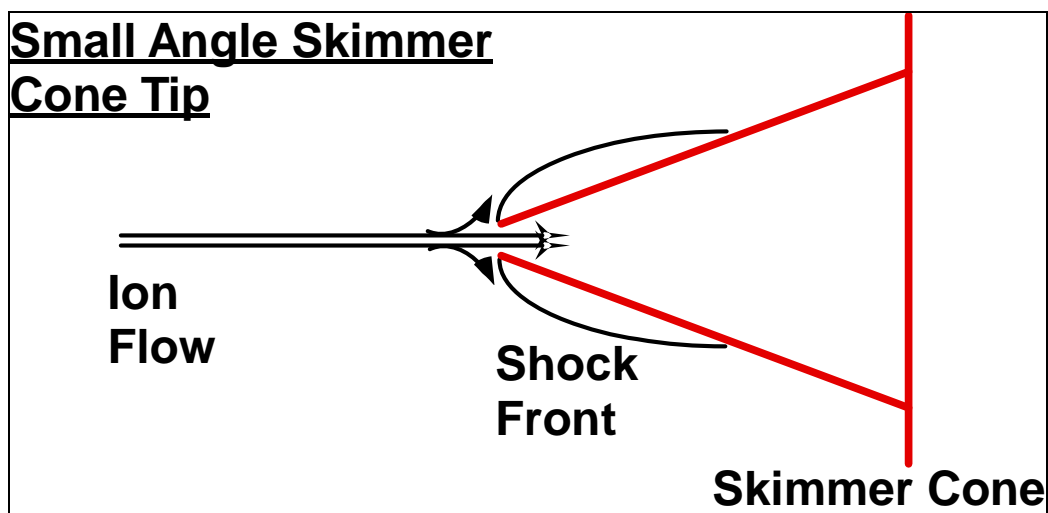


Figure 83. The Deflected Shock at a Small Tip Angle Skimmer Cone.

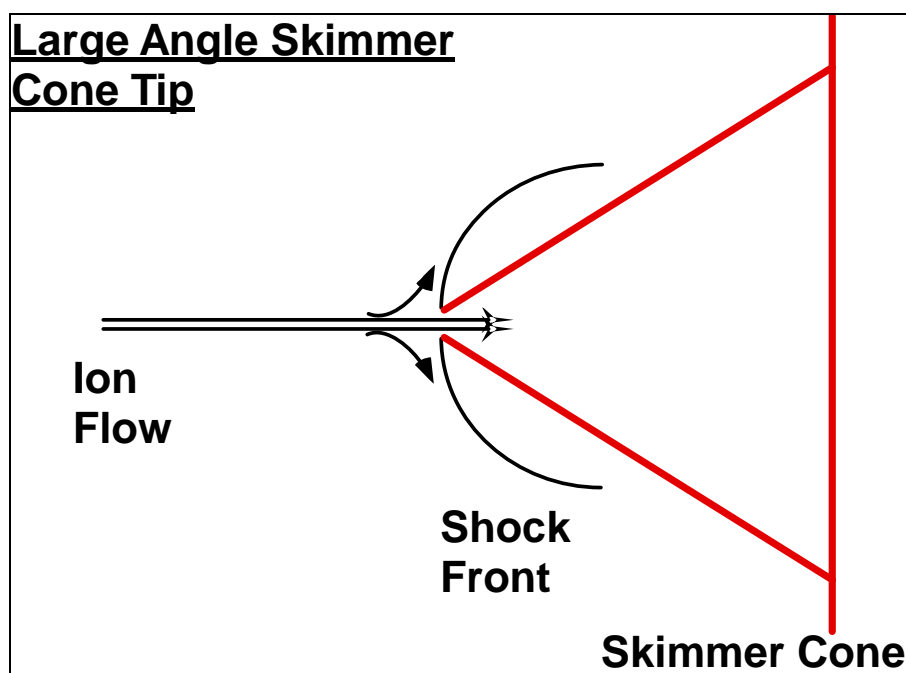


Figure 84. The Deflected Shock at a Large Tip Angle Skimmer Cone.

Based on the idea that a skimmer cone exhibiting a large tip angle deflects the bulk ion flow further away from the orifice a structure was proposed to fit into the ICP-MS interface that could deflect the bulk flow even further whilst allowing a limited, 'clean', ion flow through the skimmer orifice. By incorporating a plate with an orifice at the centre 1 mm ahead of the skimmer tip this enhanced deflection could be

achieved and then the majority of ion deposition could take place elsewhere in the expansion chamber. The proposed structure can be seen in Figure 85.

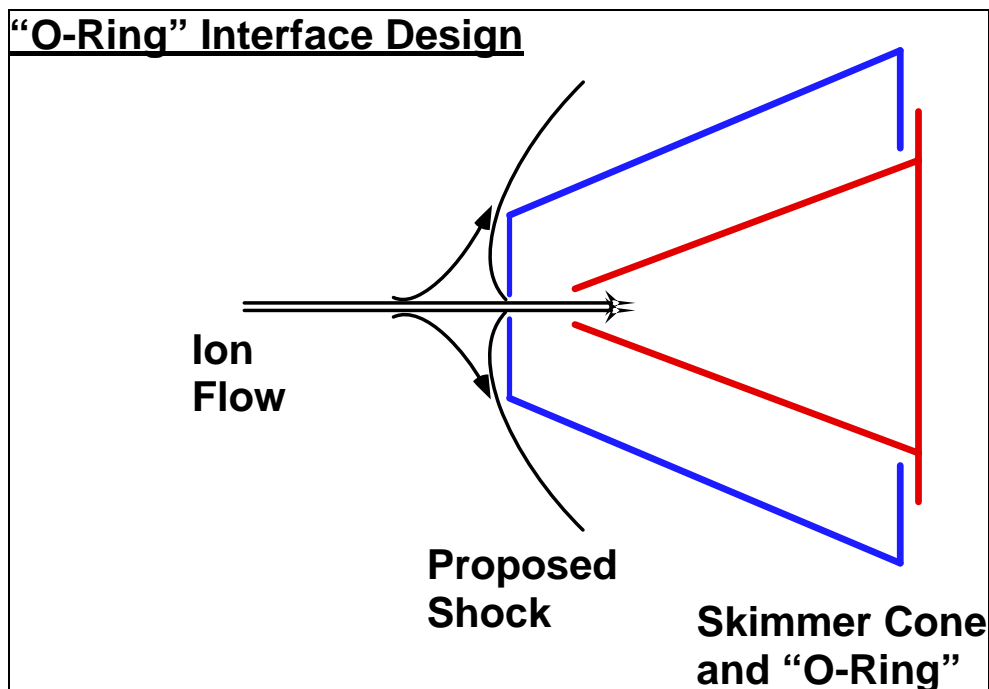


Figure 85. The Suggested Deflected Shock Arising from Supersonic Flow Against an Additional Plate and Orifice.

Prior to the manufacture and implementation of such a structure the environment of the ICP-MS interface region must first be fully appreciated. Due to the massive reduction in pressure in the expansion chamber, compared to the atmospheric pressure ICP ion source, the local volume of the ion flow is drastically increased to compensate according to the ideal gas equation ($PV = nRT$). This increase in volume is described as the adiabatic expansion. As can be seen in the equation of Figure 87, the temperature of the expansion region is related to both the temperature of the ICP source and the velocity of the ion flow (i.e. the Mach number). So, as the velocity of the flow increases the temperature within the expansion region decreases due to the conversion of energy (see section 5.3.1). An exception to this, however, is when the ion flow comes into contact with a surface and is brought to a halt. When this occurs the local temperature elevates. To accommodate such elevated temperatures at

surfaces within the region cooling is required, hence the cooling of sample and skimmer cones by a water flow system seen in all ICP-MS instruments.

It is for this reason that any additional structures, that were to be placed within the ICP-MS interface, had to be manufactured from a material exhibiting a very high melting point as they would be standing independently of the chamber cooling system. Before selection of a material that could be used for this work the temperatures of the expansion chamber were evaluated, see section 5.3.1.

5.3.1. The Temperature Environment of an ICP-MS Interface Expansion Chamber

Due to the nature and design of an ICP-MS instrument there are a number of factors that affect the temperature environment of the interface expansion chamber. The conditions at the ICP ion source, the pressure of the expansion chamber and the ion velocity through it all contribute to the local temperature. A series of equations have been published that describe the temperature, pressure and ion velocity conditions of the interface expansion chamber, many of which are employed in this chapter to justify certain work.⁴ For this section, two such equations were used to establish the temperature conditions of the expansion chamber and hence provide the information required in the selection of a material for production of an additional structure, see Figures 86 and 87.

$$\frac{P_0}{P_i} = \left(1 + \frac{\gamma - 1}{2} M^2 \right)^{\gamma/(\gamma-1)}$$

Where:

P₀: **Pressure Within the Ion Source**

P_i: **Pressure Within the Isentropic Core of the Expansion**

γ: **Ratio of Heat Capacity at Constant Pressure to Heat Capacity at Constant Volume**

M: **Mach Number**

Figure 86. An Equation Comparing Pre/Post Sampler Orifice Pressures with Mach Number.

$$\frac{T_0}{T_i} = 1 + \frac{\gamma - 1}{2} M^2$$

Where:

T₀: **Temperature Within the Ion Source**

T_i: **Temperature Within the Isentropic Core of the Expansion**

γ: **Ratio of Heat Capacity at Constant Pressure to Heat Capacity at Constant Volume**

M: **Mach Number**

Figure 87. An Equation Comparing Pre/Post Sampler Orifice Temperatures with Mach Number.

Using the equations of Figures 86 and 87 the temperature within the expansion chamber was calculated based on certain information and assumptions. This temperature was based on ICP ion source pressures and temperatures of 1 Bar and 8 000 K respectively and an expansion chamber pressure of 2 mBar. One further assumption made prior to calculation was that the ratio of heat capacity at constant

pressure to heat capacity at constant volume (γ) was 5/3, i.e. it was a parameter based on the assumption that the only gaseous species entering the expansion chamber was Ar.

So using this information and assumption the equation of Figure 86 was used to calculate the mach number of the ion flow in the chamber. This mach number data was then used to calculate a temperature of the expansion chamber, using the equation of Figure 87, of 667 K. Therefore a material had to be selected to withstand 667 K. Tantalum metal was therefore selected for manufacture of this interface structure due to its high melting point (3269 K).¹³⁵

5.3.2. Manufacture and Testing of an Adapted ICP-MS Interface for the Reduction of Ion Deposition

Two attempts were made at the construction and testing of an ICP-MS interface adaptation intended for the reduction of ion deposition on the skimmer cone. The work carried out on such an adaptation is described as follows.

Construction and Testing: First Attempt

A first attempt at the construction of a tantalum interface adaptation was carried out such that a flat plate of 4.8 mm diameter and 0.25 mm thickness was positioned 1 mm ahead of the tip of an Xi skimmer cone. This plate was held in position by tantalum rods (1.5 mm thick, rod angles of 56 degrees) attached to a base ring (17.95 mm wide and 1 mm thick) that was held in place over the skimmer cone using two screws, see Figure 135 for a schematic of the similar four rod design. Each component of this structure was welded together using a Nd:YAG laser (Starworld Performance, SWP 5002, $\lambda = 1.06 \mu\text{m}$) at the Loughborough University School of Art and Design (LUSAD).

The first attempt at construction of this adaptation involved the top plate being held in place by two parallel rods. Following welding, initial experimentation was carried out to determine whether or not this structure could withstand the expansion chamber environment. The structure was held in place, over the skimmer cone, in the expansion chamber and the ICP ion source was established. The plasma was operated for a 10 minute period whilst introducing deionised water only via the standard Micromist 100 $\mu\text{l min}^{-1}$ nebuliser and impact bead spray chamber arrangement.

Following this initial experimentation it was determined that the expansion chamber temperature was not a problem for the tantalum metal with regard to mechanical stability of the structure. However, two problems were revealed which denied the opportunity to study the effects of the presence of this adaptation on the mass spectrum.

Firstly, it appeared that within this expansion region the tantalum metal was subject to reactions due to the environment to which it was exposed. On removal of the structure from the expansion chamber, sections of the top plate and supporting rods appeared to have lost a top layer of the metal revealing a 'grainy' surface to the metal. It was also noticed that a white substance had formed on the plate which has, so far, remained unidentified as its colour did not correspond to the common tantalum reaction products.

The structure was also removed from the expansion chamber carrying a certain amount of damage. The plate had bent slightly against the rods at the points at which they were welded and a crack had appeared on one side of the plate at the origin of one of these bends. This bending may have taken place due to a 'drag' effect where the adiabatic shock within the expansion chamber met the plate.

Construction and Testing: Second Attempt

A second attempt at construction of this interface adaptation was carried out. Again tantalum was used in its construction and the individual sections were welded together with the Nd:YAG laser at LUSAD. This time the design was changed slightly with

the plate being held in place by two pairs of parallel rods rather than just one, the aim being to enhance the mechanical strength of the structure and provide greater resistance to the potential ‘drag’ effect against the plate. A diagram of this second interface adaptation design can be seen in Figure 88. Prior to testing in the ICP-MS interface, the second tantalum structure was heated in a furnace to 450 °C in order to form an oxidised surface. It was hoped that such action would render the structure surface less chemically reactive in the expansion chamber.

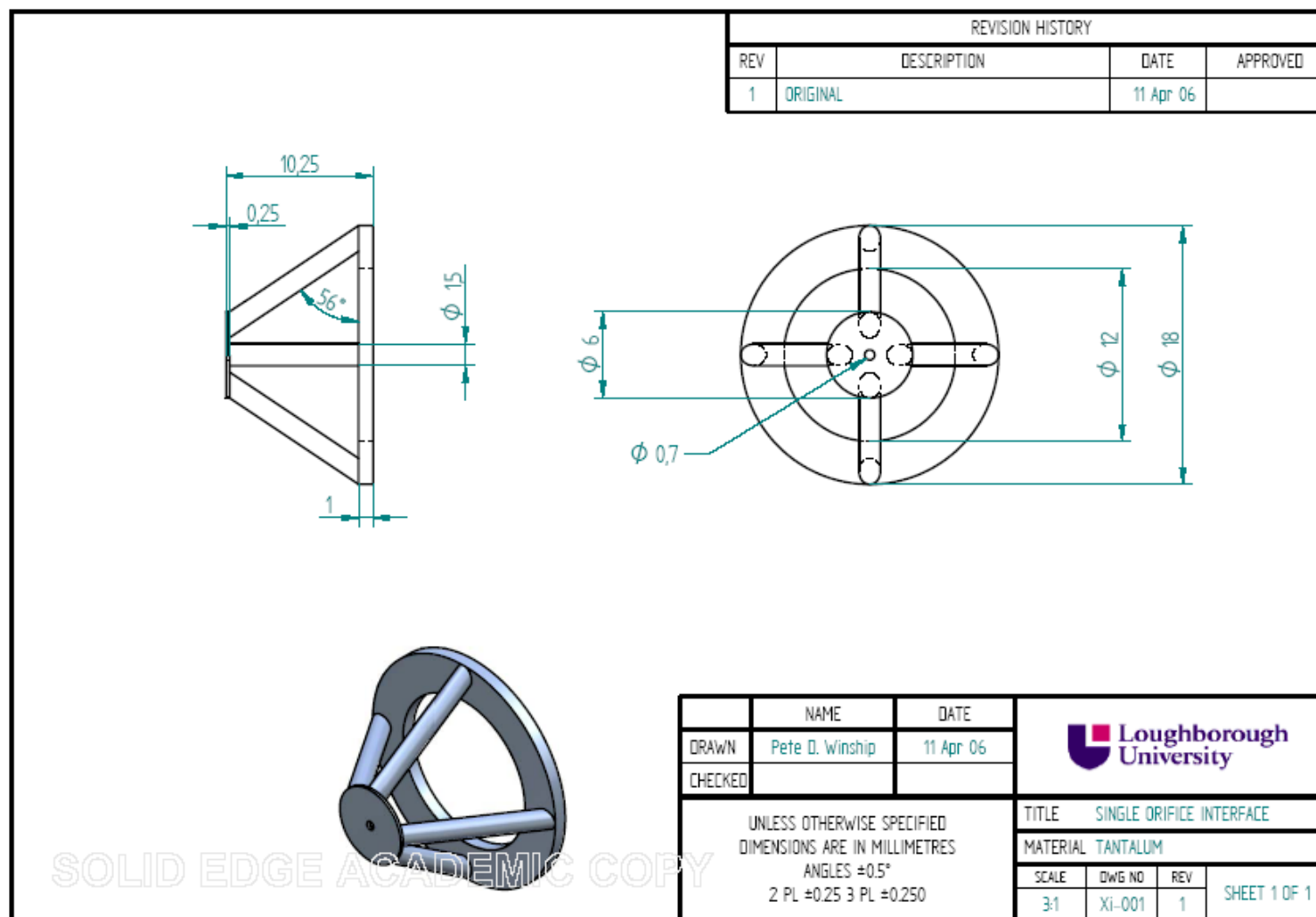


Figure 88. A Schematic of the Second (Four Rod) ICP-MS Interface Structure.

Similar to the first design, initial experimentation was carried out on this second structure to establish its stability within the expansion chamber. This time there was no damage to the structure and the degree of metal layer removal and deposition of the unknown substance was far less than with the first design. So, following this successful work, further experimentation was undertaken to establish the effect of the presence of this structure on the mass spectrum. Prior to positioning the structure in the interface the ICP-MS instrument was tuned, stabilised and tested to ensure that it was producing desirable signals. With the structure in place the mass spectrum was monitored when introducing deionised water and $1\ \mu\text{g l}^{-1}$ In, Pb, U and Li solutions. Unfortunately, with the structure in place, the signals observed at nearly all m/z 's were next to nothing and the only difference that manipulation of the instrument parameters made to this was a slight enhancement of the $^{40}\text{Ar}^+$ ($m/z = 40$) and $^{40}\text{Ar}_2^+$ ($m/z = 80$) signals.

It is believed that this limitation of the instrument signal was due to the orifice of the plate being far too small. It is thought that the shock being created at the plate is scattering the sample ions and not allowing transport through the orifice and into the skimmer cone. Therefore, a plate with a larger orifice at the centre is required.

5.3.3. The Development of an Adapted ICP-MS Interface for the Reduction of Ion Deposition: Conclusion

Although, through incorporation of both structure designs in the ICP-MS interface, there was no beneficial effect achieved there is great potential in this work to develop the interface region for the reduction of ion deposition. As mentioned in section 5.3.2 the plate of this structure may require changing with the orifice size possibly being the key to generating a beneficial shock deflection whilst allowing ions through the skimmer orifice. Such change to the structure design would be the first area of future work for this idea as well as the study of the distance between the plate and skimmer tip and the material used in production.

5.4. The Development of an ICP-MS Interface with a Gradual Pressure Reduction

As mentioned in sections 1.3 and 5.1.2 one of the significant problems associated with the ICP-MS instrument is that of the ion kinetic energy spread that occurs due to the rollercoaster to which ions are exposed. One of the greatest contributors to this ion kinetic energy spread is the acceleration of ions in the expansion chamber during the transition from atmospheric pressure (≈ 1 Bar) to low pressure (≈ 2 mBar). It is thought that the energy spread could be reduced by transporting ions from the ICP to the mass analyser whilst limiting them to subsonic velocities. This section of Chapter 5 assesses the feasibility of such an approach.

5.4.1. The Transitions Required for a Gradual Interface Pressure Reduction

Using the equation of Figure 86 the pressures required during a step-down from 1 Bar at the ICP ion source to vacuum conditions at the mass analyser ($\approx 1.33 \times 10^{-9}$ Bar) were calculated assuming that the ion velocity doesn't exceed a mach number of 1. For these calculations mach number was assumed to be 0.95. The calculated transition pressures and the number of transition 'chambers' required to achieve a subsonic reduction can be seen in Table 52.

Table 52. Calculated Transition Pressures and Numbers of Transition ‘Chambers’ for a Gradual Pressure Reduction in the ICP-MS Interface.

Transition Number	Transition ‘Chamber’ Description	Initial Pressure (mBar)	Final Pressure (mBar)
1	Atmospheric Pressure → Chamber 1	1000	630
2	Chamber 1 → Chamber 2	630	396
3	Chamber 2 → Chamber 3	396	250
4	Chamber 3 → Chamber 4	250	157
5	Chamber 4 → Chamber 5	157	98.9
6	Chamber 5 → Chamber 6	98.9	62.3
7	Chamber 6 → Chamber 7	62.3	39.2
8	Chamber 7 → Chamber 8	39.2	24.7
9	Chamber 8 → Chamber 9	24.7	15.5
10	Chamber 9 → Chamber 10	15.5	9.78
11	Chamber 10 → Chamber 11	9.78	6.16
12	Chamber 11 → Chamber 12	6.16	3.88
13	Chamber 12 → Chamber 13	3.88	2.44
14	Chamber 13 → Chamber 14	2.44	1.54
15	Chamber 14 → Chamber 15	1.54	0.97
16	Chamber 15 → Chamber 16	0.97	0.61
17	Chamber 16 → Chamber 17	0.61	0.38
18	Chamber 17 → Chamber 18	0.38	0.24
19	Chamber 18 → Chamber 19	0.24	0.15
20	Chamber 19 → Chamber 20	0.15	9.56×10^{-2}
21	Chamber 20 → Chamber 21	9.56×10^{-2}	6.02×10^{-2}
22	Chamber 21 → Chamber 22	6.02×10^{-2}	3.79×10^{-2}
23	Chamber 22 → Chamber 23	3.79×10^{-2}	2.39×10^{-2}
24	Chamber 23 → Chamber 24	2.39×10^{-2}	1.50×10^{-2}
25	Chamber 24 → Chamber 25	1.50×10^{-2}	9.46×10^{-3}
26	Chamber 25 → Chamber 26	9.46×10^{-3}	5.96×10^{-3}
27	Chamber 26 → Chamber 27	5.96×10^{-3}	3.75×10^{-3}
28	Chamber 27 → Chamber 28	3.75×10^{-3}	2.36×10^{-3}
29	Chamber 28 → Chamber 29	2.36×10^{-3}	1.49×10^{-3}
30	Chamber 29 → Chamber 30	1.49×10^{-3}	9.36×10^{-4}
31	Chamber 30 → Chamber 31	9.36×10^{-4}	5.89×10^{-4}
32	Chamber 31 → Chamber 32	5.89×10^{-4}	3.71×10^{-4}
33	Chamber 32 → Chamber 33	3.71×10^{-4}	2.33×10^{-4}
34	Chamber 33 → Chamber 34	2.33×10^{-4}	1.47×10^{-4}

Table 52 Continued. Calculated Transition Pressures and Numbers of Transition ‘Chambers’ for a Gradual Pressure Reduction in the ICP-MS Interface.

Transition Number	Transition ‘Chamber’ Description	Initial Pressure (mBar)	Final Pressure (mBar)
35	Chamber 34 → Chamber 35	1.47×10^{-4}	9.25×10^{-5}
36	Chamber 35 → Chamber 36	9.25×10^{-5}	5.82×10^{-5}
37	Chamber 36 → Chamber 37	5.82×10^{-5}	3.67×10^{-5}
38	Chamber 37 → Chamber 38	3.67×10^{-5}	2.31×10^{-5}
39	Chamber 38 → Chamber 39	2.31×10^{-5}	1.45×10^{-5}
40	Chamber 39 → Chamber 40	1.45×10^{-5}	9.15×10^{-6}
41	Chamber 40 → Chamber 41	9.15×10^{-6}	5.76×10^{-6}
42	Chamber 41 → Chamber 42	5.76×10^{-6}	3.63×10^{-6}
43	Chamber 42 → Chamber 43	3.63×10^{-6}	2.28×10^{-6}
44	Chamber 43 → Chamber 44	2.28×10^{-6}	1.44×10^{-6}
45	Chamber 44 → Chamber 45	1.44×10^{-6}	9.05×10^{-7}
46	Chamber 45 → Chamber 46	9.05×10^{-7}	5.70×10^{-7}

As can be seen from Table 52, to successfully transport ions between the ICP and the mass analyser without them exceeding a mach number of 0.95 they would have to pass through forty-six transitions. The construction of an ICP-MS interface consisting of forty-six separately pressurised chambers would be impractical unless close to 100 % ion transmission could be guaranteed between the sample cone and the mass analyser. As previously described, see section 5.2.3, it has been shown that analytical benefit can be obtained by incorporating further pressurised chambers into the interface region but this work has certainly not gone to the lengths of incorporating forty-six of them.

5.4.2. A Potential Approach to a Gradual Interface Pressure Reduction

An approach to an ICP-MS interface adaptation that could allow a gradual pressure reduction is still in the concept and design stages. It may be possible to construct a

small interface adaptation to sit between the sample and skimmer cones to restrict transport of ions at supersonic velocities. Initial ideas include the use of an open plate stack design, with orifices through the centre of each for the transmission of ions, fitted horizontally. Taking advantage of the pressure in the expansion chamber, it may be possible to create localised pressures at different points in this region. A structure composed of a series of plates held in place by parallel rods, fixed at a base plate, may allow the creation of progressively lower localised pressures between the two cones. Whilst maintaining regular pumping in the expansion chamber it is believed that varying the distance between the plates of such a structure could create the desired effect. A diagram of the potential structure described in this section can be seen in Figure 89.

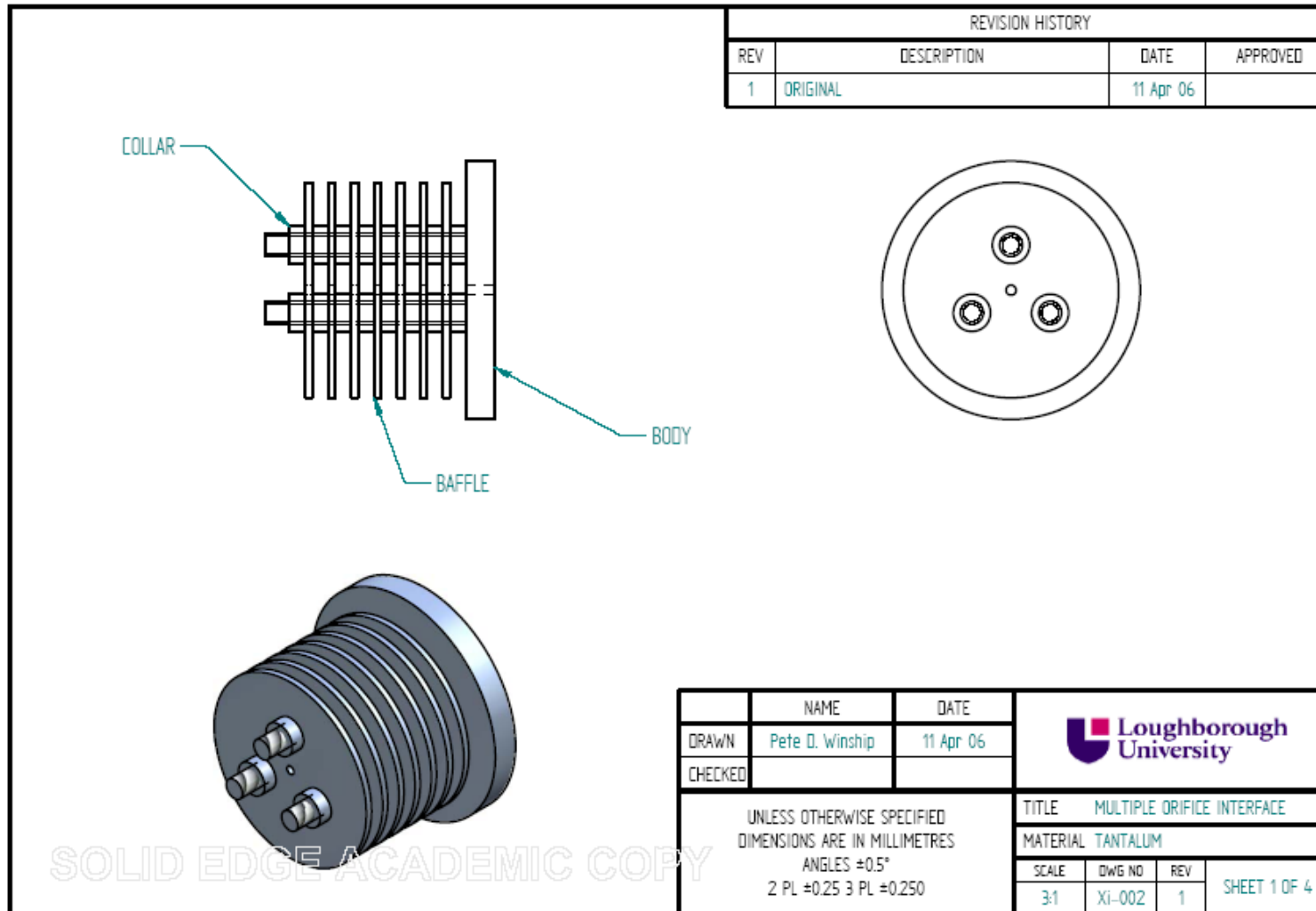


Figure 89. A Diagram Showing a Potential Plate Stack Interface Structure Design for the Gradual Reduction of Pressure in the Expansion Chamber.

5.4.3. The Development of an ICP-MS Interface with a Gradual Pressure Reduction: Conclusion

Although the transport of ions through the ICP-MS interface at subsonic velocities would require forty-six pressure transitions, a well conceived and designed interface region may be able to accomplish this. The addition of a structure between the sample cone and mass analyser may be the way forward for this kind of work but what is more likely is that the interface region may have to be completely redesigned to achieve this aim. The addition of a series of plates with an orifice at the centre of each may provide a benefit with regard to limiting ion velocity but such an arrangement would incorporate a further problem in the form a greater surface area for ion deposition and degradation of ion transmission.

5.5. Conclusions

This chapter has highlighted certain problems associated with the current ICP-MS interface region. Although the ion deposition problem can be overcome by cautious sample preparation and analysis it is the ion kinetic energy problem that, if overcome, could define the next generation of ICP-MS instrumentation.

What the work of this chapter has shown is that the positioning of additional structures within the ICP-MS interface can be a feasible approach to changing interface conditions. With good design the addition of such structures will allow research to be carried out on this region with relatively low cost and without significant change to the instrument. Within this chapter further work has been highlighted for continuation of what has been carried out so far.

Following presentation of this interface work to representatives of the Thermo Electron Corporation at the Winsford factory on 9th December 2005, interest has been shown by the sponsors of this research in furthering this work by their research and development group.

Chapter 6

General Conclusions and Future Work

6.1. The Development of Methods for the Determination of ^{31}P and ^{32}S Isotopes by ICP-MS

Collision cell technology and the ‘cold/cool plasma’ approach are two techniques used within ICP-MS that can be employed to overcome certain spectroscopic interferences. Four final methods, of six originally conceived, were successfully developed for the determination of ^{31}P and ^{32}S isotopes by quadrupole based ICP-MS. Of these four methods two were based on the use of a hexapole collision cell with He or O_2 collision/reaction gases whilst two were based on the use of a ‘cold/cool plasma’ with and without a supplementary O_2 flow through the central channel of the ICP. Each of these four methods was calibrated and limits of detection were established that were comparable to those previously published. With access to a ‘clean-room’ and ultra pure reagents the limits of detection for these methods may be superior to those previously published.

6.1.1. Hexapole Collision Cell Methods

Two collision cell methods were developed to determine ^{31}P and ^{32}S isotopes whilst overcoming the spectroscopic interferences at $m/z = 31$ and 32 , respectively. One of these methods employed an O_2 reaction gas leading to the formation of the oxide species $^{31}\text{P}^{16}\text{O}^+$ and $^{32}\text{S}^{16}\text{O}^+$ that can be measured at $m/z = 47$ and 48 , respectively therefore avoiding native spectroscopic interferences at $m/z = 31$ and 32 . The $^{47,48}\text{Ti}$ isotopes do not hinder measurement of these oxide species as they are also oxidised and moved to $m/z = 63$ and 64 in the mass spectrum. The ion kinetic energy effect (IKEE), see section 1.3.3 in Chapter 1, was used to maximise the formation of these oxide species. The limits of detection obtained by this method were $0.69 \mu\text{g l}^{-1}$ to $9.50 \mu\text{g l}^{-1}$ for ^{31}P measurement and $1.43 \mu\text{g l}^{-1}$ to $6.50 \mu\text{g l}^{-1}$ for ^{32}S measurement. The LOD’s obtained via this method are comparable to those published by Bandura *et al* showing that the measurement of ^{31}P and ^{32}S isotopes by this approach is very similar between the use of a collision cell and a dynamic reaction cell.⁹⁰

The second successfully developed collision cell method employed a He collision gas used in conjunction with kinetic energy discrimination (KED), see section 1.3.3 of Chapter 1, to allow the transmission of $^{31}\text{P}^+$ ions through the hexapole whilst restricting the passage of cell formed polyatomic ions that could interfere with the $m/z = 31$ signal. The limit of detection obtained by this method for the measurement of ^{31}P was $1.48\ \mu\text{g l}^{-1}$ to $7.78\ \mu\text{g l}^{-1}$. Such an LOD for the measurement of ^{31}P is similar to that obtained employing the O_2 collision cell method.

6.1.2. ‘Cold/Cool Plasma’ Methods

Two ‘cold/cool plasma’ methods were developed to determine ^{31}P and ^{32}S isotopes whilst overcoming the spectroscopic interferences at $m/z = 31$ and 32 . These methods are very similar with the second being a development of the first.

The first ‘cold/cool plasma’ method employed an ICP with a forward power of 800 W. Such an ICP operates at a lower temperature which leads to the significant formation of metal oxides. Similar to the first collision cell method, the oxide species $^{31}\text{P}^{16}\text{O}^+$ and $^{32}\text{S}^{16}\text{O}^+$ are readily formed at this forward power and can be measured at $m/z = 47$ and 48 therefore avoiding native spectroscopic interferences at $m/z = 31$ and 32 , respectively. The limits of detection obtained by this method were $0.89\ \mu\text{g l}^{-1}$ to $6.56\ \mu\text{g l}^{-1}$ for ^{31}P measurement and $6.84\ \mu\text{g l}^{-1}$ to $25\ \mu\text{g l}^{-1}$ for ^{32}S measurement. The second successful ‘cold/cool plasma’ method was a development of the first whereby the same 800 W ICP was employed with an additional O_2 nebuliser gas flow to maximise the formation of the $^{31}\text{P}^{16}\text{O}^+$ and $^{32}\text{S}^{16}\text{O}^+$ species ($m/z = 47$ and 48 measurement respectively). The limits of detection obtained by this method were $0.74\ \mu\text{g l}^{-1}$ to $14\ \mu\text{g l}^{-1}$ for ^{31}P measurement and $1.23\ \mu\text{g l}^{-1}$ to $80\ \mu\text{g l}^{-1}$ for ^{32}S measurement. It should be noted that the LOD’s obtained employing these two ‘cold/cool plasma’ methods are similar to those obtained by the collision cell methods. Therefore, for the determination of ^{31}P and ^{32}S isotopes in samples that are not too complex, the use of one of these ‘cold/cool plasma’ methods is recommended for laboratories that do not have access to collision cell or DRC technology.

6.2. The Application of Methods Developed for the Determination of ^{31}P and ^{32}S Isotopes by ICP-MS

The four successfully developed ICP-MS methods were evaluated for the analysis of DNA and DNA components via the measurement of the ^{31}P isotope. These methods were used in the quantification of DNA, the study of DNA components within an agarose gel, the study of polymerase chain reaction (PCR) and the study of single nucleotide polymorphisms.

Each of the four methods were evaluated for their ability to quantify DNA via the measurement of ^{31}P content. Each method produced reliable data when DNA solutions were analysed. However, the limits of detection of these methods were significantly inferior to those exhibited by fluorescence or UV methods. For this reason ICP-MS will not replace fluorescence in such applications but will be important in areas such as metallo-drug or protein-drug efficacy testing as illustrated in the work on Pt based anti-cancer drugs in Chapter 4.

The collision cell method employing an O_2 reaction gas was used in the analysis of digested agarose gels containing separated DNA. The data generated from this analysis showed that this approach can provide quantitative information but again it can't compete with the well established fluorescence or UV methods.

The progression of a PCR process was studied employing the collision cell method using an O_2 reaction gas. Unfortunately this method was not sensitive enough to measure the changes in ^{31}P concentration as the replication took place. Again, this method cannot compete with the well established fluorescence and UV methods.

The O_2 collision cell and first 'cold/cool plasma' methods were employed in the study of nucleotide sequences differing in structure by one base molecule. The aim of this work was to establish whether ICP-MS could be used to study single nucleotide polymorphisms. Online HPLC was used to separate these nucleotides before measurement via UV spectrophotometry and the ^{31}P isotope by ICP-MS. Of the two ICP-MS methods employed the collision cell approach was successful whilst the

‘cold/cool plasma’ wasn’t. The reason for this was that the standard ICP used with the collision cell was robust enough to handle the mobile phase eluting from the HPLC column whilst the reduced forward power plasma was not. The work carried out during the study of these nucleotides has shown that ICP-MS has potential for the analysis of single nucleotide polymorphisms.

6.3. The Analysis of Platinum Based Anti-Cancer Drugs and DNA by ICP-MS

Cisplatin and oxaliplatin are two platinum based complexes that are used in the treatment of a range of cancers. These two drugs bind with DNA within the cell nucleus and inhibit replication processes leading to apoptosis. Treatment with both of these drugs is relatively harsh so efficacy is a major issue. Currently there is not a fast and inexpensive test to establish efficacy of these drugs for individual patients. ICP-MS was used to study the interaction of these drugs with their DNA target and establish binding constant and adduct data that could be used as the basis of an efficacy test.

Five studies were undertaken to observe the interaction between these drugs and their biological target. Although the first of these studies was unsuccessful due to complications regarding the method employed the subsequent studies revealed several issues. Firstly ICP-QMS was capable of the measurement of Pt in these samples down to the lowest concentrations studied, i.e. in the region of 1 drug molecule to 500 000 DNA nucleotides for both drug complexes, which is beyond the suggested therapeutic region of 1 drug molecule to 400 000 DNA nucleotides. The second to fifth studies carried out showed that there is a significant difference in binding strength between inter- and intra-strand covalent binding *in vitro*. Further work in this area may be able to relate the type of covalent binding with drug efficacy. Finally the binding data calculated, in the form of 'K_f data' and the number of adducts formed, has shown that the binding between drug and target is particularly inefficient and that there is agreement with Akaboshi *et al* and Jamieson *et al* who have published data describing the number of Pt atoms that bind per DNA molecule when exposing DNA to these drugs.^{162, 186}

Further work is required in this area prior to the development of an efficacy test, however, significant advances were made through the work described here to guide the remaining work which would hopefully be straight forward.

6.4. The Development of ICP-MS Interface Structures

The work described in Chapter 5 has highlighted certain problems regarding the design of the current ICP-MS interface region. Although, as previously described, the problem of ion and material deposition can be limited through cautious sample preparation, the solution of the ion kinetic energy problem could be the defining quality of the next generation of ICP-MS instrumentation.

The work of Chapter 5 showed that the placing of additional structures within the ICP-MS interface can be a feasible approach to varying the interface conditions. Good design of such structures would allow further research to be carried out on this region at reasonable cost and without significant alteration of the instrument. As described in Chapter 5, further work has been highlighted for continuation of what has been carried out so far. It should be noted, however, that the work described in this chapter is, to a certain degree, specific for a PQ ExCell ICP-QMS instrument as the interface region is easily accessible. This is not the case for certain other types of ICP-QMS instrument, such as the Perkin Elmer Elan 6100, which are either more enclosed or exhibit less space to carry out this type of work.

As mentioned previously, following presentation of this interface work to representatives of the Thermo Electron Corporation at the Winsford factory on 9th December 2005, interest has been shown by the sponsors in furthering this work by their research and development group.

References

- 1 L. H. J. Lajunen and P. Peramaki, 'Spectrochemical Analysis by Atomic Absorption and Emission', The Royal Society of Chemistry, 2004.
- 2 D. A. Skoog, D. M. West, and F. J. Holler, 'Fundamentals of Analytical Chemistry', Harcourt Brace and Company, 1996.
- 3 L. H. J. Lajunen, 'Spectrochemical Analysis by Atomic Absorption and Emission', The Royal Society of Chemistry, 1992.
- 4 A. Montaser, 'Inductively Coupled Plasma Mass Spectrometry', Wiley-VCH, 1998.
- 5 M. Thompson and J. N. Walsh, 'Handbook of Inductively Coupled Plasma Spectrometry', Blackie Academic and Professional, 1989.
- 6 Thermo-Elemental, in 'Relative Abundance of Naturally Occurring Isotopes'.
- 7 K. E. Jarvis, A. L. Gray, and R. S. Houk, 'Handbook of Inductively Coupled Plasma Mass Spectrometry', Blackie and Son Ltd, 1992.
- 8 'Applications of Plasma Source Mass Spectrometry II', ed. G. Holland and A. N. Eaton, The Royal Society of Chemistry, 1993.
- 9 'Plasma Source Mass Spectrometry, Developments and Applications', ed. G. Holland and S. D. Tanner, The Royal Society of Chemistry, 1997.
- 10 'Plasma Source Mass Spectrometry, New Developments and Applications', ed. G. Holland and S. D. Tanner, Royal Society of Chemistry, 1999.
- 11 'Plasma Source Mass Spectrometry, The New Millenium', ed. G. Holland and S. D. Tanner, The Royal Society of Chemistry, 2001.
- 12 'Plasma Source Mass Spectrometry, Applications and Emerging Technologies', ed. G. Holland and S. D. Tanner, The Royal Society of Chemistry, 2003.
- 13 L. C. Alves, M. G. Minnich, D. R. Wiederin, and R. S. Houk, *Journal of Analytical Atomic Spectrometry*, 1994, **9**, 399.
- 14 M. Ayras, H. Niskavaara, I. Bogatyrev, V. Chekushin, V. Pavlov, P. d. Caritat, J. H. Halleraker, T. E. Finne, G. Kashulina, and C. Reimann, *Journal of Geochemical Exploration*, 1997, **58**, 269.
- 15 S. F. Boulyga and J. S. Becker, *Journal of Analytical Atomic Spectrometry*, 2002, **17**, 1202.
- 16 S. F. Boulyga, H. Dietze, and J. S. Becker, *Mikrochimica Acta*, 2001, **137**, 93.
- 17 Y. Chang and S. Jiang, *Journal of Analytical Atomic Spectrometry*, 2001, **16**, 858.
- 18 Y. Chang and S. Jiang, *Journal of Analytical Atomic Spectrometry*, 2001, **16**, 1434.
- 19 M. Edler, N. Jakubowski, and M. Linscheid, *Analytical and Bioanalytical Chemistry*, 2005, **381**, 205.
- 20 J. L. Gomez-Ariza, T. Garcia-Barrera, F. Lorenzo, V. Bernal, M. J. Villegas, and V. Oliveira, *Analytica Chimica Acta*, 2004, **524**, 15.
- 21 D. Gunther, B. Hattendorf, and A. Audetat, *Journal of Analytical Atomic Spectrometry*, 2001, **16**, 1085.
- 22 J. Hinrichs and B. Schnetger, *The Analyst*, 1999, **124**, 927.
- 23 P. Leonhard, R. Pepelnik, A. Prange, N. Yamada, and T. Yamada, *Journal of Analytical Atomic Spectrometry*, 2002, **17**, 189.
- 24 T. Lindemann and H. Hintelmann, *Analytical Chemistry*, 2002, **74**, 4602.
- 25 H. T. Liu and S. J. Jiang, *Journal of Analytical Atomic Spectrometry*, 2002, **17**, 556.
- 26 J. K. Nicholson, J. C. Lindon, G. Scarfe, I. D. Wilson, F. Abou-Shakra, J. Castro-Perez, A. Eaton, and S. Preece, *The Analyst*, 2000, **125**, 235.

- 27 J. A. Nobrega, Y. Gelinas, A. Krushevska, and R. M. Barnes, *Journal of Analytical Atomic Spectrometry*, 1997, **12**, 1243.
- 28 C. J. Park and J. K. Suh, *Journal of Analytical Atomic Spectrometry*, 1997, **12**, 573.
- 29 W. T. Perkins, N. J. G. Pearce, and R. Fuge, *Journal of Analytical Atomic Spectrometry*, 1992, **7**, 611.
- 30 M. Resano, M. Verstraete, F. Vanhaecke, L. Moens, A. van-Alphen, and E. R. Denoyer, *Journal of Analytical Atomic Spectrometry*, 2000, **15**, 389.
- 31 N. B. Roberts, H. P. J. Walsh, L. Klenerman, S. A. Kelly, and T. R. Helliwell, *Journal of Analytical Atomic Spectrometry*, 1996, **11**, 133.
- 32 A. Sanz-Medel, M. Montes-Bayon, and M. L. F. Sanchez, *Analytical and Bioanalytical Chemistry*, 2003, **377**, 236.
- 33 S. D. Tanner, V. I. Baranov, and D. R. Bandura, *Spectrochimica Acta Part B-Atomic Spectroscopy*, 2002, **57**, 1361.
- 34 J. Turner, S. J. Hill, E. H. Evans, and B. Fairman, *Journal of Analytical Atomic Spectrometry*, 1999, **14**, 121.
- 35 S. Uchida, R. Garcia-Tenorio, K. Tagami, and M. Garcia-Leon, *Journal of Analytical Atomic Spectrometry*, 2000, **0**, 1.
- 36 H. Vanhoe, J. Goossens, L. Moens, and R. Dams, *Journal of Analytical Atomic Spectrometry*, 1994, **9**, 177.
- 37 E. Webb, D. Amarasiriwardena, S. Tauch, E. F. Green, J. Jones, and A. H. Goodman, *Microchemical Journal*, 2005, **81**, 201.
- 38 H. Wildner, *Journal of Analytical Atomic Spectrometry*, 1998, **13**, 573.
- 39 E. d. Hoffmann and V. Stroobant, 'Mass Spectrometry - Principles and Applications', John Wiley and Sons, 2002.
- 40 R. S. Houk, V. A. Fassel, G. D. Flesch, H. J. Svec, A. L. Gray, and C. E. Taylor, *Analytical Chemistry*, 1980, **52**, 2283.
- 41 R. S. Houk, *Analytical Chemistry*, 1986, **58**, A97.
- 42 L. Ebdon, A. Fisher, and S. J. Hill, 'An Introduction to Analytical Atomic Spectrometry', ed. E. H. Evans, John Wiley and Sons, 1998.
- 43 Thermo-Elemental, 'PQ ExCell Infinity Lens System and Collision Cell', 0262, Thermo Elemental, 2001.
- 44 G. Schaldach, H. Berndt, and B. L. Sharp, *Journal of Analytical Atomic Spectrometry*, 2003, **18**, 742.
- 45 B. L. Sharp, *Journal of Analytical Atomic Spectrometry*, 1988, **3**, 939.
- 46 B. L. Sharp, *Journal of Analytical Atomic Spectrometry*, 1988, **3**, 613.
- 47 D. M. Hughes, D. C. Gregoire, H. Naka, and C. L. Chakrabarti, *Spectrochimica Acta Part B-Atomic Spectroscopy*, 1997, **52**, 517.
- 48 H. Y. Li, B. M. Keohane, H. Z. Sun, and P. J. Sadler, *Journal of Analytical Atomic Spectrometry*, 1997, **12**, 1111.
- 49 M. L. Magnuson, J. T. Creed, and C. A. Brockhoff, *Journal of Analytical Atomic Spectrometry*, 1997, **12**, 689.
- 50 S. J. Santosa, H. Mokudai, and S. Tanaka, *Journal of Analytical Atomic Spectrometry*, 1997, **12**, 409.
- 51 S. D. Tanner and V. I. Baranov, *Atomic Spectroscopy*, 1999, **20**, 45.
- 52 D. R. Wiedner, F. G. Smith, and R. S. Houk, *Analytical Chemistry*, 1991, **63**, 219.
- 53 J. R. Encinar, L. Ouerdane, W. Buchmann, J. Tortajada, R. Lobinski, and J. Szpunar, *Analytical Chemistry*, 2003, **75**, 3765.
- 54 R. Lobinski and J. Szpunar, *Analytica Chimica Acta*, 1999, **400**, 321.

- 55 L. F. Sanchez and J. Szpunar, *Journal of Analytical Atomic Spectrometry*, 1999, **14**, 1697.
- 56 J. Szpunar, *Trends In Analytical Chemistry*, 2000, **19**, 127.
- 57 J. Szpunar, *The Analyst*, 2000, **125**, 963.
- 58 W. M. A. Niessen, 'Liquid Chromatography-Mass Spectrometry', ed. J. Cazes, Marcel Dekker, 1999.
- 59 Q. L. Xie, R. Kerrich, E. Irving, K. Liber, and F. Abou-Shakra, *Journal of Analytical Atomic Spectrometry*, 2002, **17**, 1037.
- 60 K. S. K. Danadurai, Y. L. Hsu, and S. J. Jiang, *Journal of Analytical Atomic Spectrometry*, 2002, **17**, 552.
- 61 F. Vanhaecke, M. Resano, and L. Moens, *Analytical and Bioanalytical Chemistry*, 2002, **374**, 188.
- 62 F. Vanhaecke, M. Resano, M. Pruneda-Lopez, and L. Moens, *Analytical Chemistry*, 2002, **74**, 6040.
- 63 H. Wildner and G. Wunsch, *Fresenius Journal of Analytical Chemistry*, 1998, **360**, 520.
- 64 D. Gunther, S. E. Jackson, and H. P. Longerich, *Spectrochimica Acta B*, 1999, **54**, 381.
- 65 M. Kinter and N. E. Sherman, 'Protein Sequencing and Identification using Tandem Mass Spectrometry', ed. D. M. Desiderio and N. M. M. Nibbering, John Wiley and Sons, 2000.
- 66 J. Barker, 'Mass Spectrometry', John Wiley and Sons, 1999.
- 67 P. E. Miller and M. B. Denton, *Journal of Chemical Education*, 1986, **63**, 617.
- 68 S. Spezia, B. Bocca, G. Forte, A. Gatti, G. Mincione, A. Ronchi, P. Bavazzano, A. Alimonte, and C. Minoia, *Rapid Communications in Mass Spectrometry*, 2005, **19**, 1551.
- 69 J. S. Becker and H. J. Dietze, *Journal of Analytical Atomic Spectrometry*, 1997, **12**, 881.
- 70 S. Sturup, M. Hansen, and C. Molgaard, *Journal of Analytical Atomic Spectrometry*, 1997, **12**, 919.
- 71 H. Wildner and R. Hearn, *Fresenius Journal of Analytical Chemistry*, 1998, **360**, 800.
- 72 S. D. Tanner, L. M. Cousins, and D. J. Douglas, *Applied Spectroscopy*, 1994, **48**, 1367.
- 73 T. W. May and R. H. Wiedmeyer, *Atomic Spectroscopy*, 1998, **19**, 150.
- 74 R. Thomas, *Spectroscopy*, 2002, **17**, 24.
- 75 A. L. Gray and J. G. Williams, *Journal of Analytical Atomic Spectroscopy*, 1987, **2**, 599.
- 76 R. S. Houk and N. Praphairaksit, *Spectrochimica Acta B*, 2001, **56**, 1069.
- 77 G. K. Koyanagi, V. I. Baranov, S. D. Tanner, and D. K. Bohme, *Journal of Analytical Atomic Spectroscopy*, 2000, **15**, 1207.
- 78 N. S. Nonose, N. Matsuda, N. Fudagawa, and M. Kubota, *Spectrochimica Acta B*, 1994, **49**, 955.
- 79 J. T. Rowan and R. S. Houk, *Applied Spectroscopy*, 1989, **43**, 976.
- 80 K. Sakata and K. Kawabata, *Spectrochimica Acta B*, 1994, **49**, 1027.
- 81 A. L. Gray and J. G. Williams, *Journal of Analytical Atomic Spectroscopy*, 1987, **2**, 81.
- 82 K. E. Jarvis, A. L. Gray, and E. McCurdy, *Journal of Analytical Atomic Spectroscopy*, 1989, **4**, 743.

- 83 M. A. Dexter, H. J. Reid, and B. L. Sharp, *Journal of Analytical Atomic Spectrometry*, 2002, **17**, 676.
- 84 L. A. Iacone, W. R. L. Masamba, S. H. Nam, H. Zhang, M. G. Minnich, A. Okino, and A. Montaser, *Journal of Analytical Atomic Spectrometry*, 2000, **15**, 491.
- 85 A. Montaser, S. K. Chan, and D. W. Koppenaal, *Analytical Chemistry*, 1987, **59**, 1240.
- 86 F. G. Smith, D. R. Wiederin, and R. S. Houk, *Analytical Chemistry*, 1991, **63**, 1458.
- 87 H. Uchida and T. Ito, *Journal of Analytical Atomic Spectrometry*, 1995, **10**, 843.
- 88 H. Uchida and T. Ito, *Journal of Analytical Atomic Spectrometry*, 1997, **12**, 913.
- 89 S. Nam, W. R. L. Masamba, and A. Montaser, *Analytical Chemistry*, 1993, **65**, 2784.
- 90 D. R. Bandura, V. I. Baranov, and S. D. Tanner, *Analytical Chemistry*, 2002, **74**, 1497.
- 91 Z. Y. Du and R. S. Houk, *Journal of Analytical Atomic Spectrometry*, 2000, **15**, 383.
- 92 P. R. D. Mason, K. Kaspers, and M. J. van Bergen, *Journal of Analytical Atomic Spectrometry*, 1999, **14**, 1067.
- 93 P. R. D. Mason and W. J. Kraan, *Journal of Analytical Atomic Spectrometry*, 2002, **17**, 858.
- 94 S. Mazan, N. Gilon, G. Cretier, J. L. Rocca, and J. M. Mermet, *Journal of Analytical Atomic Spectrometry*, 2002, **17**, 366.
- 95 S. D. Tanner and V. I. Baranov, *Atomic Spectroscopy*, 1999, **20**, 45.
- 96 R. Thomas, *Spectroscopy*, 2002, **17**, 42.
- 97 S. J. Jiang, R. S. Houk, and M. A. Stevens, *Analytical Chemistry*, 1988, **60**, 1217.
- 98 K. E. Murphy, S. E. Long, M. S. Rearick, and O. S. Ertas, *Journal of Analytical Atomic Spectrometry*, 2002, **17**, 469.
- 99 K. Y. Patterson, C. Veillon, A. D. Hill, P. B. Moser-Veillon, and T. C. O'Haver, *Journal of Analytical Atomic Spectrometry*, 1999, **14**, 1673.
- 100 T. Prohaska, C. Latkoczy, and G. Stingeder, *Journal of Analytical Atomic Spectrometry*, 1999, **14**, 1501.
- 101 N. Praphairaksit and R. S. Houk, *Analytical Chemistry*, 2000, **72**, 2356.
- 102 M. A. Dexter, B. L. Sharp, and H. J. Reid, in 'Ion Energy Effects in Hexapole Collision/Reaction Cell ICP-MS: Reactivity and Control of Input Ion Energy', Garmisch-Partenkirchen, Germany, 2003.
- 103 A. K. Shukla and J. H. Futrell, *Mass Spectrometry Reviews*, 1993, **12**, 211.
- 104 E. McCurdy and G. Woods, *Journal of Analytical Atomic Spectrometry*, 2004, **19**, 607.
- 105 M. A. Dexter, P. K. Appelblad, C. P. Ingle, J. H. Batey, H. J. Reid, and B. L. Sharp, *Journal of Analytical Atomic Spectrometry*, 2002, **17**, 183.
- 106 Z. Du and R. S. Houk, *Journal of Analytical Atomic Spectrometry*, 2000, **0**, 1.
- 107 I. Feldmann, N. Jakubowski, and D. Stuewer, *Fresenius Journal of Analytical Chemistry*, 1999, **365**, 415.
- 108 J. P. Guzowski and G. M. Hieftje, *Journal of Analytical Atomic Spectrometry*, 2001, **16**, 781.

- 109 M. Iglesias, N. Gilon, E. Poussel, and J. Mermet, *Journal of Analytical Atomic Spectrometry*, 2002, **17**, 1240.
- 110 C. P. Ingle, P. K. Appelblad, M. A. Dexter, H. J. Reid, and B. L. Sharp, *Journal of Analytical Atomic Spectrometry*, 2001, **16**, 1076.
- 111 S. F. Boulyga and S. J. Becker, *Fresenius Journal of Analytical Chemistry*, 2001, **370**, 618.
- 112 S. D. Tanner, V. I. Baranov, and U. Vollkopf, *Journal of Analytical Atomic Spectrometry*, 2000, **15**, 1261.
- 113 B. Hattendorf and D. Gunther, *Journal of Analytical Atomic Spectrometry*, 2000, **15**, 1125.
- 114 B. Hattendorf, D. Gunther, M. Schonbachler, and A. Halliday, *Analytical Chemistry*, 2001, **73**, 5494.
- 115 V. I. Baranov and S. D. Tanner, *Journal of Analytical Atomic Spectrometry*, 1999, **14**, 1133.
- 116 D. R. Bandura, V. I. Baranov, and S. D. Tanner, *Journal of Analytical Atomic Spectrometry*, 2000, **15**, 921.
- 117 D. R. Bandura, V. I. Baranov, and S. D. Tanner, *Journal of the American Society for Mass Spectrometry*, 2002, **13**, 1176.
- 118 L. A. Simpson, M. Thomsen, B. J. Alloway, and A. Parker, *Journal of Analytical Atomic Spectrometry*, 2001, **16**, 1375.
- 119 S. D. Tanner, *Journal of Analytical Atomic Spectrometry*, 1995, **10**, 905.
- 120 A. Sanz-Medel, *Spectrochimica Acta B*, 1998, **53**, 197.
- 121 C. B. Hymer and J. A. Caruso, *Journal of Chromatography A*, 2006, **1114**, 1.
- 122 S. D. Ilio, N. Violante, M. D. Gregorio, O. Senofonte, and F. Petrucci, *Analytica Chimica Acta*, 2006, **579**, 202.
- 123 E. H. Larsen, J. Sloth, M. Hansen, and S. Moesgaard, *Journal of Analytical Atomic Spectroscopy*, 2003, **18**, 310.
- 124 A. Polatajko, N. Jakubowski, and J. Szpunar, *Journal of Analytical Atomic Spectroscopy*, 2006, **21**, 639.
- 125 R. R. d. I. F. S. Remy, M. L. F. Sanchez, J. B. L. Sastre, and A. S. Medal, *Journal of Analytical Atomic Spectroscopy*, 2004, **19**, 616.
- 126 O. Mestek, J. Kominkova, R. Koplik, M. Kodicek, and T. Zima, *Applied Organometallic Chemistry*, 2007, **21**, 5.
- 127 J. Goulle, L. Mahieu, J. Castermant, N. Neveu, L. Bonneau, G. Laine, D. Bouige, and C. Lacroix, *Forensic Science International*, 2005, **153**, 39.
- 128 J. Daniel, H. Ziaee, C. Pradhan, P. B. Pynsent, and D. J. W. McMinn, *The Journal of Bone and Joint Surgery (Br)*, 2007, **89-B**, 169.
- 129 A. J. Hart, T. Hester, K. Sinclair, J. J. Powell, A. E. Goodship, L. Pele, N. L. Fersht, and J. Skinner, *The Journal of Bone and Joint Surgery (Br)*, 2006, **88-B**, 449.
- 130 P. Heitland and H. D. Koster, *Journal of Trace Elements in Medicine and Biology*, 2006, **20**, 253.
- 131 M. Khan, T. Takahashi, J. H. Kuiper, C. E. Sieniawska, K. Takagi, and J. B. Richardson, *Journal of Orthopaedic Research*, 2006, 1.
- 132 J. Huang, X. Hin, J. Zhang, K. Li, Y. Yan, and X. Xu, *Journal of Pharmaceutical and Biomedical Analysis*, 2006, **40**, 227.
- 133 R. N. Rao and M. V. N. K. Talluri, *Journal of Pharmaceutical and Biomedical Analysis*, 2007, **43**, 1.
- 134 A. L. Gray, *Journal of Analytical Atomic Spectrometry*, 1992, **7**, 1151.

- 135 'Oxford Dictionary of Chemistry', ed. J. Daintith, Oxford University Press, 1996.
- 136 D. R. Bandura, O. I. Ornatsky, and L. Liao, *Journal of Analytical Atomic Spectroscopy*, 2004, **19**, 96.
- 137 J. J. R. F. d. Silva and R. J. P. Williams, 'The Biological Chemistry of the Elements', Oxford University Press, 2001.
- 138 S. C. C. Wiedemann, H. Abbes, and W. G. Hansen, *Journal of the American Oil Chemists Society*, 2004, **81**, 437.
- 139 E. H. Evans, J. J. Giglio, T. M. Castellano, and J. A. Caruso, 'Inductively Coupled and Microwave Induced Plasma Sources for Mass Spectrometry', The Royal Society of Chemistry, 1995.
- 140 PerkinElmerSciex, in 'Relative Abundance of the Natural Isotopes and Periodic Table of the Elements Exhibiting the Elan Series ICP-MS Detection Limits', Shelton, CT 06484-4794 USA, 2004.
- 141 G. C. Eiden, C. J. Barinaga, and D. W. Koppenaal, *Journal of Analytical Atomic Spectrometry*, 1996, **11**, 317.
- 142 Thermo-Electron, in 'Trace Tech Torch Design', Cambridge.
- 143 K. Harper, in 'Increasing the Performance Whilst Decreasing Interference with a New Optimised Duo Torch Design for the iCAP 6000 Series Emission Spectrometer'.
- 144 J. N. Miller and J. C. Miller, 'Statistics and Chemometrics for Analytical Chemistry', Pearson Education Limited, 2000.
- 145 S. A. Soper, C. Owens, S. Lassiter, Y. Xu, and E. Waddell, 'DNA Technology: Topics in Fluorescence Spectroscopy', ed. J. R. Lakowicz, Kluwer Academic, 2003.
- 146 M. Kovacevic and W. Goessler, *Spectrochimica Acta B*, 2005, **60**, 1357.
- 147 J. N. Miller and J. C. Miller, 'Statistics and Chemometrics for Analytical Chemistry', Pearson Education Limited, 2005.
- 148 'DNA Profiling and DNA Fingerprinting', ed. J. T. Epplen and T. Lubjuhn, Birkhauser Verlag, 1999.
- 149 A. J. Flavell, 'Nucleic Acids in Chemistry and Biology', ed. G. M. Blackburn and M. J. Gait, Oxford University Press, 1990.
- 150 M. Vincent, Y. Xu, and H. M. Kong, *Embo Reports*, 2004, **5**, 795.
- 151 N. C. f. B. Information, 'SNPs: Variations on a Theme', Internet Website, National Centre for Biotechnology Information.
- 152 B. Hoogendoorn, M. J. Owen, P. J. Oefner, N. Williams, J. Austin, and M. C. O'Donovan, *Human Genetics*, 1999, **104**, 89.
- 153 'Platinum Coordination Complexes in Cancer Chemotherapy', ed. T. A. Connors and J. J. Roberts, Springer-Verlag Berlin, 1973.
- 154 R. R. Barefoot and J. C. V. Loon, *Analytica Chimica Acta*, 1996, **334**, 5.
- 155 P. C. Wilkins and R. G. Wilkins, 'Inorganic Chemistry in Biology', Oxford University Press, 1997.
- 156 C. X. Zhang and S. J. Lippard, *Current Opinion in Chemical Biology*, 2003, **7**, 481.
- 157 S. E. Harpstrite, A. A. Beatty, S. D. Collins, A. Oksman, D. E. Goldberg, and V. Sharma, *Inorganic Chemistry*, 2003, **42**, 2294.
- 158 H. Daghriri, F. Huq, and P. Beale, *Journal of Inorganic Biochemistry*, 2004, **98**, 1722.
- 159 F. Huq, H. Daghriri, J. Q. Yu, H. Tayyem, P. Beale, and M. Zhang, *European Journal of Medicinal Chemistry*, 2004, **39**, 947.

- 160 S. J. Scales, H. Zhang, P. A. Chapman, C. P. McRory, E. J. Derrah, C. M. Vogels, M. T. Saleh, A. Decken, and S. A. Westcott, *Polyhedron*, 2004, **23**, 2169.
- 161 F. P. Intini, A. Boccarelli, V. C. Francia, C. Pacifico, M. F. Sivo, G. Natile, D. Giordano, P. D. Rinaldis, and M. Coluccia, *Journal of Biological Inorganic Chemistry*, 2004, **9**, 768.
- 162 E. R. Jamieson and S. J. Lippard, *Chemical Reviews*, 1999, **99**, 2467.
- 163 M. Yang, R. Pang, X. Jia, Q. Li, and K. Wang, *Journal of Inorganic Biochemistry*, 2005, **99**, 376.
- 164 L. J. K. Boerner and J. M. Zaleski, *Current Opinion in Chemical Biology*, 2005, **9**, 135.
- 165 M. S. Deshpande and A. V. Kumbhar, *Journal of Chemical Science*, 2005, **117**, 153.
- 166 Y. Liu, H. Chao, J. Yao, L. Tan, Y. Yuan, and L. Ji, *Inorganica Chimica Acta*, 2005, **358**, 1904.
- 167 S. Nafisi, A. Sobhanmanesh, M. Esm-Hosseini, K. Alimoghaddam, and H. A. Tajmir-Riahi, *Journal of Molecular Structure*, 2005, **750**, 22.
- 168 D. C. Menezes, F. T. Vieira, G. M. d. Lima, A. O. Porto, M. E. Cortes, J. D. Ardisson, and T. E. Albrecht-Schmitt, *European Journal of Medicinal Chemistry*, 2005, **40**, 1277.
- 169 W. B. Pratt and R. W. Ruddon, 'The Anticancer Drugs', Oxford University Press, 1979.
- 170 M. Wei, O. Burenkova, and S. J. Lippard, *The Journal of Biological Chemistry*, 2003, **278**, 1769.
- 171 R. Mandal, R. Kalke, and X. Li, *Rapid Communications in Mass Spectrometry*, 2003, **17**, 2748.
- 172 E. S. McDonald, K. R. Randon, A. Knight, and A. J. Windebank, *Neurobiology of Disease*, 2005, **18**, 305.
- 173 S. G. Chaney, S. L. Campbell, E. Bassett, and Y. Wu, *Critical Reviews in Oncology/Hematology*, 2005, **53**, 3.
- 174 K. Wang, J. Lu, and R. Li, *Coordination Chemistry Reviews*, 1996, **151**, 53.
- 175 S. Hector, W. Bolanowska-Higdon, J. Zdanowicz, S. Hitt, and L. Pendyala, *Cancer Chemotherapy Pharmacology*, 2001, **48**, 398.
- 176 E. Raymond, S. Faivre, S. Chaney, J. Woynarowski, and E. Cvitkovic, *Molecular Cancer Therapeutics*, 2002, **1**, 227.
- 177 J. M. Woynarowski, S. Faivre, M. C. S. Herzig, B. Arnett, W. G. Chapman, A. V. Trevino, E. Raymond, S. G. Chaney, A. Vaisman, M. Varchenko, and P. E. Juniewicz, *Molecular Pharmacology*, 2000, **58**, 920.
- 178 J. M. Woynarowski, W. G. Chapman, C. Napier, M. C. S. Herzig, and P. Juniewicz, *Molecular Pharmacology*, 1998, **54**, 770.
- 179 M. Galanski, A. Yasemi, S. Slaby, M. A. Jakupc, V. B. Arion, M. Rausch, A. A. Nazarov, and B. K. Keppler, *European Journal of Medicinal Chemistry*, 2004, **39**, 707.
- 180 J. M. Malinge, M. J. Giraud-Panis, and M. Leng, *Journal of Inorganic Biochemistry*, 1999, **77**, 23.
- 181 S. G. Chaney, S. L. Campbell, B. Temple, E. Bassett, Y. Wu, and M. Faldu, *Journal of Inorganic Biochemistry*, 2004, **98**, 1551.
- 182 D. E. Graves and L. M. Velea, *Current Organic Chemistry*, 2000, **4**, 915.
- 183 R. Sinha, M. Islam, K. Bhadra, G. S. Kumar, A. Banerjee, and M. Maiti, *Bioorganic and Medicinal Chemistry*, 2006, **14**, 800.

- 184 A. R. Ghezzi, M. Aceto, C. Cassino, E. Gabano, and D. Osella, *Journal of Inorganic Biochemistry*, 2004, **98**, 73.
- 185 S. Rauf, J. J. Gooding, K. Akhtar, M. A. Ghauri, M. Rahman, M. A. Anwar, and A. M. Khalid, *Journal of Pharmaceutical and Biomedical Analysis*, 2005, **37**, 205.
- 186 M. Akaboshi, K. Kawai, H. Maki, K. Akuta, Y. Ujeno, and T. Miyahara, *Japanese Journal of Cancer Research*, 1992, **83**, 522.
- 187 R. Mandal, R. Kalke, and X. Li, *Chemical Research in Toxicology*, 2004, **17**, 1391.
- 188 G. Weber, J. Messerschmidt, A. C. Pieck, A. M. Junker, A. Wehmeier, and U. Jaehde, *Analytical and Bioanalytical Chemistry*, 2004, **380**, 54.
- 189 J. Batey, P. D. Winship, B. L. Sharp, and H. J. Reid, in 'Personal Communication - A Discussion of the ICP-MS Interface Design', 2005.
- 190 J. H. Macedone and P. B. Farnsworth, *Spectrochimica Acta B*, 2006, **61**, 1031.
- 191 H. Niu and R. S. Houk, *Spectrochimica Acta B*, 1996, **51**, 779.
- 192 W. N. Radicic, J. B. Olsen, R. V. Nielson, J. H. Macedone, and P. B. Farnsworth, *Spectrochimica Acta B*, 2006, **61**, 686.
- 193 K. Sakata, N. Yamada, and N. Sugiyama, *Spectrochimica Acta B*, 2001, **56**, 1249.
- 194 K. E. Jarvis, P. Mason, T. Platzner, and J. G. Williams, *Journal of Analytical Atomic Spectrometry*, 1998, **13**, 689.
- 195 J. W. H. Lam and G. Horlick, *Spectrochimica Acta Part B-Atomic Spectroscopy*, 1990, **45**, 1327.
- 196 R. Courant and K. O. Friedrichs, 'Supersonic Flow and Shockwaves, Pure and Applied Mathematics', ed. H. Bohr, Interscience Publishers, 1948.
- 197 P. Leong-Sit, D. Redfearn, R. Yee, and A. D. Krahn, *Journal of Cardiovascular Electrophysiology*, 2006, **17**, 917.
- 198 H. Loertzer, J. Soukup, A. Hamza, A. Wicht, O. Rettkowski, E. Koch, and P. Fornara, *Transplantation Proceedings*, 2006, **38**, 707.
- 199 D. Z. Uslan and L. M. Baddour, *Current Opinion in Infectious Diseases*, 2006, **19**, 345.
- 200 D. Warren and P. D. Winship, in 'Personal Communication - A Discussion of Implantable Devices in the Human Body', 2006.
- 201 B. Walder, D. Pittet, and M. R. Tramer, *Infection Control and Hospital Epidemiology*, 2002, **23**, 748.
- 202 G. M. L. Bearman, C. Munro, C. N. Sessler, and R. P. Wenzel, *Seminars in Respiratory and Critical Care Medicine*, 2006, **27**, 310.
- 203 E. P. J. M. Everaert, B. V. D. Belt-Gritter, H. C. V. D. Mei, H. J. Busscher, G. J. Verkerke, and F. Dijk, *Journal of Materials Science: Materials in Medicine*, 1998, **9**, 147.
- 204 P. M. Arnow, E. M. Quimosing, and M. Beach, *Clinical Infectious Diseases*, 1993, **16**, 778.
- 205 R. O. Darouiche, I. I. Raad, S. O. Hearn, J. I. Thornby, O. C. Wenker, A. Gabrielli, J. Berg, N. Khardori, H. Hanna, R. Hachem, R. L. Harris, and G. Mayhall, *The New England Journal of Medicine*, 1999, **340**, 1.
- 206 'Human Pharmacology: Molecular to Clinical', ed. T. M. Brody, J. Larner, and K. P. Minneman, Mosby, 1998.
- 207 J. M. Schierholz, L. J. Lucas, A. Rump, and G. Pulverer, *Journal of Hospital Infection*, 1998, **40**, 257.

- 208 B. M. Farr, P. D. Ellner, and H. C. Neu, in 'Antiseptics and Disinfectants', ed.
T. M. Brody, J. Larner, and K. P. Minneman, St Louis, 1998.
- 209 Y. Li, P. Leung, L. Yao, Q. W. Song, and E. Newton, *Journal of Hospital
Infection*, 2006, **62**, 58.
- 210 F. Furno, K. S. Morley, B. Wong, B. L. Sharp, P. L. Arnold, S. M. Howdle, R.
Bayston, P. D. Brown, P. D. Winship, and H. J. Reid, *Journal of Antimicrobial
Chemotherapy*, 2004, **54**, 1019.

